University of Strathclyde

Department of Electronics and Electrical Engineering

Wind Power Utilization Improvement by Using Hierarchical Controlled Microgrid

Cheng Ding

M.Sc.

Supervisor: Professor K. L. Lo

A thesis presented in fulfilment of the requirements for the degree of Doctor of Philosophy

2019

Declaration of Authenticity and Author's Rights

This thesis is the result of the author's original research. It has been composed by the author and has not been previously submitted for the examination which has led to the award of a degree.

Signed: Cheng Ding Date: 14/07/2019

Acknowledgements

I would like to thank my supervisor, Prof. K. L. Lo and Mrs Lo for their supervision, guidance and encouragement during my Ph.D. study, I appreciate so much that Prof. Lo provided me the opportunity to work on a such a meaningful and challenging subject.

I also would like to thank my colleagues in the PSRG for their company and encouragement in this long journey of Ph.D. study.

To my families, I would like to thank my girlfriend Yiyi Zhao who has graduated as Ph.D. from University of Strathclyde two years ago, for her unceasing encouragement and support.

Most importantly, I am very grateful to my parents, Guohe Ding and Minhui Chen, for their encouragement and financial support during the entire study of my Ph.D. study.

Abstract

In this thesis, a possible solution for improving the utilization of wind power energy without causing impact to the power grid by using microgrid concept, which promises the function of making a cluster of generators and loads behave like a controllable unit, is proposed. This microgrid concept is achieved by a proposed hierarchical control method which contains three levels: decentralized level 1 (primary or bottom level) is of fast response and can satisfy the essential power system operation requirements; centralized level 2 (secondary or middle level) eliminates control target deviation and rely on low band width communication channels to achieve accurate control objectives within several seconds; level 3(tertiary or top level) is the system organization level in which on-site functions such as seamless states transition operation and off-site functions such as setting points optimization are executed.

A 4-bus microgrid model built in MATLAB/Simulink is used for individual validation tests of the different control level. The following experiments are executed in the wind power generators integrated CERTS 20-bus microgrid system. The simulation results show the system variations caused by wind power can be digested within the microgrid system with cooperation of the local loads, backup generators and energy storage devices which are operated by the hierarchical control system. In which case, the impact of wind power fluctuation can be absorbed by using microgrid concept with the proposed hierarchical control method.

Table of contents

List of Figures

List of Tables

List of Abbreviations and symbols

AC	Alternating Current
DC	Direct Current
DER	Distributed Energy Resource
DFIG	Doubly-Fed Induction Generator
DG	Distributed Generator
DNO	Distribution Network Operator
FESS	Flywheel Energy Storage System
LC	Local Controller
MGCC	Microgrid Central Controller
MPPT	Maximum Power Point Tracking
NRF	Natural Reference Frame
p.u.	per unit
PLL	Phase Locked Loop
PMSG	Permanent Magnet Synchronous Generator
PWM	Pulse-Width Modulation
SPWM	Sinusoidal Pulse-Width Modulation
SRF	Stationary Reference Frame
SRRF	Synchronously Rotating Reference Frame
TOC	Temporary Optimized Capacity
TOS	Temporary Optimized Setting

VPLL	Virtual Phase Locked Loop
WECS	Wind Energy Conversion System
E	Electromotive force at the output port of the energy source
V	Voltage at a certain point

Chapter 1: Introduction

1.1 Research backgrounds

When environment issues such as greenhouse gas emission and global temperature rise become more and more serious, many countries turn to clean energy technologies. With the features of being environmentally friendly and a mature technology, wind power becomes one of the popular renewable energy sources. Especially the Scottish government aimed to generate 100% electricity from renewable energy resources in 2020 [1]. Wind energy penetration can be defined in several ways [2-4]. In this thesis, wind power penetration is defined as the total power installed capacity of the wind farms divided by the total power installed capacity in the power grid. When the load is determined, increasing the wind power penetration level in power system means reducing carbon dioxide emissions. With environmental considerations, higher wind power penetration is preferred. However, because of the intermittent and hardly predictable characteristics of wind power, higher wind power penetration leads to more impacts on power quality and system reliability [2, 5-9]. Transmission congestion and/or temporal power mismatch caused by wind power variations could cause system instability. These drawbacks mean the wind power penetration level must be limited. To minimize the impacts and increase wind power penetration level, some methods are proposed and developed. These methods can be mainly divided into three groups:

- Improving existing power system allowance by better regulation methods, such as real-time power flow regulation, multi-area cooperation and demand side management [10-12].

- Wind power generation assisted with energy storage technologies including: battery, flywheel, compressed air, pumped hydro [13-18].
- Consuming excess energy locally: For instance, if there is plenty of water resources nearby, hydrogen production is one option [19].

The microgrid concept is defined as a cluster of loads and energy sources which are connected to the main grid through a point of common coupling (PCC). A microgrid can behaviour as a controllable unit. In this thesis, a microgrid cooperated with hierarchical control theory is used to combine the advantages of these conventional methods mentioned above. The research work is focused on the interactions between the microgrid and the main grid on PCC. In which case, the component within the microgrid do not have to follow the standards requirements of the main grid. It makes the research achievements can be conveniently extended to different countries and regions.

1.1.1 Development of power system and microgrid concept

1.1.1.1 Development of power system

The power system network has grown and become larger and larger over the last few decades, furthermore, some power grids of different countries are connected and run in parallel [20]. In which case, the traditional power system network is a centralised system. In such power network, the direction of power flow is from the high voltage transmission network to the lower voltage distribution network. In other words, the distribution network is passive and network components are designed in such manner that when they are further downstream, they generally have lower capacity. Settings for distribution network protection are also designed in a similar manner.

In a centralised power system, to maintain the system reliability, the investment cost for transmission network grows fast when the voltage level and transmission capacity increased. Some large area blackout events, for instance, the northeast blackout of 2003, proved the importance of reliability and the weakness of centralised power supply system [21, 22]. To deal with these drawbacks of centralised system, the decentralised structure is getting more widely used in modern power system.

Distributed generators (DGs), such as small gas turbines, fuel cells, photovoltaic system and wind farms, have the capacity often in the interval of several kW to tens of MW [23]. In contrast to conventional generators, DGs have the advantage of supporting demand locally as they are usually geographically located near the loads [24]. DG technologies reduces the capacity requirement for the transmission branches and provides the possibility of small-scale renewable energy sources injection. Meanwhile, there are some disadvantages of DG itself, such as relatively high generation cost, hard to be controlled and regulated by the system operator. These disadvantages limit the effect of DG applications. With the features of DG, some changes are needed in the modern power system concept. In recent years, with more and more DGs being installed in the distribution network, the traditional concept of power flow which is designed for radial network is no longer valid. The distribution network become active. New design and network control concept are needed.

1.1.1.2 Microgrid concept

The concept of microgrid was first introduced by R.H. Lasseter in the 2001 and 2002 IEEE Power Engineering Society Winter Meetings [25, 26]. It provided solutions for effectively operating distributed generators. The

benefits come from this concept include not limit to, enhance local power system reliability, reduce transmission losses, maintain voltage level, combined heat and power solution, and provide uninterruptable power supply functions. As the components in microgrid are highly controllable, it is inherently compatible for renewable energy sources such as wind power.

With the better prospects of the microgrid, many entities began to research and develop microgrid projects. Some of them have proposed their own definitions of microgrid [27]. These definitions are normally quite like each other. One of the widely accepted microgrid definitions given by US Department of Energy is "a group of interconnected loads and distributed energy resources within clearly defined electrical boundaries that acts as a single controllable entity with respect to the grid. A microgrid can connect and disconnect from the grid to enable it to operate in both grid-connected or island-mode." [28]

1.1.2 Worldwide microgrid development and ongoing projects

In the past years, the number of worldwide microgrid projects have been rapidly growing, especially in US and EU microgrid research projects play world's leading position [29, 30]. According to the Navigant Research's report [31], up to the 2nd quarter of 2018, there are over 2000 microgrid projects. The total capacity which include proposed, under development, and operational reached 25 GW. In these projects, the diesel generation technology shares the leading capacity. However, the PV solar capacity grows fast, which drops the leading role of diesel.

1.1.2.1 Microgrid development in USA

In the year 2003, The US department of Energy published a project called 'Grid 2030' [32]. It proposed the objects of power grid development in the 21st century are including: to improve the power supply reliability for important loads, provide the power meets variety quality requirements, reducing generation costs and building smart gird. Microgrid research is one of the most important parts of this smart gird. The participants involved in this project including industry practitioners, policy makers and researchers. This vision provides a development roadmap for the National Electric Delivery Technologies.

The most well-known organization in the microgrid R&D field is the Consortium for Electric Reliability Technology Solutions (CERTS) which proposed the first microgrid concept, based in the USA. The full-scale test bed used for demonstration is built near Columbus, Ohio and operated by American Electric Power. There are some other participants running their demonstrations on this test bed [33]. One of the famous projects is the Distributed Energy Resources Customer Adoption Model (DER-CAM) which is developed by Berkeley Lab since 2000 [33]. This model is focused on economic section about minimizing the operating costs. The current projects running by CERTS cover the research areas include:

- **Techniques section:** seamless mode transition methods, protection approach which is not depending on the abnormal currents, decentralised control method for voltage and frequency stability during islanded mode.
- **Enhancements section:** reduction of protection and DC storage costs, inclusion of AC storage and non-inverter-based microsources.

- **Addition and integrated testing of new hardware elements:** more flexible energy management system, conventional synchronous generator, intelligent load shedding, commercial stand-alone storage device.

1.1.2.2 Microgrid development in EU

'Framework Programs' (FP) is a continuously program which is funded by the European Commission [34]. This funding program started in the year 1984. It supports a variety of different research objectives in different periods. Up to 2018, there are 8 sections from FP 1 to FP7, and FP 8 which is also called 'Horizon 2020'. Each of the program sections lasts for several years. From FP 5, the funded research areas covered microgrid concept which is an important part of smart grid section. In the past several years, for the purpose of decarbonising the energy system, enhance renewable energy utilisation and getting more economical benefits, some visions and guidance, such as 'European Technology Platform SmartGrids', 'Strategic Energy Technology Plan', 'Energy Roadmap 2050' are published [35-37].

A well-known microgrid project called 'MICROGRIDS' funded by the European Commission is headed by the National Technical University of Athens (NTUA) in 2003 [38]. This project cooperates 14 members from 7 EU countries. The research fields for both stand-alone and grid-tied microgrid include: operation, control, protection, safety and telecommunication infrastructure of microgrid as well as the economic benefits demonstration. The followed-up project 'MORE MICROGRIDS' started in 2006 [34] with the research objectives include: increasing penetration of microgeneration by using microgrid concept, investigation

of generator control strategies and network design, developing tools for multi-microgrid management and operation, and standardising the technical and commercial protocols for microgrid. The test beds are the LV and MV microgrids built in the labs in Greece, Germany, France and UK respectively. One of the well-known test beds is the Kythnos Island addressed in the Aegean Sea near Athens [34]. This project is a village scale low voltage AC microgrid which is funded by FP 5 Microgrids program. This is an islanded microgrid used to test centralised and decentralised control strategies.

1.1.2.3 Microgrid development in Asia

New Energy and Industrial Technology Development Organization (NEDO) is one of the Japan's largest public R&D management organization in industrial, energy and environment technologies developing areas [34]. The Sendai Microgrid is one of the well-known microgrid projects funded by NEDO. This microgrid was constructed from 2004 to 2007 for demonstration purposes and is still being operated after several upgrades. There is a notable feature of this microgrid that it can provide six different power quality levels for different loads. This project is getting famous for its successfully surviving in an earthquake in the year 2011 [39].

In China, in contrast to the long-distance high voltage transmission technologies, the microgrid concept attracted the attention from government a little later than USA/EU. When the wide-area blackout happened in the winter of year 2008, only a few small power grids were supporting important loads [40]. The China government realised the weakness of the existing grid and decided to accelerate the research

progress on the robust smart grid area. With the efforts of National Development and Reform Commission microgrid concept is developing fast in recent years in China. There are over 100 pilot projects in different cities of China. The research scopes include energy saving and efficiency, economic running, renewable energy development for either decarbonization or power quality and reliability enhancement.

1.2 Research objectives

The microgrid concept has the advantages in the DG integration and system reliability enhancement. The attractive prospects attract many countries and organizations to run R&D projects. However, challenges and unsolved issues exist in the area of power electronic device techniques, control methods, specific protection techniques, system level optimization and common accepted standards [41-43]. As mentioned in the previous section, most of the existing microgrid projects are focused on maintaining the power balance and system optimization within the microgrid. In this research, how to effectively deal with the interactions between the wind power embedded microgrid and main grid is the main purpose.

The power directly generated by the renewable energy sources or the small-scale generators often do not meet the requirement of grid connection. Most of the DGs in microgrid connect to the grid need power electronic interfaces, normally inverters. It reduces the inertia in a microgrid system. Moreover, in contrast to the conventional power network, the line impedance in a microgrid is much smaller. In which case, even some small disturbances at one node may cause the whole system significantly varying, such as large circulating current, voltage swell or dips and frequency variations.

To solve the issues mentioned above, some concepts and methods have been proposed. The DC microgrid concept which can eliminate some of the AC system's drawbacks mentioned above, has been proposed as it has the advantages of no reactive power flow issues, simple system topology and no phase angle or frequency related issues [44-46]. However, the DC microgrid concept is not suited for existing power system as special DC transmission lines and devices are required.

In AC microgrid, the existing control methods can be divided into two groups: decentralized control and adaptive control [32, 47]. The most well accepted decentralized control method is droop control method [48-50]. This method achieves automatically load sharing by simulating the active power/frequency and reactive power/voltage droop characteristics of conventional generator. However, the conventional droop control method only works for the highly inductive lines. As a result, some modified droop control methods have been proposed. The P/V and Q/ω droop method is proposed by J.M. Guerrero et al. [51]. This droop method has the advantage and disadvantage like the conventional droop method as it only works for the highly resistive lines. C. K. Sao and P. W. Lehn investigated an adjustable load sharing method [52]. This method can improve system dynamic performance without affecting the droop characteristics. However, it still cannot deal with the line impedance effect. C. T. Lee et al. investigated a method which can improve the reactive power sharing accuracy and eliminate part of the line impedance effect by using $Q/\dot{V}$ droop characteristic [53]. However, the integral parts slow down the system dynamic response. The virtual impedance methods (such as complex virtual impedance method proposed by W. Yao el al. [54] and adaptive virtual impedance method proposed by H. Mahmood et al. [55])

and virtual frame method proposed by Y. Li and Y. W. Li [56] decouple the active and reactive power control and they are capable for different R/X ratios of line impedance. However, the accurate equivalent line impedance parameter is required, and these methods cannot adopt system topology changes. Besides, there are certain level of voltage and/or frequency deviations cannot be eliminated by using any of the decentralized method mentioned above. Meanwhile, the adaptive control methods, such as centralized control, master-slave control circular-chain control can achieve accurate control results and are capable for different line impedance situations [57-63]. However, the feature of relying on high speed communication channels make these adaptive methods applied in microgrid be expensive and unreliable.

The hierarchical control structure is widely used in power system control. Different control objectives are addressed in several control levels. In which case, different control methods can be combined. The main objective of this research is to investigate a three-level hierarchical control method, which can maintain the system stability, the power quality and obtain the best value of money, by combining the decentralized control and adaptive control methods. Control level 1 which uses decentralized control method satisfies the essential system operation requirements and capable for multi generators situation with high reliability. Control level 2 assists control level 1 to achieve good power quality and make system stable for different line impedance situations. For the purpose of improving wind power utilization, control level 3 is designed for system optimization and regulation.

1.3 Main contributions

There are four main contributions been established in this thesis.

- The first contribution is investigating a statistical wind power output model which is used for evaluation purpose. As the historical wind speed data is often not large enough for system planning, a method of generating the output model of wind power generator which is used to evaluate system performance is developed. This model is based on the statistical wind speed distribution which is derived from the historical data. Weibull Distribution is used to fit the wind speed historical data. After the relationship of wind speed and generator's output are derived, the infinite data of power output can be obtained by executing Monte Carlo simulation.

The second to the fourth contributions are about the unique three-level hierarchical control method which is designed for the wind power generator embedded microgrid.

- Contribution 2: The level 1 controller is a fast-responded decentralised controller. The controller is a local controller which is located at the DG side. The information used for regulation is the voltage and current values measured locally, and the references from the higher-level controller. With this level 1 controller, the DGs can be operated either in constant voltage mode or constant power output mode without a communication system assist. They also can adapt a certain level of system voltage and frequency variations. Although there are some deviations existed with the

standalone level 1 controller, system reliability and stability are guaranteed.

- Contribution 3: The level 2 controller is addressed in the microgrid control centre. This controller achieves its control objectives within several milliseconds to seconds. It generates the initial references, which is calculated by power flow calculation, for the level 1 controllers. It also eliminates the deviations on each node by adding compensations to the initial references. This level 2 controller is normally operated with the objective of minimum transmission losses. Only the low bandwidth communication channels are required for the cooperation between control level 2 and level 1. In which case, the precisely system regulation and high reliability are effectively maintained.
- Contribution 4: The level 3 controller is also addressed in the microgrid control centre. The information involved in the level 3 controller is not only within the microgrid, but also from the DNO. It provides both the real-time and non-real-time functions. The respond time of this level is from several seconds to hours. The real-times functions achieved in the level 3 controllers include long-term power flow regulation and state transition regulation. The real-time functions are achieved by cooperation with the level 2 controller. The non-real-time functions include power exchange schedule regulation on PCC and the settings optimization of WECS/FESS combined generator system.

1.4 Assumptions of this work

The studies in this thesis are based on the software simulation using MATLAB/Simulink.

The assumptions applied in this research are stated as follows:

a. To make the calculation procedures be simple, the components in the simulation system is relatively ideal. The transformers' effects are neglected. All the DGs in the system have the same rated voltage level. As the transmission distance is relatively short, the ideal R/X cable model is used to represent the transmission line. This part has no impact to the simulation results.
b. The AC microgrid is operated in three phase balanced load condition. The main grid side at Point of Common Coupling (PCC) is considered as infinite. The voltage and frequency variations caused by microgrid are not considered in this thesis. The voltage and frequency at PCC are determined by the main grid. For system transient analysis, more detailed main grid model is required.
c. The wind generator and the backup generator are connected to the grid through inverters. The generator and energy storage device cooperation control techniques are considered be well developed and not discussed in the thesis. The simulation model of inverter-based generator coupled with energy storage device is consisted of a constant source at the DC side and a detailed PWM driven two-level inverter.
d. Flywheel Energy Storage System (FESS) is used as the energy storage device which is coupled with the wind power generator. It is a short-term energy storage device, which is preferred for the continuously variation situation and has the feature of high-power density and low

energy density [39, 64]. Which means the energy stored in FESS is relatively few, but it can provide very large power output in short terms. The investment cost of FESS is much less than long-term devices such as battery. Besides, it has the advantages of good durability around 20 years, low maintenance cost, high energy exchange rate which is over 90%.

e. The wind speed data is generated randomly by using Monte Carlo Simulation method with the Weibull Distribution characteristics derived from historical data. With the properly installed energy storage devices, the wind generation output is assumed constant in every 15 minutes duration. Although the characteristics of continuity are not reflected by the Monte Carlo simulation. This data set is good at probability evaluation. In this thesis, the main purpose is the probability evaluation.
f. In this thesis, the frequency signal which is used to control the inverter is generated by virtual phase locked loop instead of the conventional phase locked loop. The local clock signal of the simulation host computer is used to present the GPS synchronization signal.

1.5 Layout of this thesis

The rest of this thesis is divided into 6 chapters:

Chapter 2 gives a glance of worldwide wind power development and trends. An introduction of fundamentals of wind power energy conversion system (WECS) technologies is provided as well. The features of two most widely used wind turbine model, the doubly fed induction generator (DFIG) and permanent magnet synchronous generator (PMSG), are introduced and compared. Based on these characteristics, this chapter

investigates a method of generating wind power generator's output model from the statistical wind speed model which is obtained from the historical data. A case study is given to help clarify the procedures of how to derive this statistical model from historical data.

In **Chapter 3**, a review of microgrid operational features and control theories is presented. The dispersed energy resources in microgrid are normally connected to the grid through inverters. The microgrid is connected to the main grid through PCC. To meet the grid code requirements, the DGs in a microgrid have to be monitored and supervised. A well accepted hierarchical control structure which contains three levels is often applied in microgrid applications. The control hierarchies are divided by the different control objectives which have different response time requirements. In this thesis, the existed control level 1 techniques, which provide the instantaneous functions of voltage stability provision, frequency stability preserving, plug and play capability of DERs and circulating current avoidance among DERs, are reviewed in two groups: droop control and active load sharing control.

Chapter 4 proposed an enhanced hierarchical control method for the wind power integrated microgrid. The physical components in this microgrid include generators (wind power generators and backup generator), energy storage devices, loads (elastic and non-elastic loads). The adjustable load sharing method is chosen as the control level 1 method in this thesis as its dynamic response can be adjusted without affecting the droop characteristics. There are two control objectives of the control level 2 in the proposed hierarchical control method: initial steady state values generation and deviations compensation. The initial steady state power flow is generated by the MATPOWER tools box in MATLAB. The

deviations compensation is achieved by recalculating power flows after adding correction parameters which is generated from the comparisons of observed values and the initial calculated results. In this chapter, there are two groups of functions are proposed in the level 3: energy storage device settings optimization and real-time operating functions.

In **Chapter 5**, an 11kV 20 buses simulation microgrid model built in MATLAB/Simulink is used to evaluate the performance of the proposed hierarchical control method in chapter 4. This simulation model contains three main classes of components: industrial and residential loads, inverter-based generators, distribution cables. The load model includes the main part which is operated under a predetermined daily load curve, randomly switched part, and controllable part. The WECS/FESS combined generator model proposed in chapter 4 is applied in this section. The output is randomly generated from the statistical wind speed model. This grid connected microgrid can performance as either controllable DG or load. A method which is used to generate the microgrid operating schedule is proposed in this chapter. The objective of this schedule is making the power exchange between the hierarchical controlled microgrid and the main grid be kept constant in a certain time periods with high reliability. There are two main scenarios of experiment in this chapter: long-term running result, and the system performances with precise control in a specific time period.

In **Chapter 6,** to make the wind power embedded microgrid be capable for state transition and islanded operation, the control strategies for smooth transition and short-term islanded operation are proposed. As there are different operations must be applied and they depend on the islanding duration, the critical time for load shedding and wind power

curtailing is proposed in this chapter. Within the critical time, the power supply and demand gap caused by the disconnection should be capable of being supported by the existed backup generator and energy storage devices. The procedure which can minimize the system disturbance during reclosing period is introduced and tested in the 20-bus simulation microgrid system. The backup generator's operation strategies during short-time islanding period is discussed in the last section.

The conclusions and suggestion for future work are presented in **Chapter 7**.

1.6 Publications

C. Ding and K. L. Lo, "Microgrid control and management of state transition period," *2012 47th International Universities Power Engineering Conference (UPEC)*, London, 2012, pp. 1-5.

Y. Zhao and C. Ding, "Wind Power Generator Output Model Based on the Statistical Wind Speed Distribution Derived From the Historical Data," *2018 2nd IEEE Conference on Energy Internet and Energy System Integration (EI2)*, Beijing, China, 2018, pp. 1-5.

Chapter 2: Wind power backgrounds and features of Wind Energy Conversion System (WECS)

2.1 Introduction

Environmental issues are increasingly of concern by the public. In contrast to fossil fuels, renewable energy sources such as wind power have much less impact on the environment. How to effectively use wind power becomes one of the most important topics in many countries.

Utility-scale wind turbine technologies was rapidly developing since 1980s. Fixed-speed wind turbine technology is considered obsolete [65]. Most of variable-speed wind turbines inject power to grid through power converters. The inertia of such type of generators is shielded from the grid, and hence they do not inherently have the droop characteristics as conventional generators [66]. When there is a certain number of dispersed wind turbines, a set of challenges related to power system control and operation emerges. For instance, dynamic performance, load flow balancing and reactive power control. The microgrid concept makes a small scale of power system behave as a controllable source or load. It leads to a reduction of the number of nodes needed to be operated by TSO/DSO in a certain power system network. To achieve these benefits, it is necessary to have a good understanding of wind power performances and power system control backgrounds.

In this chapter, Section 2.2 gives an overview of current wind power status. The worldwide wind power trends of both onshore and offshore wind farms are introduced. The next section explains fundamentals of wind energy conversion system. In this section, the main components including mechanical and electrical parts are introduced. Besides, information of the

aerodynamic performance of the wind turbines, the classification of current industrial WECS technology and the generating cost expressions for WECS is provided. Two of the most widely used wind turbine models, DFIG and PMSG, are compared in Section 2.4. It also describes the procedure of how to produce wind turbine mechanical output by aerodynamic features on certain wind speed. Although they generate same power when the rated wind speed reached, the PMSG is more effective in relatively slow wind speed conditions. Section 2.5 describes how to build wind speed statistical model by using Weibull Distribution and Monte Carlo Simulation method. A case study of how to derive the WECS output statistical model from the practical wind speed data explained in Section 2.6. Section 2.7 gives the summary.

2.2 Worldwide wind power trends

In recent years, there is an urgent demand of new energy technology which has less carbon dioxide emission to replace conventional fossil fuel energy. Wind energy especially onshore wind energy is considered as one of best the economic renewable energy. The generating cost of onshore WECS is around 7-9 p/kWh [67]. It is half the cost of offshore wind energy, a quarter of solar photovoltaic energy and on average slightly cheaper than nuclear power.

Since the first 50-kW utility-scale wind turbine is invested in the 1980s, and in the past decades the size of wind turbines is gradually increasing. Nowadays, the power of a single commercial wind turbine already reaches the level of 10 MW. The height of tower can be built to near 200 meters, and the length of rotor blades is near 100 meters. This huge size of WECS enable wind power to be used in some area with relatively slow average wind speed.

As Figure 2.1 shows, the world-wide cumulative wind power capacity is growing rapidly in last decade. The capacity has grown around 20% annually since 2001. Right now, the speed of expansion is slowing down as it already has a huge quantity of almost 500 GW.

Typically, wind turbines are geographically divided into onshore and offshore. In recent years, public shows more interests in offshore WECS. Compared to onshore wind farms, offshore wind farms have the characteristics of lower wind speed turbulence and higher annual mean wind speed. Large offshore wind farm can provide wind energy with better power quality to the utility grid. It is geographically centralized, this makes power flow control for system operator much easier than dispersed onshore wind farms. Figure 2.2 shows the offshore wind capacity of the top 15 countries in the recent two years and the worldwide cumulative capacity for the last six years. It can be sought out that UK has the world largest offshore wind capacity. European countries and PR China show more interests in offshore wind power than other countries. The offshore wind power capacity percentage of the total wind capacity grows constantly every year. As Figure 2.3 shows, the grown speed in percentage is over 25% in the last 5 years. In 2016, offshore wind power has already shared 3% of the total wind power. With this speed of expansion, it will share over 20% in next 10 years.

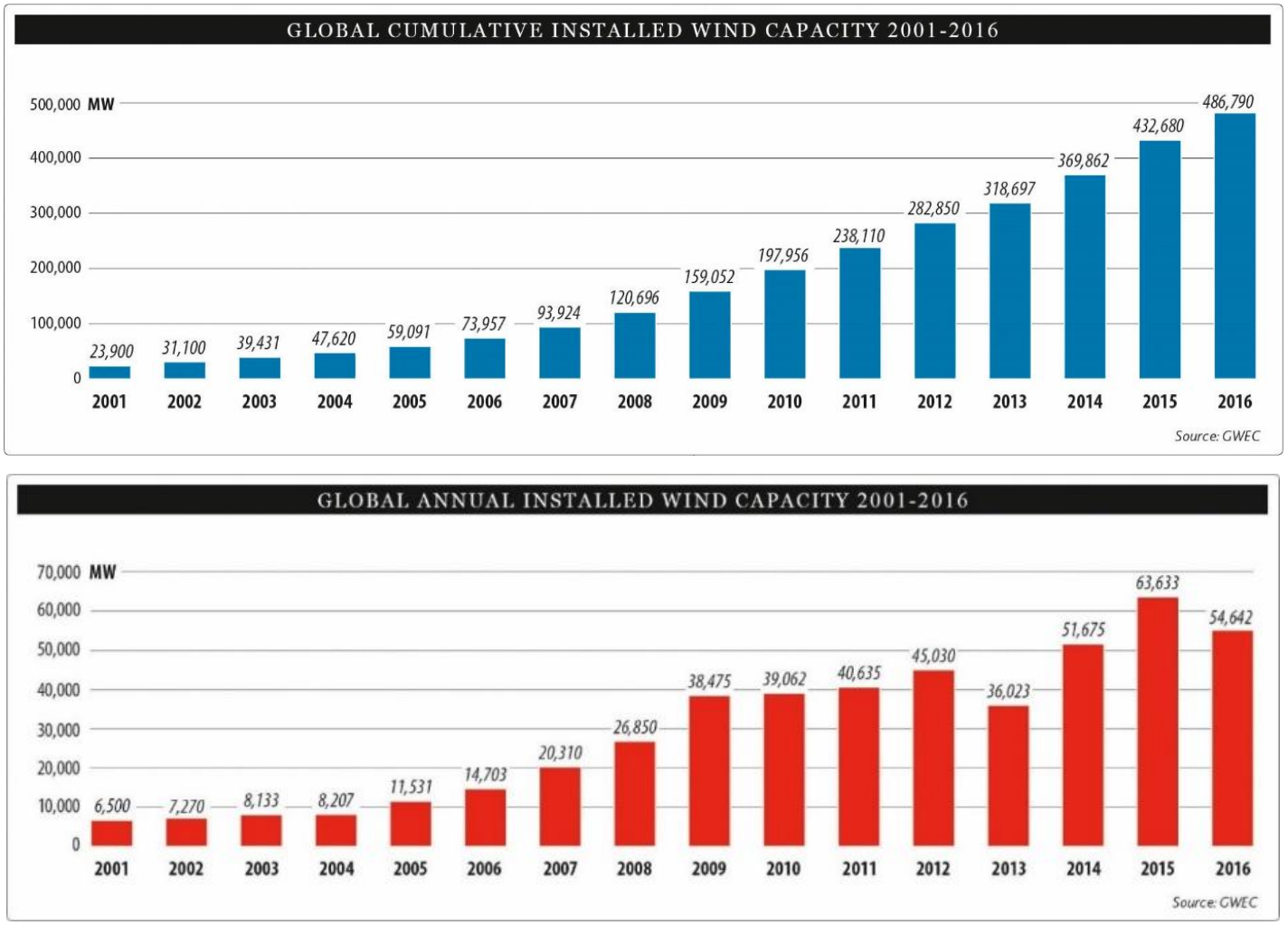

Figure 2.1 global cumulative installed wind capacity and annual installed wind capacity 2001-2016 [68]

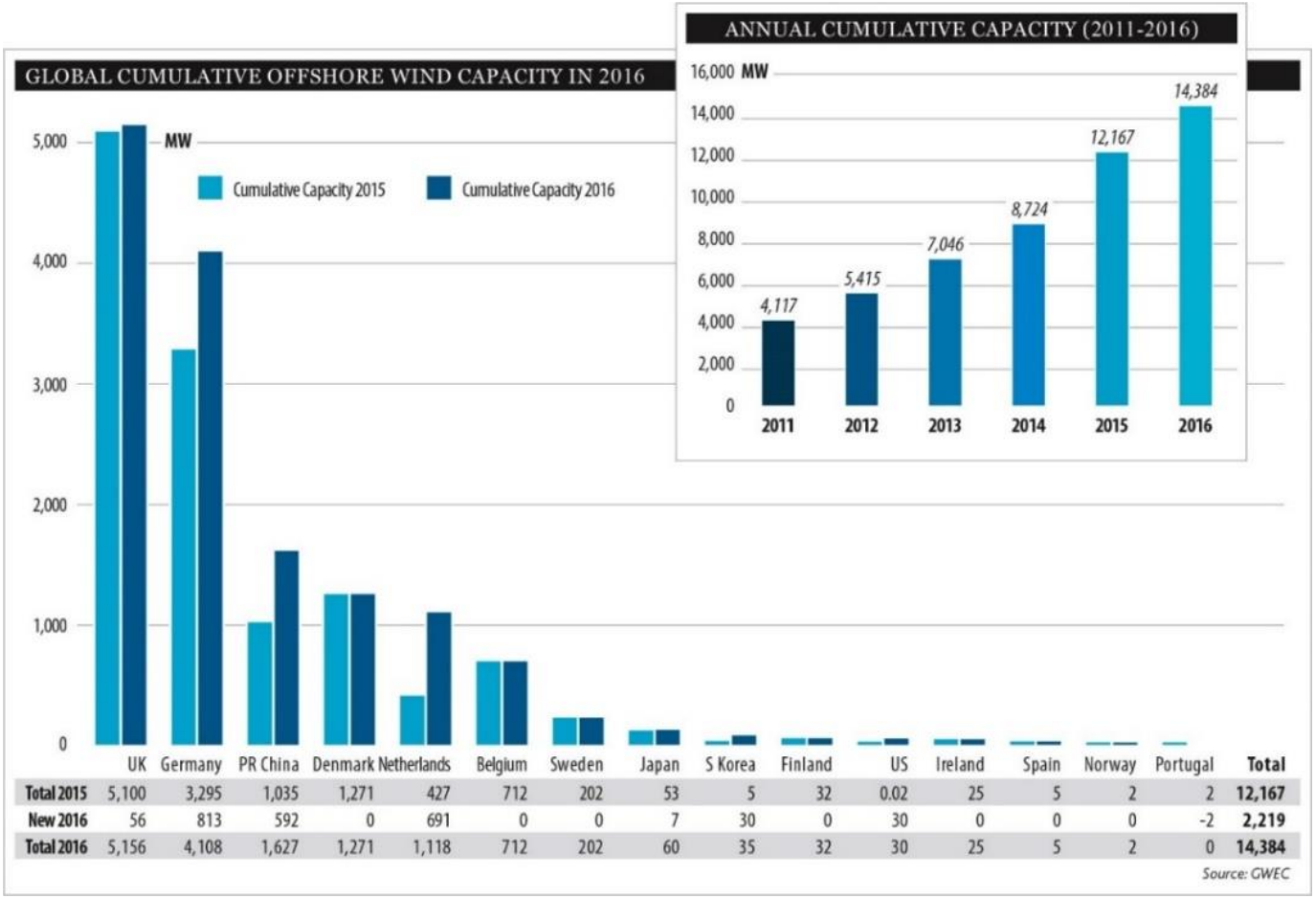

Figure 2.2 global cumulative offshore wind capacity in 2015,2016 and annual cumulative capacity 2011-2016 [68]

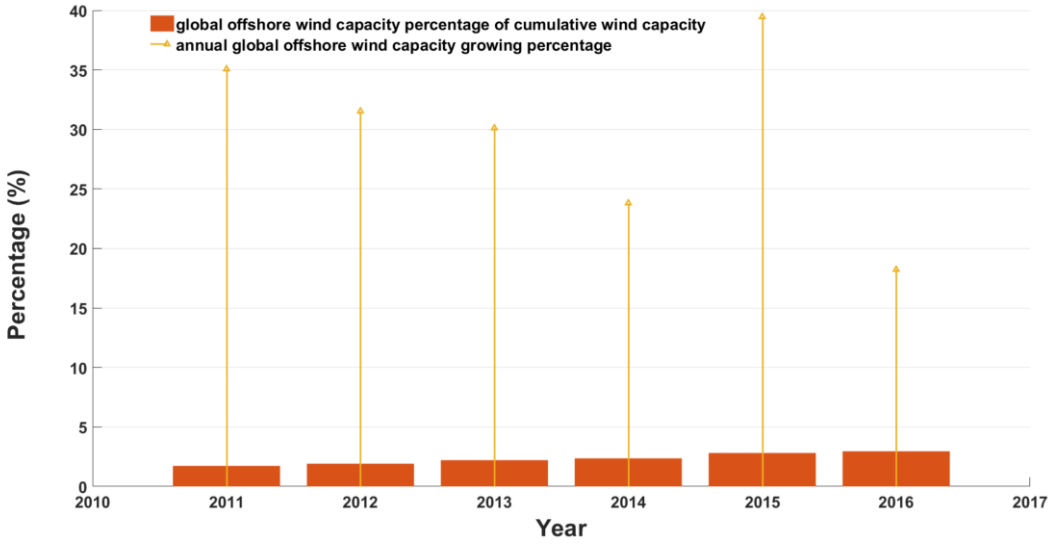

Figure 2.3 Global offshore wind capacity growing situation 2011-2016

However, for offshore wind turbines, the capital and maintenance cost are 30%-50% higher than onshore wind farms [69]. This amount results in twice the per unit cost of electricity generated of onshore wind farms. For onshore wind farms, the cost of foundation construction is not a significant part of the total cost, some high efficiency wind turbine generator technology like direct drive PMSG which is much heavier than gear drive WECS can be implemented.

With the fast development of power electronic converter technologies, by using appropriate modern control method such as microgrid concept, the power quality of WECS can be significantly improved, and the operating condition can be simplified as well. This makes parts of the drawbacks of onshore wind caused by highly randomly variable power output can be eliminated. In rural areas, when the noise and visual impacts are not major factors, the cheaper foundation of onshore wind turbine becomes very

attractive. The microgrid control theory in this research is concerned about onshore wind power.

2.3 Fundamentals of WECS

2.3.1 Main components of WECS

Figure 2.4 is an illustration of typical wind WECS from GE website. The major components of a modern WECS can be typically divided into three categories: mechanical components, electrical components and control components. The mechanical components include rotor blades, rotor hub, rotor bearings, main shaft, mechanical brake, gearbox, pitch drives, yaw drives, anemometer, nacelle, tower, foundation, heat exchange system. Wind generator, power electrical converters, filters and power cables belong to the electrical components. Control components control both mechanical related parts and electrical related parts of WECS.

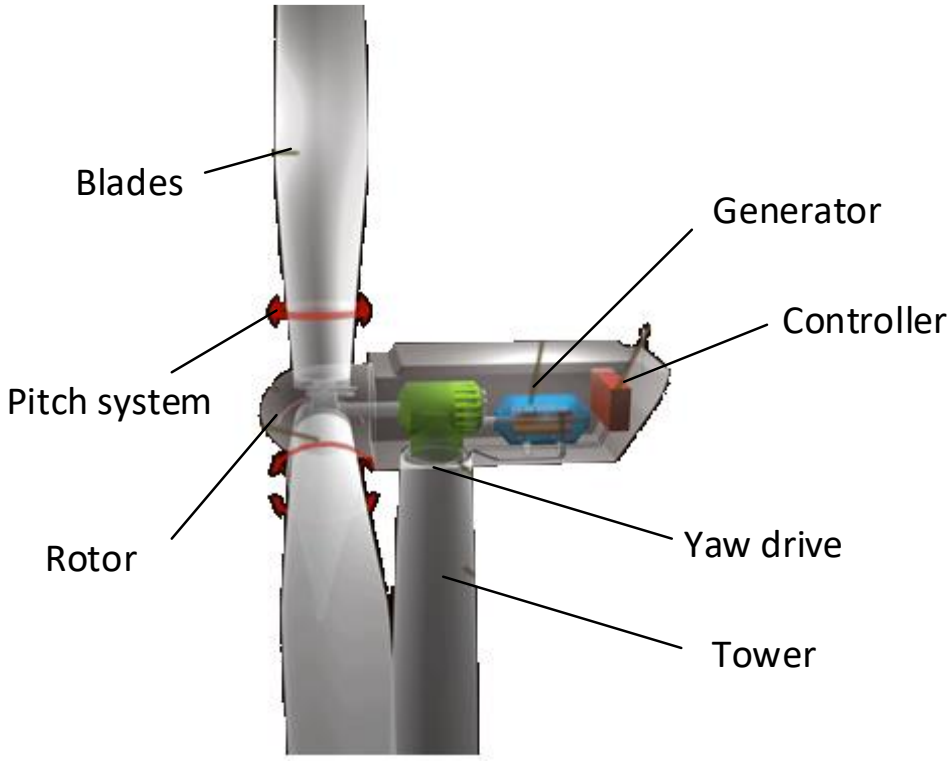

Figure 2.4 GE wind turbine [70]

Figure 2.5 is a brief diagram which explains the procedure of converting wind kinetic energy to electric energy. The wind power is captured by rotor blades and transformed into mechanical torque which drives the rotor in wind generator via gearbox. The electric power generated by wind generator is normally not well formed. There are electrical components, whether converters or transformers, used to regulate the output of wind generator. The regulated power feeds the utility grid through power cables.

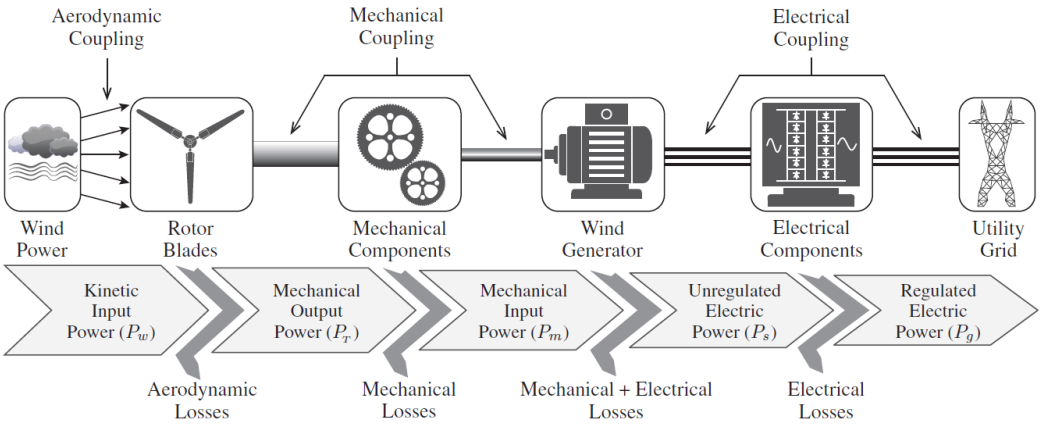

Figure 2.5 Block diagram of WECS [65]

2.3.2 Aerodynamic performance of wind turbine

Wind kinetic energy is converted into mechanical energy when it flows through the rotor blades. The wind kinetic power can be calculated by equation (2.1):

$$P_w = \frac{1}{2}\rho A v_w^3 \tag{2.1}$$

Where:

P_w is the wind kinetic power (W)

ρ is the air density, it is 1.225 kg/m^3 at sea level when temperature is 15℃

A is the area swept by rotor blades (m^2)

v_w is the wind velocity (m/s)

According to Betz's law, the mechanical power extracted from wind kinetic is

$$P_T = P_w \cdot C_p \tag{2.2}$$

Here C_p is the power conversion efficiency coefficient of rotor blades. The theoretical maximum value of C_p is 16/27 [71]. The coefficient of present commercial WECS is from 0.32 to 0.52 [65].

There are typically four wind speed intervals for different wind turbine power output characteristics respectively. Figure 2.6 shows a typical characteristic curve. The cut-in speed, rated speed and cut-out speed values are typically in the range of 3-5 m/s, 10-15 m/s and 25-30 m/s respectively. The more precise values depend on the wind turbine model. For instance, the Vestas V110-2.0 MW IEC III A model is operated with 3m/s cut-in speed and cut-out speed 20m/s respectively.

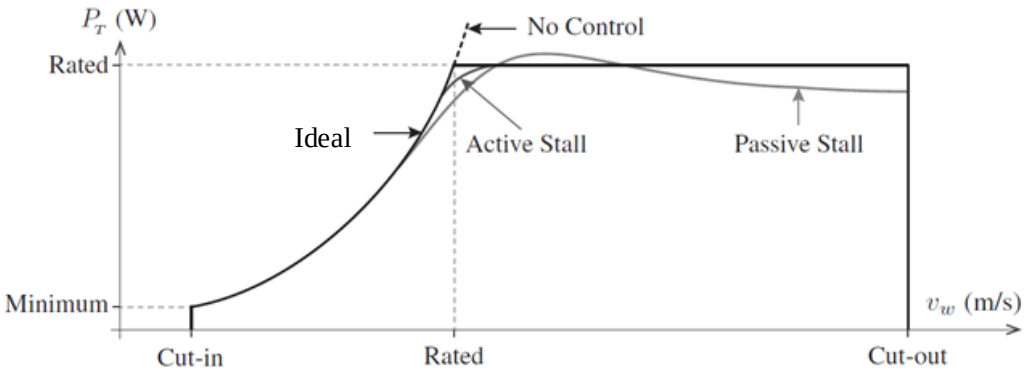

Figure 2.6 Wind turbine power output versus wind speed characteristic [65]

When the wind velocity is less than the cut-in speed, the mechanical power extracted from wind kinetic by the blades cannot drive the rotor. In this

period, there is no power generated by wind turbine. After the wind speed v_w reaches cut-in speed, the rotor starts rotating. Theoretically, the mechanical power versus wind velocity curve is a cubic curve of wind speed till the rated value. The next wind velocity interval is from rated speed to cut-out speed. The turbine's output is regulated to its rated value by the aerodynamic power control. If the wind speed exceeds the cut-out speed, for safety reason, the wind turbine will be shut down [73]. It will back online after the wind speed is reduced to a certain value. This value is called re cut-in wind speed. It is normally slightly less than the cut-out speed. To simplify analysis procedure, the re cut-in speed is not considered in the research.

In practice, there are three types of aerodynamic power regulation methods: passive stall, active stall and pitch control. The stall method is achieved by the specifically designed blade shape. Air flow turbulence formed when air flows through the blades area. The turbulence causes power coefficient C_p decreasing when wind speed increased. The blade shape used in pitch control method is like airplane wings. It controls the power coefficient by turning blade's angle. As *Figure 2.6* shows, by using different methods, the power output characteristics of wind turbines are different. The blade positions of a passive-stall turbine are fixed. The turbulence caused by wind cannot be regulated. For this reason, there are unnecessary overshoot and over reduced power coefficient exist. In contrast to the passive stall method, by using active stall control technique, the blade positions are adjusted to maintain the constant power output when the rated wind speed reached. Because of the directly aerodynamics designed blades applied in pitch control method, the pitch-controlled turbine responses faster than stall-regulated turbine. This makes its output

characteristics very close to theoretical one. In this thesis, pitch control is implemented in wind turbine model.

Overall, the wind turbine mechanical power output is described in the general expression as

$$P_T = \begin{cases} 0 & v_w < v_{ci} \\ \frac{1}{2}\rho A v_w^3 C_p & v_{ci} \le v_w < v_r \\ P_{Tr} & v_r \le v_w < v_{co} \\ 0 & v_{co} \le v_w \end{cases} \quad (2.3)$$

Where:

v_w is the wind speed (m/s)

v_{ci} is the cut-in speed of wind turbine (m/s)

v_r is the rated speed of wind turbine (m/s)

v_{co} is the cut-out speed of wind turbine (m/s)

C_p is the instantaneous power efficiency of rotor blades

P_{Tr} is the rated power output of wind turbine (W)

By combining pitch control and maximum power point tracking (MPPT) control which determines the rotor speed to maximize the mechanical power extraction during different wind speed conditions, the power efficiency C_p can be always close to the theoretical maximum value. In case of this, C_p here is considered as a constant value.

2.3.3 Classification of WECS technologies

There are many methods that can be used to classify a wind turbine. The International Electrotechnical Commission gives a definition which classified wind turbines into three classes based on wind speed as Table 2.1 shows. The turbulence classes are classified by the metric called

turbulence intensity, which is typically range from 3% to 20%. This indicator is derived as (2.4)

$$\rho = \frac{\sigma}{\bar{v}} \times 100\% \quad (2.4)$$

Where:

σ is the standard deviation of the horizontal wind speed (m/s)

$\bar{v}$ is the average wind speed over a certain time period (m/s)

Table 2.1 IEC wind speed classification [72]

Turbine class	**Annual average wind speed (m/s)**	**Extreme 50-year gust (m/s)**	**Turbulence classes**	
			A (%)	**B (%)**
IEC I	10	70	18	16
IEC II	8.5	59.5	18	16
IEC III	7.5	52.5	18	16

WECS are divided into 5 types in [65] defined by their commercial configurations:

- Type 1 is fixed-speed WECS with squirrel cage induction generator (SCIG);
- Type 2 is Semi-variable-speed WECS with wound rotor induction generator (WRIG);
- Type 3 is Semi-variable-speed WECS with doubly-fed induction generator (DFIG);
- Type 4 is full-variable speed WECS with SCIG, permanent magnet synchronous generator (PMSG), wound rotor synchronous

generator (WRSG) or high-temperature-superconducting synchronous generator (HTS-SG);

- Type 5 is full-variable-speed WECS with WRSG and mechanical converter.

Table 2.2 Top 10 WT manufacturers in 2015, along with their priority WECS configurations [63]

Rank	**WT manufacture**	**Country of manufacture**	**WECS configurations**	**Market share (%)**
1	Goldwind	PR China	PMSG	12.8
2	Vestas Siemens	Denmark	PMSG, DFIG	12
3	GE Energy	USA	PMSG, DFIG	9.2
4	Siemens	Germany	PMSG, SCIG	7.7
5	Gamesa	Spain	PMSG, DFIG	5.5
6	Enercon	Germany	WRSG	5.1
7	United Power	PR China	PMSG, DFIG	4.7
8	Ming Yang	PR China	PMSG, DFIG	3.8
9	Envision	PR China	PMSG, DFIG	3.5
10	CSIC Haizhuang	PR China	PMSG, DFIG	3.4
Total market share				67.7

Table 2.2 gives the top ten wind turbine manufacturers in 2015. The latest ranking for 2016 is: Vestas, GE, Goldwind, Gamesa, Siemens, Enercon, Nordex, United Power, Mingyang and Envision. Most of the top ten manufactures provide PMSG and DFIG solutions. As the PMSG system

has more efficiency than conventional DFIG technology, there is a trend that PMSG may replace the marketplace of DFIG. Up to year 2014, the market share of PMSG in Europe has reached 31%. The market share of DFIG is reduced from nearly 80% in 2007 to less than 40% in 2014 [73].

2.3.4 Costs of WECS

As the power generated by WECS is from wind, the operational cost of WECS is much less than conventional power plants. The capital investment cost takes the major parts of a WECS [74]. If the maintenance cost not considered, the generating cost of each kWh is defined as equation (2.5) [75]:

$$C = \frac{r(1+r)^n}{(1+r)^n - 1}\left(\frac{Q}{8760F}\right) \tag{2.5}$$

Where:

C is the cost of wind generating cost (£/kWh)

Q is the capital investment (£/kW)

r is the annual capital recovery rate

n is the operating life time of the WECS (year)

F is the generation factor of the WECS, it is defined as (2.6)

$$F = \frac{P_{ga}}{P_{Tr}} \tag{2.6}$$

Here P_{ga} is the annual mean electrical power output of WECS, P_{Tr} is the rated wind turbine output.

The generating cost of a WECS is decreased when it has less capital cost and/or higher power efficiency.

The cost composition of each components in a typical onshore WECS is shown in *Figure 2.7*. In this wind turbine model, the top three components: tower, rotor blades and gear box, cost over 60% of total investment.

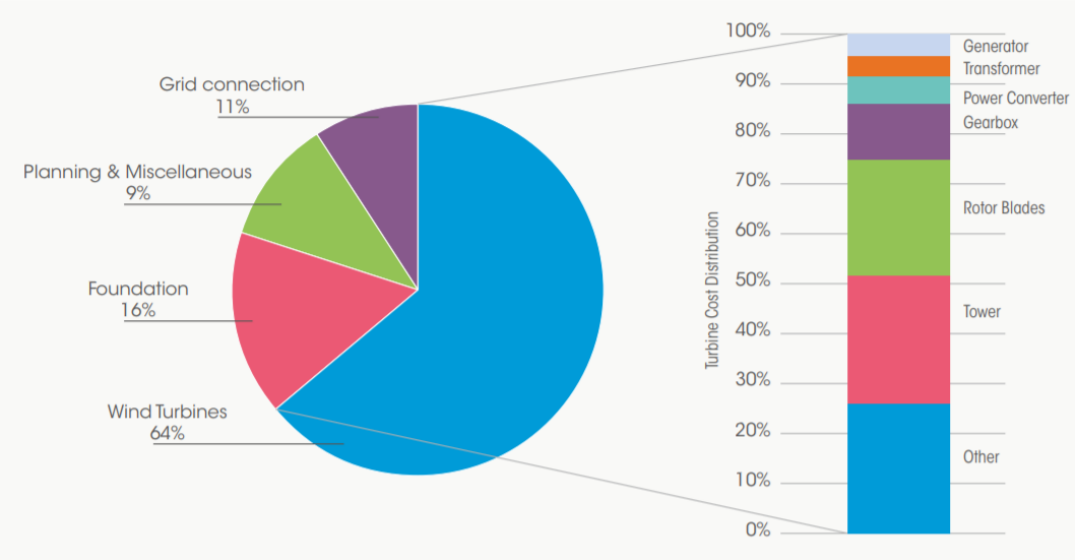

Figure 2.7 Capital cost for a typical onshore wind power system and turbine [69]

2.4 Wind turbine generator technologies

As mentioned in Section 2.3, the two commonly used wind turbine generator technologies DFIG and PMSG share over 70% market share in Europe. To build an simulation model, it is necessary to have a good understanding of how they perform energy transformation procedure.

2.4.1 DFIG model and features

Typically, the DFIG generator is wound rotor induction generator, in which the stator is directly connected to the main grid, and the rotor is connected via a back-to-back converter. This converter system normally needs to have capability to provide 30% of full-scale power

transmission.In an induction machine model, slip ratio $s = \frac{\omega_s - \omega_r}{\omega_s}$ is often used to represent the asynchronous speed states. When the MPPT control, pitch control, converter control implemented together in DFIG system, the relationships between wind speed, mechanical power generated by wind turbine, electrical power flow on stator and rotor are shown in Figure 2.8. As the wind speed increases, the slip of DFIG system decreases. There are two operating modes: sub-synchronous and super-synchronous which is based on the slip ratio.

Sub-synchronous mode: During low wind speed period, the rotor speed is less than synchronous speed, the machine is operating at sub-synchronous mode. In this condition, rotor absorbs power from grid.

Super-synchronous mode: At where $s = 0$, rotor is rotating at synchronous speed, and as such there is no power exchange between rotor and power grid. If wind speed keeps increasing, the DFIG system begins running in super-synchronous mode. The rotor speed is faster than synchronous speed. Both stator and rotor feed power to the grid. The total active power generated by DFIG system is reached its maximum when s= - 0.2.

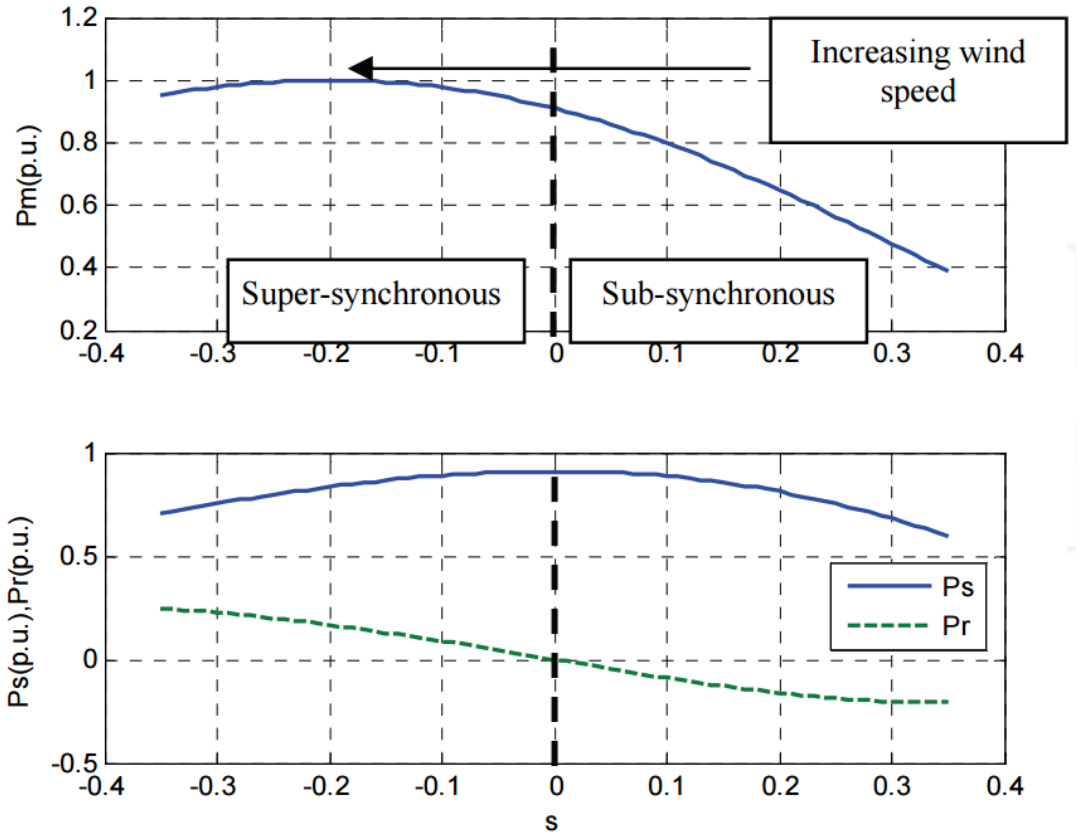

Figure 2.8 DFIG system power flows [76]

2.4.2 PMSG model and features

A PMSG generator is connected to main grid via full scale converter. The most commonly used here is back-to-back voltage converter. As the electric power generated by PMSG is not directly inject into grid, rotor speed is full scale available. This makes PMSG system more efficiency during low wind power periods. In contrast to DFIG, the rated power of converter in PMSG is over twice larger than those for DFIG. Normally, this makes the investment cost of converter increased to 7% from 5% of the whole WSCS. For the other hand, the synchronous speed of PMSG does not have to be the same as grid. A PMSG system can be geared or gearless. Figure 2.7 shows, a direct-drive PMSG can save around 10% investment on gearbox part. Besides, in a microgrid system, as the

generator output voltage is normally not required to be boosted up to a high level, the transformer part is not necessary. In a PMSG wind generator system, the rotor flux is provided by permanent magnetic materials. In this case, the electromagnetic in PMSG model is considered only on the stator.

2.4.3 Efficiency of wind generator

There are many factors which can result in power losses during the transformation from mechanical power to electrical power. Table 2.3 gives the priority parts which cause power losses need to be considered for DFIG and PMSG system.

Figure 2.9 is a typical power flow procedure for WECS. The mechanical loss happens when wind kinetic energy is transformed to mechanical torque by wind turbine. The control system for WECS tracking MPPT and load demand variation causes stray load loss. Besides, the copper loss and the iron loss exist permanently in most power generators as there are current and flux variations.

Table 2.3 losses of DFIG and PMSG

Generator Type	DFIG	PMSG
Mechanical loss	√	√
Gear loss	√	
Stray load loss	√	√
Iron loss	√	√
Copper loss	√	√
Power Converter loss	√	√

Transformer loss	√	
Filter loss		√
Windage loss	√	√
Bearing loss	√	√

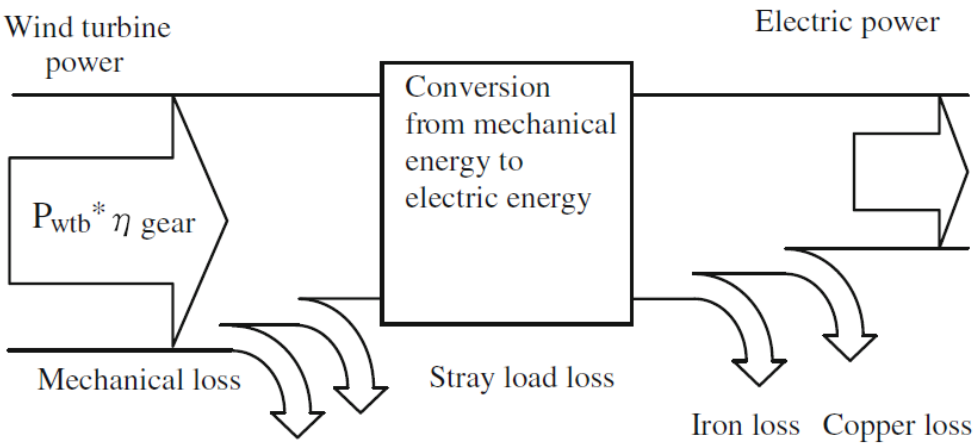

Figure 2.9 Power flow in WECS [77]

The total efficiency of a DFIG is defined as the ratio of the total electrical active power output to the mechanical power generated by the wind turbine:

$$\eta = \frac{P_{DFIG}}{P_T} = \frac{P_r + P_s}{P_T} \tag{2.7}$$

Alternatively, for a PMSG system, the total efficiency is given by

$$\eta = \frac{P_{PMSG}}{P_T} = \frac{P_s}{P_T} \tag{2.8}$$

The efficiency versus wind speed curves of three different types of 5MVA WECS with cut-in speed 4 m/s, rated speed 12 m/s, are shown in Figure 2.10. The parameters used to accurately calculate efficiency of certain commercial wind turbine model usually not openly available to the public.

For this reason, the instantaneous efficiency versus wind speed during $[v_{ci}, v_r]$ is roughly calculated based on this figure following quadratic function (2.9).

$$\eta(v_w) = \mathrm{A}{v_w}^2 + Bv_w + C \tag{2.9}$$

A, B, C parameters can be derived by pick up any three points on efficiency curve from Figure 2.10.

For a **DFIG** system,

$$\begin{cases} A = -\dfrac{0.52}{(v_r - v_{ci})^2} \\ B = \dfrac{0.98v_r + 0.06v_{ci}}{(v_r - v_{ci})^2} \\ C = \dfrac{0.49{v_r}^2 - 1.96v_r v_{ci} + 0.95{v_{ci}}^2}{(v_r - v_{ci})^2} \end{cases} \tag{2.10}$$

For a **PMSG** system,

$$\begin{cases} A = -\dfrac{0.14}{(v_r - v_{ci})^2} \\ B = \dfrac{0.31v_r - 0.03v_{ci}}{(v_r - v_{ci})^2} \\ C = \dfrac{0.78{v_r}^2 - 1.87v_r v_{ci} + 0.95{v_{ci}}^2}{(v_r - v_{ci})^2} \end{cases} \tag{2.11}$$

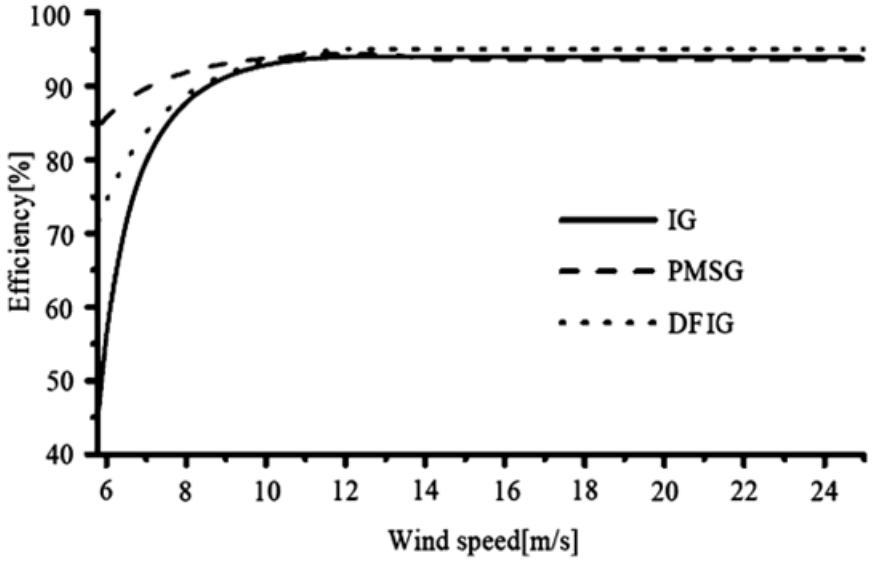

Figure 2.10 Efficiency of IG, PMSG and DFIG wind generator system [77]

2.5 Statistical model of WECS power output based on the statistical wind speed model based on Weibull Distribution

In practice, the original data available in the open access is usually not enough for evaluating a system performance as the wind speed is continuously and randomly variating. The output of WECS is highly related to the wind speed. Proper wind speed model is necessary for investigating the statistical model of WECS. Monte Carlo simulation method is widely used for modelling the probability outcomes of unpredictable processes with random variables. By using this method, a large number of wind speed samples can be generated for system evaluation. The transformation power losses from mechanical power to electrical power is discussed in section 2.3.4, the final statistics model of WECS power output can be generated from the combination of wind speed model, aerodynamics of wind turbine and generator efficiency.

2.5.1 Wind speed distribution functions

Normally, an anemometer is used to measure wind speed on site. Mean wind speed values are recorded every 10 minutes. These data are sorted by an interval of 1m/s. To evaluate wind speed distribution and wind energy potential from the statistical data, many methods are investigated. Weibull and Rayleigh distribution functions are two of most widely used methods [78].

The **Weibull distribution** function which originally a three parameters function, represents wind speed probability as a two parameters function by equations (2.12) and (2.13) :

$$p(v) = (\frac{k}{c})(\frac{v}{c})^{k-1} exp\left[-(\frac{v}{c})^{k}\right] \quad (2.12)$$

$$P(v) = 1 - exp\left[-(\frac{v}{c})^{k}\right] \quad (2.13)$$

Where:

$p(v)$ is the probability of occurrence of wind speed v

$P(v)$ is the cumulative probability

c is the Weibull scale parameter

k is the Weibull shape parameter

In the Weibull distribution function, c is proportional to the average wind speed. Parameter k determines the variation of the wind speed. When the value of k is relatively small, it means the wind speed variates significantly, and vice versa.

The **Rayleigh distribution** is a one parameter determined function. Probability density at each speed ratio is described by the equations (2.14) and (2.15)

$$p(v_i) = \frac{f_i}{\sum_{i=1}^{N} f_i} \tag{2.14}$$

$$P(v_i) = \sum_{i=1}^{N} p(v_i) \tag{2.15}$$

Where:

$p(v_i)$ is the probability of occurrence of wind speed interval i

$P(v_i)$ is the cumulative probability

f_i is the frequency of occurrence of wind speed interval i

N is the total number of wind speed intervals

f_i in the Rayleigh distribution function is directly observed from statistical data. This makes the calculation of parameters in Rayleigh function much easier than Weibull function.

However, this method is less flexible as there is only one parameter. The wind power density estimated by Weibull distribution has a probability of 30% less average errors than using Rayleigh no matter in monthly or annually [78]. For these reasons, Weibull distribution method is used for data analysis and prediction in this research. The next section introduces a method to obtain the proper Weibull parameters from statistical data.

2.5.2 Determination of Weibull distribution parameters

There are six popular methods which are used to determine the Weibull distribution parameters [79-81]. They are the graphical method, empirical method, energy pattern method, energy trend method, maximum likelihood method and moment method. There are many factors which can

be used to indicate the accuracy of the parameters generated by different methods. For instance, the root mean square error (RMSE), mean percentage error (MPE) and coefficient of determination (R^2). These three indicators are calculated in the following equations (2.16) - (2.18).

$$\text{RMSE} = \sqrt{\frac{1}{N}\sum_{i=1}^{N}\left(X_p - X_o\right)^2} \tag{2.16}$$

$$\text{MPE} = \frac{1}{N}\sum_{i=1}^{N}\left(\frac{X_p - X_o}{X_o}\right) \times 100\% \tag{2.17}$$

$$R^2 = 1 - \frac{\sum_{i=1}^{N}\left(X_p - X_o\right)^2}{\sum_{i=1}^{N}\left(X_o - \overline{X_o}\right)^2} \tag{2.18}$$

Where:

N is the total number of observations

X_p is the predicted value

X_o is the observed value

$\overline{X_o}$ is the average value of X_o

When the RMSE and MPE value close to 0, and R^2 close to 1, it means the predicting functions is accurate.

Although the moment method is one of the oldest method which is used to determine Weibull distribution parameters, the error indicators of this method are better than most of other methods in many situations [79, 80]. In this research, moment method is used to determine the Weibull distribution parameters. The Weibull distribution parameters which can be easily obtained by the moment method have the goodness of curve

fitting. The Weibull distribution parameters c and k are calculated from the values of standard deviation and average wind speed follows the equation (2.19) and (2.20) [79].

$$k = \left(\frac{0.9874}{\sigma/\overline{v}}\right)^{1.0983} \tag{2.19}$$

$$\mathrm{c} = \frac{\overline{v}}{\Gamma\left(1 + 1/k\right)} \tag{2.20}$$

where:

σ is the standard deviation of wind speed (m/s)

$\overline{v}$ is the average wind speed (m/s)

Γ is gamma function which is defined as $\Gamma(\mathrm{x}) = \int_0^\infty t^{x-1}e^{-t}\,dt$

2.5.3 Statistical wind speed model

According to equation (2.13), when the Weibull scale parameter c and shape parameter k are determined, there is a certain relationship between wind speed v and the cumulative probability $P(v)$. By reversing the original equation, (2.21) is obtained.

$$v = c \cdot \left[-\ln\left(1 - P(v)\right)^{1/k}\right] \tag{2.21}$$

The interval of cumulative probability $P(v)$ is from 0 to 1. In this case, in the Monte Carlo simulation, $1 - P(v)$ can be replaced by a uniformly distributed random variable number M within the interval [0,1]. A certain number of wind speed samples can be generated by substituting the new random number M into equation (2.22).

$$v = c \cdot \left[-\ln(M)^{1/k}\right] \tag{2.22}$$

Normally, the results become more accurate when the number of samples grows.

2.6 Case study: WECS power output near river Wensum

To clarify the procedure of derive the artificial output model, this case study is presented. The historical data is from the weather station of Wensum. It is located at the east part of England. All the following studies are based on the data from Wensum weather station. There are several steps to generate artificial wind speed and wind turbine output:

First of all, gather the original data including historical wind speed data. The type of wind turbine is chosen and is based on the wind speed character. After that, using historical wind speed data to extract Weibull distribution parameters c and k. Then wind speed samples are generated by equation (2.22). The statistical wind turbine power output is obtained by apply artificial wind speed data to equation (2.3).

The case study introduced in this section is based on the wind speed records from Wensum weather station [31]. The Figure 2.11 indicates that the wind speed in different months has different characteristics. For this reason, the Weibull parameters variates seasonally. Here it gives the procedure of how to establish statistical model of two different seasons in January and July.

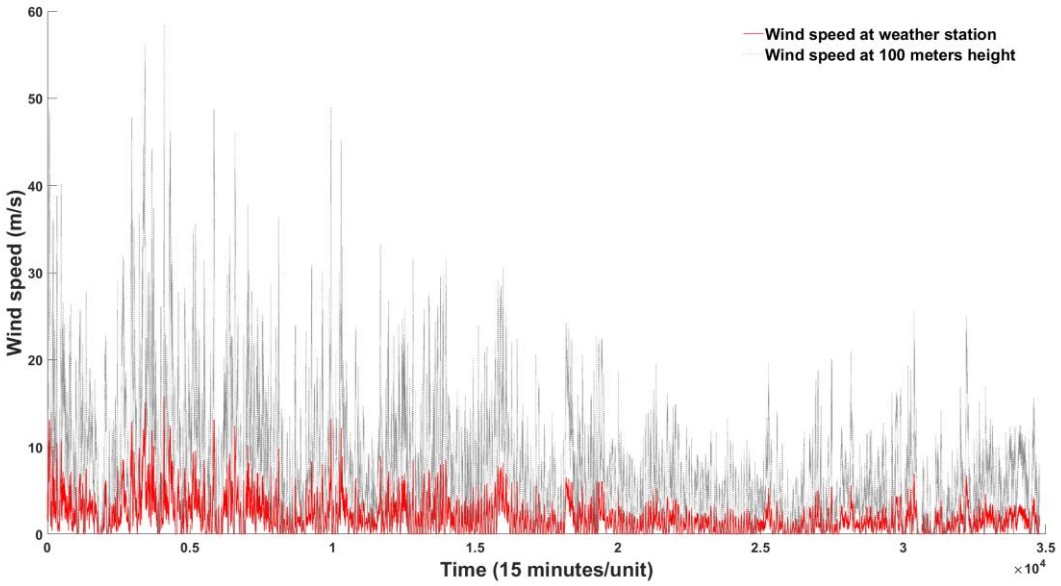

Figure 2.11 Wind speed at Wensum of year 2014

2.6.1 Historical data analysis

The height of modern wind turbine tower can be over 100 meters. However, the wind speed data used to evaluate wind type normally comes from the weather station which measures the wind speed near ground. The wind speed at 100 meters above ground for wind turbine can be estimated by equation (2.23) [82]:

$$v(h) = v_{10} \cdot \left(\frac{h}{h_{10}}\right)^{a} \tag{2.23}$$

Where:

$v(h)$ is the wind speed at height h (m/s)

v_{10} is the velocity of wind at 10 meters height (m/s)

h_{10} is constant equal to 10 meters

a is the Hellmann exponent

According to the NOABL WIND MAP [83], at the same location, the annual average wind speed is increased by the height above ground. The

wind speed profile at Wensum area as Figure 2.12 shows is 5.1 m/s at 10 meters height, 5.8 m/s at 25 meters height and 6.3 m/s at 45 meters height respectively. The Hellmann exponent α for this area can be derived from equation (2.23) as 0.14. The annual average wind speed at 100 meters height is 7.05 m/s. In this area, IEC III low wind speed WECS class should be chosen. According to Figure 2.10, PMSG wind generator system has better efficiency performance than DFIG if wind speed is less than rated speed. In this case, PMSG low wind model is preferred.

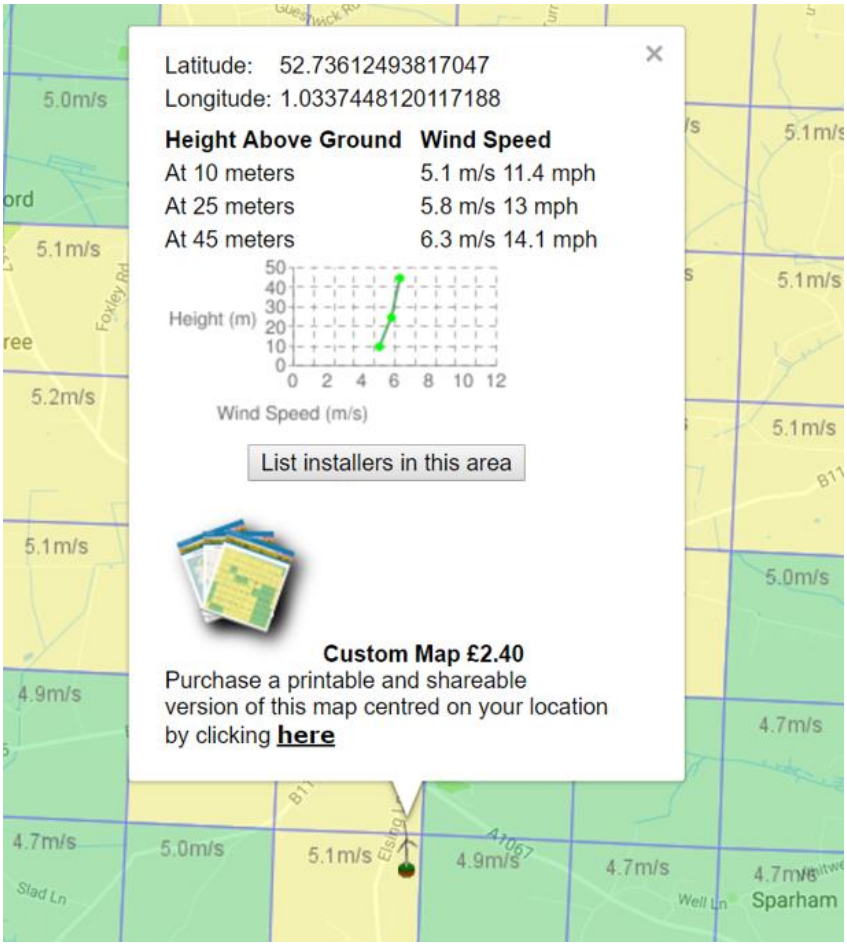

Figure 2.12 NOABL WIND MAP of Wensum [83]

2.6.2 WECS parameters

In this case, the Vestas V150-4.2 MW^{TM} IEC III B model WECS is implemented. It is a PMSG based wind turbine. This model has parameters of a cut-in speed 3 m/s, cut-out speed 22.5 m/s, and rotor swept area 17671 m^2 respectively. According to (2.1) and (2.2), and assuming that the max power coefficient of rotor blades C_p is 0.52, then the rated wind speed can be estimated using equation (2.24):

$$v_{rated} = \left(\frac{2P_T / C_p}{\rho A} \right)^{1/3} \tag{2.24}$$

The rated wind speed here is around 9 m/s. When the cut-in speed, the rated speed and cut-out speed are obtained, the expression (2.25) of mechanical output of wind turbine can be extracted from equation (2.3):

$$P_T = \begin{cases} 0 & v_w < 3 \\ 5573 \cdot v_w^3 & 3 \le v_w < 9.1 \\ 4.2 \times 10^6 & 9.1 \le v_w < 22.5 \\ 0 & 22.5 \le v_w \end{cases} \tag{2.25}$$

As this WECS model is a PMSG model, the final electrical power output of this system is derived as the product of PMSG instantaneous efficiency and the turbine mechanical power input:

$$P_g = \eta(v_w) P_T \tag{2.26}$$

According to (2.9)(2.11)(2.25), this equation can be rewritten as

$$P_g = \begin{cases} 0 & v_w < 3 \\ -21v_w^5 + 409v_w^4 + 3308v_w^3 & 3 \le v_w < 9.1 \\ 4 \times 10^6 & 9.1 \le v_w < 22.5 \\ 0 & 22.5 \le v_w \end{cases} \tag{2.27}$$

2.6.3 Generating Weibull distributed artificial wind speed

The annual average wind speed measured at the weather station is 1.9 m/s. According to (2.23), the wind speed at 100 meters height is the original wind speed at weather station level multiplied by a coefficient 3.95. Figure 2.11 gives the original wind speed and the 100 meter speed respectively.

The wind speed distribution varies in different seasons. In this case, wind speed data in January and July are chosen to stand for two different types of distributions. Weibull distribution parameters $k = 1.228$ and $c = 11.6$ derived from the January wind speed data by equations (2.19) and (2.20). Applying these parameters in (2.22), the wind speed versus the random number equation is

$$v = 11.6 \cdot \left[-\ln(M)^{1/1.228}\right] \tag{2.28}$$

Alternatively, the wind speed versus the random number equation for July is

$$v = 6.274 \cdot \left[-\ln(M)^{1/1.1215}\right] \tag{2.29}$$

Infinite wind speed samples of January can be generated by Monte Carlo simulation based on equation (2.28) and (2.29). The artificial wind speed density is shown in Figure 2.13. The wind power in winter season is stronger than in summer. Wind speed varies more in the summer.

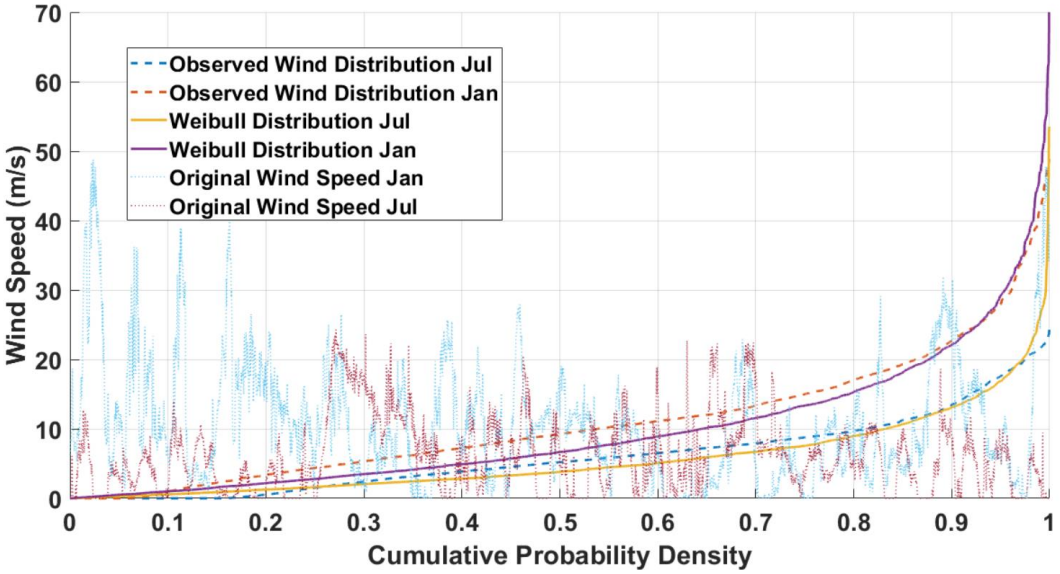

Figure 2.13Wind speed distribution of Wensum in January and July 2014

2.6.4 WECS power output based on the statistical wind speed model

In previous sections, the wind speed versus electrical power output equation (2.27), and the statistical wind speed model equation (2.28)(2.29) are obtained.

Figure 2.14 and Figure 2.15 gives the results of WECS output at artificial wind speed data respectively. The former figure is obtained within 100 times repeat calculating using Monte Carlo method. The green line and purple line represent the probability density by reforming the WECS output in ascending order. The dash lines are the original WECS output samples. The latter figure is the result after 10000 times repeat calculating. It is observed that, the simulation results are significantly closer to theoretical distribution when the repeat times increases to a relatively large number. In practise, the Monte Carlo simulation shoud be stopped when the standard deviation is reduced to an acceptable range, which is determined by the specific situations. The WECS power variations model

used in the research in this thesis is based on the statistical model investigated in this chapter.

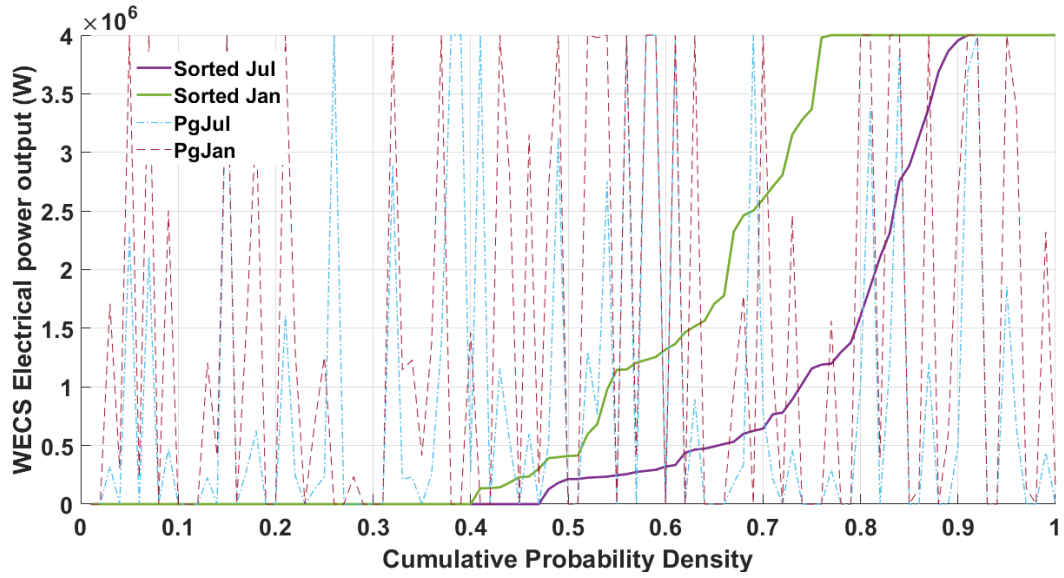

Figure 2.14 WECS output distribution of Wensum in January and July 2014 by 100 repeats Monte Carlo simulation

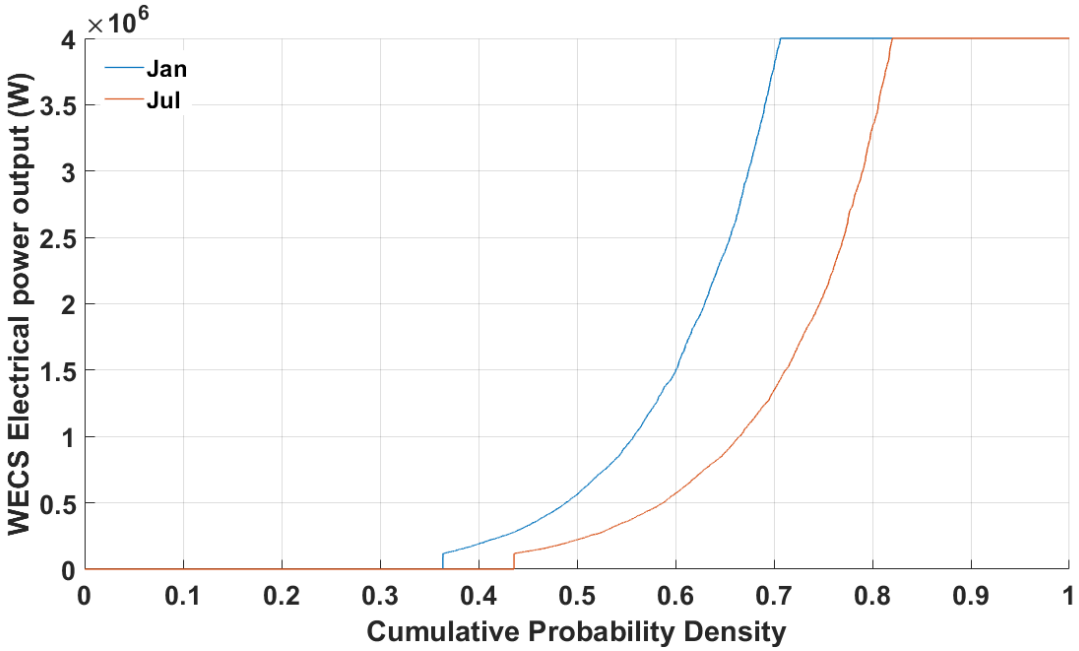

Figure 2.15 WECS output distribution of Wensum in January and July 2014 by 10000 repeats Monte Carlo

2.7 Summary

This chapter gives the background knowledge about modern wind energy issues. With the benefit of relatively stable wind speed and more centralized regulation, offshore wind farms are getting more concerns. However, up to year 2016, the worldwide onshore wind farm installed capacity remains over 97% of cumulative wind energy capacity. The combination of the microgrid concept and modern control technologies provides a feasible solution to the power quality and safety issues caused by the randomly power output feature of onshore wind farms. The following chapters of this thesis are concerned about how to achieve this combination system for the onshore WECS.

There are two most commonly used commercial wind generators types: DFIG and PMSG. DFIG has a lower capital cost as there is no need of full-scale converters and permanent magnetic rotor. However, the power efficiency of DFIG during slow wind condition is much less than PMSG. Besides, there is a potential cost reduction as the gearbox and transformer part which usually take over 10% of the total investment cost are not necessary for PMSG. The WECS using PMSG technology becomes more popular in recent years. In most place, the average onshore wind speed is less than 6.5 m/s within the height of 45m. In case of that, the WECS model used in this thesis is based on PMSG model.

The statistical model of WECS which is used to evaluate system performance is provided in this chapter. This model is created based on the artificial generated wind speed and aerodynamic features of wind turbine. The Weibull distribution is a probability distribution which has a good fit of describing wind characteristics and can be used to generate artificial wind speed. The moment method which is used to determine the

shape and scale parameters of Weibull distribution based on historical wind speed samples. A case study shows how to build this statistical model, and the simulation results proves the model has a good probability distribution feature which can be used in system evaluation.

Chapter 3: Review of microgrid operational features and control theories

3.1 Introduction

A microgrid can form an individual system with high penetration of DGs without causing power quality problems to the main grid. This provides a solution for how to effectively utilize wind power. In contrast to a conventional wind farm, the aggregate local load which is in charge of a Microgrid is highly relative to the install capacity of generators in this Microgrid. Besides, a microgrid has to be designed to operate with or without utility grid. These features make the operation and control of a microgrid more sophisticated than a wind farm. Proper control theories are needed to make a microgrid achieve multi functions such as load sharing management for each DGs and demand side management. The operational features and existed control theories is introduced in the following parts of this chapter.

Section 3.2 introduces the fundamentals of microgrid concept. Typical microgrid features and hierarchical control theory which integrated several control procedures addressed in different time scales to deal with the issues including accuracy load sharing, reference value correction, seamless mode transition, optimized energy management are briefly introduced. The inverter-based DGs models in the microgrid are also explained in this section. The basic control principles consist of current controller and voltage controller for single inverter-based DG in microgrid are provided in section 3.3. The next section gives a brief review of grid code requirements in modern transmission and distribution network, especially the UK network. This section indicates the issues that need to

be considered related to wind power embedded microgrid. Section 3.5 reviews the existing control theories on the control level 1 applied in microgrid. Most of the control theories concerned at the variations of demand side. However, for onshore wind turbines, the output of WECS is varying continuously. It is difficult to properly operate a microgrid in long term without monitoring and correction. A summary is provided in the last section.

3.2 Fundamentals of microgrid concept

3.2.1 Microgrid features and hierarchical control structure

A microgrid is typically a small-scale power grid, consisting of DGs, energy storage units and loads and control system. In normal operation conditions, the microgrid often runs connected with the utility grid, and behaves like a controllable load or embedded generator [26].

A multi-DG microgrid architecture presented by the Consortium for Electric Reliability Technology Solutions (CERT) is shown in Figure 3.1. This microgrid is connected to the utility grid through a PCC point. There are four inverter-based DGs controlled by the Microgrid Central Controller (MGCC) and the local controllers (LC) in this microgrid. The DGs are operated by the LCs following the commands sent from the MGCC which manage the overall system performance. For economic and security considerations, the MGCC is often located near the PCC. Besides, a combined heat and power function is available in the microgrid as the DGs in a microgrid is often located near demands. These inverter-based DGs in microgrid could be microturbines, fuel cells, photovoltaic cells, wind power generators, diesel generators etc. Wind power generators embedded in the microgrid are the concern of this thesis. The local

demands in this microgrid are classified into the sensitive loads and the traditional loads. The sensitive loads such as hospital and industrial loads, which are often inelastic, have the high priority of the power supply. On the other hand, the traditional loads such as lighting and some residential loads are interruptible. A microgrid is designed to secure the power supply for the sensitive loads, where the traditional loads will be dropped if necessary [84].

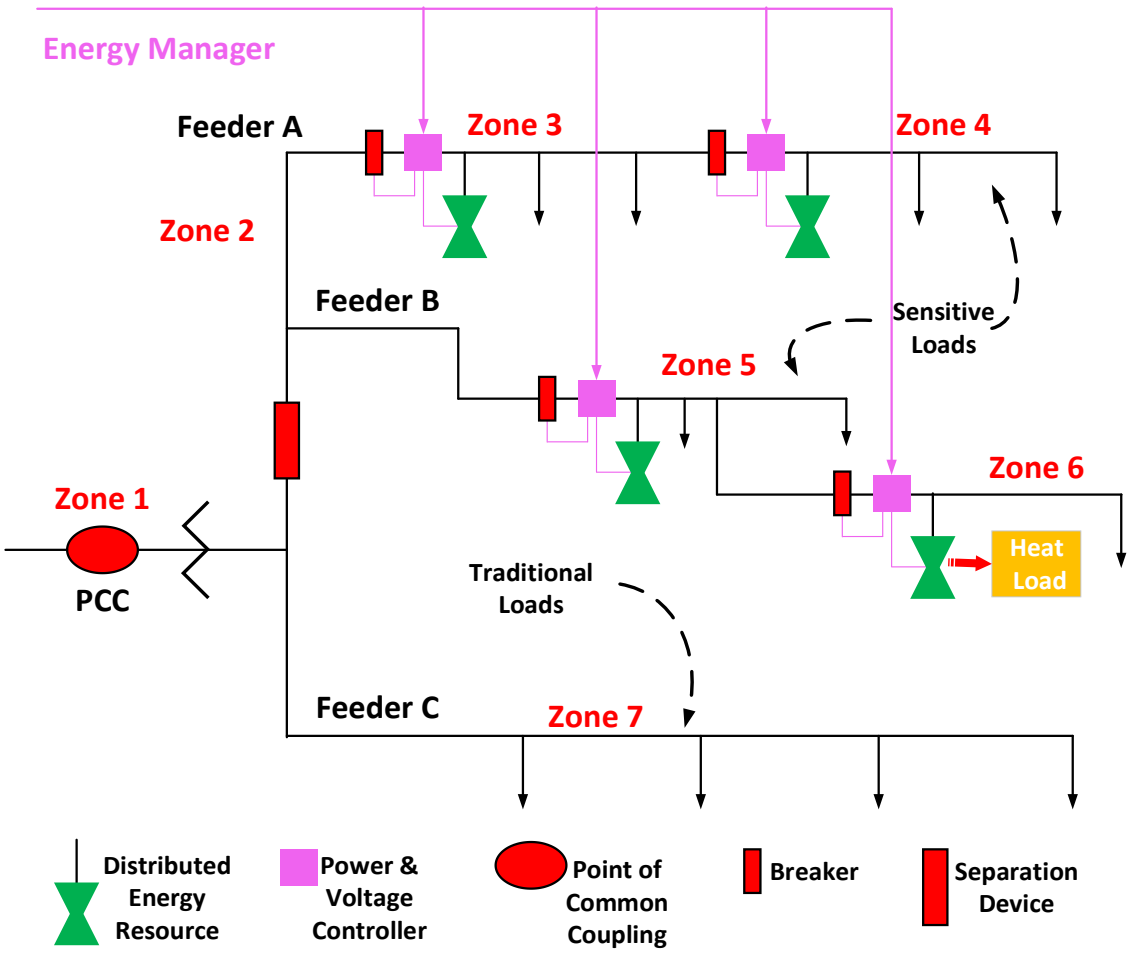

Figure 3.1 CERTS Microgrid Architecture [85]

When the microgrid is disconnected from main grid either caused by external faults in the main grid or intended, ‘islanding’ is formed. The control system has to be designed to achieve a smooth mode transition function and provide stable and secure running ability for the islanded microgrid [86]. The same control circuit and hardware which is capable of different operation modes is preferred as it has the benefits on reducing the distortions during transition periods. Besides, a microgrid should have flexible features to support load variation and DGs switching in/out. In that case, a fast responding decentralized control algorithm without communication is preferred. However, most of decentralized control methods which are based on droop theory often result in a certain level of power quality deviations such as voltage drop or frequency variation.

A well operated microgrid usually has both critical and non-critical requirements [86-89]. The critical requirements include maintaining system stability, voltage and frequency regulation, proper load sharing among DGs. The non-critical requirements include power flow regulation, system deviations compensation, microgrid operating cost optimization and resynchronization before reconnection. These control objectives often need to be achieved by different control strategies in different time scales. The hierarchical control structure which addresses these objectives at different control hierarchy is a feasible solution [54].

A commonly used hierarchical structure in a microgrid with three levels is presented in Figure 3.2. The control level 1 is often addressed in the DG local controllers. It provides the fast-response functions which can work within several milliseconds to seconds to meet the critical requirements such as voltage and frequency regulation, load sharing. Most of the

published papers are concerned about the control theories can applied at this level. The level 2 and level 3 control functions are achieved by the MGCC. The second level improves the power quality by providing the compensating functions to eliminate to voltage and frequency deviations caused by control level 1. This control level 2 takes place in several seconds. The control level 3 gives a microgrid some particular functions including either real-time or not. This level achieves the objectives within several seconds to hours, which is determined by what the control function is. For instance, economic running, constant power exchanges with the main grid, seamless state transition takes seconds; and the system optimization may take hours.

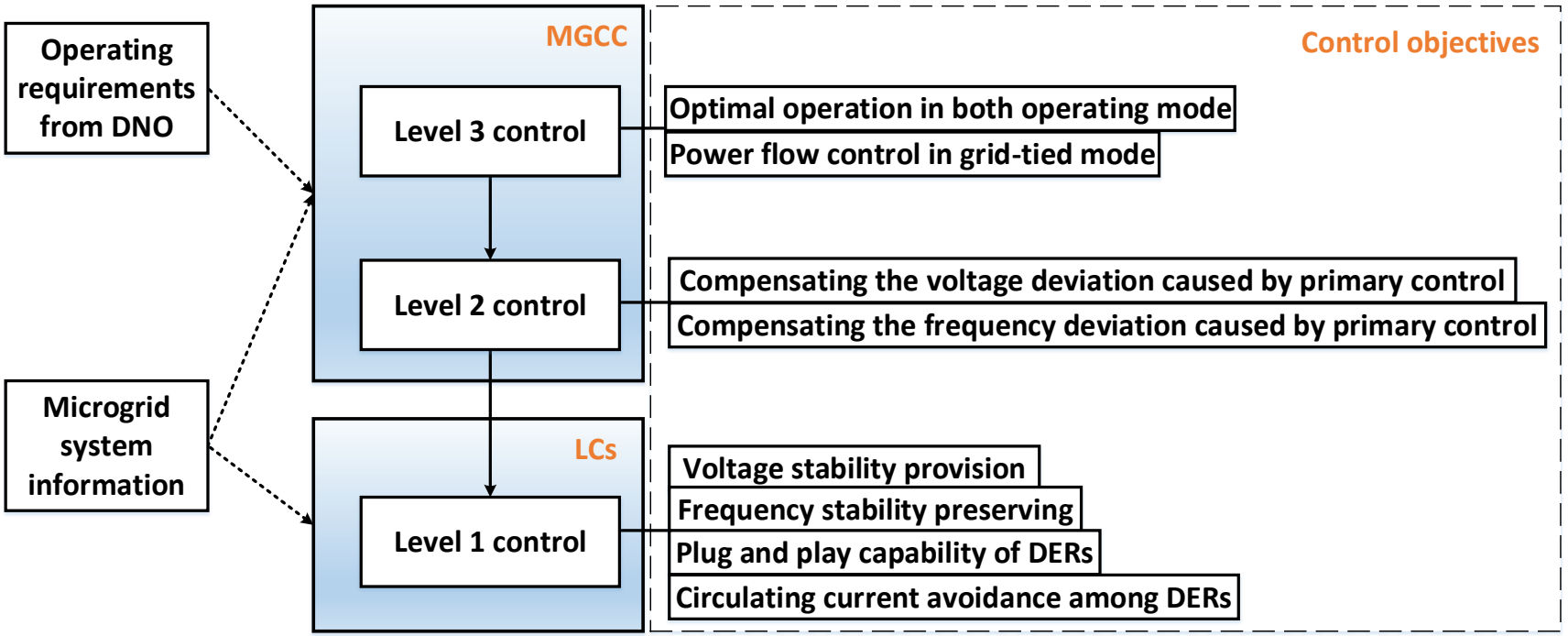

Figure 3.2 Hierarchical control levels of a microgrid [90]

3.2.2 Inverter based DG model in microgrid

Most of the power generated by distributed energy sources in microgrid cannot be directly injected into the grid. For instance, the rotor in a microturbine can rotate over 90,000 rpm [91], and the high-frequency AC power has to be transferred to 50Hz before it connected to the grid. One of the most commonly used DG structure models in microgrid is shown in Figure 3.3. The primary energy source can be either renewable energy source, fossil energy source or chemical energy source. The output power from primary energy source can be AC or DC depending on the type of the generator. The inverter here converts the power from energy source to AC form. For DC energy source, for instance PV array, before the power is passed to a DC to AC inverter, normally there is a DC to DC boost circuit used to transform the voltage level to a certain value. If the energy source is an AC source, for instance wind turbine, the AC/DC/AC back to back converter is often used. The AC power converted from an inverter, even multilevel inverter, normally contains square waves which may cause damages. To eliminate the harmonics, a filter has to be placed in most cases. A transformer is needed if there is a requirement of transforming voltage to a certain level out of the operating range of the inverters.

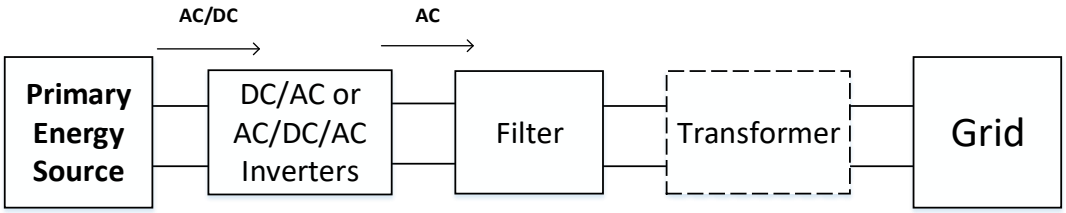

Figure 3.3 Single-phase model of DG in microgrid

For either AC or DC sources, the electricity power has to be transformed into DC form and passed through the DC to AC inverter. The DG model used in this thesis is reduced as Figure 3.4 shows. In this model, the primary energy source is replaced by a constant DC source. There is only one DC to AC inverter here used to convert DC input to AC output. The control techniques which makes the primary energy source behaviour like a constant DC source is not considered in this research. This reduced structure is widely used in microgrid modelling [23, 32, 47, 92].

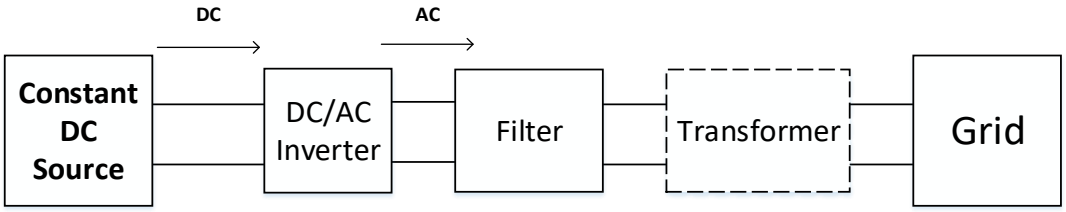

Figure 3.4 Reduced single-phase model of DG in microgrid

The control theories discussed in the following sections are based on this simplified structure of DG model. The control theories are concerned about the DC to AC inverter part. Control of primary generators, DC link voltage stabilizer control, filter design and transformer design are not considered in this thesis.

3.3 Basic control principles for an inverter-based DG in microgrid

3.3.1 Reference frame transformations

When a controller designed with the original three phase AC signals under Natural Reference Frame (NRF), it has to treat three phases separately. To make the control procedure for a three phase AC power system be easier, three phase voltage/current signals in NRF are usually transformed to

Stationary Reference Frame (SRF) or Synchronously Rotating Reference Frame (SRRF) signals. The biggest advantage of using SRRF is the control components are DC signals which can be easily controlled by PI controller. It has good performances on eliminate steady state errors with this widely used PI control theory. PR controller which relatively more complicated is used for SRF control [23]. This PR controller has advantages in solving unbalanced conditions and harmonic problems [93, 94]. However, it is not cost-effective compared with PI control. In this thesis, the power system is assumed to be operated under balanced three phase condition, in case of that the SRRF is preferred. This NRF to SRRF transformation usually called direct-quadrature-zero (dq0) transformation which is derived from Clarke transform(3.1) and Park transform(3.2).

$$\begin{bmatrix} x_\alpha \\ x_\beta \\ x_\gamma \end{bmatrix} = \frac{2}{3}\begin{bmatrix} 1 & -\frac{1}{2} & -\frac{1}{2} \\ 0 & \frac{\sqrt{3}}{2} & -\frac{\sqrt{3}}{2} \\ \frac{1}{2} & \frac{1}{2} & \frac{1}{2} \end{bmatrix} \cdot \begin{bmatrix} x_a \\ x_b \\ x_c \end{bmatrix} \tag{3.1}$$

$$\begin{bmatrix} x_d \\ x_q \\ x_0 \end{bmatrix} = \begin{bmatrix} \cos\omega t & \sin\omega t & 0 \\ -\sin\omega t & \cos\omega t & 0 \\ 0 & 0 & 1 \end{bmatrix} \cdot \begin{bmatrix} x_\alpha \\ x_\beta \\ x_\gamma \end{bmatrix} \tag{3.2}$$

When the balanced three phase condition is considered in the power system design here, both the x_γ in (3.1) and x_0 in (3.2) are kept zero. In case of that, the SRRF which is applied in this thesis has two axis, d-axis and q-axis. The d-axis rotates with the same Angular velocity of original AC signal. The q-axis is perpendicular to d-axis. Equation (3.3) gives the relationship of three-phase AC signal and SRRF DC signal.

$$\begin{bmatrix} x_d \\ x_q \end{bmatrix} = \frac{2}{3}\begin{bmatrix} \cos\omega t & \cos(\omega t - 120°) & \cos(\omega t + 120°) \\ -\sin\omega t & -\sin(\omega t - 120°) & -\sin(\omega t + 120°) \end{bmatrix} \cdot \begin{bmatrix} x_a \\ x_b \\ x_c \end{bmatrix} \tag{3.3}$$

Where:

x_α is the instantaneous variant on α-axis of SRF

x_β is the instantaneous variant on β-axis of SRF

x_d is the instantaneous variant on d-axis of SRRF

x_q is the instantaneous variant on q-axis of SRRF

x_a, x_b and x_c are the original instantaneous three phase signals

ω is the Angular velocity of original AC signal (degrees/s)

3.3.2 Inverter-based DG components

An inverter-based DG model with control components is shown in Figure 3.5. There are several main components used in this DC-AC power conversion system: inverter, phase-locked loop (PLL), current or/and voltage control loops and switching signal modulation [47]. Both instantaneous voltage and current information v_i, i_i at the inverter output ports and v_o, i_o which are injected to the main grid are gathered and passed to the controller. $P_{ref}, Q_{ref}, f_{ref}, V_{ref}$ are the reference output values of active power, reactive power, frequency, voltage magnitude respectively.

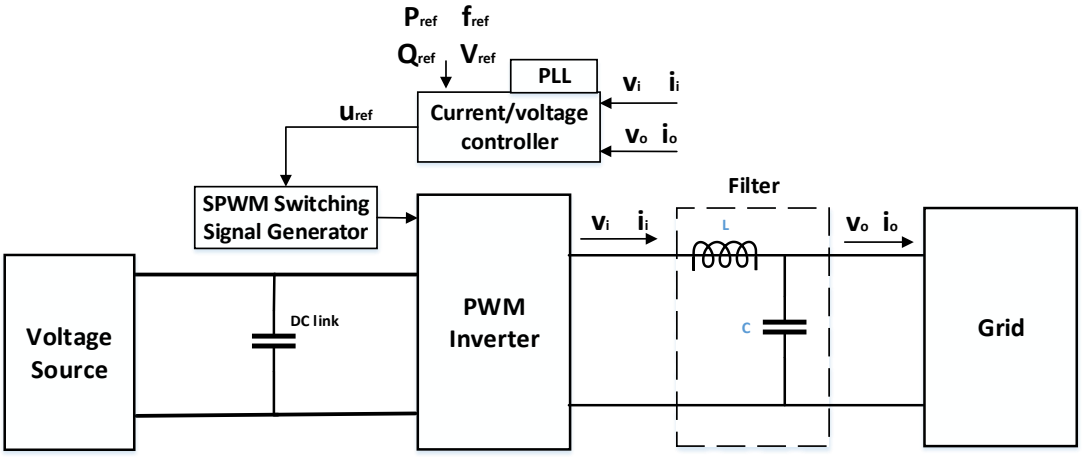

Figure 3.5 Single phase diagram of Inverter

3.3.2.1 PLL and current/voltage controller

The PLL is an important and well-developed tool for signal frequency synchronization and generation [95]. A PLL normally has a filter part which can eliminate the noise in the original signal. In this control system, the PLL is used to track the instantaneous frequency of three-phase voltage or current signal gathered from original electricity circuit and passes the phase angle information to the controller which deals with NRF-SRRF and SRRF-NRF transformation. In this thesis, the phase angle of v_o is tracked.

The reference voltage signal u_{ref} for Sinusoidal Pulse-Width Modulation (SPWM) is generated by the controller based on different control strategies. The power conversion system here can perform as either current-controlled voltage source or voltage-controlled voltage source depends on the controller. The detailed controller structure is introduced in the following section 3.3.3.

3.3.2.2 Pulse-width modulated inverter and SPWM technique

Pulse-Width Modulated (PWM) inverter is widely used for converting DC input to three-phase AC output in power system. Figure 3.6 gives a common circuit topology of a PWM voltage-source inverter. The power electronic valves are switching follow the gate signals generated by the modulation device.

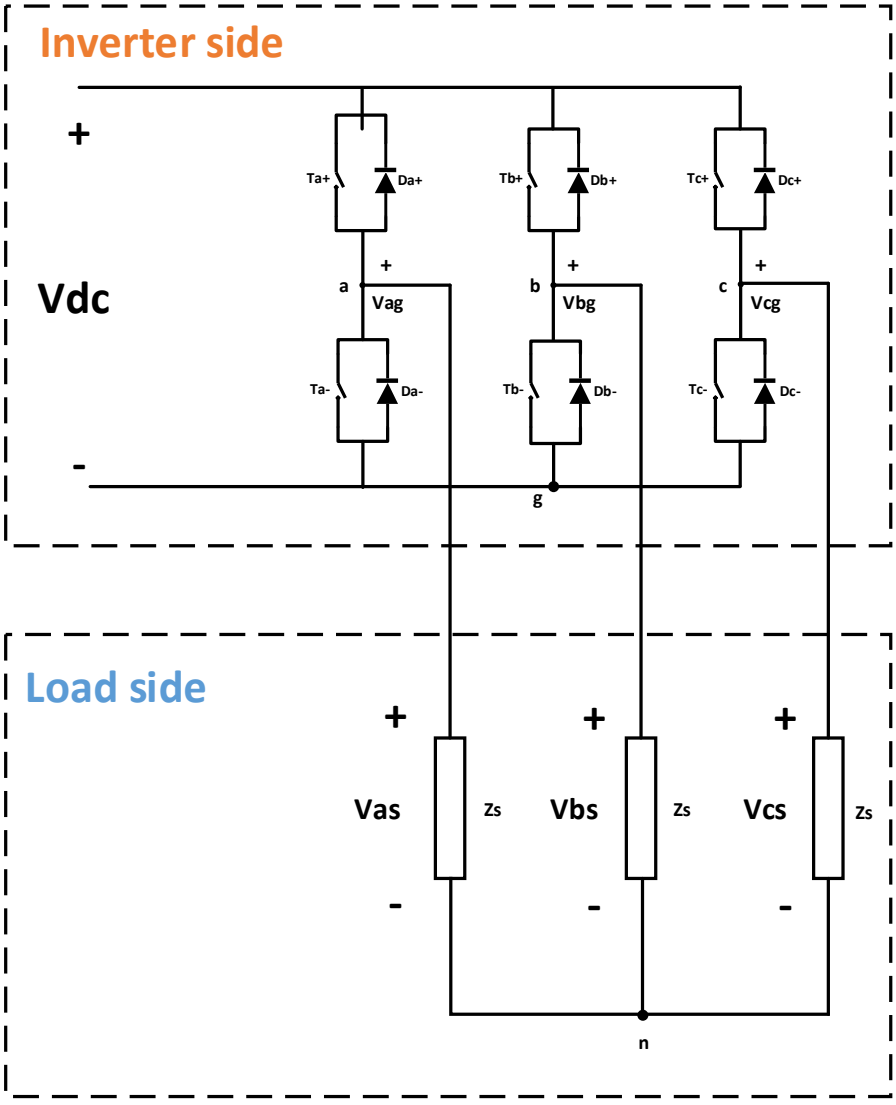

Figure 3.6 PWM voltage-source inverter [96]

One of the most commonly used modulation techniques in modern power systems is the SPWM. Normally, the gate driven signal is generated by

the comparisons of a high frequency triangular carrier wave and the desired reference waveform. Figure 3.6 shows a typical characteristic of single-phase voltage output of a SPWM driven inverter. When the amplitude of carrier signal is larger than the desired waveform, the negative dc bus voltage is applied for the output of inverter, and vice versa, positive voltage output is applied. The root mean square value of the ac voltage waveform is equal to the original dc voltage. In this figure, A_m is the amplitude of desired sinusoid waveform, and A_c is the amplitude of carrier waveform. The ratio $m = {A_m}/{A_c}$ is called modulation index. The high frequency harmonics is filtered after passing through low pass filter. This square waveform is transformed to the desired sinusoid waveform. The final output voltage quality will be better when the carrier frequency increased. However, the larger number of switching per cycle causes more power losses. In power system applications, the carrier frequency is normally chosen in the range of 2kHz to 15kHz. For a three-phase system, this number has to be multiples of 3.

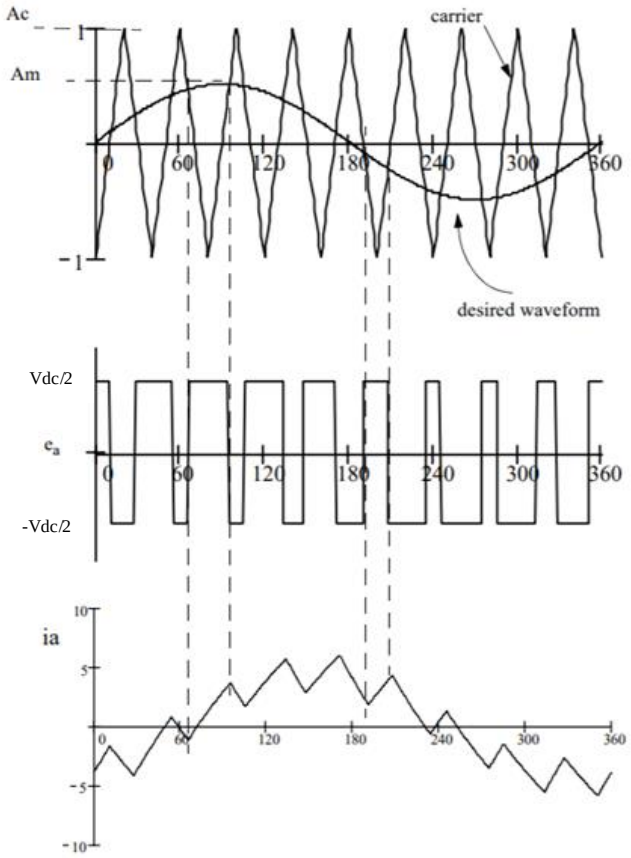

Figure 3.7 Principle of SPWM [97]

3.3.3 Inverter controller design

3.3.3.1 Equivalent voltage and current circuit

When a power conversion system equipped with a LC filter in Figure 3.5, single-phase equations (3.4) (3.5) which are used for control loop design can be obtained. The design procedure of the power conversion system with other types of filter is the same as the LC filter situation discussed in this section.

$$v_i = v_o + L_f \frac{di_i}{dt} \tag{3.4}$$

$$i_i = i_o + C_f \frac{dv_o}{dt} \tag{3.5}$$

Where:

v_i is the per-phase instantaneous voltage value at the output port of the inverter (V)

i_i is the per-phase instantaneous current value at the output port of the inverter (A)

v_o is the per-phase instantaneous voltage value at the grid connection point (V)

i_o is the per-phase instantaneous current value at the grid connection point (A)

L_f is the per-phase inductance value of the inductive part of the LC filter (H)

C_f is the per-phase capacitance value of the capacitor part of the LC filter (F)

This equation can be re-written as equation (3.6)(3.7)

$$\frac{di_i}{dt} = \frac{1}{L_f}\Delta v \tag{3.6}$$

$$\frac{dv_o}{dt} = \frac{1}{C_f}\Delta i \tag{3.7}$$

Where:

$\Delta v = v_i - v_o$ is the voltage difference value between inverter port and grid side (V)

$\Delta i = i_i - i_o$ is the current difference value between inverter port and grid side (A)

For a three-phase system, the equations (3.4) can be expanded as equations

$$\begin{bmatrix} v_{ia} \\ v_{ib} \\ v_{ic} \end{bmatrix} = \begin{bmatrix} v_{oa} \\ v_{ob} \\ v_{oc} \end{bmatrix} + \begin{bmatrix} L_f & 0 & 0 \\ 0 & L_f & 0 \\ 0 & 0 & L_f \end{bmatrix} \begin{bmatrix} \frac{di_{ia}}{dt} \\ \frac{di_{ib}}{dt} \\ \frac{di_{ic}}{dt} \end{bmatrix} \tag{3.8}$$

$$\begin{bmatrix} i_{ia} \\ i_{ib} \\ i_{ic} \end{bmatrix} = \begin{bmatrix} i_{oa} \\ i_{ob} \\ i_{oc} \end{bmatrix} + \begin{bmatrix} C_f & 0 & 0 \\ 0 & C_f & 0 \\ 0 & 0 & C_f \end{bmatrix} \begin{bmatrix} \frac{dv_{oa}}{dt} \\ \frac{dv_{ob}}{dt} \\ \frac{dv_{oc}}{dt} \end{bmatrix} \tag{3.9}$$

The dq-frame inverter output current i_{id}, i_{iq} and the filter output voltage v_{od}, v_{oq} are given in the equations (3.10)(3.11)(3.12)(3.13) which are obtained from the NRF-SRRF transformation equation (3.3). The reference frequency ω is the frequency of grid side voltage v_o tracked by PLL.

$$i_{id} = \frac{2}{3}[i_{ia}\cos\omega t + i_{ib}\cos(\omega t - 120°) + i_{ic}\cos(\omega t + 120°)] \tag{3.10}$$

$$i_{iq} = -\frac{2}{3}[i_{ia}\sin\omega t + i_{ib}\sin(\omega t - 120°) + i_{ic}\sin(\omega t + 120°)] \tag{3.11}$$

$$v_{od} = \frac{2}{3}[v_{oa}\cos\omega t + v_{ob}\cos(\omega t - 120°) + v_{oc}\cos(\omega t + 120°)] \tag{3.12}$$

$$v_{oq} = -\frac{2}{3}[v_{oa}\sin\omega t + v_{ob}\sin(\omega t - 120°) + v_{oc}\sin(\omega t + 120°)] \tag{3.13}$$

Alternatively, the current and voltage differences equation in SRRF can be obtained as equations (3.14)(3.15)(3.16)(3.17)

$$\Delta i_d = \frac{2}{3}[\Delta i_a\cos\omega t + \Delta i_b\cos(\omega t - 120°) + \Delta i_c\cos(\omega t + 120°)] \tag{3.14}$$

$$\Delta i_q = -\frac{2}{3}[\Delta i_a\sin\omega t + \Delta i_b\sin(\omega t - 120°) + \Delta i_c\sin(\omega t + 120°)] \tag{3.15}$$

$$\Delta v_d = \frac{2}{3}[\Delta v_a\cos\omega t + \Delta v_b\cos(\omega t - 120°) + \Delta v_c\cos(\omega t + 120°)] \tag{3.16}$$

$$\Delta v_q = -\frac{2}{3}[\Delta v_a \sin \omega t + \Delta v_b \sin(\omega t - 120°) + \Delta v_c \sin(\omega t + 120°)] \quad (3.17)$$

Equations (3.18)(3.19)are obtained by applying derivation of time to equations (3.10)(3.11)

$$\frac{di_{id}}{dt} = \frac{2}{3}\left[\frac{di_{ia}}{dt}\cos \omega t + \frac{di_{ib}}{dt}\cos(\omega t - 120°) + \frac{di_{ic}}{dt}\cos(\omega t + 120°)\right] - \frac{2}{3}\omega[i_{ia} \sin \omega t + i_{ib}\sin(\omega t - 120°) + i_{ic}\sin(\omega t + 120°)] \quad (3.18)$$

$$\frac{di_{iq}}{dt} = -\frac{2}{3}\left[\frac{di_{ia}}{dt}\sin \omega t + \frac{di_{ib}}{dt}\sin(\omega t - 120°) + \frac{di_{ic}}{dt}\sin(\omega t + 120°)\right] - \frac{2}{3}\omega[i_{ia} \cos \omega t + i_{ib}\cos(\omega t - 120°) + i_{ic}\cos(\omega t + 120°)] \quad (3.19)$$

According to equations (3.6)(3.16)(3.17), the equations (3.18)(3.19) are reformed as

$$\frac{di_{id}}{dt} = \frac{1}{L_f}\Delta v_d + \omega i_{iq} \quad (3.20)$$

$$\frac{di_{iq}}{dt} = \frac{1}{L_f}\Delta v_q - \omega i_{id} \quad (3.21)$$

After doing Laplace Transformation to equations (3.20)(3.21), new equations (3.22)(3.23)are obtained.

$$sL_f\mathbf{I_{id}} = \Delta\mathbf{V_d} + \omega L_f\mathbf{I_{iq}} \quad (3.22)$$

$$sL_f\mathbf{I_{iq}} = \Delta\mathbf{V_q} - \omega L_f\mathbf{I_{id}} \quad (3.23)$$

The equivalent block diagram Figure 3.8 of current circuit can be derived from the equations (3.22)(3.23).

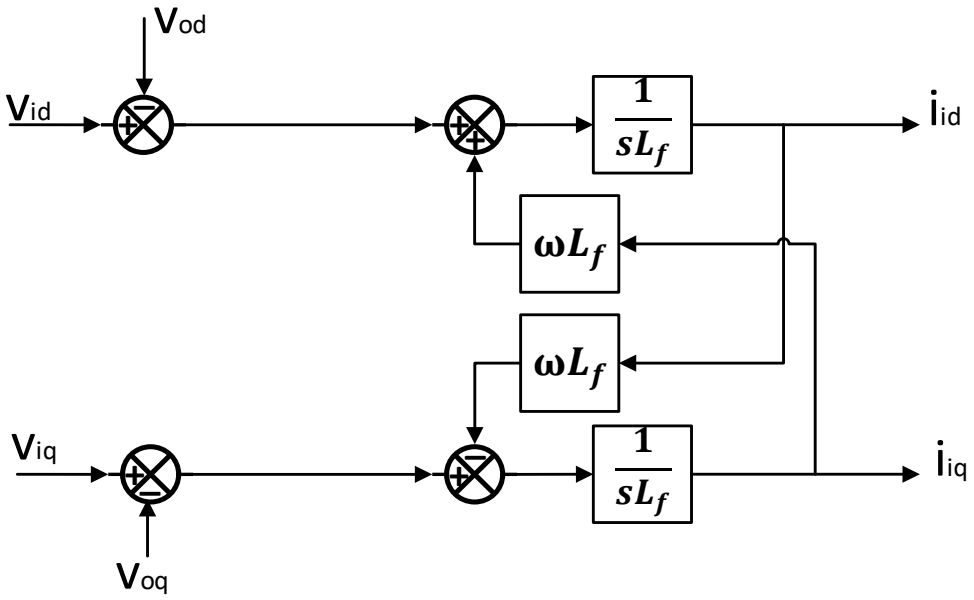

Figure 3.8 Current circuit equivalent circuit

Similarly, the voltage circuit equations(3.24)(3.25) and equivalent block diagram Figure 3.9 can be obtained.

$$sC_f\mathbf{V_{od}} = \Delta\mathbf{I_d} + \omega C_f\mathbf{V_{oq}} \quad (3.24)$$

$$sC_f\mathbf{V_{oq}} = \Delta\mathbf{I_q} - \omega C_f\mathbf{V_{od}} \quad (3.25)$$

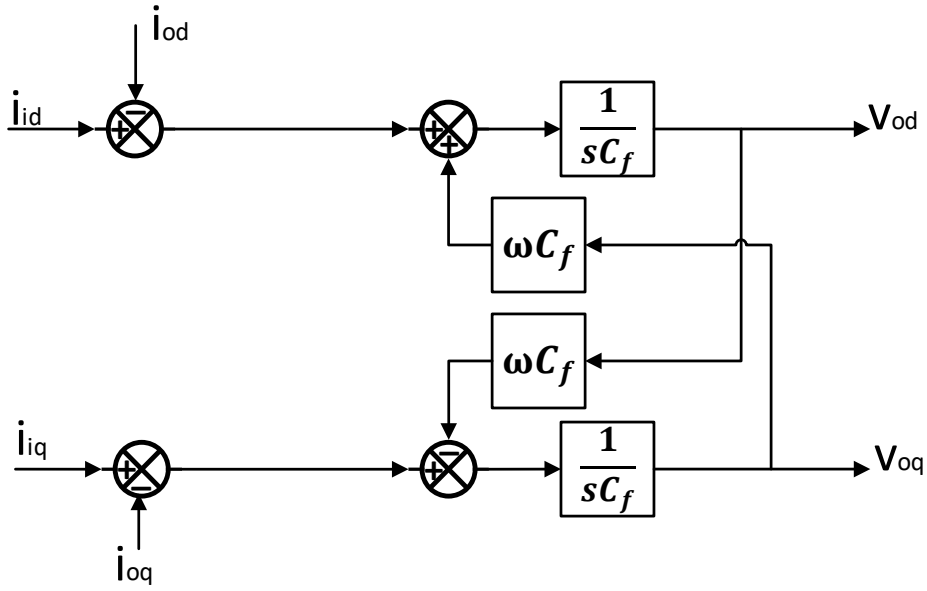

Figure 3.9 Voltage circuit equivalent circuit

3.3.3.2 Current controller

A current controller needs to compare the input current and reference current differentials and generate reference inverter output voltage to the SPWM. The current control loop can be obtained from inverse of current equivalent circuit in Figure 3.8. The $\frac{1}{sL_f}$ block which contains proportional and integral part can be replaced by a PI controller. Finally, the current controller is given in Figure 3.10.

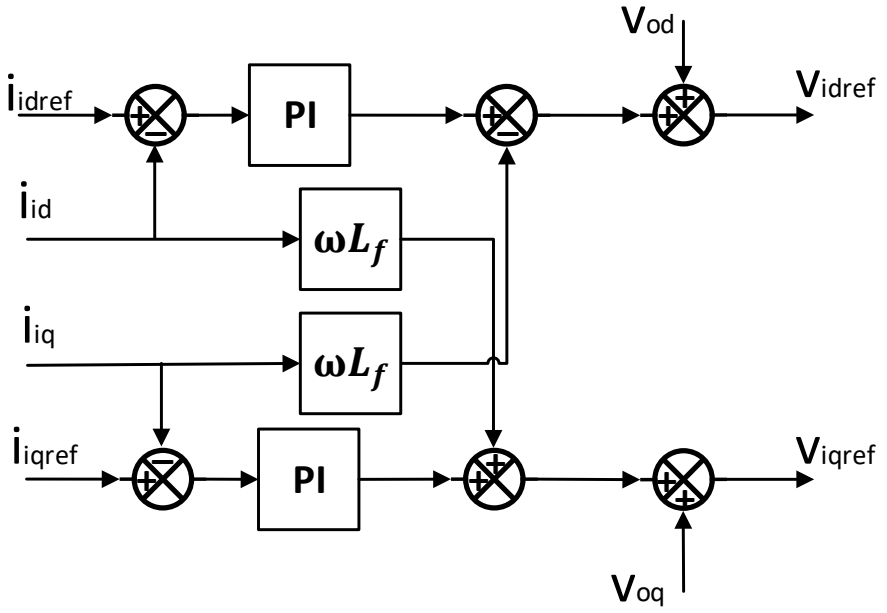

Figure 3.10 Current controller loop

In power system, the complex power provided by a DG can be calculated by equation (3.26).

$$S = \vec{E} \cdot \vec{I}^{*} = (E_d + jE_q) \times (I_d - jI_q) = (E_d I_d + E_q I_q) + j(E_q I_d - E_d I_q) \quad (3.26)$$

Where:

S is the complex power generated by the DG (VA)

$\vec{E}$ is the injection potential (V)

E_d, E_q are the projections of $\vec{E}$ on d-axis and q-axis (V)

$\vec{I}^*$ is the conjugate of injection current (A)

$I_d, -I_q$ are the projections of $\vec{I}^*$ on d-axis and q-axis (A)

As the SRRF rotates synchronized to the grid side voltage, E_q here is equal to 0. Then relationships among voltage, current, active power and reactive power output of previous section are simply expressed in equations

$$P_o = v_{od} \cdot i_{od} \tag{3.27}$$

$$Q_o = -v_{od} \cdot i_{oq} \tag{3.28}$$

When the microgrid is running under grid-connected mode, the grid side voltage magnitude is often set at a fixed value which is close to the nominal voltage. The frequency of this microgrid system is determined by the main grid. The DGs in this situation usually runs to provide certain power to the grid. In this case, if active power P_o, reactive power Q_o and grid side voltage v_{od} are predetermined, the reference injection current i_{od} and i_{oq} can be easily obtained by equations (3.27)(3.28). A typical structure of current controlled inverter structure running in power support mode is shown in Figure 3.11.

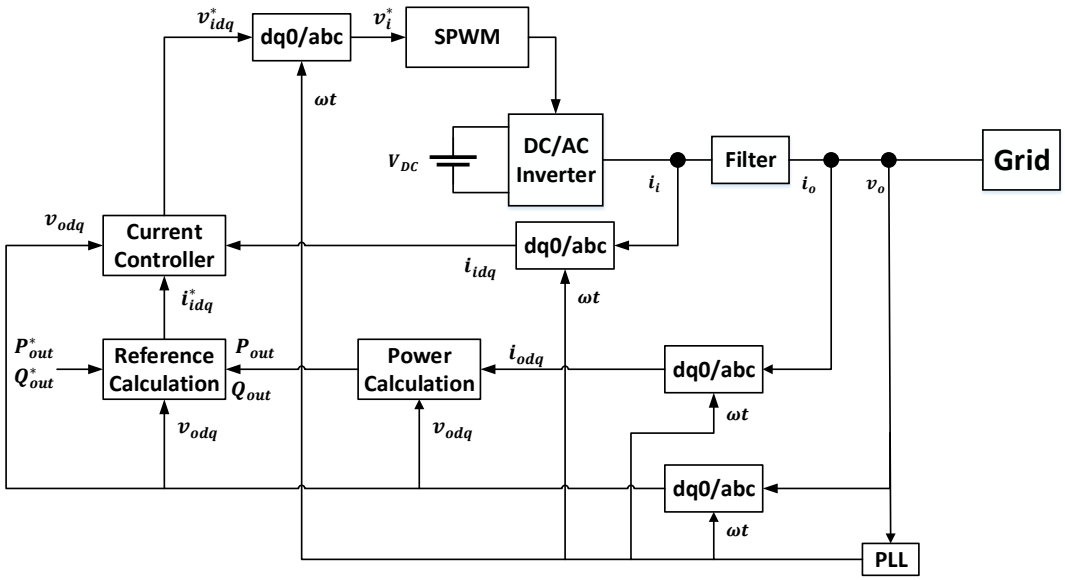

Figure 3.11 Control block diagram of the current based controller for a single grid-connected inverter [23, 98]

3.3.3.3 Voltage controller

The input parameters for a voltage controller are the voltage differentials, and the outputs are the inverter current values. Like the current control block, the voltage control block is given in Figure 3.12.

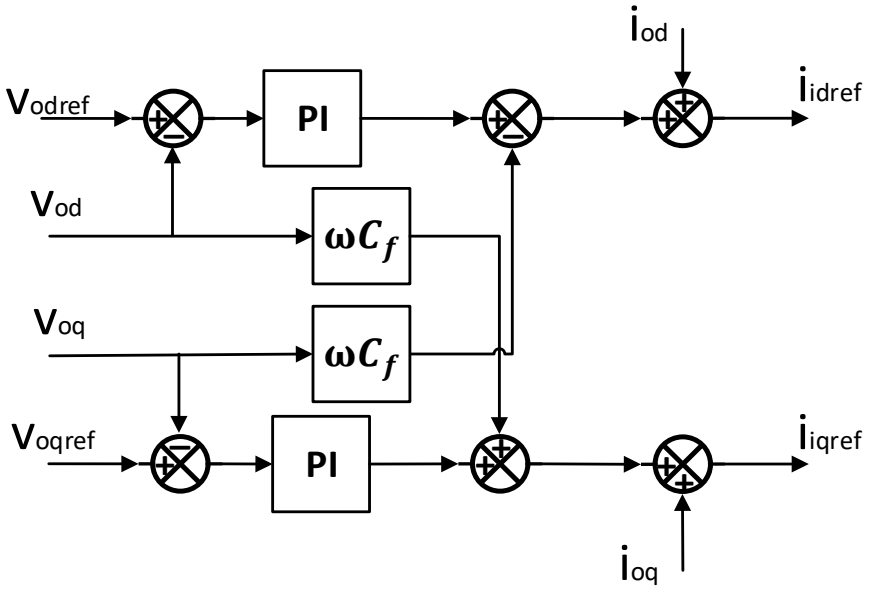

Figure 3.12 Voltage controller loop

When a microgrid is islanded, which means it is operated standalone without the connection to the main grid, there has to be one or more DGs provide support of the frequency and voltage regulation. In this case, voltage controller is applied. However, the controller with only voltage control loop has poor performance for transient over current. The nested loop structure with a current controller in the inner loop is preferred. A typical structure is shown in Figure 3.13.

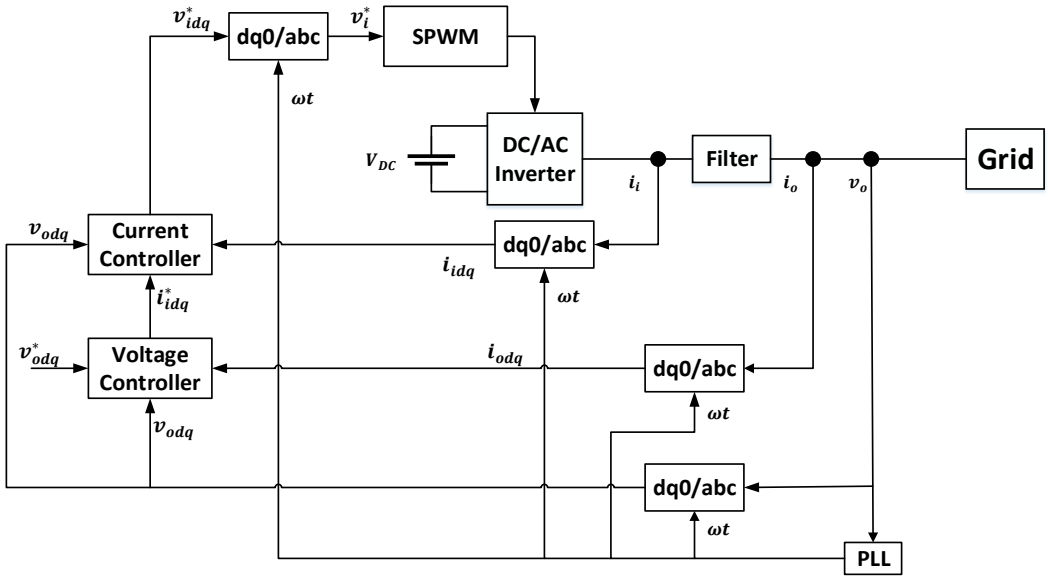

Figure 3.13 Control block diagram of the nested controller for a single standalone inverter [23]

3.4 Power system control issues and challenges with high wind power penetrated microgrids

3.4.1 General Grid Code requirements

To meet the demands of the secure, safe and economy, many specific technical requirements called ‘grid codes’ define the operating procedures and principles of all participants involved in the electricity grid. The contents of grid codes vary in different countries as the

transmission/distribution systems are operated by different TSOs/DSOs [70, 99-102]. For example, according to Spanish grid codes, wind farms have to stop drawing reactive power within 100ms of voltage dips and inject reactive power within 150ms of system recovery. In UK, the grid codes which published by National Grid requires wind farms producing their maximum reactive current for the period of voltage dip caused by a network fault [103]. System design requirements in this thesis are based on UK grid codes.

In a conventional grid, high voltage level wind farm which directly connected to utility grid is often integrated by a group of wind turbines. Wind power is classified as intermittent power source in the UK grid code, the primary source of power for a WECS cannot be considered as controllable. There are specific grid codes provided for the purpose of improving WECS performances and making WECS behaviour with the operational characteristics similar to conventional power plants during normal and abnormal grid conditions [104]. The most common requirements related to high voltage wind farms include fault ride-through capability, frequency and voltage operating range, active power and frequency control, reactive power and voltage regulation [105]. These requirements are often specified at the PCC. Wind turbine manufactures specify individual WECS performance rather than entire wind farm.

3.4.1.1 Frequency and voltage operating range

3.4.1.1 Frequency operating range

According to connection conditions CC.6.1.3 in the UK grid code, the system frequency could variate between 47Hz and 52Hz in exceptional circumstances. The plants and apparatus must be designed to operate with

this frequency variation. For over frequency conditions, they must be capable of operating for 15 minutes at system frequency over 51.5Hz, and 90 minutes if the frequency is above 51Hz. In low frequency situation, the operation period is at least 90 minutes for the system frequency between 47.5Hz and 49Hz, and 20 seconds when the frequency is less than 47.5Hz. Besides, all the devices need to be continuously operating when he system frequency is in the range from 49Hz to 50Hz.

3.4.1.2 Voltage operating range

When doing control category research, most of the contemporary microgrid researchers consider the voltage at PCC as a constant value. However, the voltage at PCC does variate when a microgrid runs as a subsystem in a main grid. There are 3 categories in CC.6.1.7 that give the constraints of voltage changes at a PCC of onshore transmission system. These 3 categories are classified by the indicators $\%\Delta V_{steadystate}$ and $\%\Delta V_{max}$ in equations (3.29) and (3.30). For offshore system, which usually depends on the user's bilateral agreements is not discussed in this section.

$$\%\Delta V_{steadystate} = \left|\frac{V_{steadystate} - V_o}{V_o}\right| \times 100\% \qquad (3.29)$$

$$\%\Delta V_{max} = \begin{cases} \frac{V_{max} - V_o}{V_o} \times 100\% & \text{voltage increases} \\ \frac{V_o - V_{min}}{V_o} \times 100\% & \text{voltage decreases} \end{cases} \qquad (3.30)$$

Where:

All voltages are the root mean square value measured over one cycle and refreshed every half a cycle based on IEC 61000-4-30

V_o is the initial steady state system voltage (kV)

$V_{steadystate}$ is the system voltage with less than 0.5% rate of change over 1 second (kV)

$\%\Delta V_{steadystate}$ is the absolute percentage value of difference between V_o and $V_{steadystate}$

V_{max} is the maximum system voltage when voltage is increased (kV)

V_{min} is the minimum system voltage when voltage is decreased (kV)

$\%\Delta V_{max}$ is the percentage value of maximum differential between V_o and current system voltage

When both absolute values of $\%\Delta V_{max}$ and $\%\Delta V_{steadystate}$ are less than 1%, the system is running under category 1. There is no limit of occurrence number for this category. Both categories 2 and 3 have the condition of $1\% \leq \%\Delta V_{steadystate} \leq 3\%$, they are classified by the differences of $\%\Delta V_{max}$. In category 2, the voltage variations with $\%\Delta V_{max}$ less than 3% occur evenly distributed. The maximum number allowance of occurrence in one hour is $\frac{3600}{\sqrt[0.304]{2.5\times\%\Delta V_{max}}}$.

If the voltage deviation from the V_0 is up to 12% decrease or 5% increase, category 3 happens. Figure 3.14 gives the time and voltage magnitude restrictions of category 3 for the system. Each time the voltage drops up to 12% happened, it has to be modified to no more than 10% in 80ms. The voltage deviation has to be reduced to less than 3% within 2 seconds. Alternatively, if the voltage is increased within 5%, operations are needed to maintain it in the steady state with up to 3% deviation in 0.5 seconds. After that, category 3 is transferred into category 2.

The maximum number of occurrences of category 3 is strictly limited. Normally, it only happens when commissioning, maintenance and fault restoration which is notified to the TSO. It can happen no more than 4 times per day. At the PCC, category 3 happens no more than once per year on average.

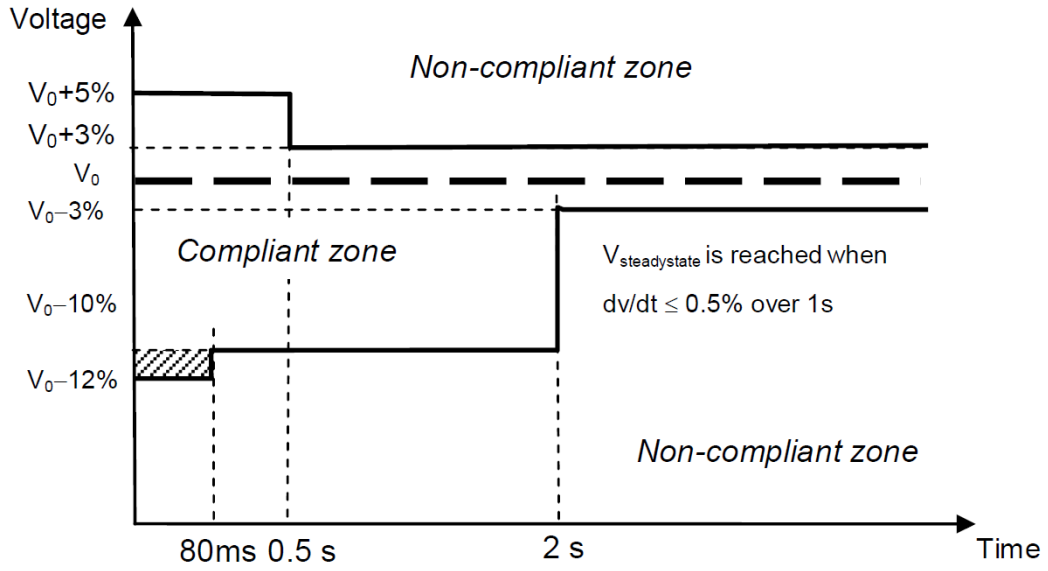

Figure 3.14 Time and magnitude limits for a category 3 Rapid Voltage Change [103]

3.4.1.3 Power factor regulation

In the UK grid code section OC2, the power output zone of a subsystem at PCC is given as Figure 3.15. The MVAr values at point A and point B present 0.95 leading power factor and 0.95 lagging power factor at rated active power output respectively. At point E, the subsystem absorbs reactive power which is 12% of rated MW output. When the active power output is 20% of rated MW, the power factor at PCC reaches minimum value of 0.8575 leading. Under normal operating conditions, the power output at PCC is located inside the bold line area. The power factor has to locate in the intervals [0.8575, 1] leading and [0.54, 1] lagging. The

dashed lines C and D represent the leading power factor and lagging power factor restrictions of the reactive dispatched on the power network. These restrictions are depending on local voltage requirements.

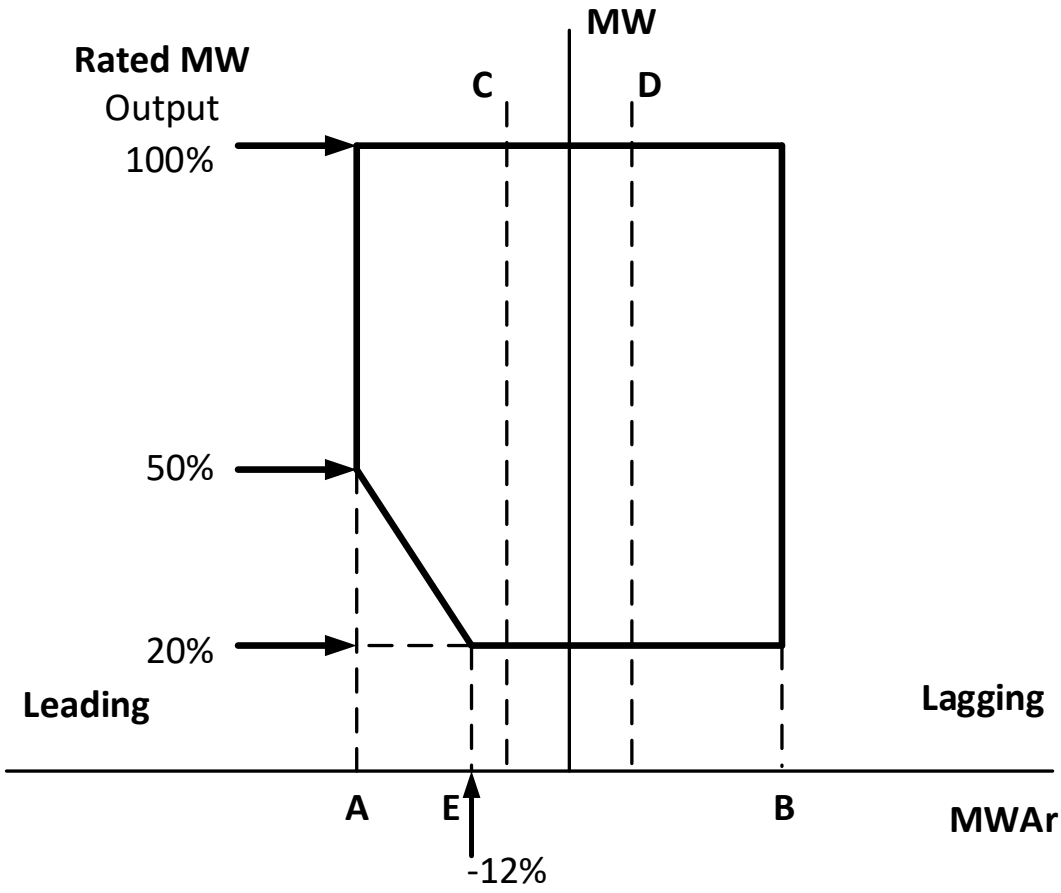

Figure 3.15 Power park module performance chart at the connection point or user's system entry point [103]

3.4.2 UK distribution network connected microgrid design requirements

A microgrid system is often at a low voltage level (less than 6.3kV) or medium voltage level (up to 33kV). It means this microgrid system is

normally operated part of a distribution network rather than directly connected to transmission network. There are mainly 10 licensed DNOs and IDNOs in the UK as Figure 3.16 shows. They are Electricity North West, Northern Powergrid, Scottish and Southern Electricity Networks, SP Energy Networks, UK Power Networks, Western Power Distribution, Energetics Limited, ESP Utilities Group, GTC, UK power Distribution Limited. When a microgrid power system operated as a part of a utility grid, its design has to follow the Distribution Code [106, 107].

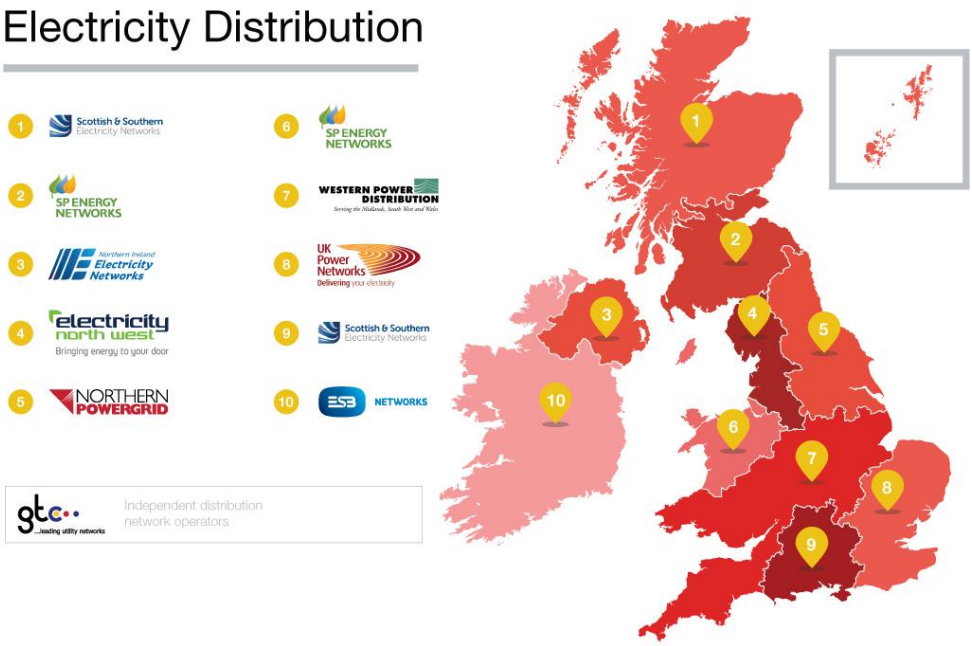

Figure 3.16 UK Electricity Distribution Map [108]

According to section DPC4.2.3.3, there could be a ±3% voltage step changes due to infrequent planned switching event or outages. A microgrid need to be designed working properly with this short-term voltage changes at the PCC bus. With different operating features, a microgrid can be either considered as an embedded generator module or a demand [109]. Section DPC7 indicates the requirements for embedded

generators. A microgrid need to be operated with the registered power output within the system frequency range 49.5Hz to 50.5Hz. It should not be affected by voltage changes in the permitted operating range.

According to section DOC1.5.4, if the power flow deviation at the PCC of a microgrid is greater than 5MW over any half-hour period, the information has to be passed to the DNO within a reasonable time. For this requirement, a high wind power penetrated microgrid needs sufficient back up energy sources or energy storage devices that restrain the fluctuation of total power output or consumption within 5MW. Otherwise, the loading shedding process need to be applied.

3.5 Review of Existed microgrid control theories

3.5.1 Conventional droop control method

For a conventional rotating generator, when the active power output exceeds the rotor driven mechanical power, the generator will slow down until the power balance is restored. During this procedure, the frequency continuously to decrease. In a high voltage power system, the transmission line is normally inductive in characteristic. In this situation, the voltage magnitude drops if the reactive power provided by the generator increases. This inherently P/ω and Q/V droop characteristics makes conventional generators achieves good autonomous load sharing performances. Inverter control method performs with this conventional droop characteristics has been proposed and applied in microgrid [48-50].

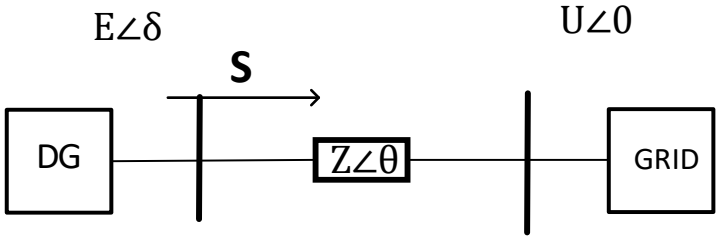

Figure 3.17 Simplified diagram of a DG connected to main grid

In a microgrid, if DGs are connected to a common AC bus, and the switching ripples and high frequency harmonics are neglected, a simplified single-phase system of a DG connected to the grid through line with impedance $Z\angle\theta$ can be modeled as Figure 3.17. $E\angle\delta$ is the DG side bus voltage. For a single DG, the grid side bus is considered as a reference bus with the voltage $U\angle 0$. The grid received complex power from this DG is calculated as (3.31)

$$S = \vec{U} \cdot \vec{I}^{*} = \vec{U} \times \left(\frac{\vec{E} - \vec{U}}{\vec{Z}}\right)^{*} = Ue^{j0}\left(\frac{Ee^{j\delta} - Ue^{j0}}{Ze^{j\theta}}\right)^{*} = \frac{EUe^{j(\theta-\delta)} - U^{2}e^{j\theta}}{Z} \quad (3.31)$$

The real part and imagine part of this complex power are represent as active power P and reactive power Q as equations (3.32)

$$P = \frac{EU\cos(\theta - \delta) - U^{2}\cos\theta}{Z}$$
$$Q = \frac{EU\sin(\theta - \delta) - U^{2}\sin\theta}{Z} \quad (3.32)$$

The line impedance in the conventional droop theory is considered as highly inductive. In this case, θ is replaced by $90°$. When the DG bus

voltage angle δ is relatively small, $\sin\delta$ can be considered be equal to δ in radian. (3.32) can be reduced as

$$P = \frac{EU}{Z}\delta$$
$$Q = \frac{U(E-U)}{Z} \tag{3.33}$$

As the angle δ is the integral of the angular frequency ω in time domain, the P/ω and Q/V droop characteristics can be obtained in the interval around a steady-state point as

$$\omega = \omega_0 - k_P(P - P_0)$$
$$E = E_0 - k_Q(Q - Q_0) \tag{3.34}$$

Where:

P_0 is the active power injected to the common bus at the original steady-state point (W)

Q_0 is the reactive power injected to the common bus at the original steady-state point (Var)

ω_0 is the original angular frequency of the DG output (rad/s)

E_0 is the original voltage RMS value at DG bus (V)

k_P and k_Q are the droop coefficients of active power and reactive power respectively

When the idle values are chosen as the original steady-state operating point, these droop expressions in (3.34) is simplified as

$$\omega = \omega_0 - k_P P$$
$$E = E_0 - k_Q Q \tag{3.35}$$

The active load sharing can be adjusted by the droop characteristics of each DG. A two DG load sharing algorithm is given in Figure 3.18. P_{10} and P_{20} represent the active power output of these two DGs at their maximum frequency ω_{max}. When the system being stable with the frequency of ω, the output of each DG is determined by the different droop characteristics. If the microgrid is running connected to the main grid, the system frequency is forced to be the same as main grid frequency, the active load sharing can be easily achieved. When the microgrid runs in islanded mode, the system frequency is determined by the DGs in the grid, they can also share the active load properly after system steady state is reached. Because of advantages of the simple structure and no communication is needed, this conventional droop control method has high reliability.

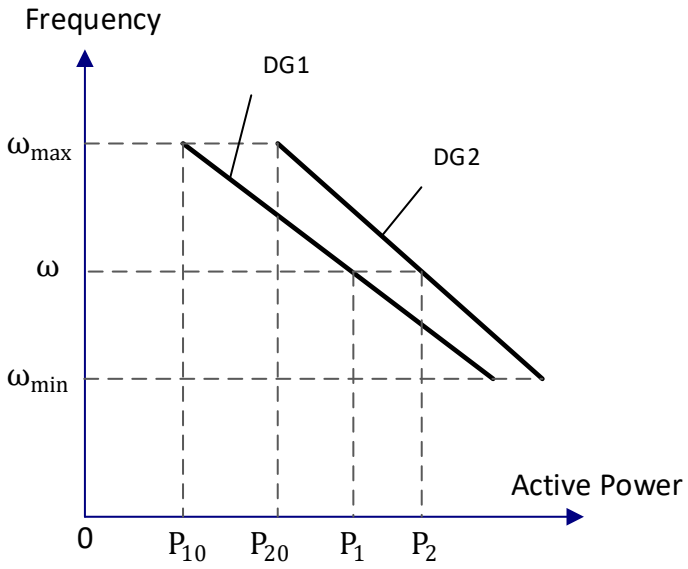

Figure 3.18 P/ω droop characteristics of two paralleled inverter based DGs

For a nonlinear system, the dynamic response of a control system at a certain operating point can be evaluated by the small signal assessment [37, 110, 111]. Although if the inverter control loops and filters do not take places, this conventional droop control system itself is inherently linear, it can be analysed by the small signal assessment as well. When the conventional droop-controlled system running from a steady-state point at U_0, E_0, ω_0, the linearized equations of this DG simplified model can be derived from (3.33) as

$$\begin{aligned} \Delta \mathrm{P} &= \mathrm{G}_P \Delta\delta \\ \Delta \mathrm{Q} &= \mathrm{G}_Q \Delta \mathrm{E} \end{aligned} \tag{3.36}$$

Where:

$\mathrm{G}_P = \frac{E_0 U_0}{Z}$, $\mathrm{G}_Q = \frac{U_0}{Z}$ are constant values.

And the linearized equations of the controller itself are obtained from (3.34) as

$$\Delta\omega = -k_P \Delta P$$
$$\Delta \mathrm{E} = -k_Q \Delta Q \tag{3.37}$$

The differential of angle $\Delta\delta$ is the integral of the differential angular frequency $\Delta\omega$ in time domain. The small-signal model of this DG system can be obtained by injecting a small disturbing signal as shown in Figure 3.19. $\Delta\hat{\omega}$ and $\Delta\hat{\mathrm{E}}$ are the disturbing signals.

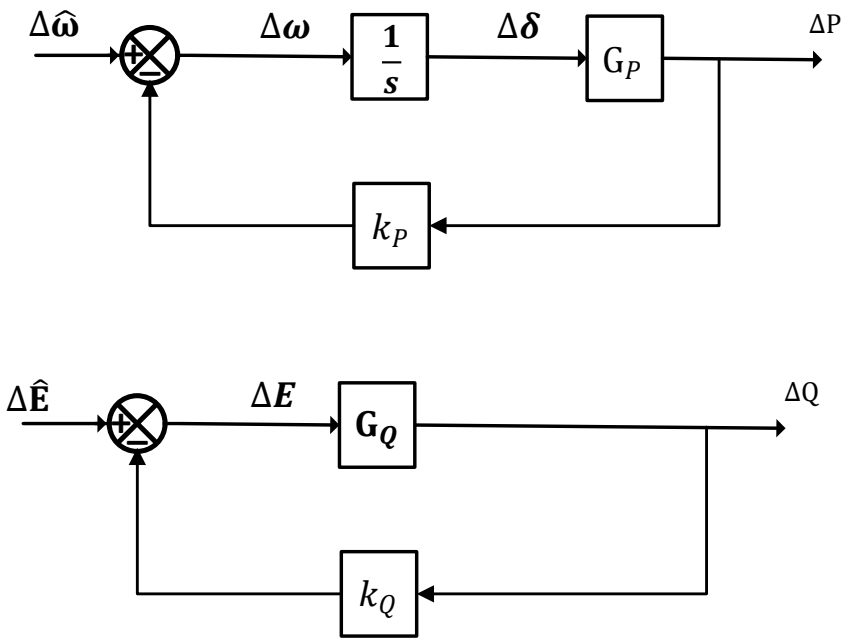

Figure 3.19 Block diagram of small-signal model of the conventional droop control

The transfer functions of this small-signal for active power and reactive power are

$$S_P(s) = \frac{\Delta P(s)}{\Delta \hat{\omega}(s)} = \frac{G_P}{s + k_P G_P}$$
$$S_Q(s) = \frac{\Delta Q(s)}{\Delta \hat{E}(s)} = \frac{G_Q}{1 + k_Q G_Q} \quad (3.38)$$

The time constant of active power controller is $\frac{1}{k_P G_P}$. G_P is a constant value at a steady-state operating point. By using large k_P, it can improve the dynamic performance of load sharing. However, a large droop coefficient causes large steady-state frequency deviation. This makes this control system response relatively slow. For the reactive control part, the controller presents as a proportional gain. Non-closed loop makes this reactive power control lack of accuracy. Besides, some assumptions used to develop this control algorithm not applicable in a microgrid:

a) In the conventional droop theory, pure inductive line model is used to develop the control system. The line impedance in a microgrid is usually not inductive but resistive. This feature causes active power and reactive power control decouple failure.
b) DGs in a microgrid may not connect to a common bus. The different grid side bus voltages may cause reactive power regulation failure.

3.5.2 Modified droop control methods

The shortcomings of a conventional droop algorithm have already been discussed in many literatures. Many modified methods have been proposed to solve these problems.

3.5.2.1 P/V and Q/ω droop method

As mentioned in previous sections, the transmission line in a microgrid could be highly resistive. An algorithm has been developed by assuming pure resistive line [51]. The new droop characteristics are developed by introducing $\theta = 0$ into (3.32). This control theory is described in (3.39) alternatively.

$$\begin{cases} P = \dfrac{U(E - U)}{Z} \\ Q = -\dfrac{EU}{Z}\delta \\ E = E_0 - k_P P \\ \omega = \omega_0 + k_Q Q \end{cases} \tag{3.39}$$

This method has the same advantages of conventional droop. However, they share the same drawbacks as well. This method only performances well for highly resistive line. For a medium voltage level microgrid, the R/X ratio varies depends on the materials and length of the transmission line. It could be inductive or resistive, or even around 1. This transmission impedance variations impacts on the control performance [92].

3.5.2.2 Adjustable load sharing method [90]

To improve the dynamic response without affecting the droop characteristics, a proportional gain $k_{P\omega}$ for the angular frequency is introduced into the active power control loop. To eliminate the impact on reactive power sharing caused by different gird side bus voltages, a grid side voltage regulation part takes place inside the reactive power droop control loop [52, 112]. The small-signal model block diagram of this improved control method is described in Figure 3.20. The transfer function (3.40) is given alternatively.

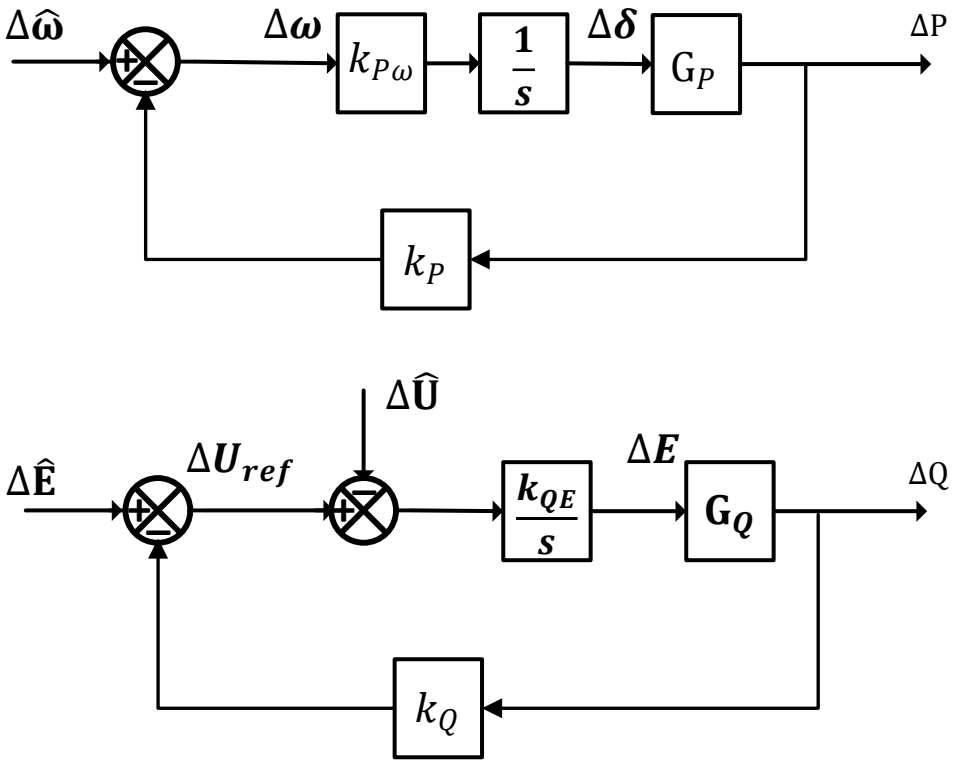

Figure 3.20 Block diagram of small-signal model of the adjustable load sharing method

$$S_P(s) = \frac{\Delta P(s)}{\Delta\hat{\omega}(s)} = \frac{G_P}{s + k_{P\omega}k_P G_P}$$

$$\begin{cases} S_{QE}(s) = \dfrac{\Delta Q(s)}{\Delta\hat{E}(s)} = \dfrac{k_{QE}}{s + k_{QE}k_Q G_Q} \\ S_{QU}(s) = \dfrac{\Delta Q(s)}{\Delta\hat{U}(s)} = -\dfrac{k_{QE}}{s + k_{QE}k_Q G_Q} \end{cases} \tag{3.40}$$

By using this control method, the time constant of active power can be adjusted by changing the value of $k_{P\omega}$. The original droop gain is kept constant, which makes this system voltage deviation relatively small.

Furthermore, the reactive control part forms a close loop system, and there is an adjustable coefficient k_{QE} as well. It makes the reactive power regulation of this control theory have good performance on both dynamic response and steady-state deviation. Because of this feature of no impact to original droop characteristics, this method can be applied to the $\mathrm{P/V}$ and $\mathrm{Q/\omega}$ droop as well. However, the active power and reactive power cross-coupling issue caused by line impedance impacts are still not solved in this method. The system stable operating ranges are affected by the voltage differences between DG bus and Grid side bus.

3.5.2.3 $\mathrm{Q}/\dot{V}$ droop method

A method which improves the accuracy of reactive power sharing by replacing voltage by the rate of change of inverter voltage in the conventional droop method as (3.41) was proposed [53].

$$\dot{E} = \dot{\mathrm{E}}_0 - \mathrm{k_Q}(\mathrm{Q_0} - \mathrm{Q})$$
$$E_{ref} = E_0 + \int \dot{E}\, dt \tag{3.41}$$

Where:

$\dot{E}$ is the rate of change of inverter voltage in time domain (V/s)

$\dot{\mathrm{E}}_0$ is the nominal $\dot{E}$, it is set to 0 V/s here

$\mathrm{Q_0}$ is the reactive power set point at $\dot{\mathrm{E}}_0$ (Var)

E_{ref} is the voltage magnitude value reference for inverter voltage output (V)

E_0 is the nominal phase voltage magnitude (V)

For a multi DGs microgrid system, the reactive power output of DGs continuously variates until the rate of change of frequency of DGs settled at a same value. This method eliminates some line impedance impacts on the reactive power sharing. However, the additional differential and integral parts slow down the dynamic response of this system.

3.5.2.4 Active and reactive power decoupling control methods

As mentions in previous sections, the active power and reactive power cross-coupling issues caused by the resistive part of line impedance significantly affect the performances of droop control. Some decoupling theories have been proposed to eliminate the line impedance impacts.

a) Virtual output impedance method

A feedback path with a virtual impedance as proportional gain is added to this control system as shown in Figure 3.21. This virtual impedance could be complex impedance [54], inductive impedance [113] or adaptive virtual impedance [55]. With an accurate designed virtual impedance, the line impedance angle appears there changed. This provides a possible way to decouple the relationship of active and reactive power. Furthermore, a feedback loop has positive effect on damping harmonic current. However, this virtual impedance needs to be carefully designed, otherwise it may cause voltage and frequency deviations.

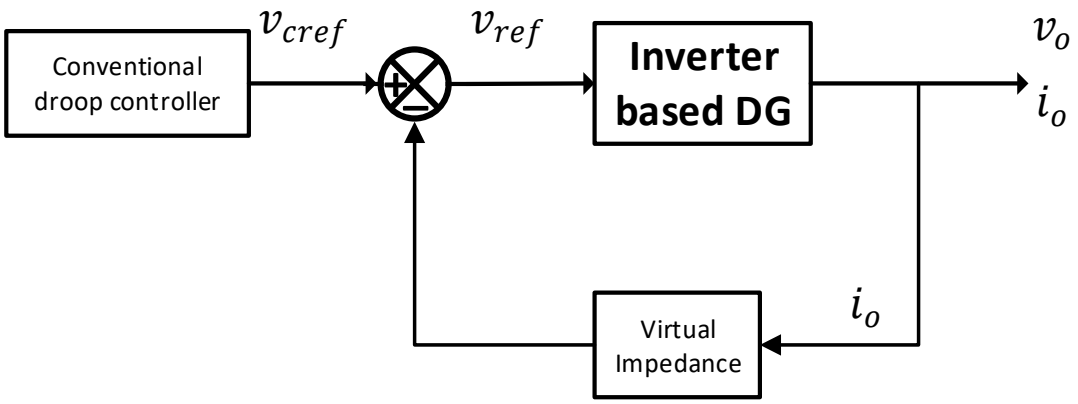

Figure 3.21 Simplified diagram of virtual impedance

b) Virtual frame method

The control components including active/reactive power and frequency/voltage are transferred to a new reference frame which can eliminate the line impedance impact [56] as (3.42).

$$\begin{cases} \begin{bmatrix} P' \\ Q' \end{bmatrix} = \begin{bmatrix} \sin\varphi & -\cos\varphi \\ \cos\varphi & \sin\varphi \end{bmatrix} \begin{bmatrix} P \\ Q \end{bmatrix} \\ \begin{bmatrix} \omega' \\ E' \end{bmatrix} = \begin{bmatrix} \sin\varphi & \cos\varphi \\ -\cos\varphi & \sin\varphi \end{bmatrix} \begin{bmatrix} \omega \\ E \end{bmatrix} \end{cases} \quad (3.42)$$

This method gives a good performance on the decoupling control. However, the line impedance information is required for the orthogonal transformation matrix design. The voltage regulation is not guaranteed.

3.5.3 Active load sharing control methods

The references for the inverters in the active load sharing controlled system are generated from central controller or somewhere else where it is not local. Because of the requirement of fast and high bandwidth

communication channel, most of these active load sharing techniques are used in UPS applications rather than distributed power system.

3.5.3.1 Centralized control method

In this type of control system, all the system performances and inverter references are regulated by the central controller [57]. Depends on the signal generating procedure and algorithm, there could be some particular variants, for instance current distribution [58] or average load sharing [59].

3.5.3.2 Master-slave control method

In a master-slave control system, a DG is considered as a master unit. This master DG regulates the system voltage and frequency during islanded period. Other slave DGs performances as current sources [60, 61, 114]. The reference current for slave inverters is normally generated from central controller or the master unit. There are some variants of this method. The master unit can be fixed or rotating selected by features. A decentralized master-slave control is proposed in [62]. Because there are no requirements for communication channel by using the decentralized master-slave method, it can be easily applied in microgrid. As in all the methods, the master unit takes the responsibility for the whole system regulation, there is risk of transient over current during stats transition.

3.5.3.3 3C method

A 3C strategy is proposed by [63]. In this 3C strategy, there are two loop controls, inner current loop controller and outer voltage controller. The current controller loop forms a circular chain as Figure 3.22 shows. The inductor current of inverter n-1 is used as the reference for the nth inverter to regulate its inductor current. The outer voltage controller regulates the

sinusoidal output voltage. This strategy has good performance on current sharing. However, if any of the inverters failed, the rests will lose current references. It causes the whole system down. As the interconnections of inverters are used to deliver signals, the inverters have to be geographically closed to others.

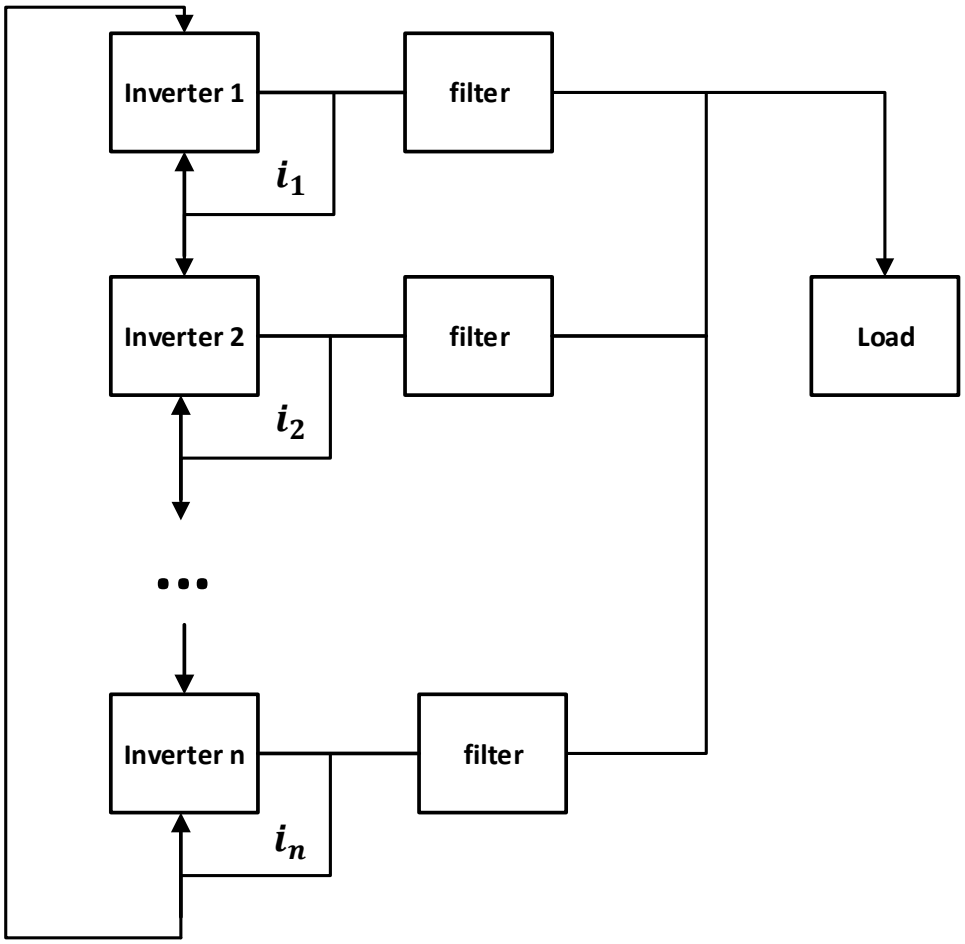

Figure 3.22 Block diagram of the multimodule inverter system controlled with 3C strategy [63]

3.5.4 A summary of the DG control techniques in microgrid

A summarization of the centralized and decentralized control methods discussed above is present in Table 3.1 and Table 3.2 respectively.

Table 3.1 A summary of the decentralized DG control techniques in microgrid

Control method	**Main concepts**	**Advantages**	**Disadvantages**
Conventional droop	P/ω and Q/V droop	• Simple implementation • No communication required • High reliability	• Voltage and frequency deviations cannot be eliminated • Only work for highly inductive line impedance • Poor transient performances • Cannot deal with harmonic distortions
Modified droop	P/V and Q/ω droop	Same as conventional droop	Only work for highly resistive line impedance
	Adjustable load sharing	• Dynamic response speed improved • Improved reactive power regulation • Robust to the system parameter variations	• Not suit for nonlinear load • The line impedance affects the stable running range
	$Q/\dot{V}$ droop method	Accurate reactive power sharing	Slow dynamic response
	Virtual impedance	• Decoupled active and reactive power control • Inherently harmonic damp	• Voltage regulation not guaranteed • Need properly designed
	Virtual frame	Decoupled active and reactive power control	• Voltage regulation not guaranteed • Effective line impedance value needed

Table 3.2 A summary of the active load sharing DG control techniques in microgrid

Control method	**Main concepts**	**Advantages**	**Disadvantages**
Centralized control	Reference signal generated by central controller	• Easy software programming • Good voltage and frequency regulation • Accurate load sharing	High communication bandwidth needed for current signal
Master-slave control	One master DG runs as VSC, other slave DGs runs as CSC	• Good voltage and frequency regulation • Accurate steady-state load sharing • No communication required for decentralized master-slave	• Fast and high bandwidth communication required for centralized master-slave • Risks of losing master unit during transition
Circular chain control (3C)	Current reference comes from the previous inverter	Good current sharing	Any inverter failure cause whole system down

3.6 Summary

In this chapter, the key features of the Microgrid and a commonly used three level hierarchical control structure utilized in such a microgrid have been briefly introduced. The inverter-based DG model and the current/voltage control loops are also summarized. The operating issues of the microgrid that need to be considered in the UK power system are discussed. Most of contemporary researchers build microgrid consider the voltage at the PCC as a constant. However, it does vary during operation when issues happen in the main grid. The power exchange, voltage and frequency variations at the PCC all need to be considered. The rest of the chapter gives a review of existed control techniques, which is divided into two groups: droop control and active load sharing control. Most of the droop control techniques have the advantages of non-communication required and certain level of autonomy.

The adjustable load sharing method is chosen as the level 1 control method in this thesis because its dynamic response can be adjusted without affecting the droop characteristics. In the following study, the lack of accuracy regulation caused by the droop controllers are expected be eliminated by applying higher level controller which is used to actively modify the settings of the local controller. These features are suitable for the microgrid with the WECS where output power is continuously variating.

Chapter 4: Enhanced hierarchical control method for the wind power integrated Microgrid

4.1 Introduction

The commonly used three level hierarchical control structure has been briefly introduced in chapter 3. However, for different power system, the essential requirements and control methods applied in certain hierarchical level are dependent on some system features. For instance, in contrast to the conventional generators which often have inherently larger inertia, the output of inverter-based DGs in the microgrid have to be instantaneously regulated. In this chapter, an enhanced hierarchical control method specifically designed for the high wind power penetrated microgrid is proposed. Section 4.2 introduces the proposed control system in physical domain. The components and how information is exchanged between them are briefly explained.

As reviewed in chapter 3, most of the droop control techniques uses the frequency signal as the global reference [51, 53, 62, 115-118]. The PLL tracks the system frequency and generates phase angle signal for the frame transformation which is used in the inverter voltage and current control loops. For a microgrid with many inverter-based DGs, small deviations of the reference signal can cause large voltage fluctuations. The filters have to be carefully designed to eliminate the high frequency signal distortion impact on the PLL. A robust droop control method which uses the GPS signal synchronized clock as the global reference is proposed in section 4.3. The conventional PLL is replaced by the virtual PLL which generates the reference signal directly from the predetermined phase angle and frequency. The control level 2 which regulates the load flow of this entire microgrid is present in the subsequent section. Besides generating the first

guess settings for the level 1 controllers, it also provides compensation functions. The control level 3 which contains real-time and non-real-time functions is briefly introduced in the section 4.5. To minimize the output variance of wind power generators, section 4.6 proposes a method, which is classified as a non-real-time function, for the settings optimization of wind power generator and energy storage device combined system. A case study is presented in this section to explain the design optimization procedures for the generator and energy storage device combined system.

The simulation results and discussion are given in the section 4.7. The proposed hierarchical control method is tested in a 3-DGs low voltage microgrid model which is built in MATLAB/Simulink. The result demonstrates the power system control objectives in different operation modes can be achieved by the proposed hierarchical control system. A summary is concluded in the last section.

4.2 Proposed high wind power penetrated microgrid control system

In a microgrid with large amount of WECSs, the whole power system has to be monitored and regulated to maintain the system stability. Figure *4.1* is a proposed information exchange map among the components in the microgrid. There are different types of information exchanges which is determined by what the component is. For the renewable DGs, the information is complex than others. It contains request information, admission information and the references information. The other components such as backup DGs, circuit breakers and loads only exchange very simple information with the control centre. The non-elastic loads must always be satisfied. The only send the demand information to

the control centre. Meanwhile, the interruptible loads can be cut off if necessary. There is dual channel between them and the control centre. Figure 4.2 shows the physical structure of this information exchange system. In this system a microgrid is divided into 6 sectors: Control centre, communication channels, system information gathering and local controllers, demands, generators and the power grid itself. The control centre is consisted of two groups of servers. The level 2 and level 3 control operation commands are generated in the decision-making server. The information used for determination is gathered and stored in the communication and data storage server. This communication server also takes the job of sending command to the remote devices through communication channels.

The response time requirements for different components are not the same. The power consumption status of the loads in the microgrid is not frequently updated. The reporting frequency can be from once per several seconds to minutes, or even waiting until receiving the uploading request from the control centre. The message exchanged between the control centre and demand side includes the amount of demands, and the switch on/off signal which is used to control the interruptible loads. In case of this, the relatively slow and low bandwidth wireless communication techniques should be applied as the cost-effective option.

Although the decentralized control technique is applied in the level 1 controller, some abnormal conditions, for example large voltage or frequency deviations at PCC, which are beyond the stable operating capability of the decentralized controllers may cause voltage fluctuations in several cycles. The ethernet system should be used to form a local area

network to secure the fast communication channel. The time latency of signal communication process in an enterprise ethernet can be limited around 2ms [113, 119]. This latency may increase depends on the signal processing hardware and the number of switches the message is passed. Normally, better hardware means more cost, and longer distance leads to more repeaters which cause larger network latency. Hence, the control centre is usually located close to the PCC to achieve fast tracking. For system stability consideration, the output of WECS in this proposed hierarchical controlled microgrid is not allowed to instantaneously changes following the automatic MPPT. It has to send requests to the control centre and maintain the output till it receives the new settings and permission from the control centre. This process usually takes several seconds.

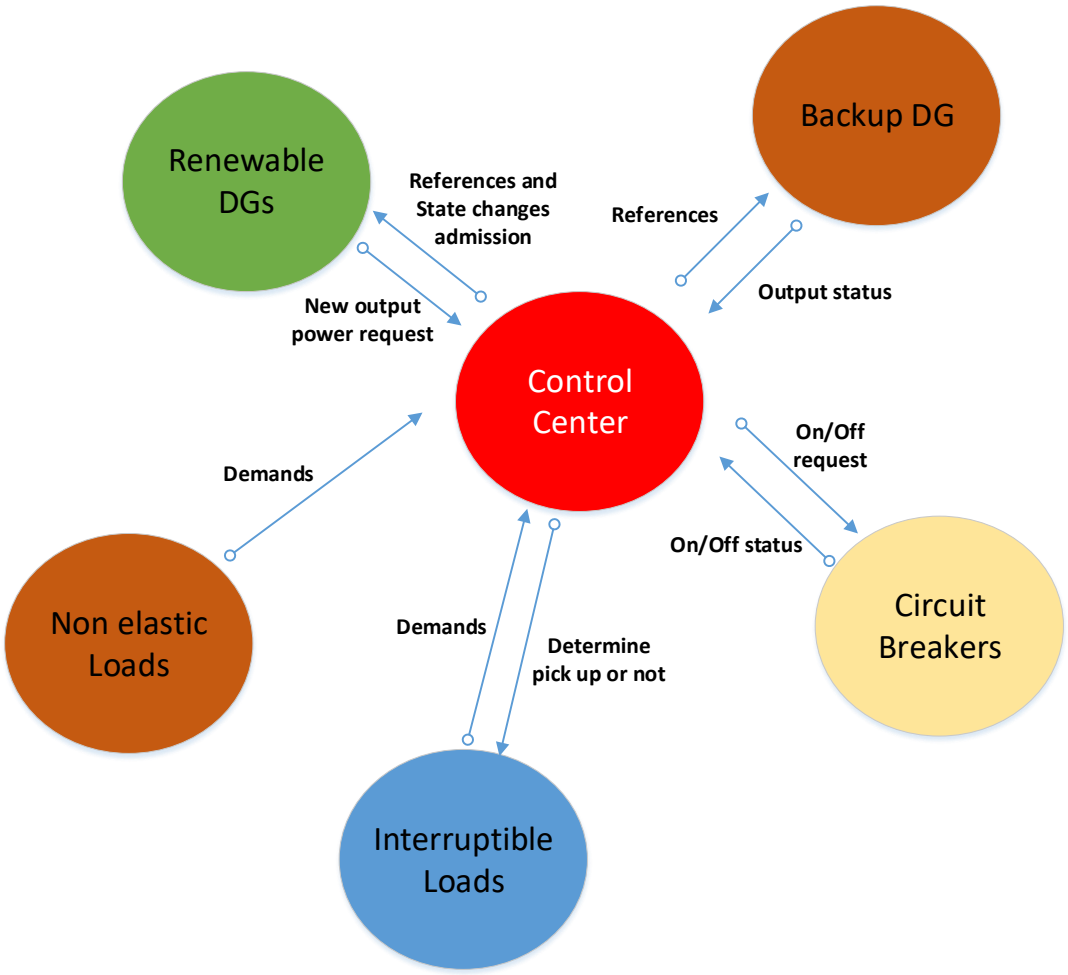

Figure 4.1 Information exchanged between control centre and controllable components

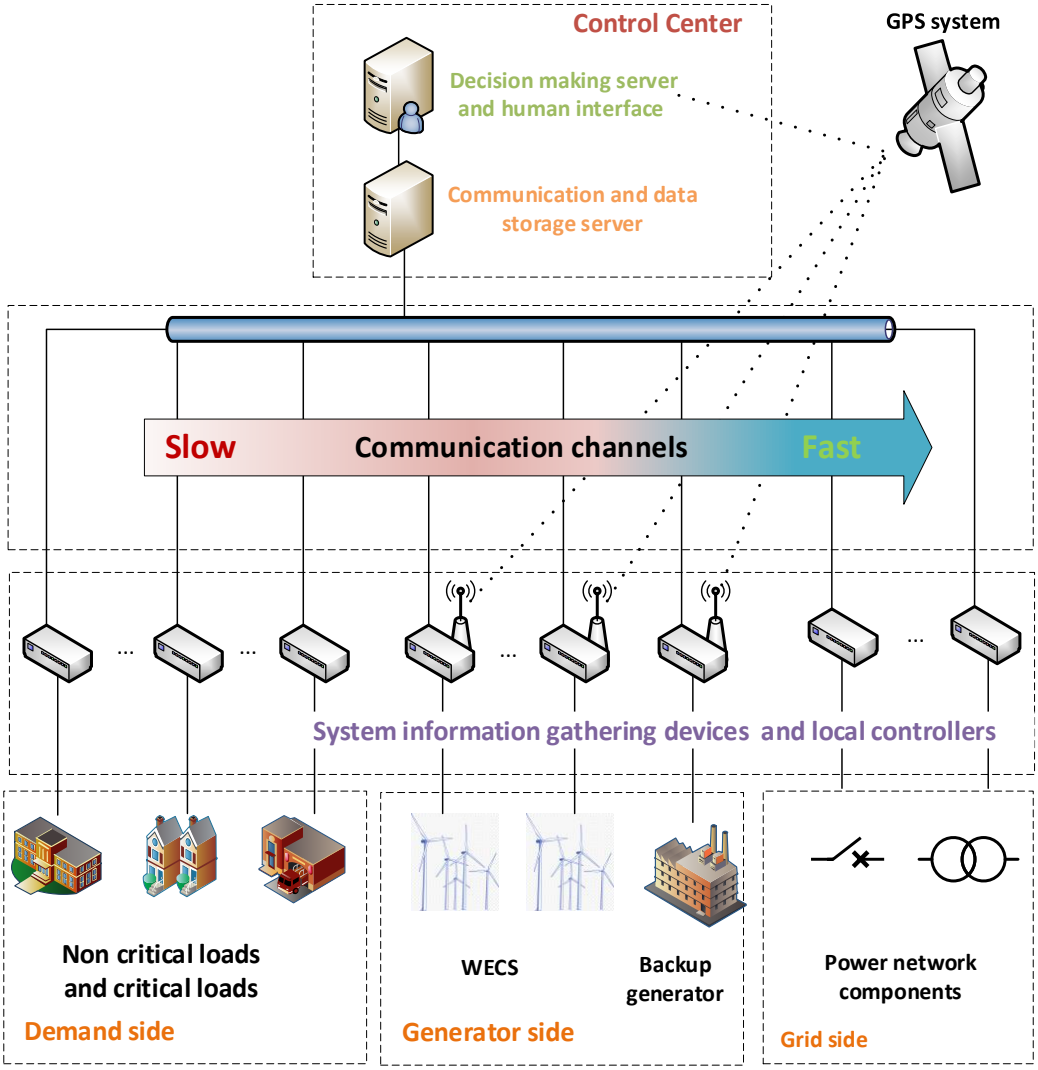

Figure 4.2 Information transmission system for proposed hierarchical control method

4.3 Control level 1 design

With the requirement of high efficiently utilizing the wind power, the WECSs in a microgrid supply power depends on how much power it can provide rather than sharing power follow droop characteristics either in islanded or connected mode. When the microgrid is connected to main grid, the backup DG generate power to maintain the power exchange level at PCC. If an islanded microgrid is formed, the backup DG will behave as a master unit to regulate the system voltage level and frequency which are determined by the main grid before. It also covers the supply-demand gap caused by WECS output variations.

4.3.1 Virtual PLL (VPLL)

The accuracy level of a civilian GPS timing synchronizing system error can be less than $4 \times 10^{-7} s$ [120]. It means for a 50Hz system, phase angle error caused by this time error is within $\pm 4 \times 10^{-4}$ degree. This amount of error can be neglected in the local droop control process. It makes a clock signal have the potential of taking place of system frequency to be a global reference in different locations. With this benefit, VPLL which generates the angular frequency signal directly from the reference angle and frequency can be used instead of conventional PLL in this microgrid control system.

Figure 4.3 shows a VPLL block diagram which is used in MATLAB/Simulink. The output triangular waveform is provided as well. It generates the angle signal in radian by using the global clock signal, frequency signal and phase angle signal. As mentioned in chapter 3, in a practical distribution network connected microgrid system, the frequency on PCC are variable. The frequency deviation causes system fluctuation.

The PCC frequency has to be continuously tracked and sent to the local controllers from the control centre. However, if this microgrid disconnected from the utility grid, the frequency reference can be set as a constant value. Because this VPLL does not use the practical voltage or current signals, there is no need of filters for eliminating high frequency interference signals. It makes the control system harmonic resistive. Meanwhile, the phase angle replaces the frequency which represents one of the controllable parameters in conventional droop control technique. The frequency deviation problem is eliminated with this VPLL.

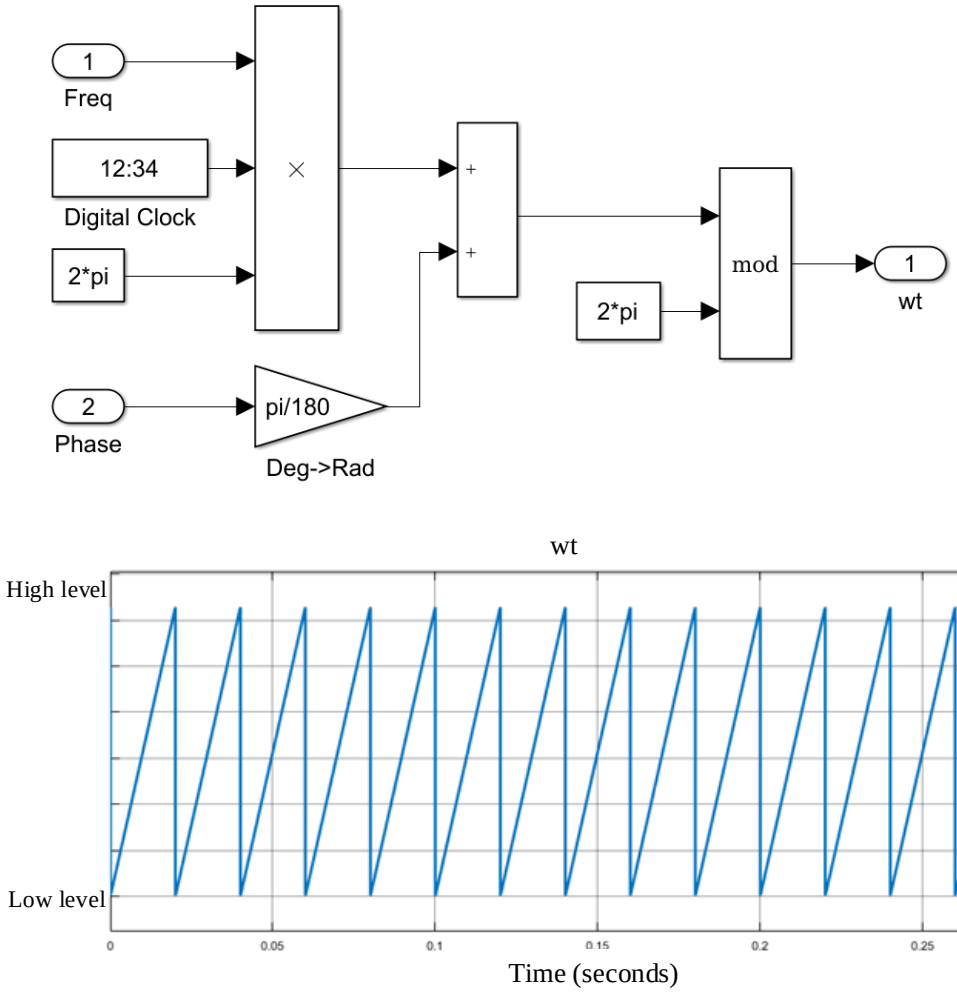

Figure 4.3 MATLAB/Simulink block diagram and the generated signal of a VPLL

4.3.2 Backup DG control

Because of the roles the backup DG plays in this microgrid mentioned above, it is usually geographically close to the PCC. The output power of it is regulated by control centre to meet requirements, such as economic operation or constant power exchange in connected running microgrid. In this state, a PQ control mode need to be applied. If the microgrid is islanded, either intended to be or because of abnormal conditions, the backup DG has to output constant voltage to do its duty.

Figure *4.4* is the control block diagram of the backup DG. The virtual output impedance method and virtual frame method mentioned in chapter 3 are good for the active power and reactive power decoupling control. However, because of the parameters of decoupling components used in these two methods are derived based on the line impedance between the DG and the common bus, the performances are highly affected by the network topology. For a microgrid with several potential system topologies, these power-decouple methods are hard to perform good decentralized features with high reliability. As the backup DG is close to the PCC, the line impedance between the DG bus and PCC bus is considered as pure resistive. The $\mathrm{P/V}$ and Q/δ droop is applied when the microgrid is connected to main grid. Adjustable load sharing method is used to improve the dynamic performance of this droop control system. K_{PV} and $K_{Q\delta}$ are used to tune the control system without changing droop characteristics. There is a saturation limiter which is used to limit the voltage magnitude deviations from the initial steady state voltage V_0 attached on the PI blocks $\frac{K_{PV}}{s}$. The initial steady state voltage can be modified by the higher-level controller or just set to 1 p.u.. Alternatively,

there is a limiter attached with the block $\frac{K_{Q\delta}}{s}$ as well. The control loop generates reference voltage magnitude and voltage angle of the DG bus. G_P and G_Q are the transfer function of the inverter base DG with inner inverter voltage control and current control loops which are introduced in chapter 3. The inner inverter control loops are used to transfer the bus voltage reference to the inverter reference voltage. In the event of islanding, a constant voltage output operation can be achieved without physical switching by setting the limiters on both active and reactive power control loops to the interval [0,0] respectively.

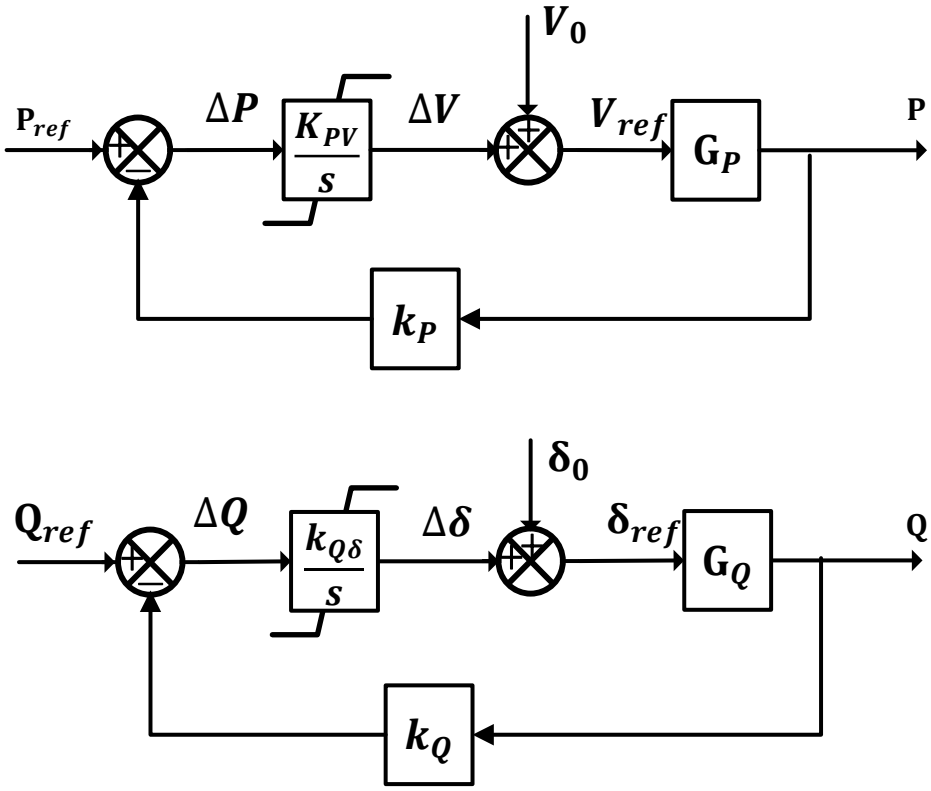

Figure 4.4 Control system block diagram of backup DG

4.3.3 WECS control

The two commonly used wind turbine techniques DFIG and PMSG can provide a certain level of reactive power [121-123]. However, the reactive power is preferred to be compensated locally by compensation devices such as SVC. To limit the circulating current, the reactive power output of WECS is usually be set to zero. The WECS outputs active power as much as it can, it is not necessary to apply the conventional droop characteristics in the control system. In such case, there are some differences between the control loop for WECS in *Figure 4.5* and the backup DG in *Figure 4.4*. The droop coefficients are taken away. The output active power and reactive power are used as the feedback signal instead of the voltage magnitude and phase angle signals in the backup DG control loops. As the transmission lines in microgrid are usually short lines with relatively high R/X ratio, the P/V and Q/δ droop relationships are still applicable here.

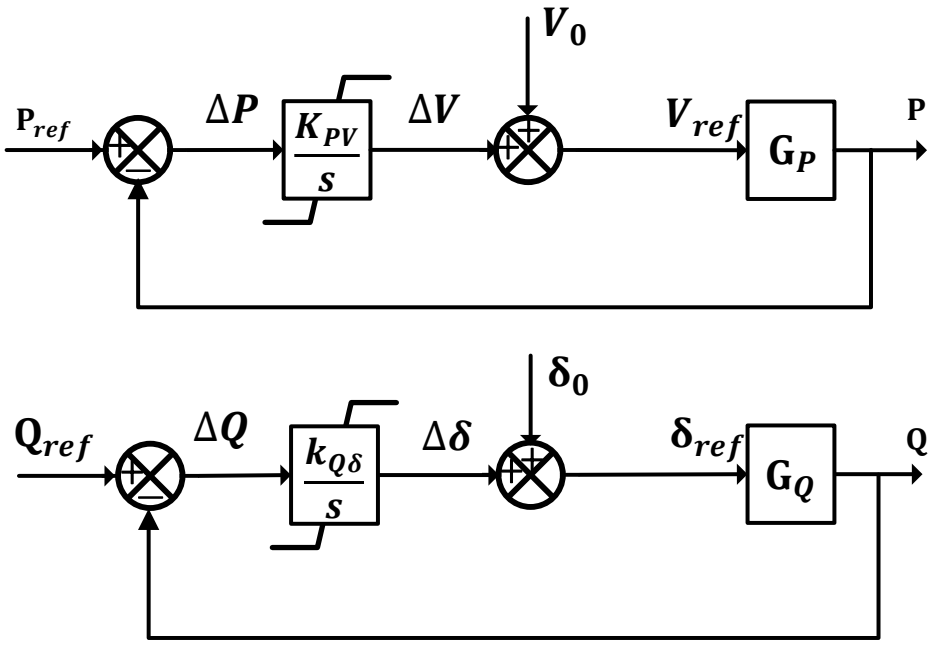

Figure 4.5 Control system block of WECS

4.4 Control level 2 design

4.4.1 Initial references generation based on the steady state analysis

To maintain a stable system, the controllable parameters V_{ref} and δ_{ref} mentioned in control level 1 can only vary within a relatively small interval around the initial steady state values. A guessed initial voltage magnitude and angle information which will be sent to the level 1 controller is necessary. Load flow calculation methods are well developed decades ago [124]. There are many existing tools can be used to solve load flow questions. In this thesis, the MATPOWER toolbox [125] with Newton-Raphson method is applied to the power flow calculation.

The information required for load flow calculation here are mainly divided into three sections: buses, branches and generators. The Bus section includes bus numbers, bus types, bus voltage variations limits and demand on certain buses. The bus type for a certain DG connected bus may vary depends on the running mode of connected DG. The branch section contains the impedance parameters, bus connected information for each branch line, and the load ability constraints. The system topology is formed by this branch section. There is information about the generator's output limits and the bus number where it is connected. Besides, the calculation procedure is based on per unit value, the system MVA rating value and base voltage values for each bus are required as well. While recording the information in a particular format, an initial steady state information can be calculated by MATPOWER toolbox.

4.4.2 Deviations compensation

There are many nonlinear components in a power system, for instance, power electronic switches, circuit breakers and nonlinear loads. It is very

difficult to build an accurate equivalent model. A certain level of deviations always exists, compensation procedures have to be introduced to make the deviations within an acceptable interval.

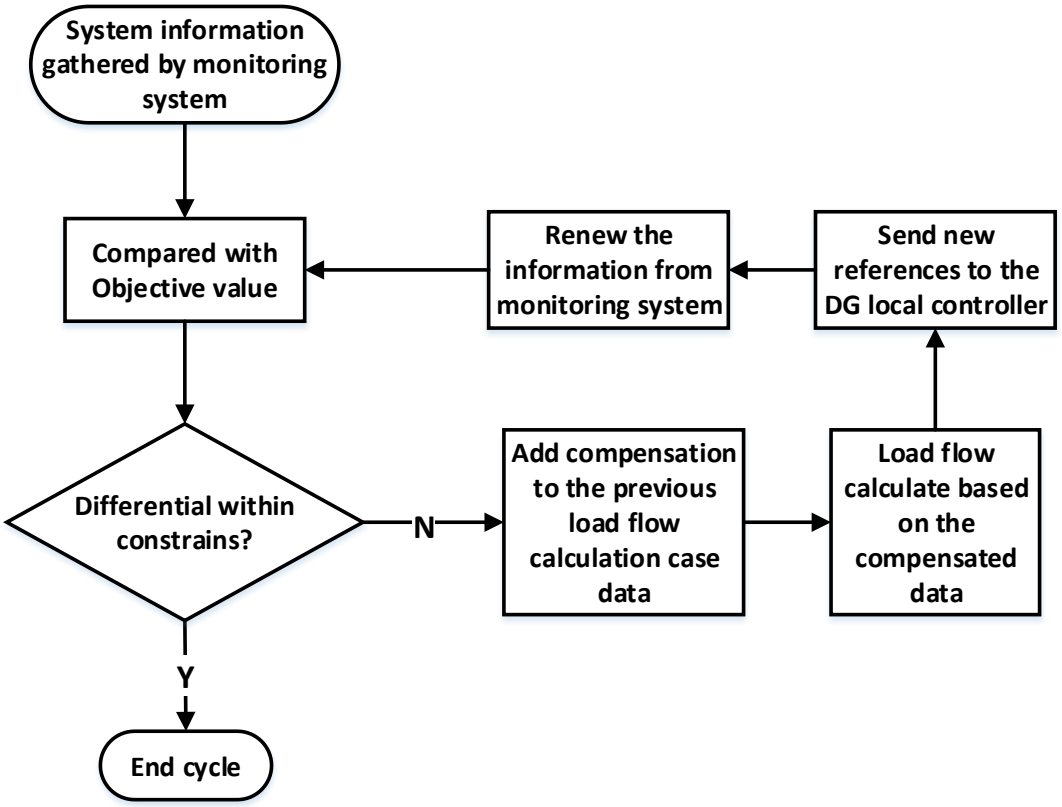

Figure 4.6 Deviations compensation procedure

Figure 4.6 gives the closed loop compensation procedures. There is a monitoring system continuously gathering the system information including demands, bus voltages, DGs' output. If some of the system parameters are outside their constraints, the compensation based on the differentials will be added to the original power flow case data mentioned in section 4.4.1. A new load flow calculation is then executed from the latest data set, and the new references will be sent to the level 1 controllers. After that, a comparison will be executed based on the latest information.

This process loop repeats until the differentials is reduced to within an acceptable range.

4.5 Control level 3 design

4.5.1 Real-time operating functions

In practical long-term operating period, the demand, WECS output keep variating. The control functions provided by the level 2 controller are focused on a certain short-term period in which the system parameters only changed once. The real-time operating functions can be achieved by utilizing an infinite loop in level 3 control system which send requests continuously to the level 2 controller to renew the system information and recalculate the settings for the leve1 1 controllers.

When the power provide by the main grid are chosen as the control object for the level 2 control system, the power flow and compensation function are kept on executed follow the requests sent from level 3 controller. The power exchange on PCC can be maintained as the original reference value. A constant power exchange mode is formed. Alternatively, in an islanded microgrid, if the voltage magnitude and angle on PCC bus are picked as the control object, and the values are set the same as the main grid side.

4.5.2 Non-real-time operating functions

Besides the real-time operating functions, the non-real-time operating functions, such as load prediction and wind speed prediction, are also addressed in the control level 3. These functions can either effectively improve the system performances or achieve more economic benefits. In this thesis, a WECS and Flywheel Energy Storage System (FESS) combined system, which can reduce the output variation of standalone

WECS and provide a certain level of backup capability, is proposed in the following section. The settings optimization procedures for this system are executed in the level 3 controller as a non-real-time operating function.

4.6 Proposed wind power generator and energy storage device combined system and the settings optimization

4.6.1 Backup devices applied in high wind power penetrated microgrid

As mentioned in chapter 2, the electrical power output of an onshore WECS is highly intermittent. For this reason, there has to be backup generators or/and energy storage devices which are used for maintaining the microgrid reliability and power quality. For a microgrid with low voltage and small installed capacity, a backup generator can be used as a master unit to maintain the voltage magnitude and provide power support for the system. Diesel generator has fast dynamic characteristics. It can pick up load quickly. Besides, it can work with very heavy load for a short duration [35, 36, 126, 127]. Because of these advantages, diesel generators are often selected to supply the gap of load demand which cannot be supplied by wind power in a small-scale power system.

When the installed capacity of WECSs increased to MW level, it is not cost effective to use only backup generators. Energy storage devices are required to reduce the power output fluctuations. Short-term energy storage devices are preferred as the continuously variation characteristics of WECS and relatively small investment cost compared with long-term devices such as battery. The Flywheel Energy Storage System is a very commonly used short-term energy storage technique as it has the feature of high-power density and low energy density [39, 64]. Which means the

energy stored in FESS is relatively few, but it can provide very large power output in short terms. Besides, it has the advantages of good durability around 20 years, low maintenance cost, high energy exchange rate which is over 90%. The transient stability of a high WECS penetrated system will be improved by using flywheel as energy storage device [40]. The FESS can be placed centralized in one place to provide stability support or distributed with other local DGs to improve their performances. In commercial applications, less investment cost is always preferred, it is important to find the smallest amount of capacity of energy storage device which can meet the essential requirements. An optimization setting generating procedures are proposed in the following sections. Distributed FESS with WECS combined system is proposed.

4.6.2 FESS charging and discharging rules

Figure *4.7* gives a proposed WECS and FESS combined system. The left bar is the output indicates of the WECS with an installed capacity of P_{max}, the unit is MW. The right bar is the different energy stored states of the FESS with an installed capacity of C, the unit is MWh or Jules. There are two reservation intervals used to prevent over charging or rotation stopped situations. Table 4.1 indicates the charging and discharging rules for this system.

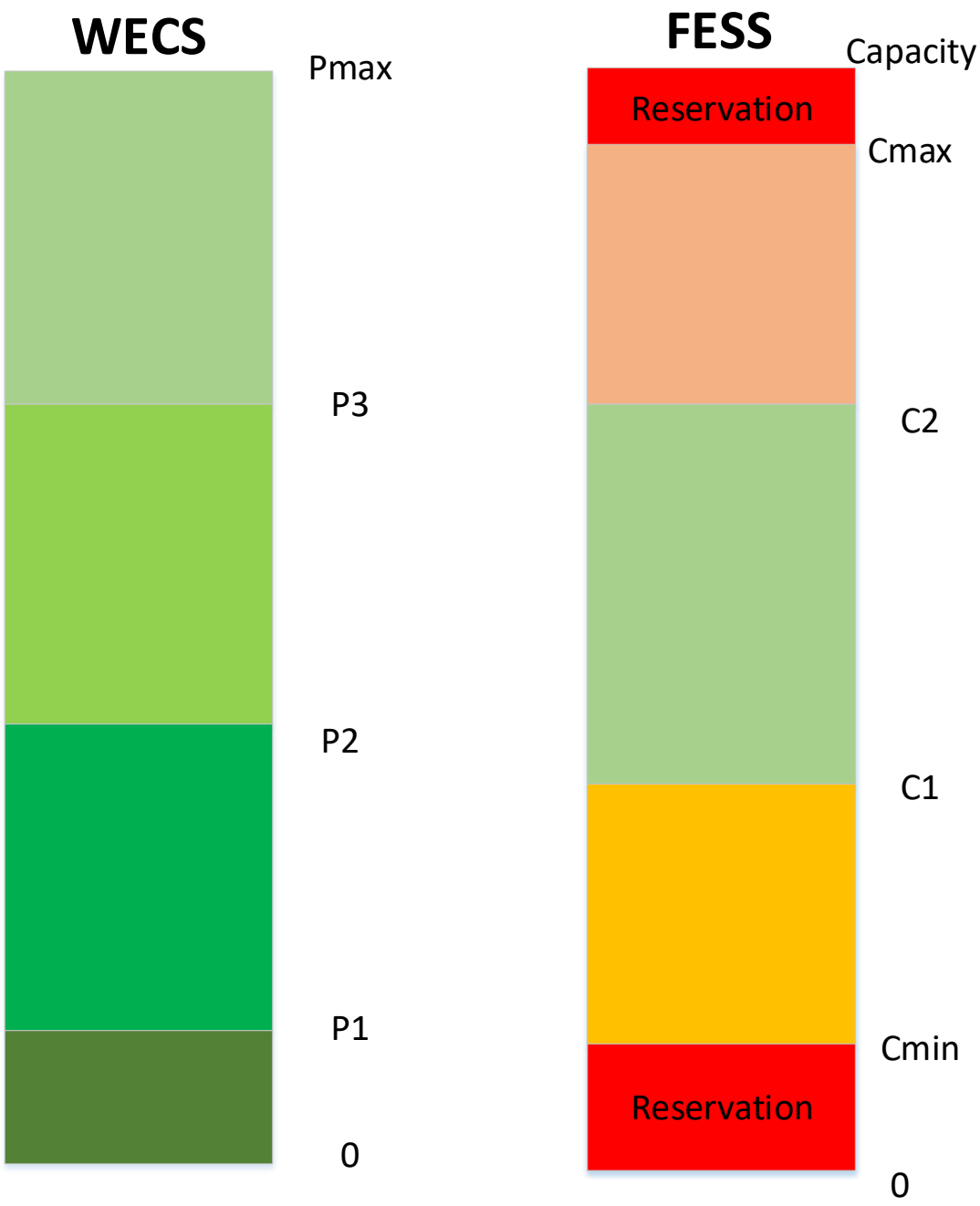

Figure 4.7 WECS power output and FESS states

Table 4.1 Charging and discharging rules

	$C \leq C_{min}$	$C_{min} < C \leq C_1$	$C_1 < C \leq C_2$	$C_2 < C \leq C_{max}$
$P \leq P_1$	Standby	Discharge (P_1)	Discharge (P_1)	Discharge (P_2)
$P_1 < P \leq P_2$	Charge (P_1)	Standby	Discharge (P_2)	Discharge (P_3)
$P_2 < P \leq P_3$	Charge (P_1)	Charge (P_2)	Standby	Discharge (P_3)
$P_3 < P \leq P_{max}$	Charge (P_2)	Charge (P_2)	Charge (P_3)	Charge (P_3)

***P in brackets indicate the supposed combined system output**

When the wind speed is relatively low, the output of the WECS is below the point P_1. To meet the power balance of the system, FESS need to discharge and provide a certain level of power output and this depends on the its energy stored level. If the energy stored in the FESS is lower than C_{min}, it cannot provide power support for the system. The backup generator and other DGs have to provide the energy gap for power balance requirement. When the energy stored level is higher than C_1, the FESS discharges to make the combined system output P_1. When the FESS energy stored level reaches C_2, it is well charged, and it can pull the total output to P_2. The alternative charging and discharging cooperation rules for the WECS power output in other intervals are displayed in Table 4.1.

Case: an example of WECS/FESS combined system output

A 1500 minutes result sample of output power with the settings $P_1 = 10\%, P_2 = 20\%, P_3 = 40\%, P_{max} = 2MW$, $C_{min} = 0$, $C_1 = 45\%$, $C_2 =$

55%, $C_{max} = 2.5MWh$ is shown in Figure *4.8*. Here C_{max} is the reference value for the percentage values C_1, C_2.

The FESS is charged if the output of WECS at a high level. As part of the wind power generator's power output is absorbed by the FESS, the overall output of the combined system is less than the original WECS output. Alternatively, it is discharging during the periods with low output power from WECS. The overall power output rises to a higher level. Besides, there are some intervals the output of WECS and the charging level of FESS both in medium condition. The FESS operated in standby mode for these periods. The output of the combined system keeps the same as the WECS output. It can be observed from this figure, when this WECS and FESS combined system operating followed the proposed energy management rules, the total power variating interval is effectively narrowed.

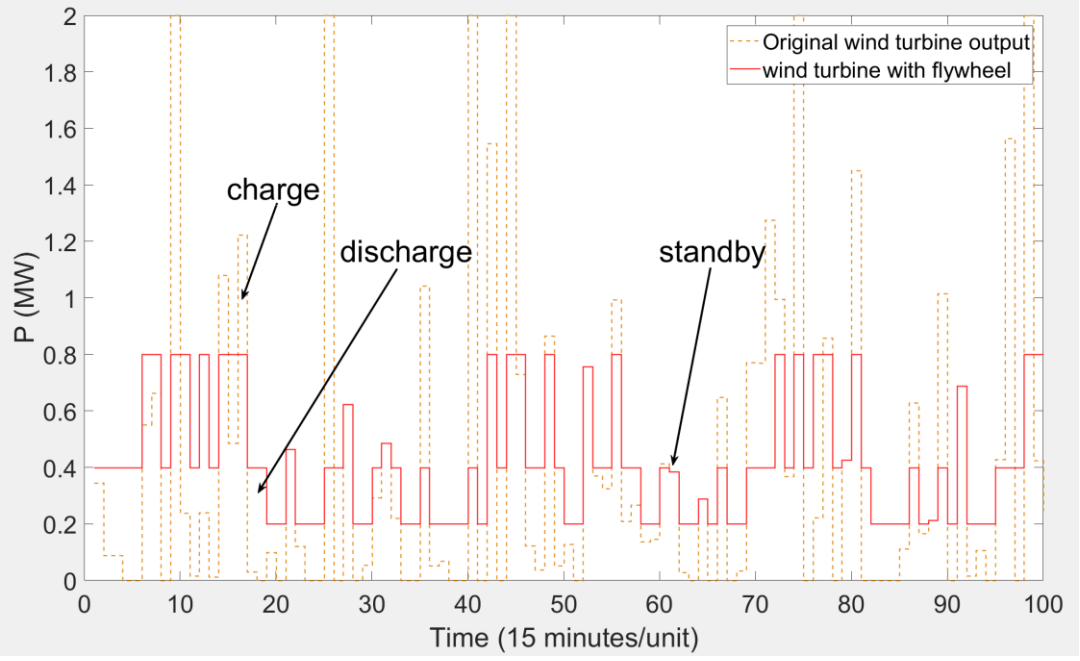

Figure 4.8 Combined system power output in 1500 minutes

4.6.3 FESS installed capacity and combined system settings optimization

The output characteristic of a WECS at a particular location is highly seasons related. The capacity of FESS must be capable for different situations. The setting points can be adjusted for different seasons to obtain a better performance. This optimization procedure is separated in two sections: to obtain the minimum FESS installed capacity which is capable for the optimization requirements, and the setting points which improve the system performance with a certain installed capacity.

4.6.3.1 Installed capacity minimization object and constraints

The minimum investment cost is often used as the optimization object. In this section the investment cost is proportional to the FESS installed capacity, in case of that, the optimization object here is minimizing the installed capacity. The expression of the installed capacity and the constraints are presented in *(4.1)* and *(4.2)* respectively.

$$C_{inst} = C_{max} + C_{res-upper} \tag{4.1}$$

$$\text{Constraints} \begin{cases} C_{min} = C_{res-lower} \\ 1 \geq P_3 \geq P_2 \geq P_1 > 0 \\ 1 \geq C_2 \geq C_1 \geq C_{min} \\ \min(Re_1, Re_2, \cdots Re_{12}) > 0.9 \end{cases} \tag{4.2}$$

Where:

C_{inst} is the installed capacity of the FESS (MWh)

C_{max} is the maximum energy stored in the FESS (MWh)

C_{min} is the minimum energy stored in the FESS (MWh)

$C_{res-upper}$ is the reservation capacity to meet the over charged situation (MWh)

$C_{res-lower}$ is the reservation capacity to prevent the flywheel completely stopping (MWh)

P_1, P_2, P_3 are the setting points which are the percentage values of the rated WECS power output (%)

C_1, C_2 are the setting points which are the percentage values of C_{max}

Re_n is the system reliability of nth month, when the variance of the combined system output is less than 0.5, it is considered as reliable

In this section, the variance σ^2 which defined as equation *(4.3)* is used to evaluate the performances of optimized settings.

$$\sigma^2 = \frac{\sum_{i=1}^{N}(X_i - \bar{X})^2}{N} \quad (4.3)$$

Where:

N is the total number of samples

X_i is the value of i^{th} sample

$\bar{X}$ is the average value of samples

4.6.3.2 Setting points optimization object and constraints

The optimization object in this section is finding a set of setting points to minimize the variation σ^2 of the combined system output. Alternatively,

the expression and constraints are presented in *(4.4)* and *(4.5)* respectively. The variation σ^2 here is calculated from the combined system output with a particular set of setting points. In contrast to the FESS installed capacity minimization, the reliability constraint here is based on the σ^2 in the same trial loop.

$$\sigma^2 = f(P_1, P_2, P_3, C_{max}, C_1, C_2) \tag{4.4}$$

$$\text{Constraints} \begin{cases} C_{min} = C_{res-lower} \\ 1 \geq P_3 \geq P_2 \geq P_1 > 0 \\ 1 \geq C_2 \geq C_1 \geq C_{min} \\ \min(Re_1, Re_2, \cdots Re_{12}) > 0.9 \end{cases} \tag{4.5}$$

4.6.3.3 Optimization procedures

The flowcharts for the optimization procedures are given in *Figure 4.9*. There are two main streams to achieve this optimization: FESS Installed capacity optimization and combined system setting points optimization.

a) FESS installed capacity optimization

The left part of Figure 4.9 is the procedure for finding minimum installed capacity of FESS. It starts with an initial guess of capacity and settings including $P_1, P_2, P_3, C_{min}, C_1, C_2, C_{max}$ which defined in *Figure 4.7*. The output of combined system is calculated and continuously repeated with a Monte Carlo simulation procedure for different wind speed situations. If the result meets the predetermined constraints, the capacity value here is recorded as a temporary optimized capacity (TOC). Then a reduced capacity value is used to do the Monte Carlo simulation. This loop is executed again and again till the output couldn't satisfy the constraints. The TOC is replaced by the latest capacity which makes the constraints satisfied. The setting values are continuously changed to check if there is

setting group which makes this capacity feasible. When a possible solution has been found, this procedure will go back to the top loop by using the latest capacity value and the settings. If all possible settings have been tried, and there is no one meets the constraints, an increased capacity will be compared with TOC. If it is less than the TOC, it will be put in the Monte Carlo simulation and start the first loop. Otherwise, the TOC is recorded as the final optimized capacity value.

b) Combined system setting points optimization

The right part of Figure 4.9 presents the procedure of finding optimized settings with a certain installed capacity. It starts with the optimized capacity value from the left procedure and an initial guess of settings. This settings group is recorded as a temporary optimized settings (TOS). After that, a Monte Carlo simulation similar to the capacity optimization is placed to evaluate if the initial settings meet the constraints. The settings keep changing until there is a setting value makes this system performance good enough. If the performance of the latest settings is better than previous TOS, it will be recorded instead of previous one. Otherwise, the settings are kept on changing till a better one be found, or all settings have been tested. The latest TOS is considered as the optimized settings.

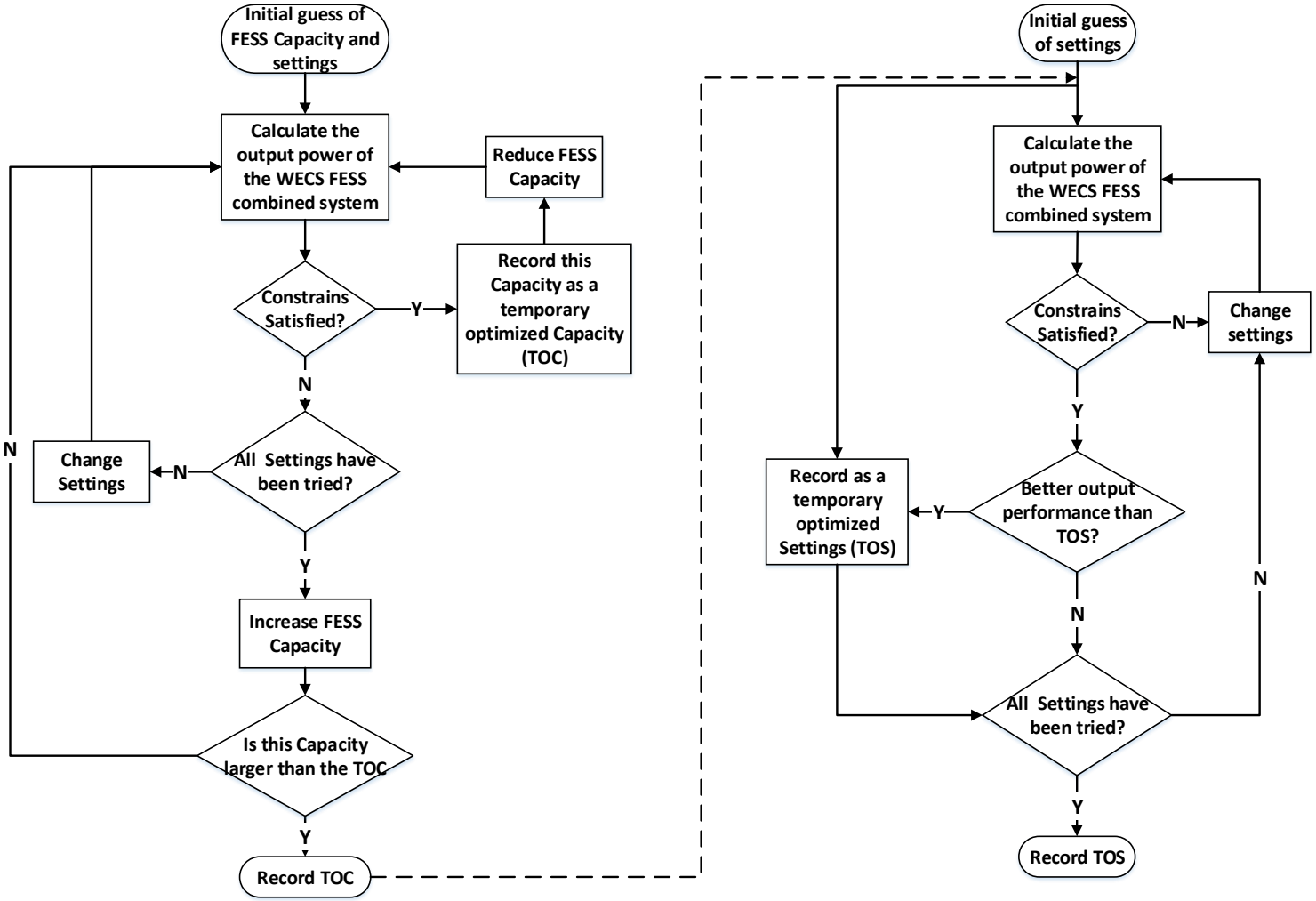

Figure 4.9 FESS Capacity and Combined System Setting points optimization procedure

4.6.4 Case study: WECS/FESS combined system design optimization procedure

A case study is based on the wind speed data recorded by weather station in Wensum England which has been introduced in chapter 2. The statistical model of WECS output and Monte Carlo simulation method have been discussed in chapter 2 as well. This section is going to give the procedure of how to optimize a WECS/FESS. The generator power output data used in the Chapter 5 and Chapter 6 is based on the optimized WECS/FESS combination system.

4.6.4.1 Artificial Wind speed and WECS output generating

The Weibull distribution parameters generated by the moment method for 12 months wind speed of Wensum in year 2014 are listed in Table 4.2.

Table 4.2 Wind speed distribution parameters of Wensum 2014

Month	Weibull Shape Parameter k	Weibull Scale Parameter c
Jan	1.2285	11.6642
Feb	1.3741	15.4889
Mar	1.0725	9.5832
Apr	1.1010	7.6686
May	1.2515	8.9463
Jun	1.0334	6.6980
Jul	1.1169	6.2448
Aug	1.2155	4.5742
Sep	0.9622	3.0555
Oct	1.2695	4.7300
Nov	1.0267	4.4539

Dec	1.6089	6.5354
Annually	**0.9855**	**6.9812**

The artificial wind speed data used for Monte Carlo simulations are generated from the equation (2.49) in chapter 2. The WECS electrical power output depends on the parameters: wind speed, cut in speed, cut out speed, rated speed, rated electrical power output as *(4.6)* which is derived from the equations (2.3) and (2.36) in chapter 2.

$$P_g = \begin{cases} 0 & v_w < v_{cut-in} \\ \dfrac{Av_w^5 + Bv_w^4 + Cv_w^3}{Av_r^2 + Bv_r + C} P_r & v_{cut-in} \le v_w < v_r \\ P_r & v_r \le v_w < v_{cut-out} \\ 0 & v_{cut-out} \le v_w \end{cases} \quad (4.6)$$

Where:

P_g is the electrical power output of the WECS (MW)

P_r is the rated power output of the WECS (MW)

v_w is the wind speed (m/s)

v_r is the rated wind speed (m/s)

A, B, C are three constants which introduced in equations (2.37) and (2.38)

4.6.4.2 FESS capacity and the settings of WECS/FESS combined system optimization

There are some experiences based initial guessing rules can accelerate the optimization procedure. The guessing of P_1 is start from half of average

WECS output power. The initial guessed FESS capacity value $C_{initial}$ is equal to the rated power of WECS. As the reservation is needed for preventing stopping, C_{min} is larger than $\frac{P_1 * P_r * 0.25}{0.9} \Big/ C_{initial}$. The guessing value of C_1 is between twice C_{min} and 50%.

The objects and constraints of this optimization is: minimum combined system output over 50% average output level of standalone WECS with over 99% reliability, and the achieve the smallest variance.

4.6.4.3 Simulation results

Table 4.3 gives the optimization results for a 2MW rated WECS and FESS combines system. The individual FESS capacity is the smallest capacity which meets the constraints for each month individually. The numbers in the brackets are the C_{max} values without reservations. The final FESS capacity is the capacity capable for whole year. The optimized setting points are calculated with the final FESS capacity. P_1, P_2, P_3 are percentage value of the rated power output of the WECS. C_1, C_2 are percentage value of the C_{max}. Re is the reliability of this combined system with the optimized settings. The minimum FESS capacities are calculated by 10000 times repeat Monte Carlo simulation. The optimized setting points, optimized variance and reliabilities are calculated by 100000 times repeat Monte Carlo simulation. Better results could be existed with more repeat times.

Table 4.3 Optimized settings and FESS capacity for a 2MW rated WECS

Months	**Individual FESS Capacity (MWh)**	**Final FESS Capacity (MWh)**	P_1	P_2	P_3	C_1	C_2	**Re**	**WECS Variance**	**Combined system Variance**
			%							
Jan	1.1580(0.85)	1.35(0.95)	19.91	25.93	34.04	48.66	51.23	99	0.7598	0.2394
Feb	1.1698(0.85)		20.51	26.41	31.77	50	52.5	99.09	0.7835	0.2655
Mar	1.0667(0.75)		19.54	24.11	29.70	50	52.5	99.01	0.7523	0.2760
Apr	1.1095(0.8)		17.21	22.13	27.92	50	52.5	99	0.6922	0.2293
May	1.1363(0.8)		17.09	22.02	30.72	50	52.5	99	0.6878	0.2134
Jun	1.1129(0.8)		16.25	19.63	25.67	50	52.5	99.06	0.6622	0.2448
Jul	1.1986(0.85)		14.23	16.02	25.62	50	55	99.14	0.6041	0.2288
Aug	1.3197(0.95)		8.81	10.87	21.24	50	52.5	99.05	0.3836	0.1061
Sep	1.3120(0.95)		6.54	8.72	12.28	50	55	99.09	0.2862	0.0827
Oct	1.3197(0.95)		8.56	10.63	17.57	50	52.5	99.03	0.3887	0.1142
Nov	1.2636(0.9)		10.65	12.62	19.35	50	52.5	99.03	0.4722	0.1666
Dec	1.2148(0.85)		9.79	11.8	18.62	50	55	99.02	0.4388	0.1480

The WECS and combined system output distributions generated from the Monte Carlo simulation is given in Figure *4.10*. The blue line indicates that the standalone wind power generator system has over 35 percentage probability outputs no power. It keeps generating the maximum power in around 30 percentage intervals. Besides, the output power variates from 0 to 2 MW at the rest part. This performance characteristics makes the power quality of a microgrid with the standalone WECS very difficult to regulate. When a well-tuned WECS/FESS combined system formed, the output has over 85 percentage probability drops in the interval from 0.4 to 0.68 MW. This interval is less than 1/7 of original variation room. The chance without output power is reduced to less than 1 percentage probability. The heavy variation probability also be limited in less than 4%. The combined system output 2MW rated power for the rest 11 percent chance. This less fluctuation feature makes this combined system be friend to regulation. Meanwhile, the purple dashed line indicates the energy stored in the FESS. The probability is close to evenly distributed, which means it is used efficiently.

Alternatively, the annual combined system performance characteristics with the rest 11 months are given in *Figure 4.11*. The dashed lines represent the standalone WECS outputs and the dotted lines represents the energy stored in FESS. The solid lines are the combined system outputs. It is easy to figure out, the average power outputs are different for each month as the wind speed characteristics not the same. With the optimized settings, the combined system output of all the 12 months are narrowed in relatively small intervals for over 80 percentage probability. These results demonstrate the variance improvement listed in Table 4.3. The variances

of combined system reduced to around 1/3 of standalone WECS for all 12 months.

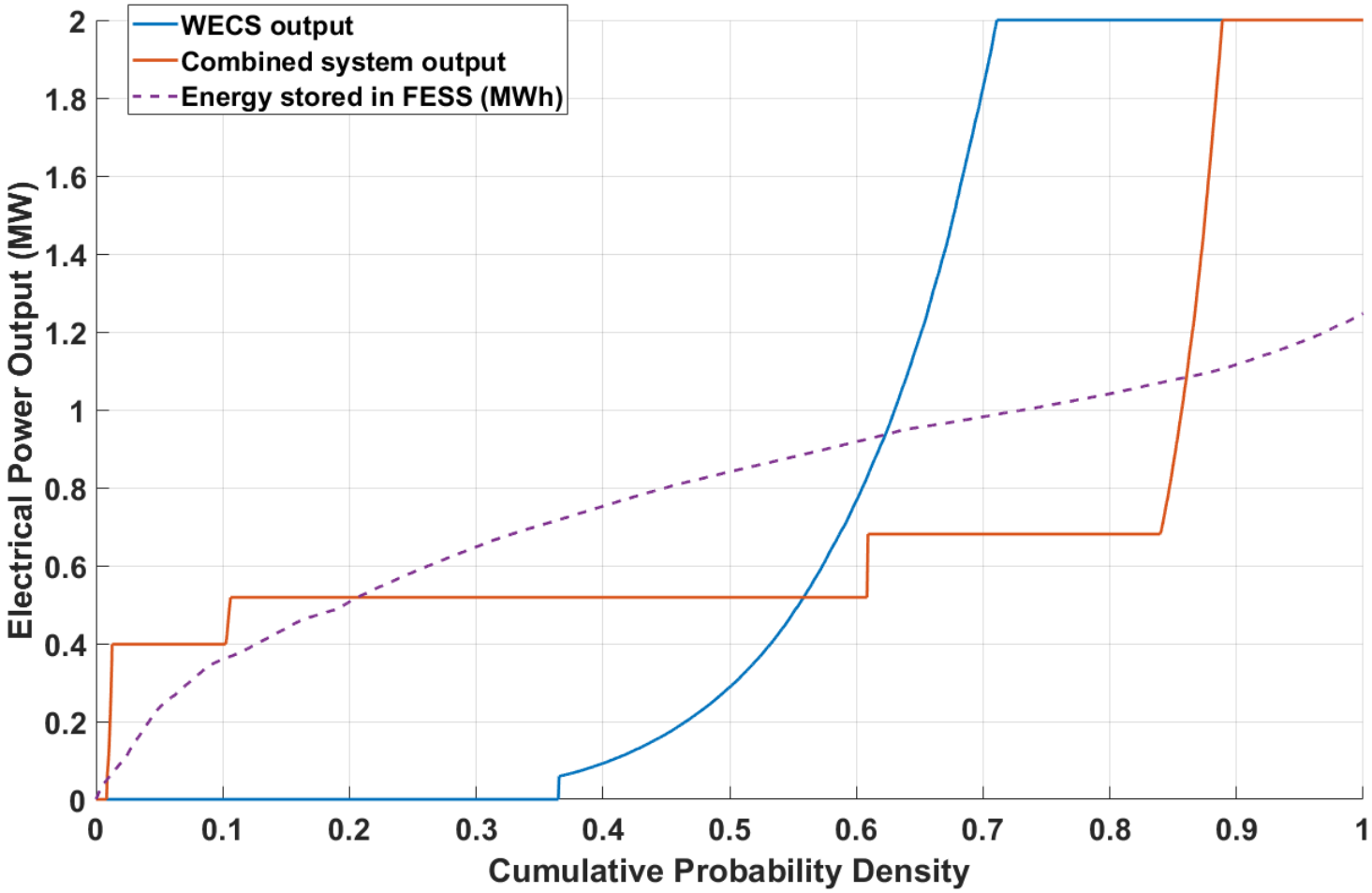

Figure 4.10 Power output distribution of Wensum in January 2014 by 1000000 repeats Monte Carlo Simulation

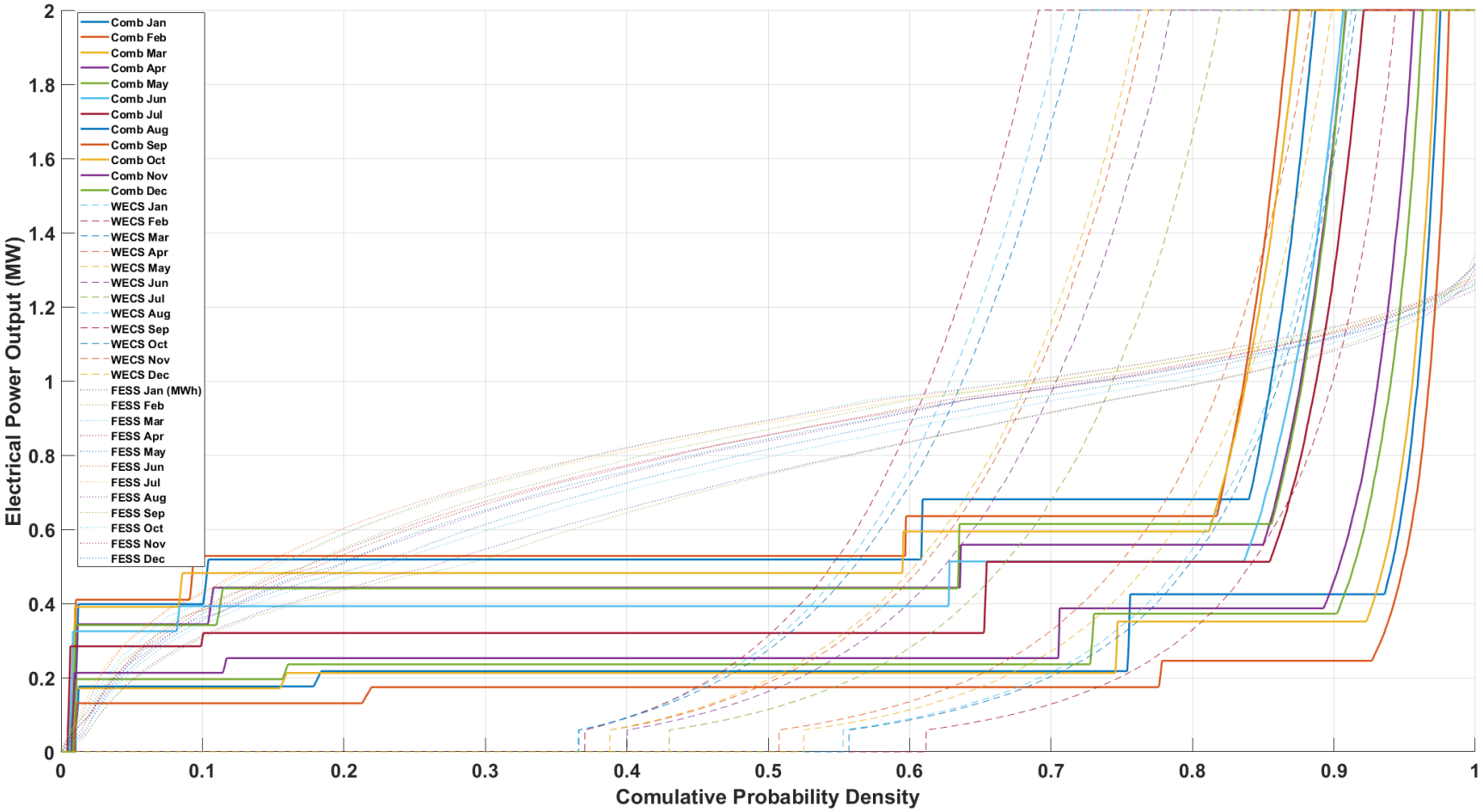

Figure 4.11 Annual power output Probability distribution of Wensum 2014

4.7 Simulation results and discussion

4.7.1 Simulation model description

In this section, a simple low voltage level microgrid which is used to evaluate the proposed control theory and built in MATLAB/Simulink is shown in *Figure 4.12*. The MATPOWER toolbox is used for the power flow calculation. This microgrid is connected to the main grid through a transformer. There are three inverter-based DGs in this test model. G2 and G3 represent two WECS/FESS combined DGs. The power output of them do not automatically change when the loads vary. G1 is the backup unit which regulates the power exchange between the microgrid and the main grid in connected mode and plays the master unit role when islanded. Load 2 and load 3 are two local loads attached on the WECS local buses. Load 1 can perform step changes of demand as it consists of 4 individual loads. The main parameters of this test system are given in Table 4.4.

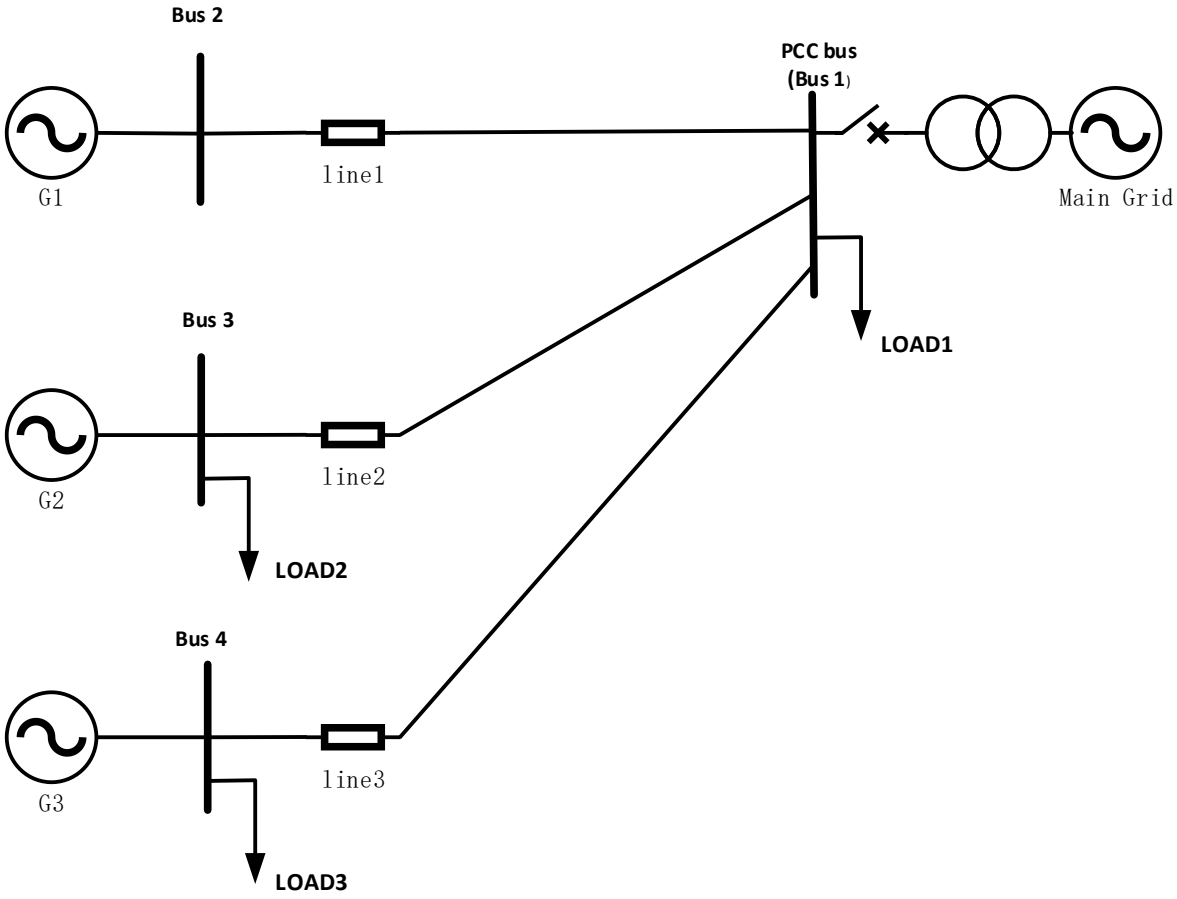

Figure 4.12 A simple 3-DG 4-Bus microgrid structure

Table 4.4 Test system parameters

DGs	DG type	Operating mode
DG1	Backup Generator	Constant V/Constant Power
DG2	WECS/FESS Combined	Constant Power
DG3	WECS/FESS Combined	Constant Power

Branches	Resistance ($p.u.$)	Reactance ($p.u.$)
Line 1	0.0313	0.0029
Line 2	0.1563	0.0982
Line 3	0.1563	0.0982

Demands	Active power (kW)	Reactive power ($kVar$)
Load 1	50*4	5*4
Load 2	50	0
Load 3	50	0

System frequency	Base voltage (phase-phase)	Base MVA rating
50Hz	400 V	*50* kVA

Figure 4.13 shows the block diagram of the DGs' level 1 controllers built in the MATLAB/Simulink model. There are seven input parameters for this controller: DG bus voltage V_o, DG bus current I_o, initial voltage

magnitude, active power output reference, frequency reference, initial voltage angle and reactive power output reference. V_o and I_o are gathered from the DG bus. The other five parameters come from upper level controllers.

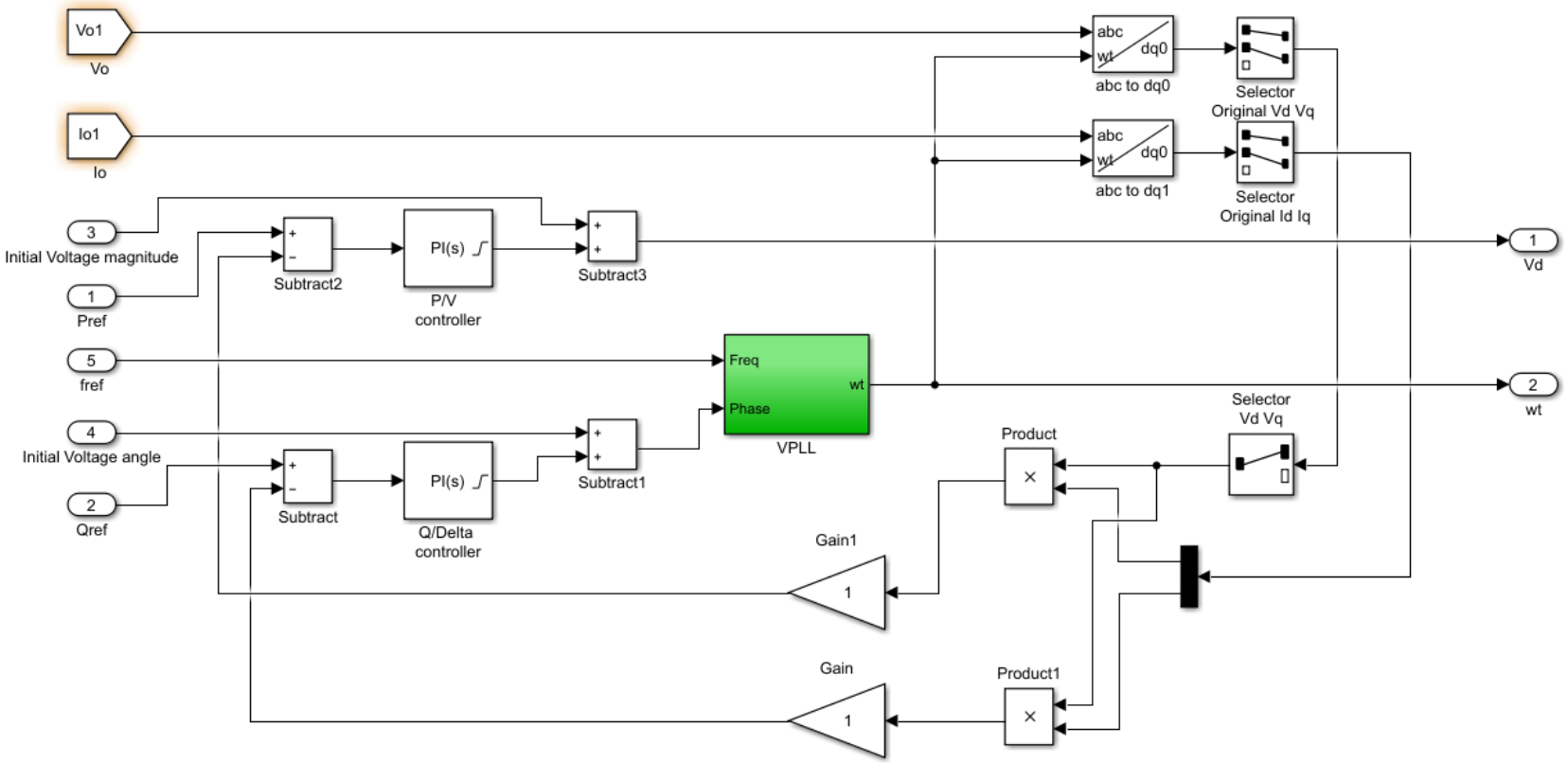

Figure 4.13 Controller block for the DGs

There are two control loops in this controller: P/V control loop and Q/δ control loop. The settings of these controllers for each DGs are given in Table 4.5.

Table 4.5 Level 1 controller settings

DG	Controller	Proportional (P)	Integral (I)	Upper saturation limit	Lower saturation limit
DG1	P/V	1	1	0/0.03	0/-0.03
	Q/Delta	1	10	0/90	0/-90
DG2, DG3	P/V	0.5	10	0.03	-0.03
	Q/Delta	5	500	inf	-inf

There are two parameters generated by this controller: voltage magnitude V_d and instantaneous phase angle signal wt. These two parameters are used as the references for generating the PWM modulation signal. In this section, the backup DG is operated under either constant voltage or constant power output mode. During the constant voltage output mode, the upper saturation limit and the lower saturation limit are set to 0 to makes the output signal the same as the initial input signal. In this case, only the VPLL function in this block is activated.

4.7.2 Scenario 1: Microgrid operated under grid connected mode

In the grid connected mode, the PCC bus is considered as the swing bus. The voltage at the PCC bus can be consider as constant. It makes Bus2, Bus3 and Bus4 be isolated from each other. The DGs' output and load variations on each DG bus do not affect others. The load variations can be supported by the main grid.

4.7.2.1 System reactions with level 1 controllers

In this section, all DG1, DG2 and DG3 are operated in constant power output mode. To present wind speed changes, the active power output of DG2 is initialled with 40 kW and changed to 50kW at t = 1s. Similarly, the DG3 is started with 50kW and changed to 40kW at t = 1.75s, and then back to 50kW at t = 2.75s. This schedule of power output changes is presented in the Table 4.6. This section is designed to test the system automatically reaction for the wind speed variations.

Table 4.6 Experiment schedule

Time Scales	Output of DG1	Output of DG2	Output of DG3
0-1s	200kW/10kVAr	40kW/0VAr	50kW/0VAr
1-1.75s	200kW/10kVAr	50kW/0VAr	50kW/0VAr
1.75s-2.75s	200kW/10kVAr	50kW/0VAr	40kW/0VAr
2.75s-3s	200kW/10kVAr	50kW/0VAr	50kW/0VAr

The test results are given in Figure 4.14. Whenever the output of DG2 and DG3 increased or decreased, only the main grid power flow follows the changes. The DGs in this microgrid with the proposed de-centralized control theory can reach the steady state within 0.2 second with accurate reference tracking. Both active power and reactive power output of DGs are regulated without deviations.

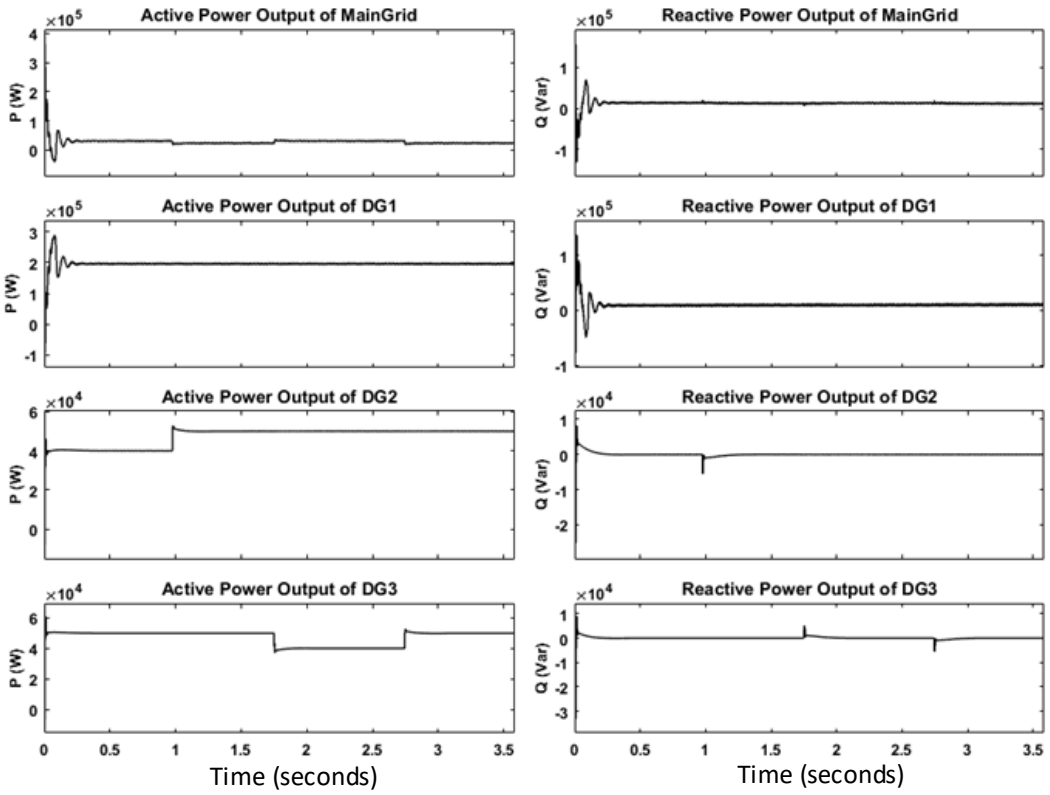

Figure 4.14 DG output power variations

4.7.2.2 System reactions with level 2 controllers

In practical applications, rather than keeping the output of DGs within the microgrid constant, the constant power exchange at PCC is preferred. However, with the standalone level 1 controllers, only the power output of the DGs can be guaranteed. The deviation compensation approach which eliminates the power exchange deviation is applied to maintain the objective power exchange at PCC. In this section, as it is representing a relatively short time period, the DG2 and DG3 which are two WECSs are assumed constantly generating 75kW and 50kW respectively. The compensation is achieved by tuning the output of DG1.

Figure 4.15 shows the system reactions on exchange power regulation. The object is absorbing 50kW active power and 0 reactive power from main grid. The test system started with an initial guess calculated by MATPOWER. The active power is well performed with the initial guess references. There is less than 10% more active power supplied from the main grid compared with the object. However, the reactive part is far away from the scheduled value. With four times repeat compensation procedure which processed by the level 2 controller, the reactive power absorbed from the main grid successfully reached 0. The active power generated from the main grid became exactly 50kW. Furthermore, there is no impact on the output regulation of DG2 and DG3 during the compensation procedure.

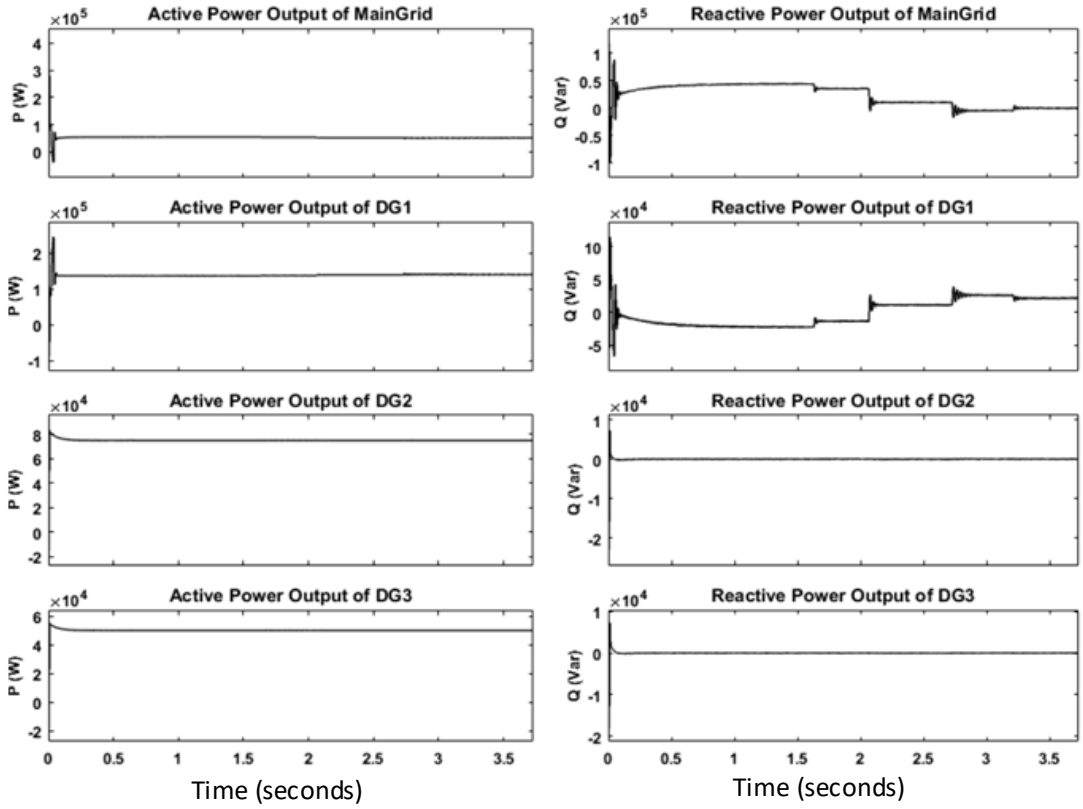

Figure 4.15 Grid exchange power regulation

4.7.3 Scenario 2: Microgrid operated under islanded mode

When this microgrid is switched to islanded mode, the backup DG (DG1) will be operated in constant voltage mode. The operation tested in this model is scheduled in Table 4.7 as two sections: only decentralized controllers activated and cooperated with higher level controller. In contrast to the grid connected mode, the voltage at PCC bus is constant. The DGs in the microgrid are not isolated from each other anymore. A set of system behaviours including power output of each DGs and the voltage variations on each bus during islanded period are presented in Figure *4.16* and Figure *4.17* respectively. As the microgrid was disconnected from the main grid, the power from main grid was kept 0 during all the time periods.

Table 4.7 Schedule of operating actions

Time scales		**Actions**
Section 1: Only decentralized control applied	0-0.5s	System initialization
	0.5-1s	Drop ¼ Load 1
	1-1.5s	Drop another ¼ Load 1
Section 2: Assisted with control level 2	1.5-2s	System parameters renewed
	2-2.5s	Reduce DG2 output
	2.5-3s	Continuously reduce DG2 output

4.7.3.1 System reactions with control level 1

This section is scheduled from t = 0s to t =1.5s. In this section, only decentralized local controllers without communication are applied. This simulation system was initialized in the first 0.5s. The output of DG2, DG3 were set to 100 kW/0 VAr and 75 kW/0 VAr respectively. This microgrid became steady state within 0.2s. Demands were well shared among DGs.

At the time point of 0.5s, one of the four individual loads in Load1 was disconnected. This event was successfully dealt without the help of centralized controller. There were no active and reactive power output deviations of both DG2 and DG3. Another ¼ of Load 1 was dropped in the next 0.5s period. This amount of load changes was over the capability of this system with standalone level 1 controllers. Although the voltage of DG3, the active power of DG2 and the reactive power were still well regulated. There was an active power shift of DG3. The DG1's bus (bus2) voltage was maintained constant during all the time periods. The voltage on the other two DG buses were increased following the droop control characteristics.

The results show the standalone decentralized control method has the ability deal with a certain level of system changes. However, it has the limitation which cannot guarantee good performance when system parameters heavily changed.

4.7.3.2 System reactions with control level 2 assisted

The control level 2 was introduced in the time interval (1.5s, 3s). At t = 1.5s, the new references settings were calculated and posted to the local controllers. The DG1's output voltage reference was changed to 0.95 p.u.. The system with new references became stable within 0.3s. The active power output of DG3 was recovered to the original objective value of 75 kW.

To simulate the WECS output variations, in the next 1s, the active power output object of DG2 was manually reduced to a half of the original value with two steps. To maintain the system stability, the bus voltage reference of DG1 was changed to 1.0 p.u.. The output voltages of DG2 and DG3

were modified when the power flow changed. In this scenario, when the power output of DG2 changed, the power gap was provided by DG1, and the power output of DG3 kept constant.

The simulation results show that, with the assistant of level 2 controller, the bus voltages and power outputs of all DGs were well regulated during all time periods. The system stable operating range was greatly expanded with the control level 2 introduced.

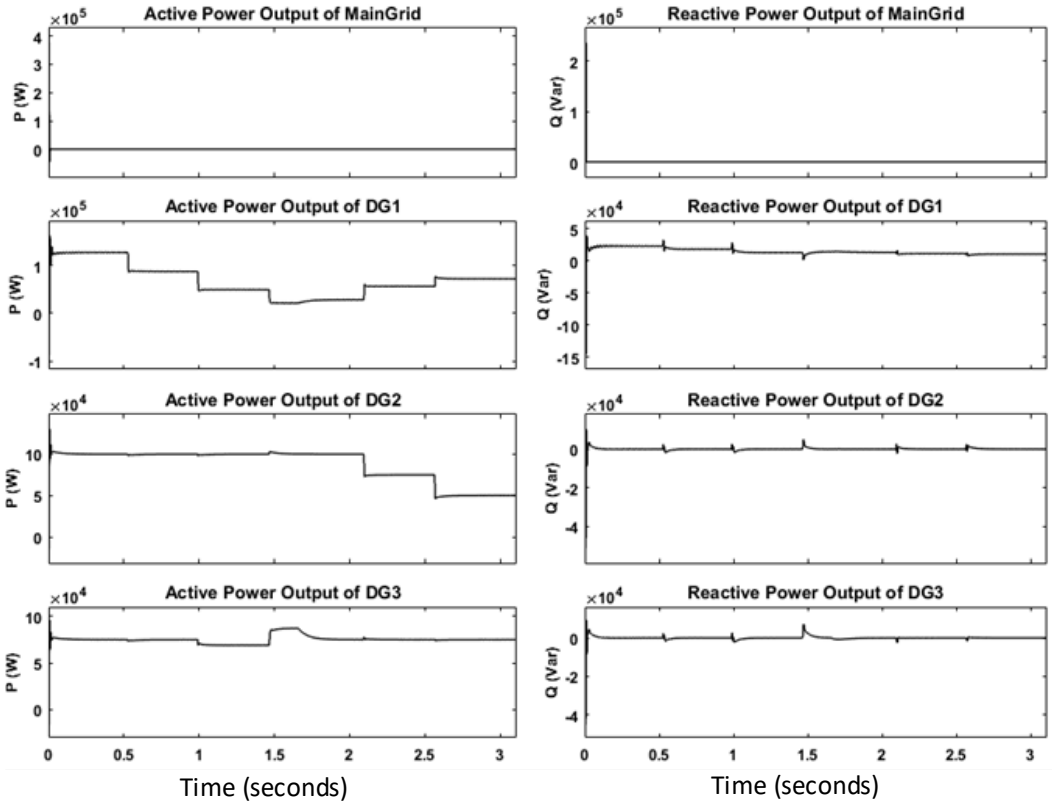

Figure 4.16 DG output during islanded periods

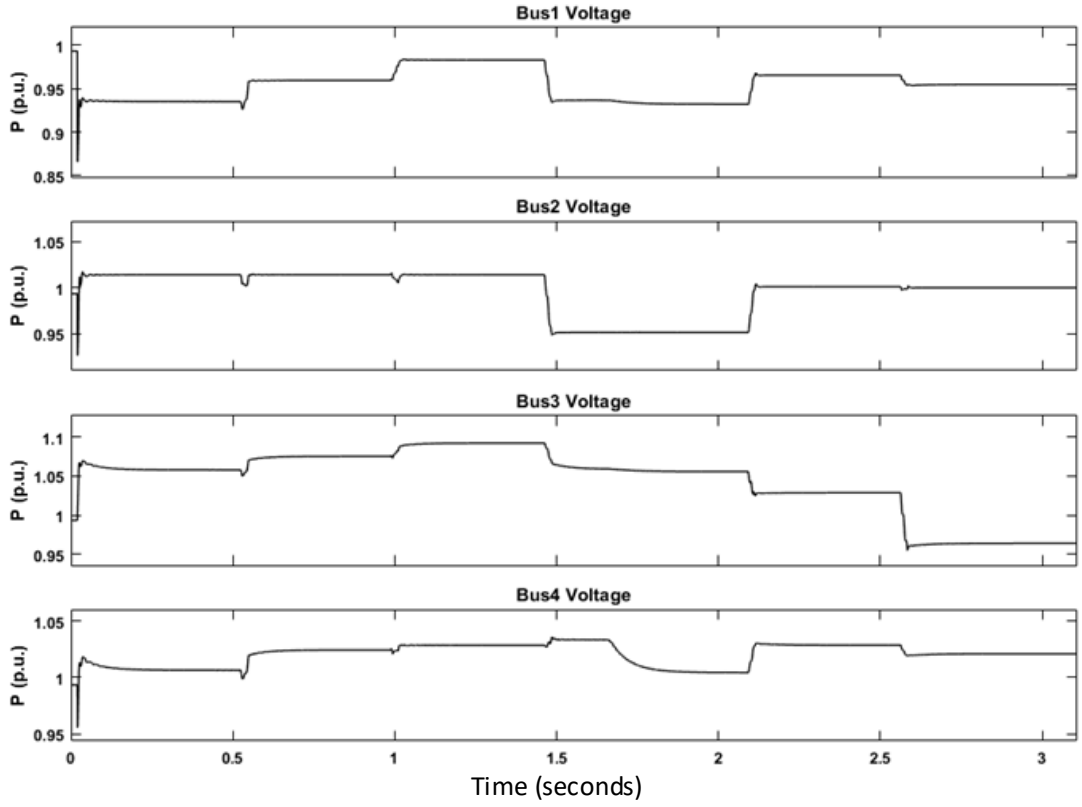

Figure 4.17 Bus voltage during islanded periods

4.7.4 Scenario 3: Microgrid reconnection from islanded mode

In this section, the microgrid is reconnected to the main grid from islanded state. This smoothly transition is achieved by applying a compensation operation. This operation tracks the main grid side voltage magnitude and phase angle at the PCC bus, and makes them as the control objectives for the voltage magnitude and phase angle at bus 1. As the reconnecting operation happened in s short time period, the DGs output and load variations are neglected. Figure 4.19 gives the overall simulation results of the output of each DGs and the buses' voltages.

The simulation initialized and stabled in the first 0.1s. Then the voltage regulation for smooth reclosing was started at the time point 0.4s. The

system reached the steady-state point within 0.1s. After that, the microgrid was reconnected to the main grid at t=1s.

The voltages at each bus and output of each DGs kept the same during transition period. There is almost no impact to either the main grid or the microgrid during the reclosing time point. The smooth transition function is achieved as there are not voltage differential on the two sides of PCC.

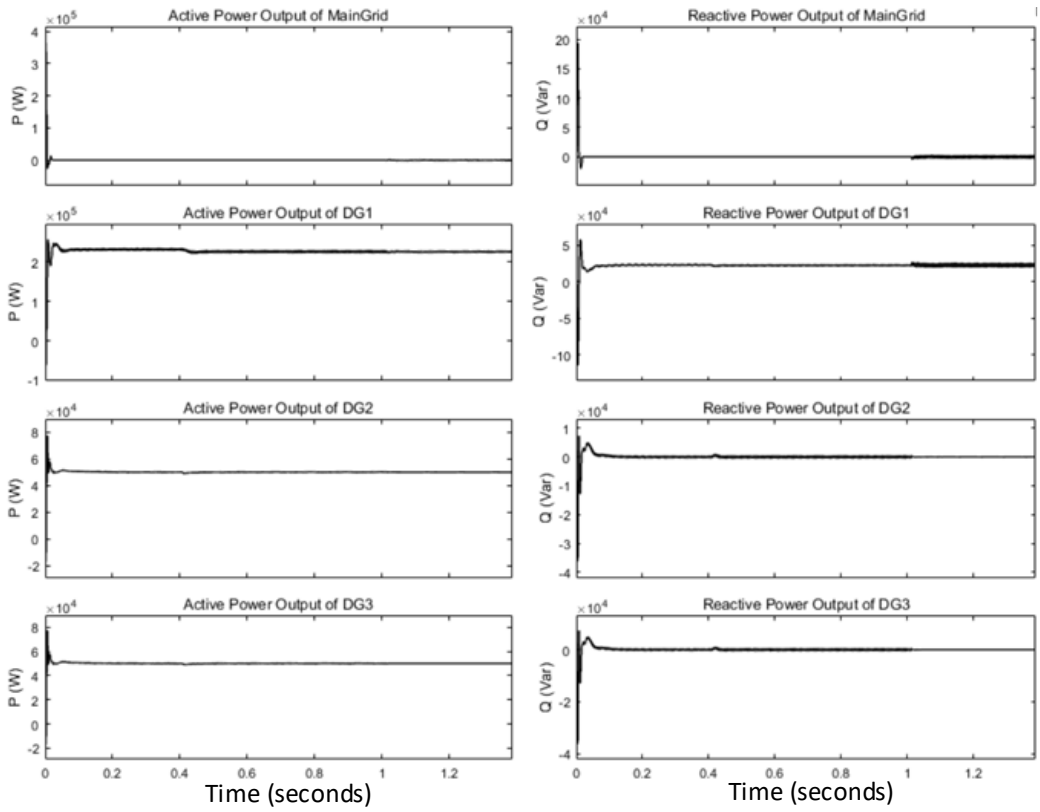

Figure 4.18 DG output during reconnection period

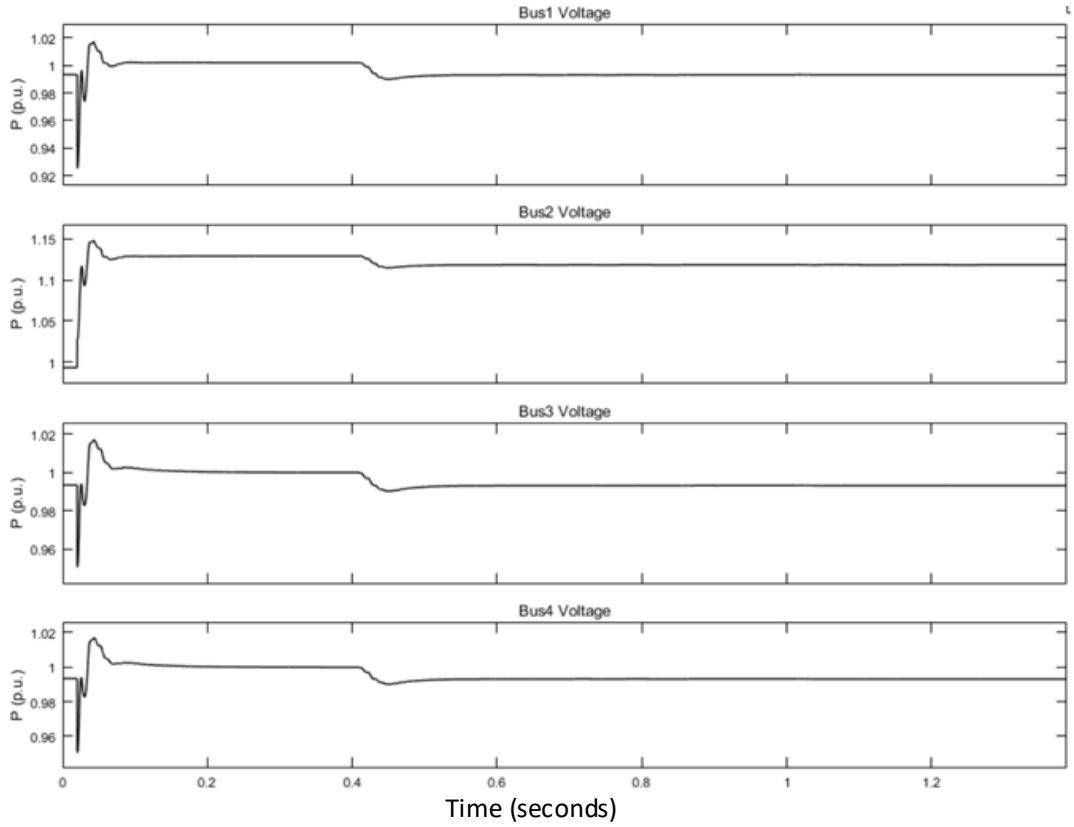

Figure 4.19 Bus voltage during reconnection period

4.8 Summary

The specific enhanced hierarchical control system designed for WECS embedded microgrid is introduced in this chapter. A modified P/V and Q/δ control method with GPS synchronized VPLL is applied in the level 1 control system. The backup DG operated with either grid supporting mode in connected running period or constant voltage output mode in islanded microgrid. The WECSs are always running in constant power output mode. A 4-bus microgrid model built in MATLAB/Simulink is used to evaluate this control system. The simulation results show that this decentralized level 1 control performs automatically non-error power output regulation. With this specific control method, there is always no frequency deviation. However, to maintain the system stability and restrict the voltage deviation in a certain

area, there is a limitation of load change capability of this standalone level 1 control system. The simulation results demonstrated that, the control level 2 system which provide power flow regulation and deviation compensation functions eliminates the drawbacks of the level 1 control. The control objects are always well regulated with the cooperation of these control systems in different two levels.

A WECS/FESS combined system which improves the system performance is proposed. The settings optimization procedure is applied in the control level 3. The output variance is reduced to 1/3 of the original WECS after optimized. Besides, the real time optimization functions, such as economic operating and smooth state transition, are applied in this level as well. These functions are achieved by sending compensation requests to the level 2 controller. A simulation result of reclosing procedure demonstrates the good cooperation among the control systems in these different three levels.

Overall, this proposed hierarchical control method is easy applied and robust with the simple level 1 control structure. It is also good at system parameters regulation and function flexible with the assistant of the higher-level control systems. This proposed control system can be extended to any inverter-based energy source with randomly power output as well.

Chapter 5: High wind power penetrated medium voltage microgrid operation in grid connected mode with hierarchical control theory

5.1 Introduction

In this chapter, a 20-Bus medium voltage level(11kV) microgrid is built in MATLAB/Simulink to evaluate the proposed hierarchical control theory of microgrid. In Section 5.2, the main components of this microgrid including load, DG and distribution line are described separately. There are two groups of loads in this model: industrial load and residential load. The 24-hour pre-set load curve is applied in the experiment. DGs in this microgrid are also divided in two classes: the diesel generator which is used as the backup generator and the WECS/FESS combined generator. As the microgrid is normally geographically small, the underground cables are chosen as distribution lines.

In the wind power embedded microgrid, the behaviour of the system is depending on the wind speed and demand states. In contrast to operation with a constant power exchange rate, to operate under a schedule which has relatively low requirements for backup capacity would be more cost effective. Section 5.3 gives the analysis for the microgrid operating schedule based on the wind speed statistical model which has been introduced in Chapter 2. A case study introduces how to derive the operating schedule for the simulation microgrid is presented in this section. The schedules for different months are presented in the results as well.

The simulation results and discussion are given in subsequent section. The experiment includes two scenarios: 24-hour overall running result, and the system performances with precise control in a specific time period. The

first scenario evaluates the long-term system stability and prove the feasibility of the power exchange schedule which is proposed in the previous section. The second scenario is focused on the control accuracy and robustness. Both the voltage magnitude and frequency on PCC bus variations are introduced in this scenario. The last section gives the summary.

5.2 Simulation microgrid system configuration

The microgrid model presented in Figure 5.1 consists of 4 DGs, 11 loads, 20 buses, 19 branches, an infinite generator representing the main grid and a number of circuit breakers. Per unit values are used in the input signals for the control system. Transformers are not considered in this simulation model. The base MVA value for this microgrid is 5MVA.

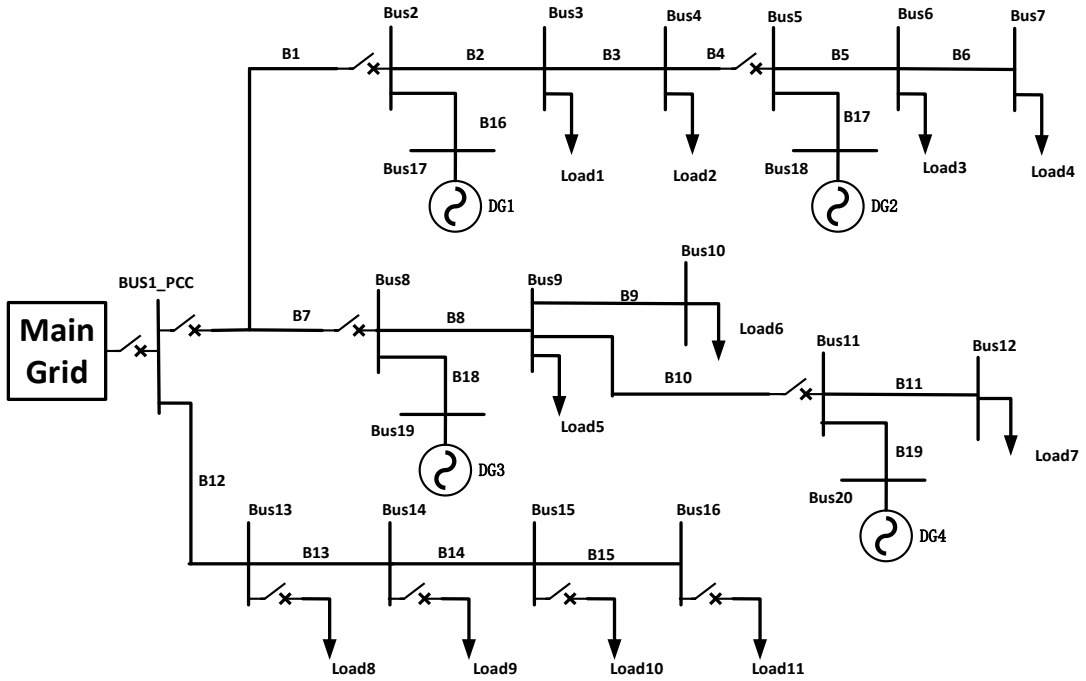

Figure 5.1 Single line diagram of CERTS microgrid model [26]

5.2.1 Loads in the simulation model

There are many well developed demands prediction methods [128, 129]. A load variation model based on the daily load curve characteristics is used in this chapter. Figure *5.2* gives two typical daily load curves for industrial load and residential load. The machines in industrial factories usually start warming up from 5am. The demand reaches the peak value at 8am as the workers come on duty. It falls a little during the lunch time around 1pm. This industrial load backs to the full-load condition till 6pm. After that, people are leaving for home, and only part of the industrial load are still running during evening time. Alternatively, the residential load keeps on a low level as people works on daytime. It grows from 6pm because people start leaving job and back home. The residential load reaches its peak value around 10pm. Then it decreases as people go to sleep. In some temperate climate countries, such as China, the residential demand in summer is higher than it is in winter because of air conditioning load. By the same time, in high latitude countries such as UK, the heating load in winter makes the winter curve over it in summer. In this study, the differences between countries is not considered.

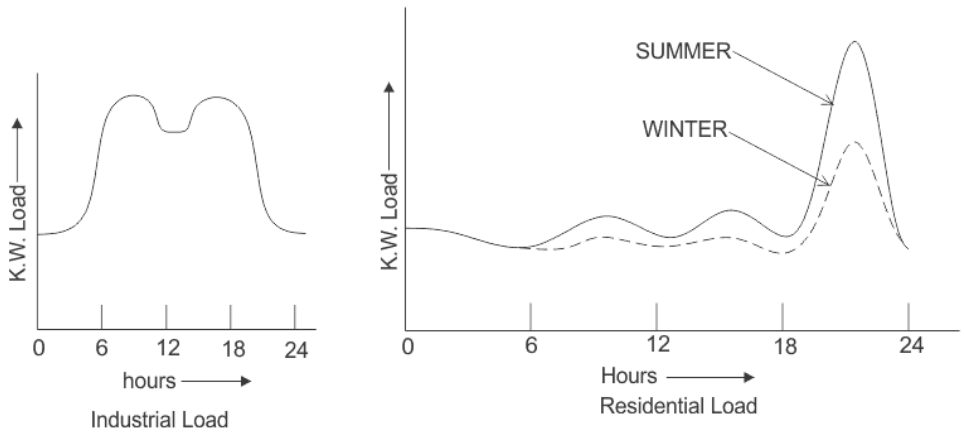

Figure 5.2 Daily industrial and residential load curve [130]

In this MATLAB/Simulink simulation model, loads 1-7 are the inelastic industrial loads. They must be supplied in any situations. To reduce the power losses and voltage drops on the transmission lines, the reactive power consumption of them are usually supplied locally by the reactive power compensation devices such as SVC. Loads 8-11are the residential loads. Each of the residential loads contains normal loads and controllable loads. The controllable loads can be either plugged in or dropped off. They could be washing machines, fridges, heaters, batteries or electrical vehicles etc. A bilateral contract usually needs to be signed to control this type of load [131]. A flatter total load curve can be obtained by properly modifying the controllable load. To simulate the load variations, each of the load models consists of 4 sub-loads L1, L2, L3 and L4 as *Figure 5.3* shows. Alternatively, the different sub-loads configurations are given in Table 5.1.

Table 5.1 Load configurations

Industrial Loads			
Load 1-Load 7 (each load consists of the following)			
On/off	On/off	On/off	On/off
0.15MW	0.15MW	0.15MW	0.15MW

Residential Loads			
Load 8 (consists of the following)			
Random	On/off	On/off	Controllable
0.2MW	0.2MW	0.2MW	0.4MW
Load 9-Load 11 (each load consists of the following)			
On/off	On/off	On/off	Controllable
0.2MW	0.2MW	0.2MW	0.4MW

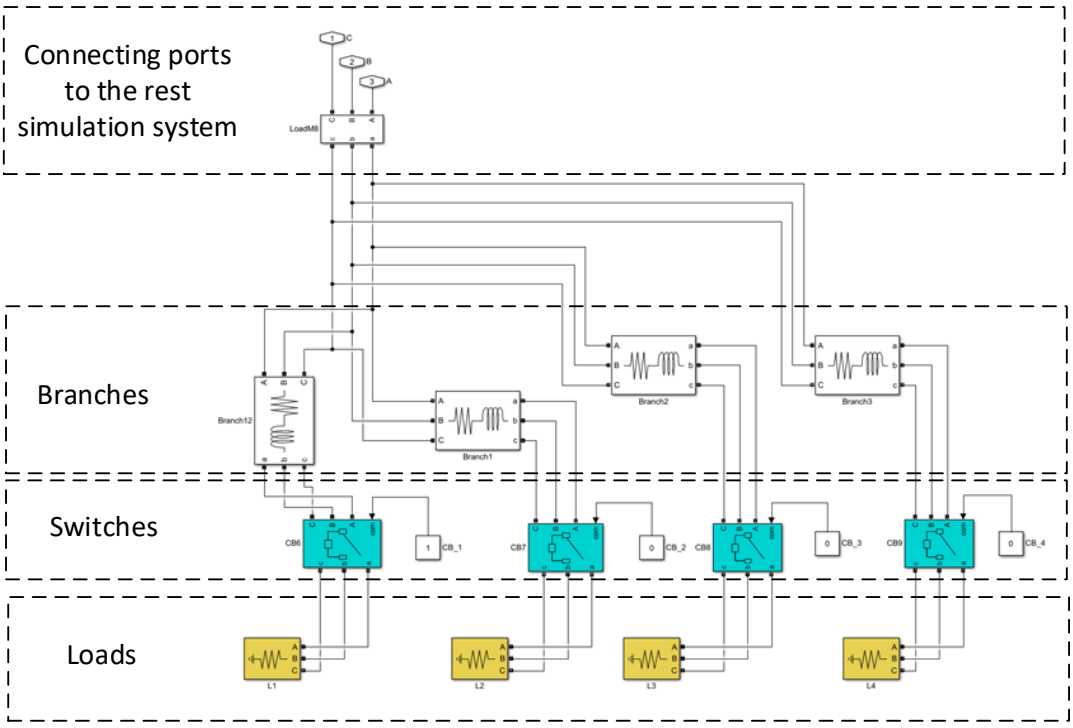

Figure 5.3 Load model in MATLAB/Simulink

Each of the industrial loads in this simulation model is consisted of four 0.15MW loads. The minimum situation for industrial load is that only one of the four loads is connected. Alternatively, the residential load is a combination of three 0.2MW normal loads and one 0.4MW controllable load. The 24-hours demands of both industrial and normal residential loads in this simulation system are concluded in Table 5.2. There are randomly load variations for the residential load as the plug and play function supported in the microgrid concept. In this section, a 0.2MW load of Load8 is randomly added in or dropped off to represent these situations. The minimum situation for Load8 is 0. The load curves of individual and total loads are plotted in *Figure 5.4* alternatively. As the Total load curve shows, the total demand remains at a very low level during the period of 23:00 to the next day 6:00, picking up controllable loads in this time period is cost effective.

Table 5.2 24-hours load schedule

Time periods	**0:00-6:00**	**6:00-7:00**	**7:00-8:00**	**8:00-12:00**	**12:00-14:00**	**14:00-18:00**	**18:00-19:00**	**19:00-20:00**	**20:00-21:00**	**21:00-22:00**	**22:00-23:00**	**23:00-0:00**
Individual Industrial load (MW)	1*0.15	2*0.15	3*0.15	4*0.15	3*0.15	4*0.15	3*0.15	2*0.15	1*0.15			
Individual Residential load (MW)	1*0.2						2*0.2	2*0.2	3*0.2		2*0.2	1*0.2

**there is randomly plug and play variation for Load 8 as described in Table 5.1*

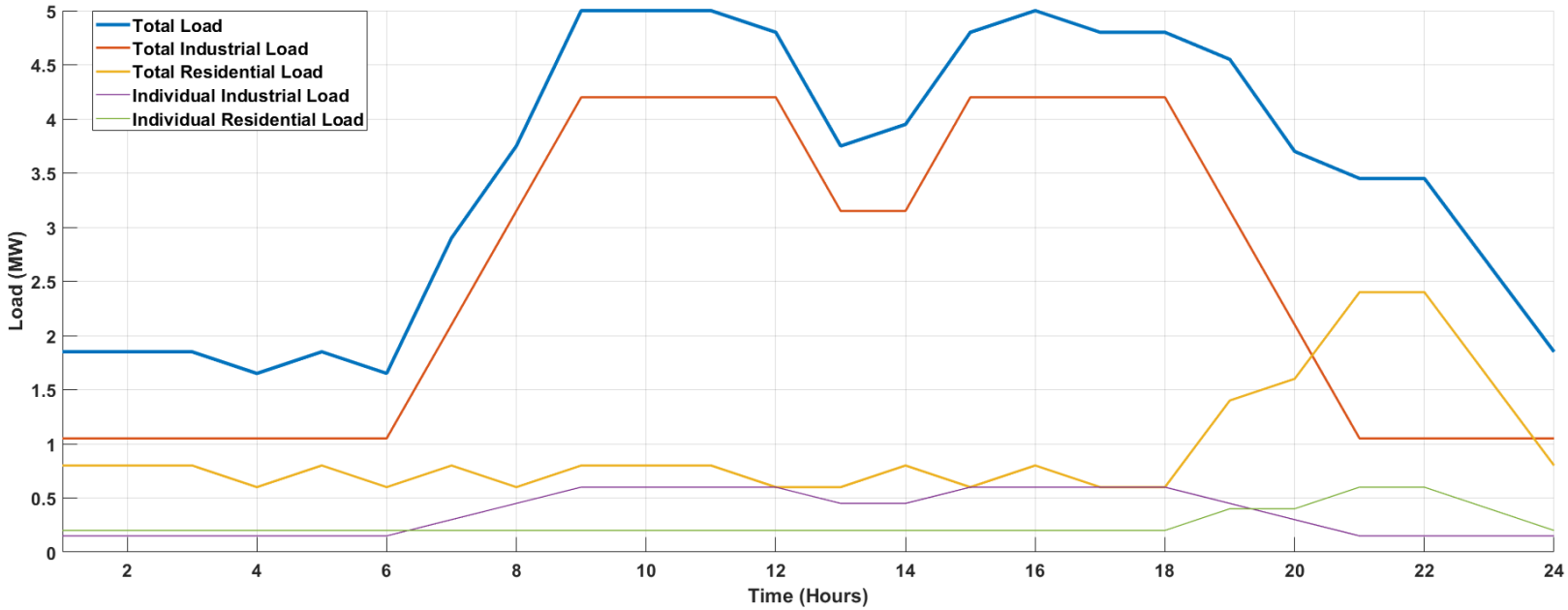

Figure 5.4 Daily load curves of the simulation microgrid system

5.2.2 DGs in the simulation model

5.2.2.1 Backup DG

There has to be a backup generator to provide the system voltage level and/or frequency reference in an islanded microgrid. It also feeds the power supply and demand gap to assist better power regulation at PCC when the microgrid operated in grid connected mode. To achieve fast and good voltage regulation on the PCC, the backup DG should be placed close to the PCC bus. In this case, DG1 which is a diesel generator the installed capacity of 2MW plays the role of backup DG. The operating feature of DG1 is based on the FG WILSON P2000/P2250E diesel generator set [132]. It has two operating mode, prime and standby. The prime mode can be continuously operated and capable for 10% overload running for 1 hour every 12 hours. The fuel cost with class A2 diesel fuel for this type of generator is given in Table 5.3. Due to the equipment safety requirements, when this diesel generator is operated in standby mode, it is normally operated above 50% rated power output.

Table 5.3 P2000/P2250E fuel cost in prime running mode [132]

%load	110%	100%	75%	50%
Fuel cost (L/hr)	483.4	422.8	311.5	212.2

The diesel fuel price in UK is around 120 pence per liter [133]. When it is running with unit power factor, the generator cost of this diesel generator can be simply presented in a third order function as *(5.1)*.

$$\text{Cost} = 91P^3 - 380P^2 + 756P - 213 \qquad (5.1)$$

Where:

Cost is the generation cost, in this chapter, it is equal to the fuel cost (Pound/hour)

P is the real power output of the diesel generator (MW)

Figure 5.5 is the fuel cost curve plotted based on the equation *(5.1)*. The four points on the curve are the prices derived from the fuel cost data in Table 5.3 multiply by 1.2 Pounds/liter. It can be observed from this figure that the generator cost function expression fits these four points well. The generating cost of this type of diesel generator is between 250 £/MWh and 580 £/MWh. According to the report published by the Department for Business, Energy & Industrial Strategy, in year 2017, the UK average industrial electricity prices including tax for small (consuming 20-499 MWh per annum), medium (consuming 2,000-19,999 MWh per annum), large (20,000-69,999 MWh per annum) and extra-large (consuming 70,000-150,000 MWh per annum) consumers are 125.5 £/MWh, 103.9 £/MWh, 103.4 £/MWh and 102£/MWh respectively [134]. All these industrial energy prices are much less than the generating cost of the diesel generator, in case of that, the electrical power generated by diesel generator has the relatively low priority to maintain the microgrid system be economically operated.

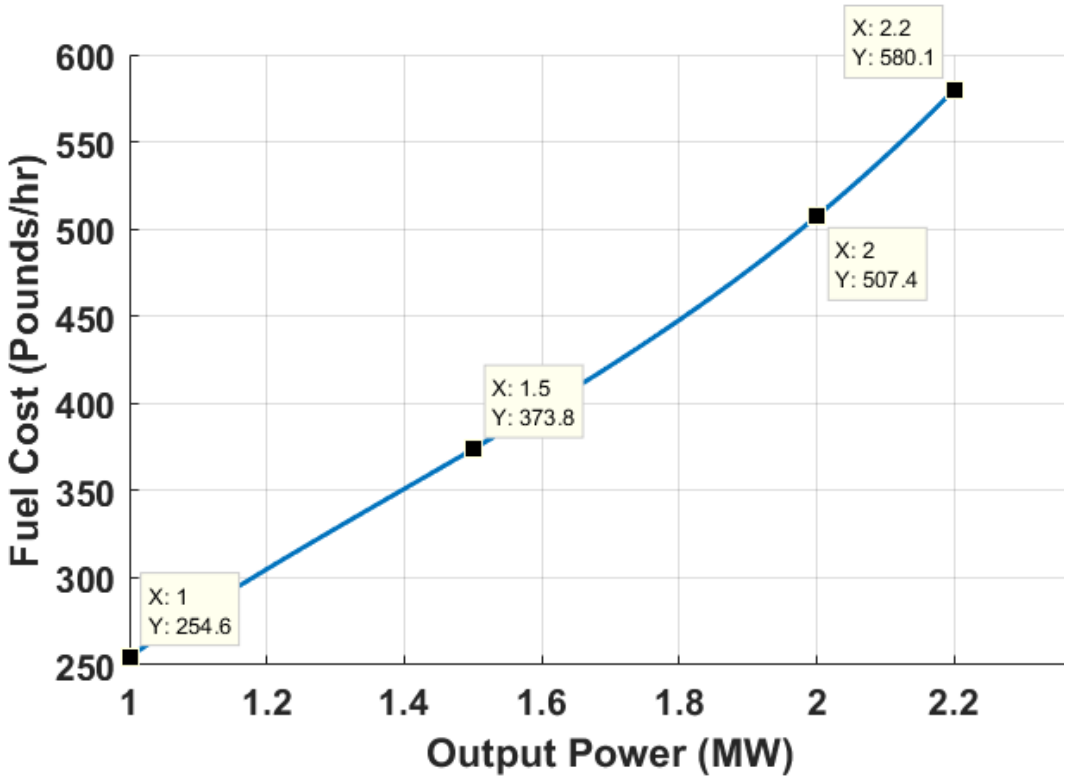

Figure 5.5 Fuel cost curve of the diesel generator

5.2.2.2 Wind power DGs

DG2, DG3, DG4 are the WECS and FESS combined generation systems which is proposed in chapter 4. The Vestas V150-4.2MW^{TM} IEC III B model WECS is utilized. It has the features of cut-in wind speed 3 m/s, rated wind speed 9.1 m/s, cut-out wind speed 22.5 m/s, and rated electrical power output 4MW. The power output data of the WECS here is generated by the artificial wind speed derived from the historical wind speed data of Wensum weather station [31]. The method which is used for generating artificial WECS output is introduced in Chapter 2. In contrast to the diesel generator, the generating cost of WECS can be neglected, the electrical power generated by WECS has the highest priority in the microgrid system.

5.2.2.3 Control block parameters of MATLAB/Simulink model

The DG models built in the MATLAB/Simulink uses the same block diagram which is introduced in the section 4.7 of Chapter 4. The parameters of the controllers are given in Table 5.4. In contrast to the low voltage microgrid in chapter 4, the backup DG is not operating under constant V mode as its installed capacity is relatively small compared with that of the whole system. Hence, the constant voltage level output cannot be guaranteed.

Table 5.4 level 1 controller settings

DG	Controller	Proportional (P)	Integral (I)	Upper saturation limit	Lower saturation limit
DG1	P/V	0.01	1	0.05	-0.05
	Q/Delta	0.1	50	90	-90
DG2, DG3, DG4	P/V	0.05	10	0.03	-0.03
	Q/Delta	1	500	inf	-inf

5.2.3 Distribution lines in the simulation model

The transmission line in this microgrid is built by using the R/L short line model which often applied for distance less than 80km or voltage level less than 20kV [135]. The transmission lines in this simulation model are Nexans three core unarmoured copper conductor underground cables [136]. The line resistance and inductance parameters are given in Table 5.5.

Table 5.6 shows the transmission line impedances of these 19 branches. There are four branches linking the DG bus and the grid, and DG1 is the backup DG which is located close to the PCC bus. Branches B1, B16, B17,

B18 and B19 are relatively short. Branches B2, B3, B5, B6, B8, B9, B11, B12 are relatively long distribution cables. To constrain the power losses and voltage drop with economic consideration, the 3*240 mm^2 conductors are used. The branches B13, B14, B15 connect the four buses with non-critical loads in a relatively small area. As the DG2, DG3, DG4 can provide certain level of power and voltage supports locally, the investment costs of branches B4, B10, B7 can be reduced without causing reliability or power quality problems. The cheaper transmission lines with smaller conductors are applied for these six branches.

Table 5.5 Voltage 6.35/11 (12) kV Three Core unarmored copper conductors [136]

Nominal cross-sectional area (mm^2)	**3*70**	**3*95**	**3*120**	**3*150**	**3*185**	**3*240**	**3*300**	**3*400**
Maximum AC resistance @90℃ (Ω/ km)	0.342	0.247	0.196	0.159	0.128	0.098	0.079	0.063
Inductance (mH/km)	0.396	0.378	0.361	0.351	0.343	0.328	0.316	0.305
Reactance @50Hz (Ω/ km)	0.124	0.119	0.114	0.11	0.108	0.103	0.099	0.096

Table 5.6 Branches impedances of simulation system

Branches	**Conductor diameter (mm^2)**	**Length (km)**	**Impedance (Ω)**
B1, B16, B17, B18, B19	3*400	0.1	0.0063+j0.0096
B2, B3, B5, B6, B8, B9, B11, B12	3*240	1	0.098+j0.103
B13, B14, B15	3*150	0.5	0.0795+j0.055
B4, B10, B7	3*150	1	0.159+j0.11

5.3 Microgrid operating schedule analysis based on the wind speed statistical model

The operating modes analysis in this chapter is based on the WECS model proposed in Chapter 2, the WECS/FESS combination system mentioned in Chapter 4, and the 20-buses microgrid system introduced in this Chapter. To be noticed, for different microgrid systems, the results are not the same. In practical applications, better system performances can be achieved by using more accuracy wind speed and load prediction methods. However, the analysis procedure can be extended for different situations.

5.3.1 Power exchange on PCC

The active power P_{mg} exchanged at the PCC is presented in equation *(5.2*).

$$P_{mg} = P_{backup} + P_G - P_L - P_{rand} - P_{con} - P_{loss} \qquad (5.2)$$

Where:

P_{backup} is the active power generated by DG1 (MW)

P_G is the total active power generated by DG2, DG3 and DG4 (MW)

P_L is the sum of the industrial and residential loads which follow the daily curve (MW)

P_{rand} is the randomly connected load (MW)

P_{con} is the controllable load (MW)

P_{loss} is the transmission line loss (MW)

The range of the parameters in this equation is given in equation *(5.3)*. The transmission line losses are relatively small, and it is highly related to the power flow regulation, to make a simple analysis procedure, the power losses in this section is neglected.

$$\begin{cases} P_{backup} \in 0 \text{ or } [0.8,2.2] \\ P_G \in [0,12] \\ P_L \in [1.05,5] \\ P_{rand} \in [0,0.2] \\ P_{con} \in [0,1.6] \end{cases} \quad (5.3)$$

5.3.2 Microgrid operating modes schedule

The average wind speed varies in different seasons, the mean power output of a WECS is not the same in different time periods. As discussed before, a microgrid can be operated to behave as either a generator or a load. The behaviours of the microgrid with large amount of WECSs installed capacity depend on the wind speed features.

Figure 5.6 gives the 12-months scale parameters of Weibull Distribution which derived from the wind speed data recorded by Wensum weather station in 2014. In January, February, March and May, the scale parameter is over 9, it means the wind power is relatively strong in these months. In these time periods, the microgrid has more chance to behave as a generator unit. Alternatively, in August, September, October and November, with

the weak wind power, the microgrid behaves like a controllable load rather than generator.

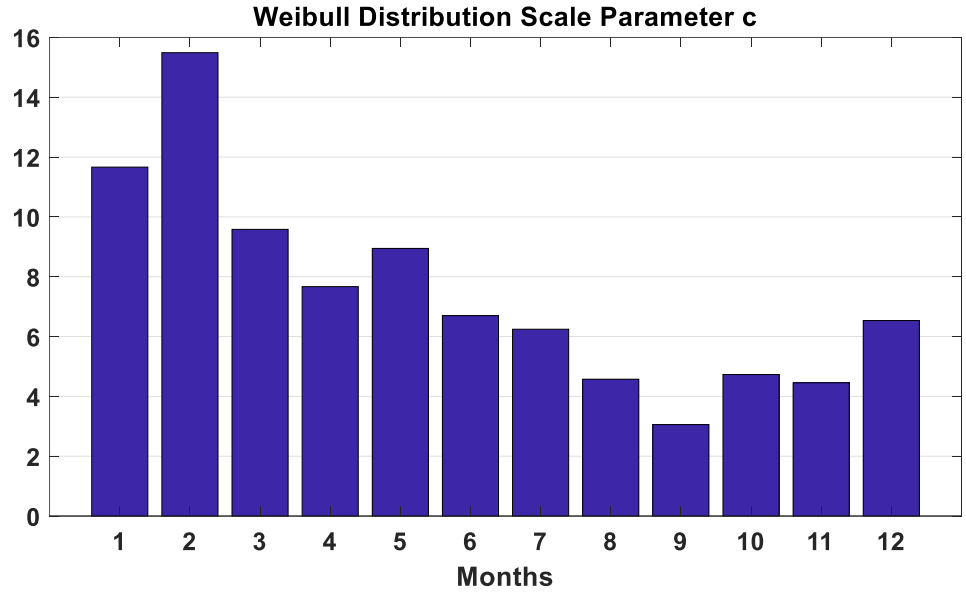

Figure 5.6 12-months wind speed Weibull Distribution Scale Parameter c of Wensum 2014

5.3.3 Case study: Operating schedule for the simulation microgrid

The probability density of the total power generated by DG2, DG3 and DG4 is given in *Figure 5.7*. P_G has a 5% chance of generating less than 3 MW, which means even with the 2MW backup generator, the microgrid generator system cannot meet the demand in peak hours. In this situation, this microgrid has to either absorb power from main grid or cut off part of the residential load. Both actions cause extra compensation costs. Meanwhile, there is a chance of less than 1% that the power generated by the DGs is over 10MW. It makes this microgrid have a risk of over 5MW power flow mismatch at the PCC from the schedule. As discussed in chapter 3, it has to be reported to the DNO if this situation lasts over half an hour. Another possible solution for this situation is abandoning the over

generated wind power which cause a certain level of energy waste. Due to this probability is very small here, the wind power abandon is preferred to achieve a better system performance.

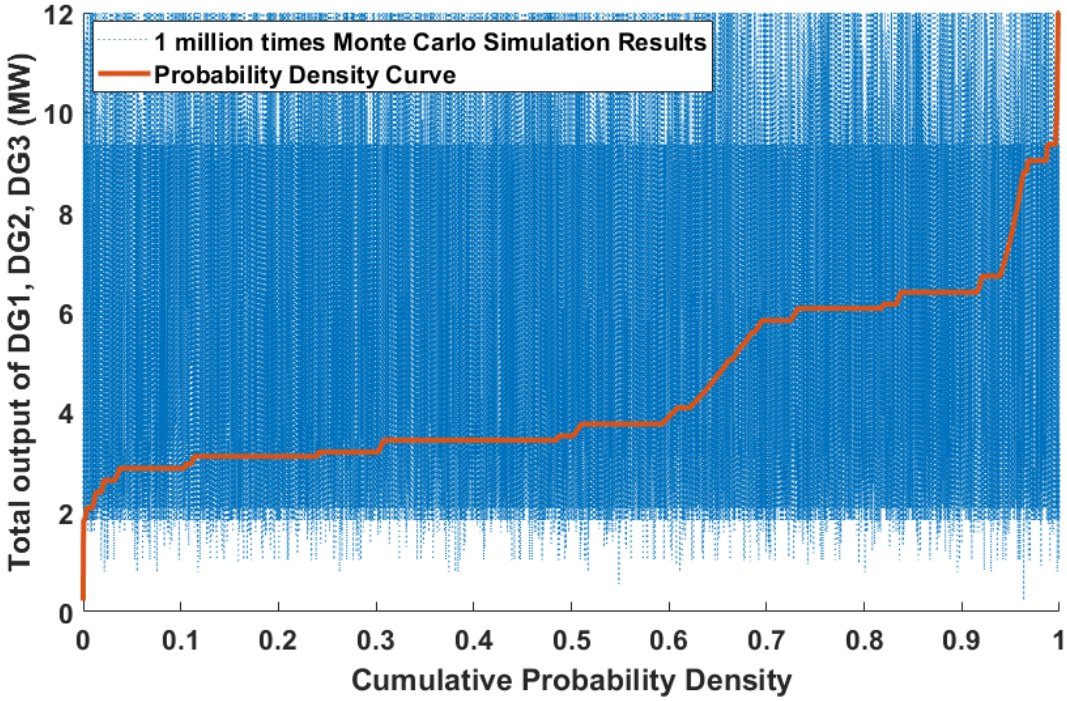

Figure 5.7 Total power output probability of DG2, DG3, DG4 in January

Besides just managing power balance, a microgrid has to provide better power quality and be friend to the utility grid. In case of that, the power exchange on PCC should be scheduled. As discussed in previous section, the daily load variations can be divided into 11 sections which is summarized in Table 5.7. A procedure in *Figure 5.8* is used to determine the operating mode of this microgrid for certain time period. This procedure starts with the initial guessed P_{mg} and a reliability constraint $Re > 80\%$. These initial values are recorded in the memory as a temporary best solution. After that, a Monte Carlo simulation is executed to derive the probability distribution of power difference between the

objective microgrid power output P_{mg} and the power it can provide without the backup DG and controllable loads. If this differential value is less than -1.6MW, it means even with all controllable loads picked up and shutting down the backup DG, the power inject to the main grid by this microgrid is more than P_{mg}. In this section, this probability is recorded as the over generated probability. Alternatively, all the controllable loads are dropped and the backup DG running in overload mode can feed a power unbalanced gap of 2.2MW. When the differential value is larger than 2.2MW, it is recorded as the probability of over loaded. The probability besides the over generated and the over loaded probability is considered as the reliability of this system with this certain value of P_{mg}. If this reliability is better than the temporary solution, the new solution will be recorded and replace the previous one. This procedure is continuously executed until all possible P_{mg} values are tested. At last, the temporary best solution is recorded as the final best solution.

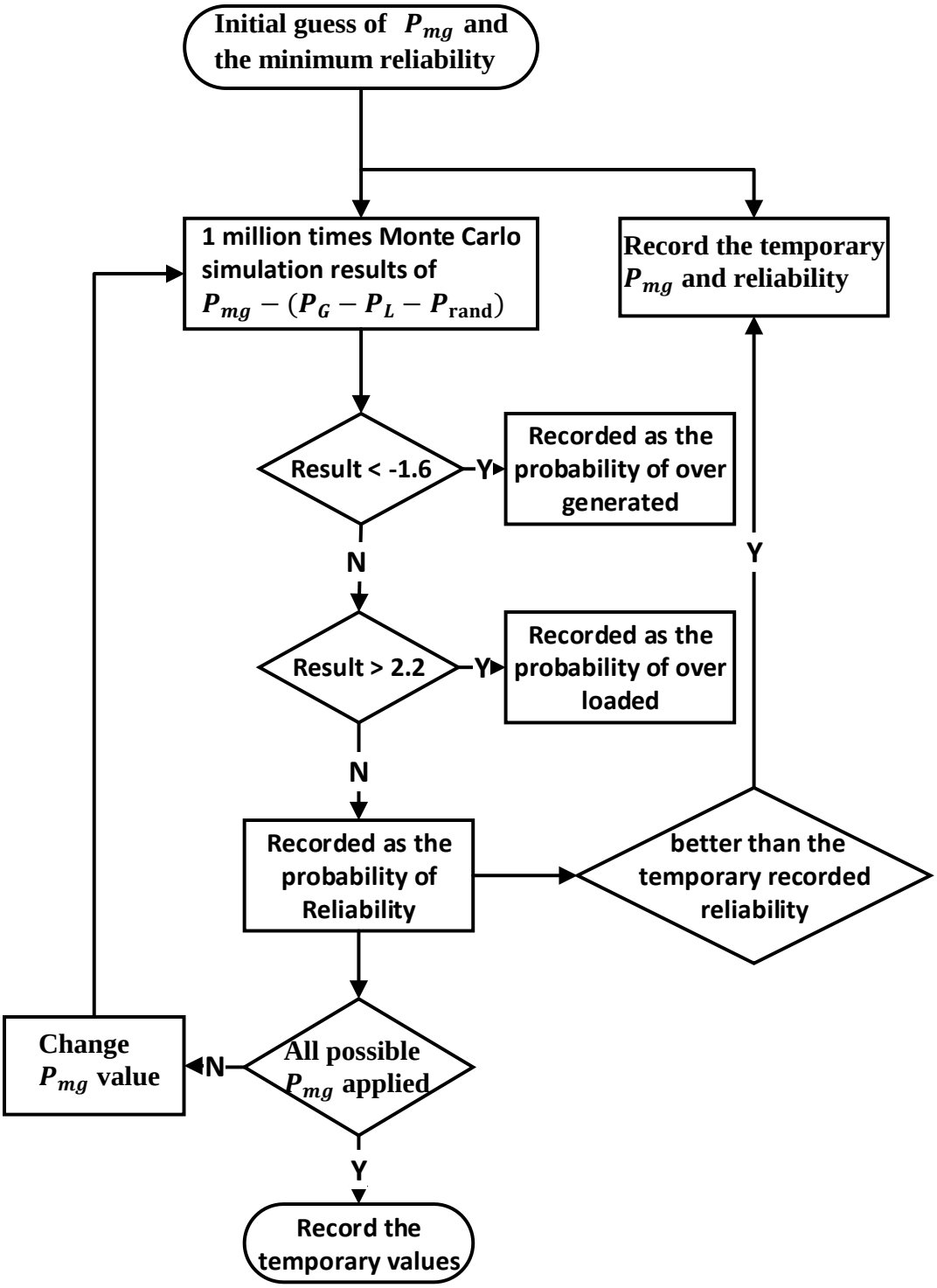

Figure 5.8 Determination procedure of P_{mg} for a certain time period

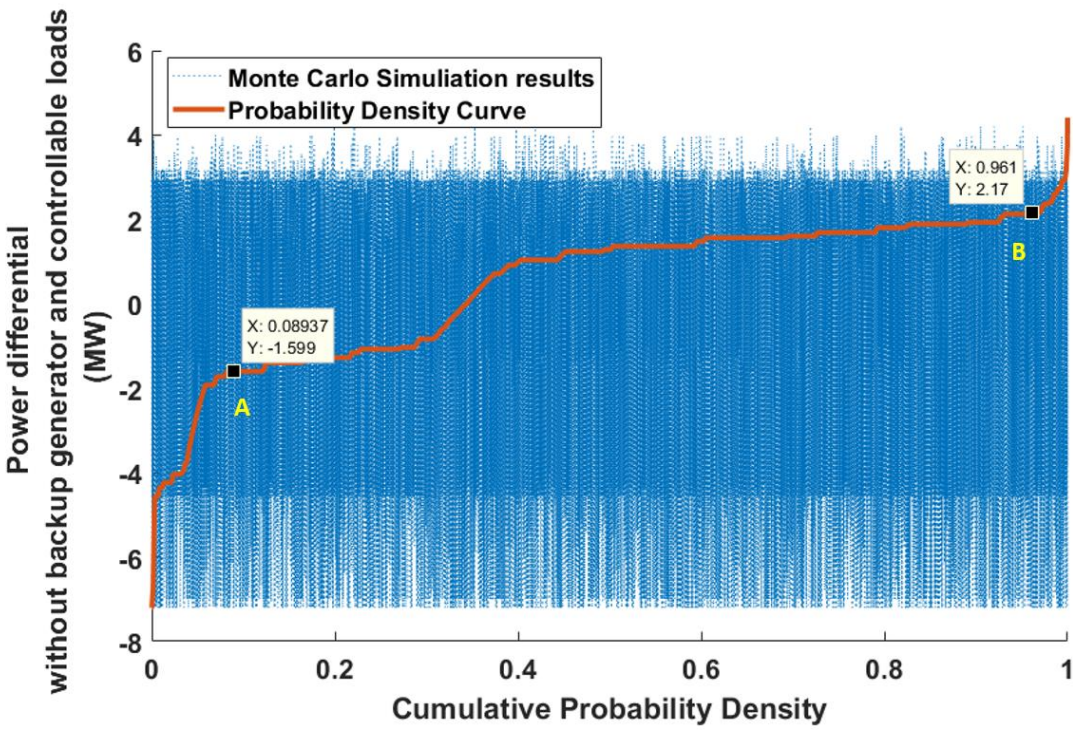

Figure 5.9 Power differential probability distribution during 14:00-18:00

A probability distribution sample of the P_{mg} solution is given in *Figure 5.9*. The P_{mg} value for 14:00-18:00 time period is set to 0 in January. There are two points A and B on the cumulative probability density curve. The area on the left side of point A represents the probability of over generated. The area on the right side of point B represents the probability of over loaded. Due to the transmission power losses not considered, the positions of point A and B will be slightly moved to the left in practice. The slopes of this probability curve in both these two areas are relatively large. Which means a large amount controllable loads or energy storage devices need to be installed to narrow the over generated area. Alternatively, a double sized backup generator is needed to be installed to eliminate the over loaded area. As there are large investment costs and

little reliability improvements, the reliability improving solutions are not cost effective. Making compensation contracts of residentials/microgrid owner and microgrid owner/DNO for these situations is preferred. How to make a contract with most benefits which related to the electricity market behaviours is not covered in this thesis.

Table 5.7 Microgrid daily operating schedule in January

P_L+P_{rand} (MW)	Time period	P_{mg} (MW)	Reliability (%)	Probability of over generation (%)	Probability of over loaded (%)
1.65+0.2	0:00-6:00	3.2	88.32	8.2	3.47
2.7+0.2	6:00-7:00	2.1	88.88	8.23	2.89
3.75+0.2	7:00-8:00	1.1	88.4	8.07	3.53
4.8+0.2	8:00-12:00	0	88.81	8.28	2.91
3.75+0.2	12:00-14:00	1.1	88.33	8.14	3.53
4.8+0.2	14:00-18:00	0	88.82	8.3	2.88
4.55+0.2	18:00-19:00	0.3	88.21	8.26	3.53
3.5+0.2	19:00-20:00	1.3	88.89	8.2	2.91
3.25+0.2	20:00-22:00	1.6	88.41	8.11	3.48
2.45+0.2	22:00-23:00	2.4	88.25	8.18	3.57
1.65+0.2	23:00-0:00	3.2	88.32	8.15	3.53

Table 5.7 gives the daily microgrid output schedule with the reliability in January. The column P_{mg} represents the anticipated power flow at PCC. There is a certain level of probability for over generation and overload situations. Table **5.8** is the annual operating schedule. The daily operating schedules for 12 months are plotted in *Figure 5.10*. The power output curves for each month has the similar shape. The magnitudes have the similar trends of the Weibull scale parameters given in *Figure 5.6* as well. To be noticed, although the Weibull scale parameter in February is 25% larger than it in January, the operating schedules are the same at these two months. This is because they have the different Weibull shape parameters. The average total generator output in these two months are 4.45MW and 4.61MW. There is only 3.6% differential on electrical power output rather than 25% of the wind power differential. This causes the over generated probability in February is around 9% which is 1% larger than it in January. The over loaded probability is 1% less than January. The reliability of the daily operating schedule is shown in *Figure 5.11*. The lowest reliability for the whole year is over 86.5% which happened in July. Meanwhile, the schedule in September with the lowest mean wind power has the highest reliability. This is because with the optimised schedule, when the average wind power speed goes slow, this microgrid can absorb power from the main grid. The load needs to be shared by wind power generator also be decreased. In which case, with a certain amount of energy storage devices installed, the electrical power output distributes more concentrated with less average wind power.

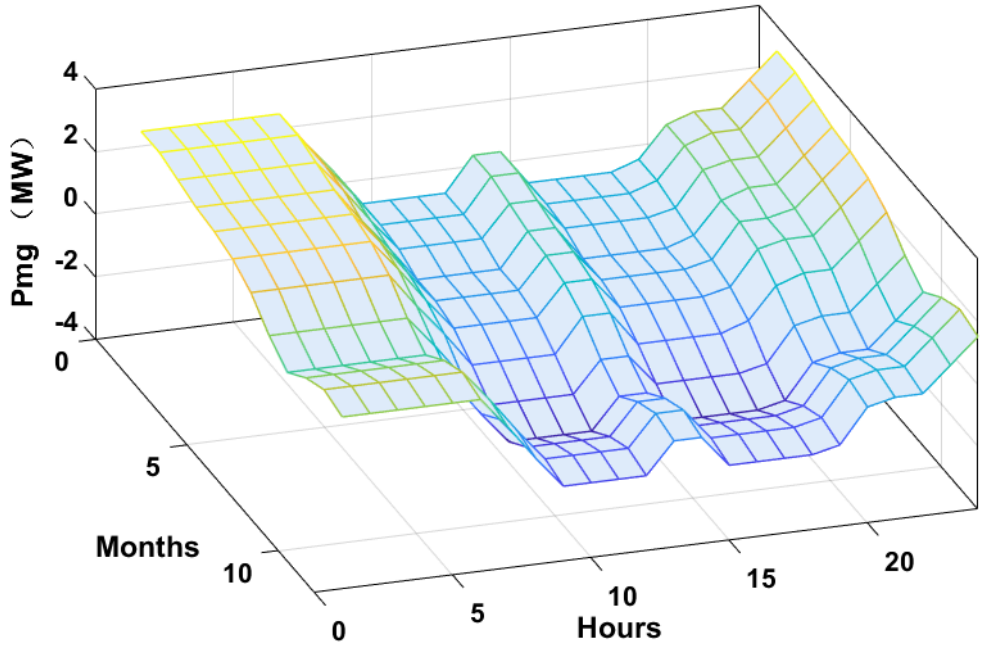

Figure 5.10 Annual daily operating schedule of the simulation microgrid system

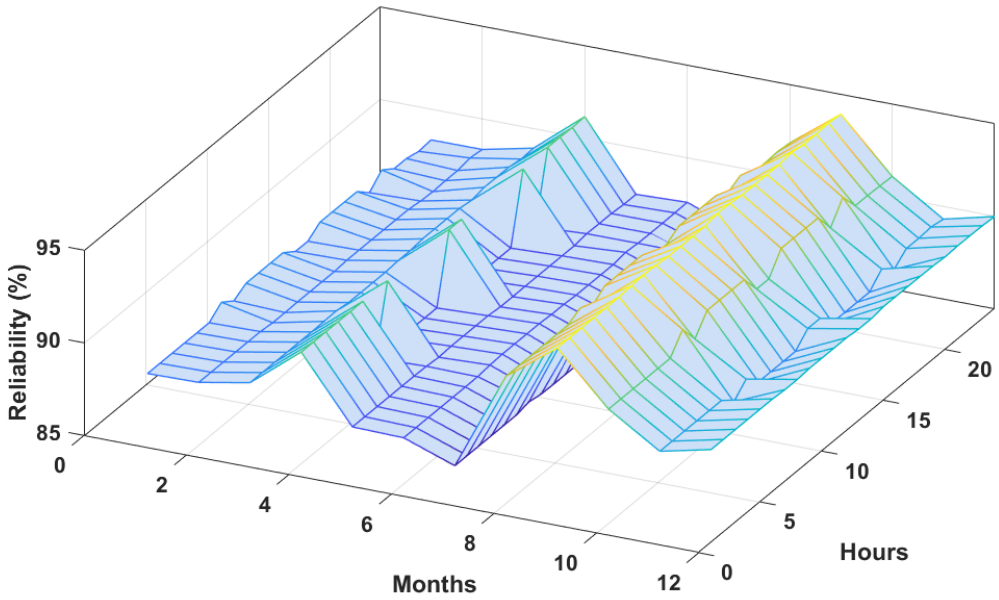

Figure 5.11 Reliability of the annual daily operating schedule

Table 5.8 Annual operating schedule and Reliability

	Time Period	0:00-6:00	6:00-7:00	7:00-8:00	8:00-12:00	12:00-14:00	14:00-18:00	18:00-19:00	19:00-20:00	20:00-22:00	22:00-23:00	23:00-0:00
Jan	P_{mg} **(MW)**	3.2	2.1	1.1	0	1.1	0	0.3	1.3	1.6	2.4	3.2
	Reliability (%)	88.32	88.88	88.4	88.81	88.33	88.82	88.21	88.89	88.41	88.25	88.32
Feb	P_{mg} **(MW)**	3.2	2.1	1.1	0	1.1	0	0.3	1.3	1.6	2.4	3.2
	Reliability (%)	88.37	88.3	88.3	88.32	88.38	88.38	88.29	88.25	88.29	88.42	88.33
Mar	P_{mg} **(MW)**	3	2	0.9	-0.1	0.9	-0.1	0.1	1.2	1.4	2.2	3
	Reliability (%)	88.88	88.9	88.92	88.82	88.88	88.97	88.87	89.01	89	88.89	88.93
Apr	P_{mg} **(MW)**	2.8	1.7	0.7	-0.4	0.7	-0.4	-0.1	0.9	1.2	2	2.8
	Reliability (%)	91.06	87.45	91.07	87.41	91.1	87.35	91.07	87.41	91.15	91.12	91.16
May	P_{mg} **(MW)**	2.7	1.7	0.6	-0.4	0.6	-0.4	-0.2	0.9	1.1	1.9	2.7
	Reliability (%)	87.55	87.53	87.47	87.52	87.45	87.46	87.46	87.56	87.55	87.49	87.49
Jun	P_{mg} **(MW)**	2.5	1.5	0.4	-0.6	0.4	-0.6	-0.4	0.7	0.9	1.7	2.5
	Reliability (%)	87.49	87.5	87.58	87.62	87.57	87.52	87.63	87.57	87.56	87.57	87.59
Jul	P_{mg} **(MW)**	2.1	1	0	-1.1	0	-1.1	-0.8	0.2	0.5	1.3	2.1

	Reliability (%)	86.51	86.66	86.54	86.52	86.61	86.63	86.59	86.56	86.62	86.62	86.58
Aug	P_{mg} **(MW)**	1.4	0.4	-0.7	-1.7	-0.7	-1.7	-1.5	-0.4	-0.2	0.6	1.4
	Reliability (%)	91.88	92.25	91.84	92.36	91.85	92.29	91.92	92.29	91.87	91.92	91.85
Sep	P_{mg} **(MW)**	0.9	-0.1	-1.2	-2.2	-1.2	-2.2	-2	-0.9	-0.7	0.1	0.9
	Reliability (%)	93.93	93.99	94.03	94	93.93	94.06	93.96	94.06	93.95	94	93.93
Oct	P_{mg} **(MW)**	1.4	0.4	-0.7	-1.7	-0.7	-1.7	-1.5	-0.4	-0.2	0.6	1.4
	Reliability (%)	91.15	92.16	91.1	92.1	91.05	92.15	91.06	92.16	91.16	91.13	91.1
Nov	P_{mg} **(MW)**	1.7	0.7	-0.4	-1.4	-0.4	-1.4	-1.2	-0.1	0.1	0.9	1.7
	Reliability (%)	89.4	88.78	89.46	88.76	89.45	88.67	89.37	88.8	89.38	89.44	89.32
Dec	P_{mg} **(MW)**	1.5	0.5	-0.6	-1.6	-0.6	-1.6	-1.4	-0.3	-0.1	0.7	1.5
	Reliability (%)	90.02	89.97	89.97	90.03	89.96	90.07	90.06	90.01	90.05	90.04	89.99

5.4 Simulation results and discussions

5.4.1 Scenario1: 24-hour overall running results

5.4.1.1 Backgrounds of this experiment

As discussed above, the daily operating schedule has the lowest reliability in July. The power exchange at PCC has all the values of positive, negative and zero in July. The WECS/FESS combined system outputs are generated by the wind speed data of July is chosen to be used to verify the reliability of the proposed hierarchical controlled system as it has this strictly condition.

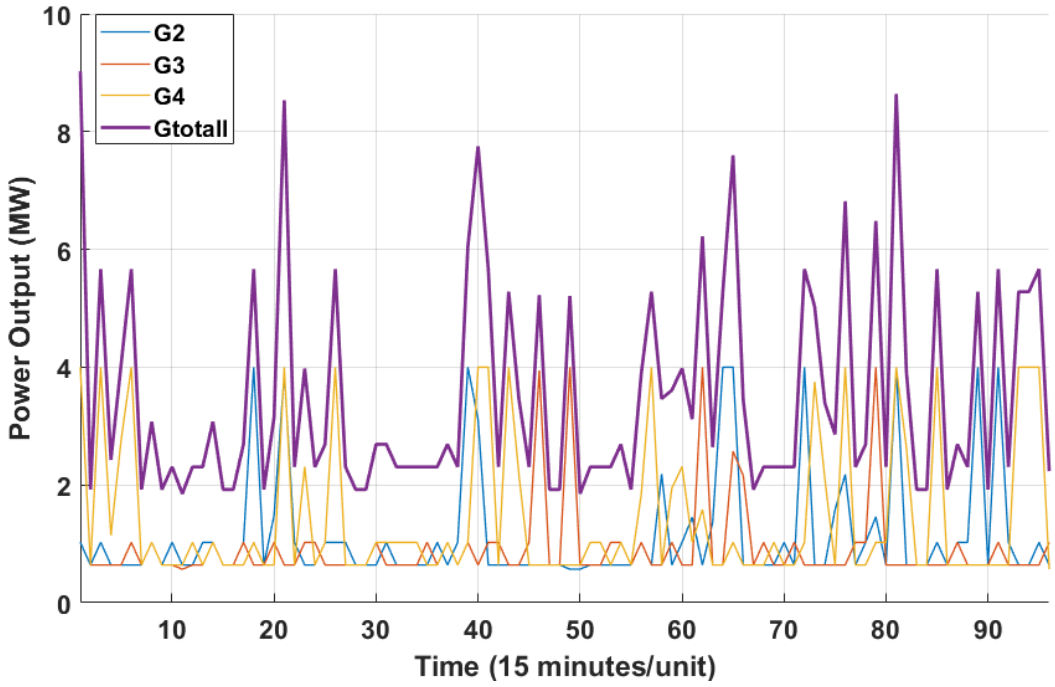

Figure 5.12 24-hours generator output

Figure 5.12 shows the randomly generated 24-hours DGs power output data which is used in the experiment. In this experiment, it is assumed that there is only a little variation of wind speed in every 15 minutes periods. This means the power output of a DG keeps constant within 15 munities. These data are generated by randomly picking up 96 continuous points in

a Monte Carlo simulation result points series. The curves G2, G3, G4 and Gtotal represent the power output of DG2, DG3, DG4 and the sum of these three DGs respectively.

Figure 5.13 is the original Main grid output schedule. It is derived by reversing the P_{mg} schedule values given in previous section. This microgrid generates power during evening and early morning time. It represents a load absorbing power from main grid in peaking hours.

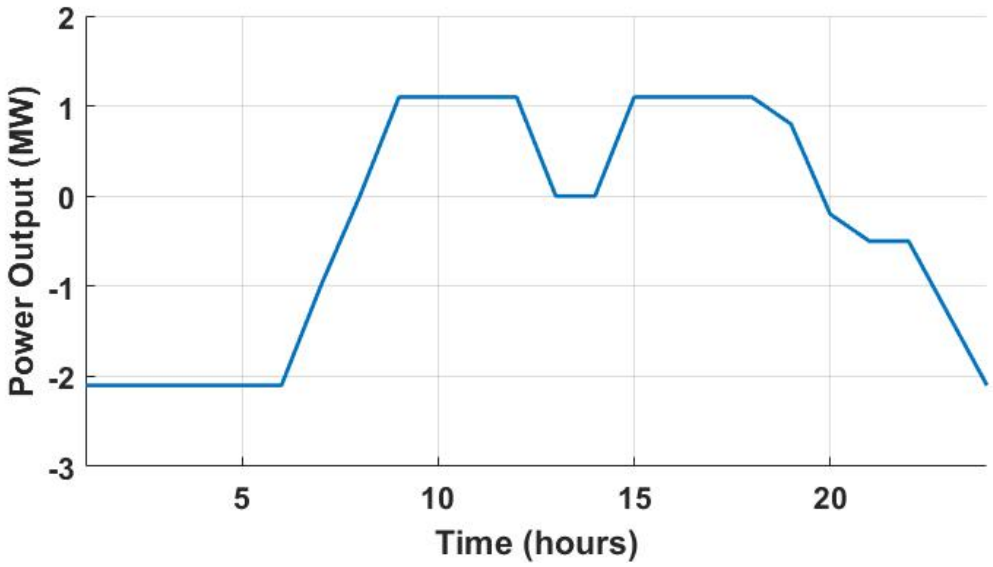

Figure 5.13 Scheduled Power output of Main grid

The fast-response operating rules of commitment for the backup DG and controllable loads has to be introduced in the control procedure to maintain a high reliability of this system. The operating rules are given in Table 5.9. The total power gap here is the differential between the generated power and the demands, which is derived from *(5.4)*.

$$P_{Gap} = P_G - P_L - P_{rand} - P_{mg} \qquad (5.4)$$

P_{mg} here is the scheduled microgrid output.

Table 5.9 Operating rules for the backup DG and controllable loads

Total power gap (MW)	**Backup DG**	**Controllable Load 1**	**Controllable Load 2**	**Controllable Load 3**	**Controllable Load 4**
Over 1.6	Shut down	Picked up	Picked up	Picked up	Picked up
1.2 to 1.6	Shut down	Picked up	Picked up	Picked up	Dropped off
0.8 to 1.2	Shut down	Picked up	Picked up	Dropped off	Dropped off
0.4 to 0.8	Shut down	Picked up	Dropped off	Dropped off	Dropped off
0 to 0.4	Shut down	Dropped off	Dropped off	Dropped off	Dropped off
-0.4 to 0	Start	Picked up	Picked up	Dropped off	Dropped off
-0.8 to -0.4	Start	Picked up	Dropped off	Dropped off	Dropped off
-7.2 to -0.8	Start	Dropped off	Dropped off	Dropped off	Dropped off
Below -7.2	Report to the DNO				

As there are only 1.6MW controllable load in total, when $P_{Gap} > 1.6$, even all the controllable loads are picked up, there is over generated power injected into the main grid. If the P_{Gap} is in the range of 0.4MW to 1.6MW,

the power exchange objects at PCC can be achieved by amending the controllable loads.

Due to power losses which practically exist but are not being considered in *(5.4)*, when $0.4 > P_{Gap} > 0$, all controllable loads need to be dropped. Part of the rest power supply support the power losses, and the other is not used. In the interval of (-0.8, -0.4), extra power from the backup generator is needed to maintain the power balance. Because the diesel generator is normally being operated above the half-rated power point, to meet the power exchange schedule, the backup DG has to be started and operated accompanying with controllable loads.

If $P_{Gap} < -7.2$, which means the deviation of the power exchange on PCC bus is over 5MW, a report has to be passed to the DNO. However, in this microgrid system, there are 4.8MW scheduled loads and 1.6 MW controllable loads in total, this strict situation happens only with heavily system failure, in which backup DG fails and all loads connected during off peak time at the same time. This situation does not occur normally.

5.4.1.2 Simulation results and discussion

In this section, the total simulation time is 960 seconds. Each 10s periods in simulation represent 15 minutes in real world. Wind speed and loads changes every 10s. To be noticed, the DGs' output changes after it received the new references from control centre, and the load variation happens before any regulation actions. Besides the scheduled load curve, a 0.2 MW load randomly plug in and out every when load changes.

Figure 5.14 gives the logs of the power output of DGs in the microgrid. The periods of DG1 without power output are evenly distributed which

means the probability of situations with positive or negative P_{Gap} happens is equal with the operating schedule. According to the DGs' output curve in *Figure 5.12*, there are 6 peak periods of G2 around the points 20, 40, 65, 70, 80, 90. Alternatively, 3 peak periods of G3 around points 50, 60, 80, and 7 peak periods of G4 around points 5, 25, 30, 60, 75, 85, 95. These particular features can be found in *Figure 5.14* as well.

Figure *5.15* is a snap shot of the DGs' power output response at the time point of system parameters changing. As DG1 is very close to the PCC bus, the transmission line impedance between them are relatively small. To prevent system oscillations, small PI controller setting values are applied in the local controller of DG1. This makes it has a relatively slow response characteristic. Compare to the DG1's 0.2s settling time, the active power of DG2-4 reached steady state within 0.02s, and the reactive power reached steady state in 0.06s. As the reactive power of DGs are well regulated to 0, the reactive circulating current problem is well eliminated in this system.

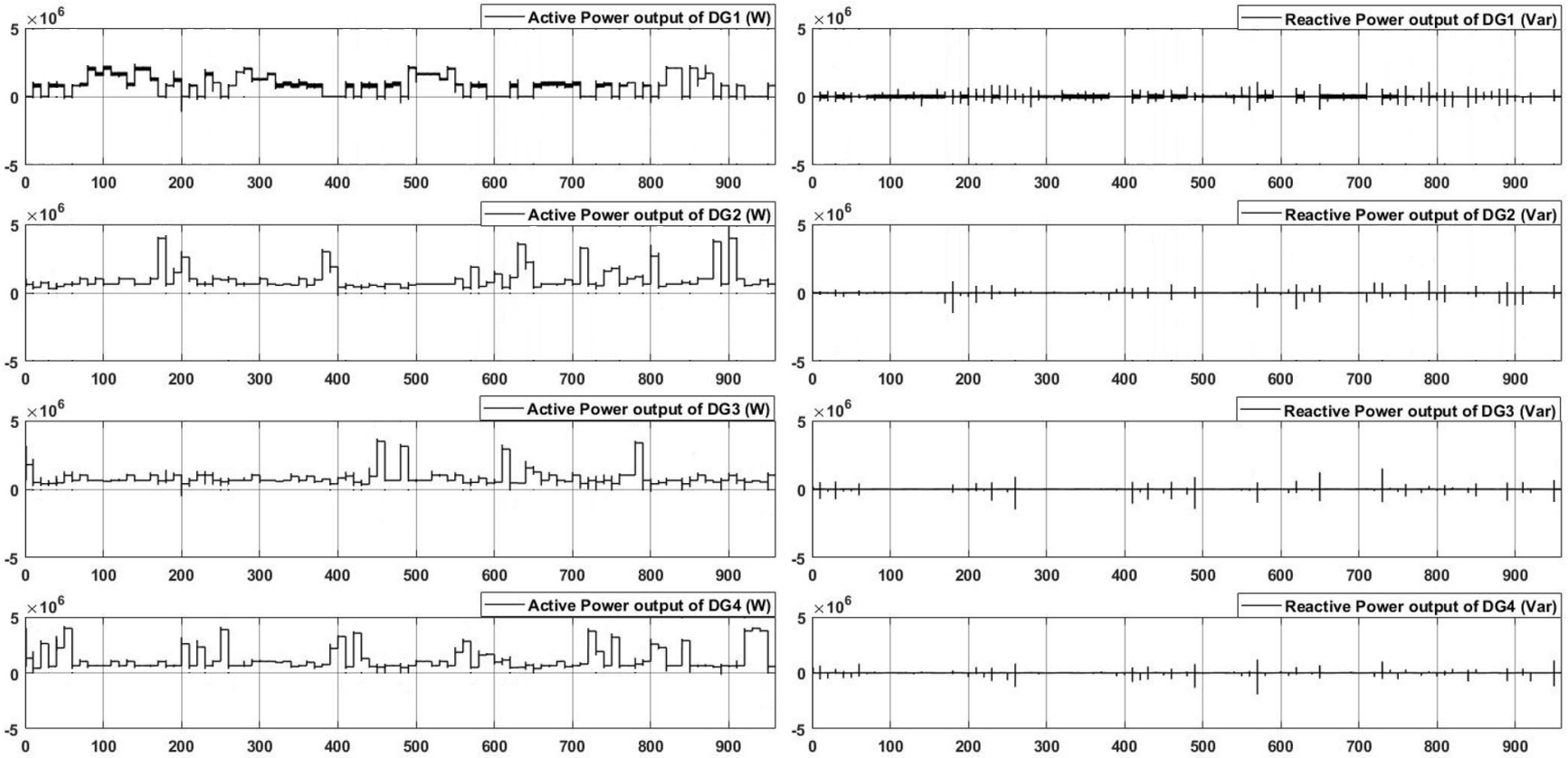

Figure 5.14 Power output of DG1, DG2, DG3, DG4

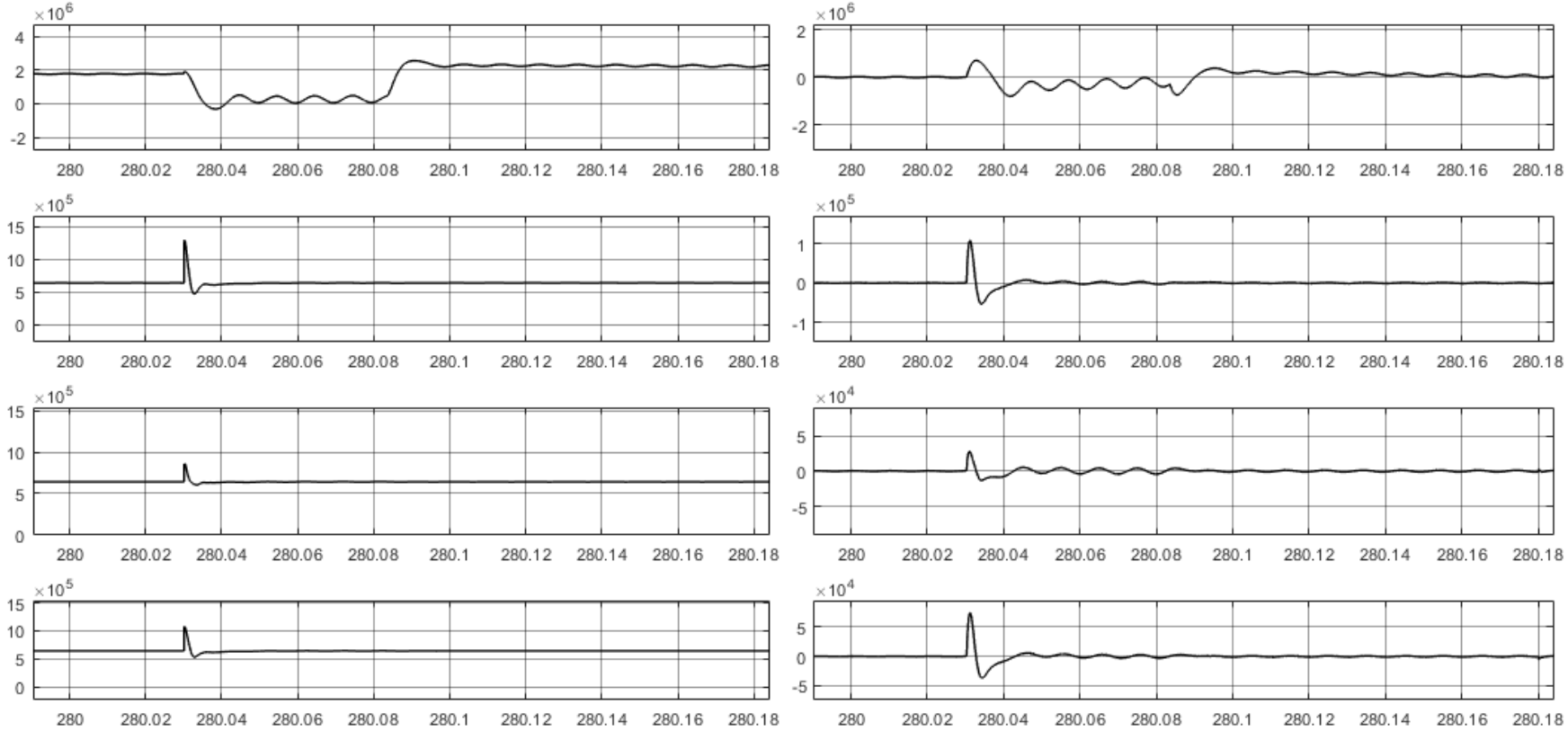

Figure 5.15 Snap shot of power response of DGs

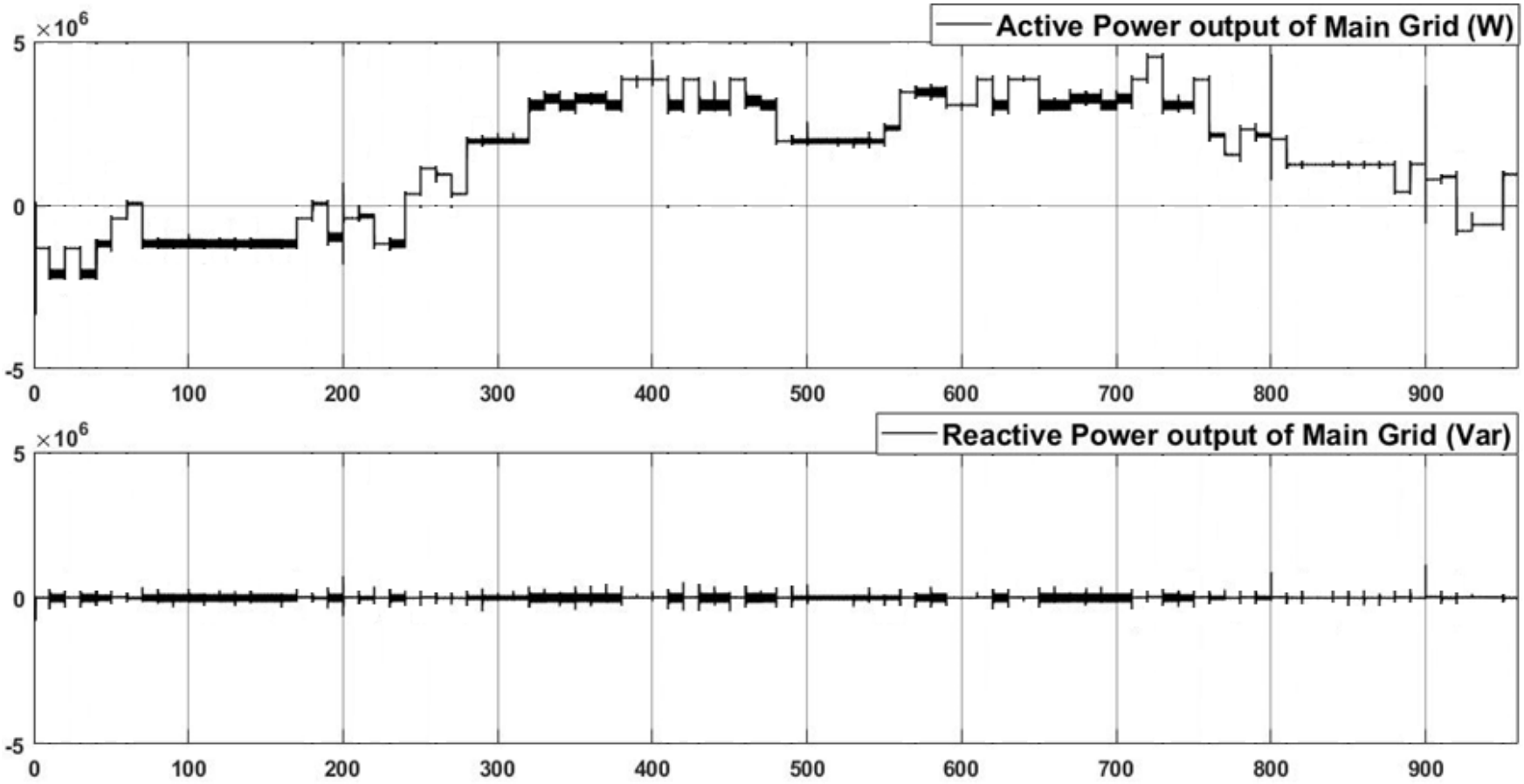

Figure 5.16 Power flow from main grid to microgrid

Figure 5.16 presents the power flow from main grid to the microgrid. The active power curve of the simulation result and the scheduled curve in *Figure 5.13* have similar shape. However, there are always deviations between them. This is because of there are nonlinear components, and the impedance of circuit breakers are not considered in the power flow calculation. The compensation strategy which can deal with this power deviation issue without using a complex power system model is applied in the following sections.

5.4.2 Scenario2: The microgrid system performances with precise control in a specific time period

5.4.2.1 Backgrounds of this experiment

The overall system behaviours of DGs output and loads variations have been tested in the previous section. The simulation results demonstrate the long-term stability of the control system. The experiment in this section is focused on the accurate system performance control.

As mentioned in chapter 3, when a microgrid operated as a generator, it should be operating within the frequency range of 49.5Hz to 50.5Hz. There could be step voltage changes at PCC bus within $\pm 3\%$ in UK distribution network. The experiment in this section is designed to evaluate the system performance under voltage and frequency variation.

Table 5.10 gives the events schedule of the experiment in this section. At the time point of 5:00, the power output of DG2, DG3 and DG4 are 3.89MW, 0.64MW, 4.0MW respectively. The industrial loads demand, residential loads demand and controllable loads demand are 1.05MW, 0.8MW and 1.6MW respectively. The scheduled microgrid output is 2.1MW. Due to the wind power at this time point meets the demand, and

the diesel generator has to be operated over 50% rated power output, DG1 is shut down in this section.

Table 5.10 Experiment events schedule

Time period	Events
0s-0.5s	Simulation initialization and system parameters of 5:00 applied
0.5s-1.5s	PCC Power deviation compensation
1.5s-2s	Voltage Step change to 1.03pu
2s-2.5s	Frequency step change to 50.5Hz
2.5-3s	System regulation from control centre
3s-4s	PCC Power deviation compensation

5.4.2.2 Simulation results and discussion

An overall system performance information on PCC during the simulation periods are shown in Figure *5.17*. The total simulation duration is 4s as given in Table 5.10. There is a voltage step change of the main grid at t=1.5s, this causes an overshoot of instantaneous power exchange on PCC before the system became steady. Alternatively, the frequency change at t=2s also caused power exchange fluctuation.

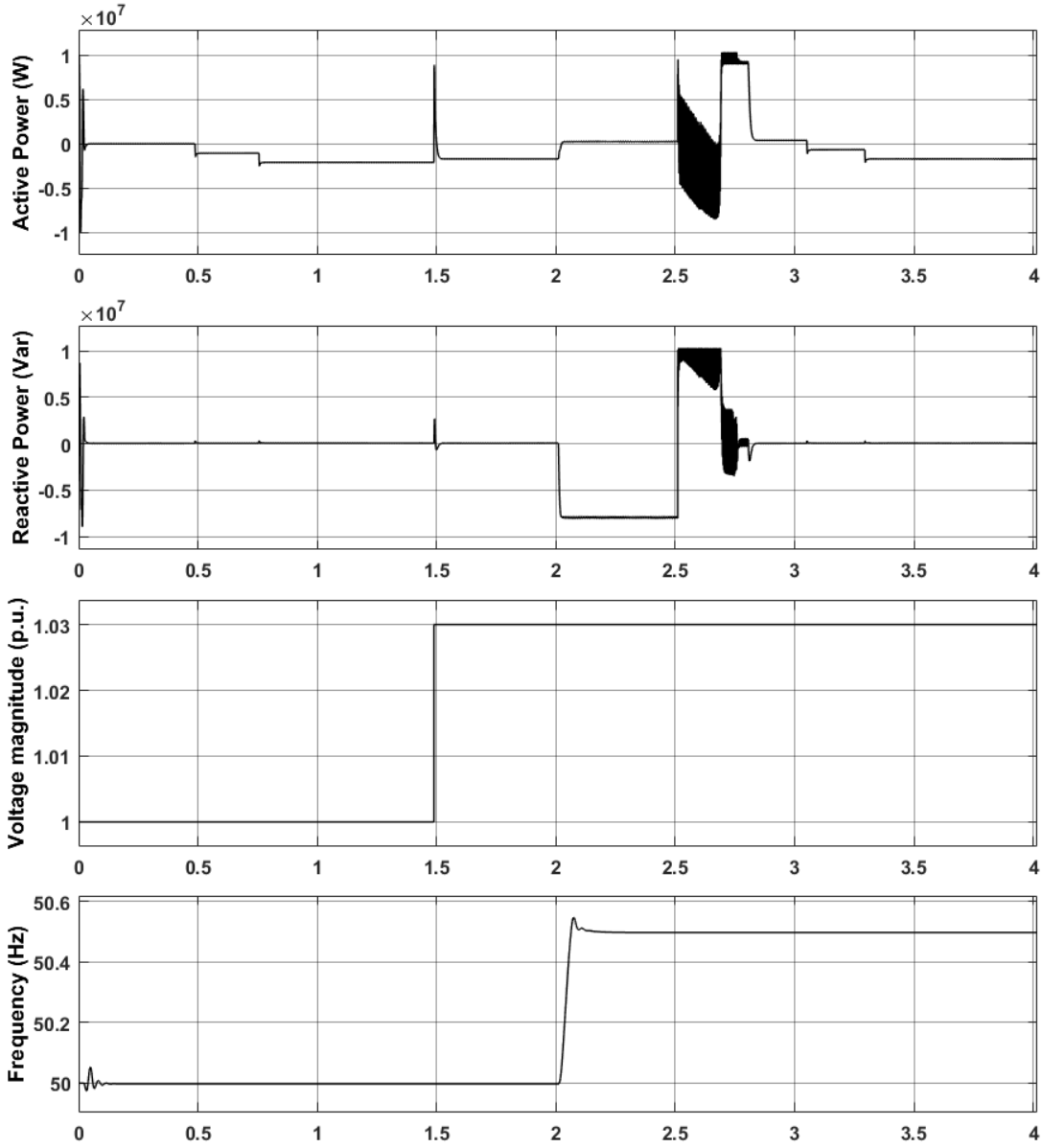

Figure 5.17 PCC bus states variations

a) PCC power exchange deviation compensation

In this section, the PCC power deviation compensation procedure is taken place. *Figure 5.18* shows the power follow from the main grid to the microgrid at the PCC bus. *Figure 5.19* gives the power output of DGs alternatively. It is observed form the figures that the initial system settings cannot meet the scheduled microgrid output. The power exchange at the

PCC bus was close to 0. With the two steps of deviation compensations, the power injected into the main grid reached the scheduled value of 2.1MW. The active power output of DG2-4 were increased from 3MW, 0.4MW, 3MW to 3.89MW, 0.64MW, 4MW respectively. The steady-state reactive power output of DGs were closed to 0 during all these procedures. There is no power output from DG1 as it was shut down in this section. The time duration from each compensation settings applied to steady state achieved is less than 0.2s.

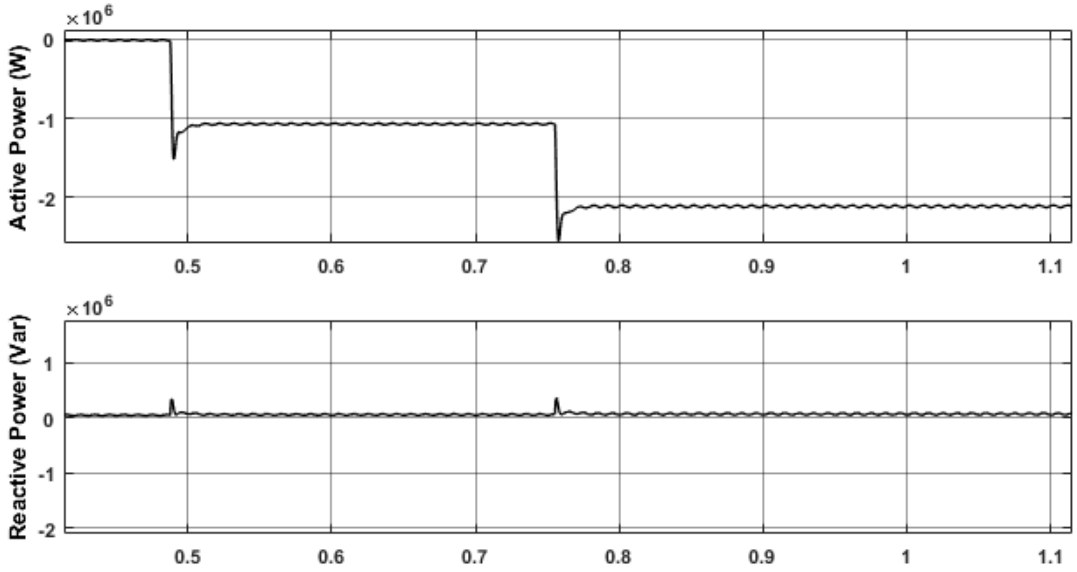

Figure 5.18 Power flow on PCC during the time period 0.4s-1.1s

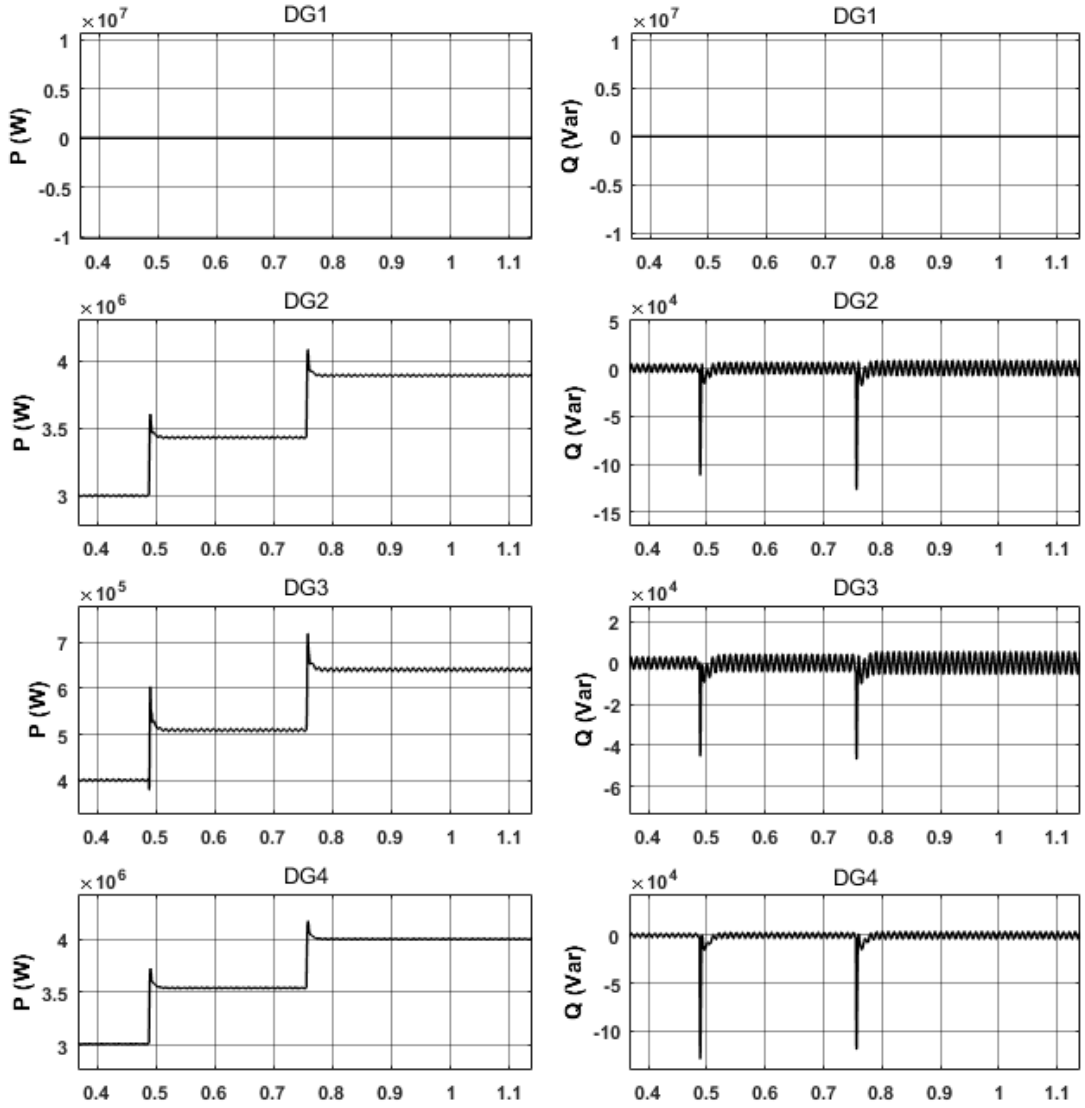

Figure 5.19 Power output of DGs during the time period 0.4s-1.1s

b) PCC voltage and frequency step changes

The system capability for voltage and frequency variation at PCC bus is evaluated in this section. To make the result clear, during this time period, the microgrid system performed with local controller only. *Figure 5.21* gives the variation information of the active power, reactive power, voltage magnitude and frequency on the PCC bus. *Figure 5.20* shows the voltage magnitude and phase angle control signals in DG3 local controller.

Figure 5.22 shows the output power variations of DGs when the voltage and frequency step changes.

At the time point near 1.5s, the PCC bus voltage step changed from 1.0 p.u. to 1.03 p.u.. A transient large power flow on PCC bus occurred due to the voltage differential between PCC bus and other microgrid buses increased. The DG output power references stay the same in the local controller before new settings from control centre are updated. As mentioned above, in the proposed hierarchical control system, P/V and Q/δ droop control is applied in local controller. As observed in *Figure 5.20*, to maintain the active and reactive power output of DG, both the voltage magnitude and phase angle control signals were changed. This microgrid system is back to steady state within 0.03 seconds. The power consumed by this system increased as long as the voltage of this entire system increased. As the power output of DGs is kept the same, the power low to main grid was reduced from 2.1MW to 1.8MW.

At the time point near 2s, the frequency of main grid is increased to 50.5Hz. The phase angle differential between the PCC bus and the DG buses grows 90° every second as there is 0.5Hz frequency differential. Due to there are cross-coupling effects by using the droop control method, the phase angle differential caused by both active and reactive power flows changed. To maintain the stability of the local controller, a saturation limiter is used for the voltage magnitude control signal. In this case, this saturation limiter is set to 0.03 p.u. from the initial voltage setting value. In contrast to the voltage magnitude control loop, there is no saturation limiter applied in the phase angle control loop. When the voltage magnitude control signal reached its limitation, the phase angle control signal kept increasing the

meet the reactive power differential eliminating requirement. This continuously phase angle increase compensates the frequency differential and maintains microgrid system stability. However, there are time delays in the control system, for this reason, a certain deviation between objective power output always exists. Although this microgrid system can be operated stably without communication with central controller, the power quality cannot be guaranteed. The new system settings from control centre should be applied as soon as possible.

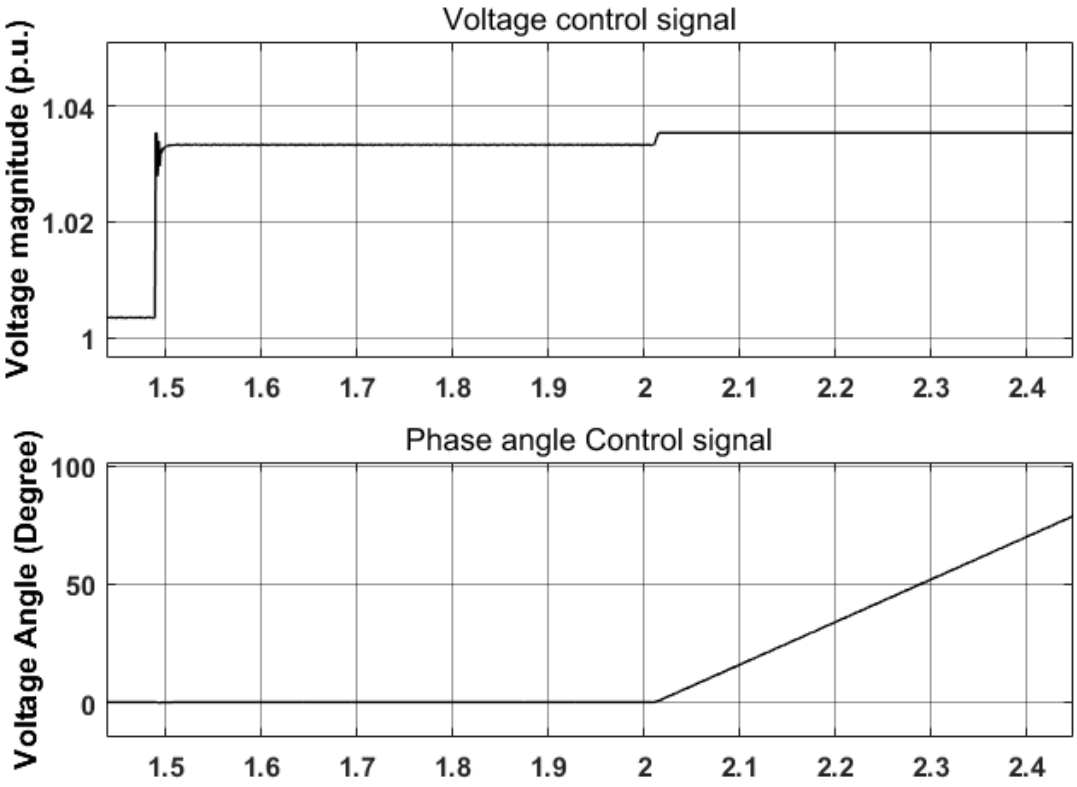

Figure 5.20 Control signals of DG3 during the time period 1.5s-2.5s

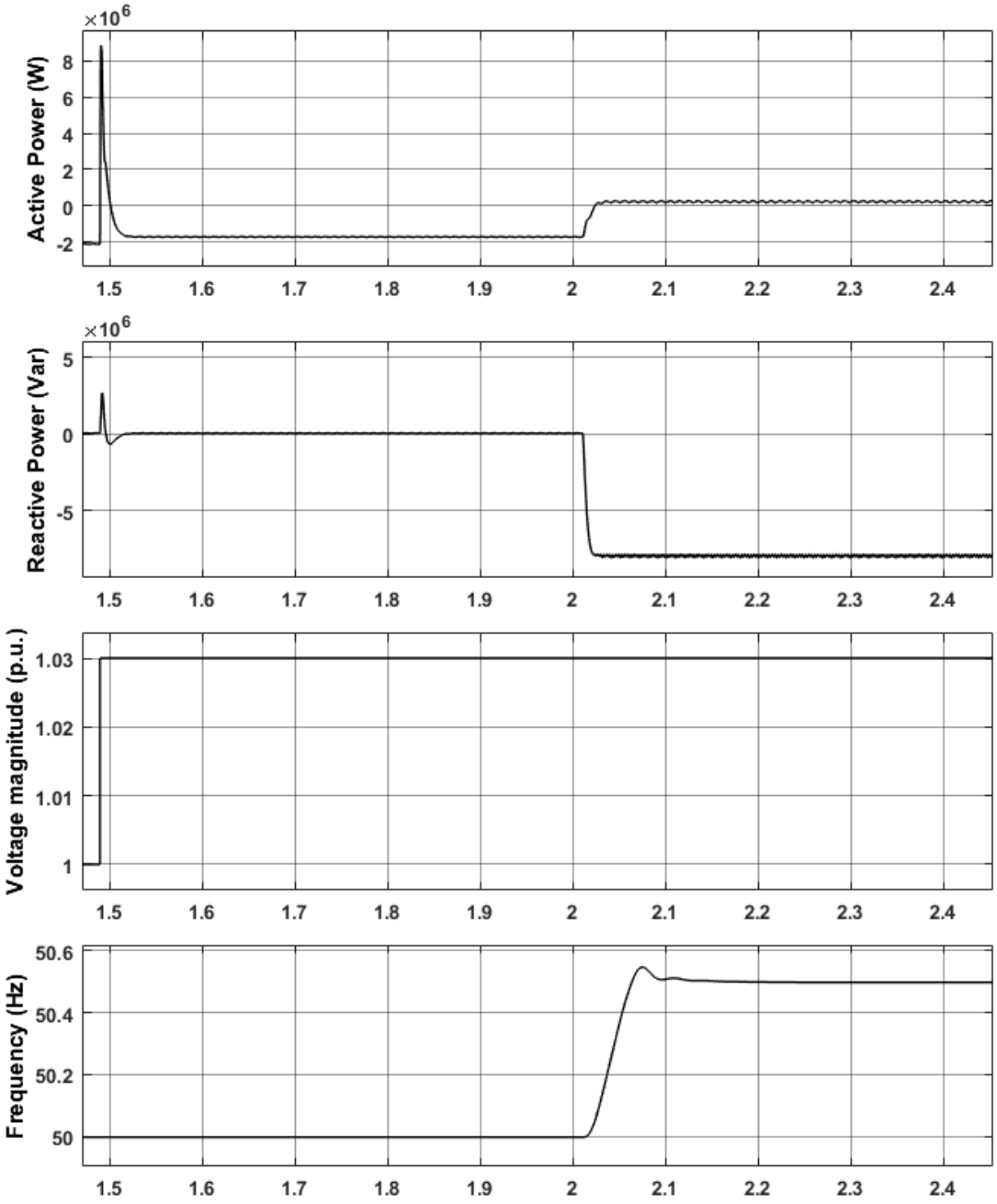

Figure 5.21 PCC bus states variation during the time period 1.5s-2.5s

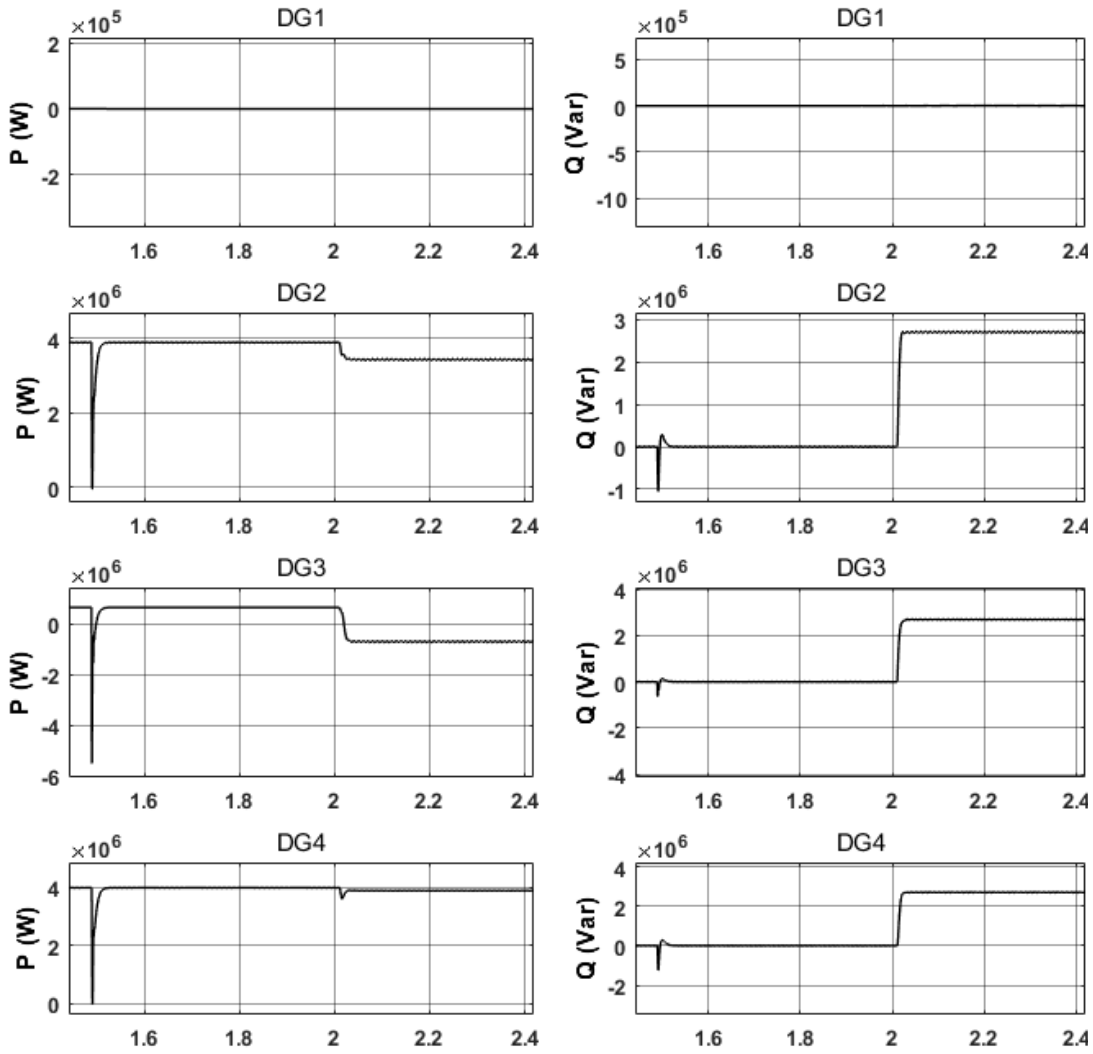

Figure 5.22 Power output of DGs during the time period of 1.5s-2.5s

c) System regulation based on the new PCC voltage and system frequency

A set of system settings generated by control centre was applied to the DGs' local controllers in this section. *Figure 5.24* gives the PCC bus states variations information. *Figure 5.25* is the log of power output of the DGs in the microgrid. *Figure 5.23* shows the control signal changes procedure.

At the time point near 2.5s, the settings of local controllers were updated by control centre. The output frequency of DGs were changed to 50.5Hz. As observed from *Figure 5.23*, the initial voltage magnitude reference for DG3 was change to 1.032 p.u.. Due to the large active output deviation from the reference value, the voltage magnitude control signal immediately hit the upper limit. The power flow oscillation happened as the phase angle signal in the local controller continuously decreasing for near 0.2s. There is a saturation limiter in the feedback path of the phase angle control loop to maintain system stability during normal condition. This saturation limiter slows down the angle control loop response speed. The power flow oscillation stopped at the time point 2.76s. After that, the controller functions were effectively achieved. The system is back to steady state within 0.1s. As *Figure 5.25* shows, both the active and reactive power output of DGs were well regulated.

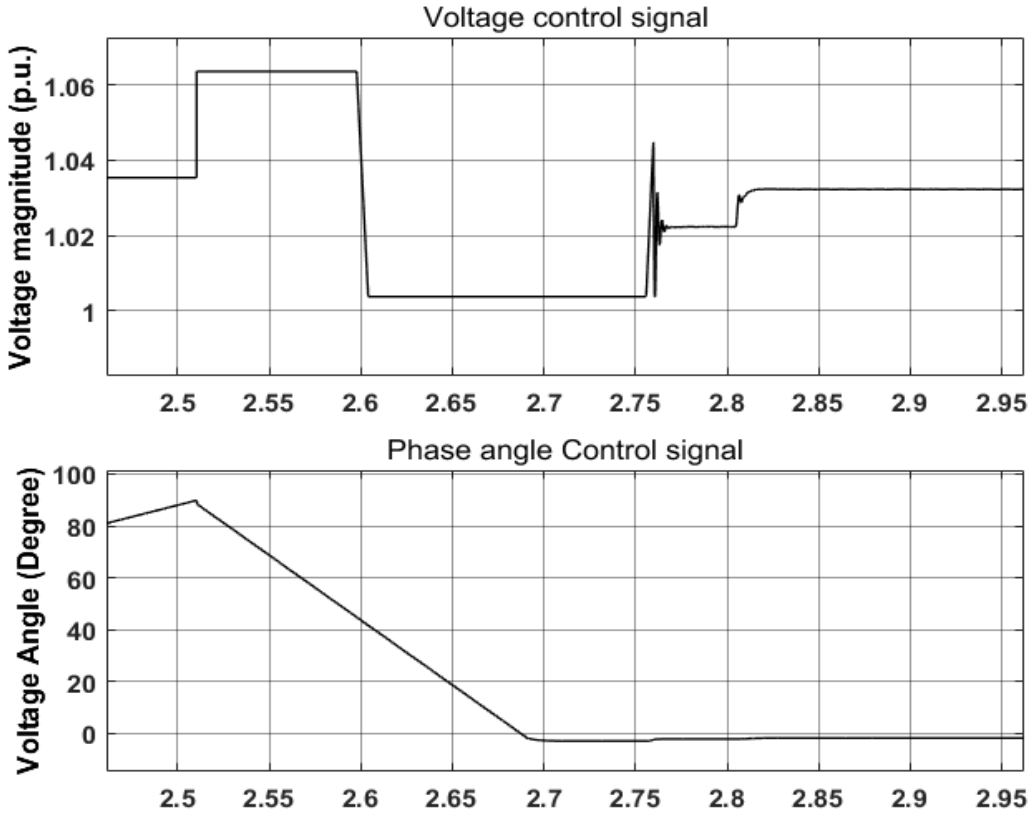

Figure 5.23 Control signals of DG3 during the time period 2.5s-3s

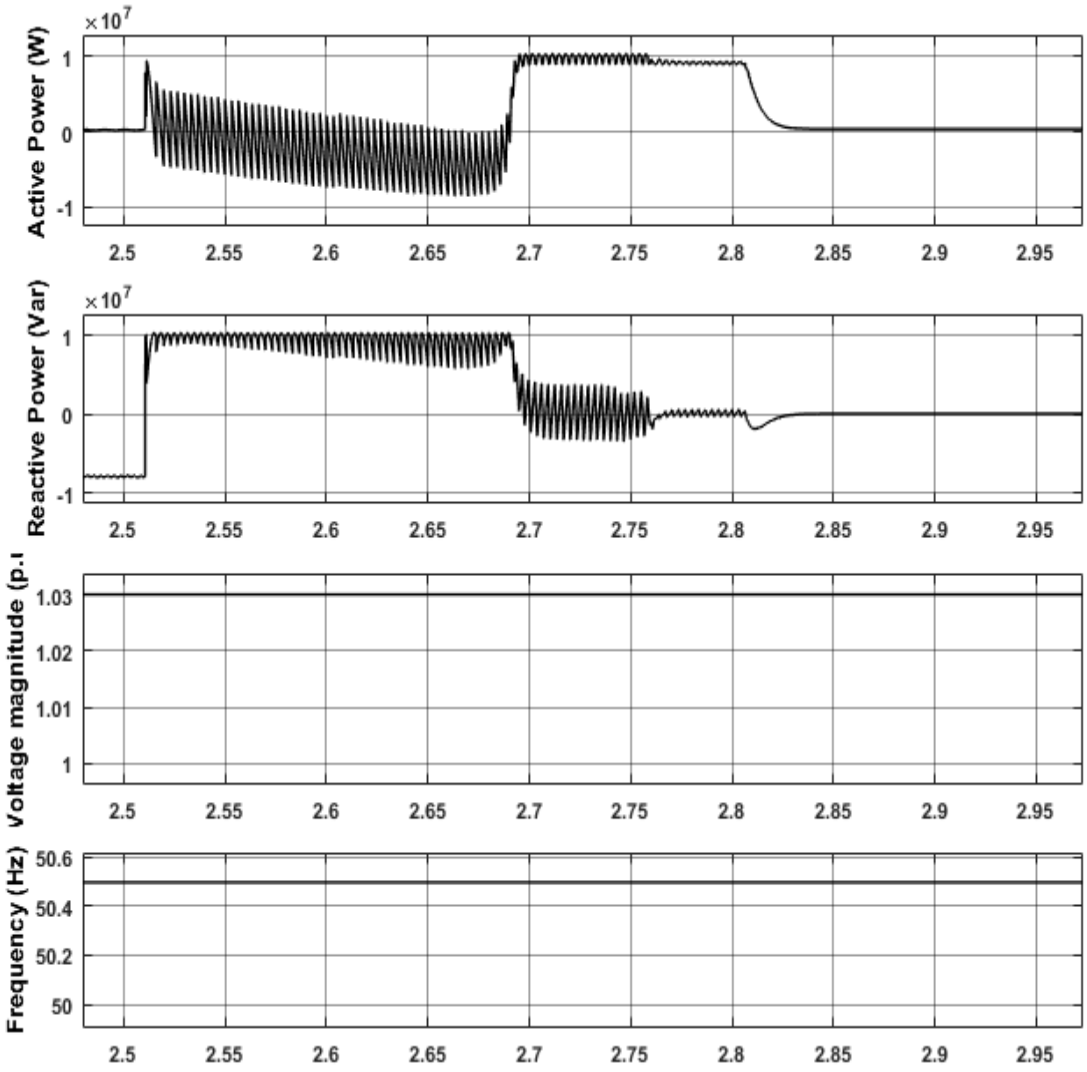

Figure 5.24 PCC bus states variation during the time period 2.5s-3s

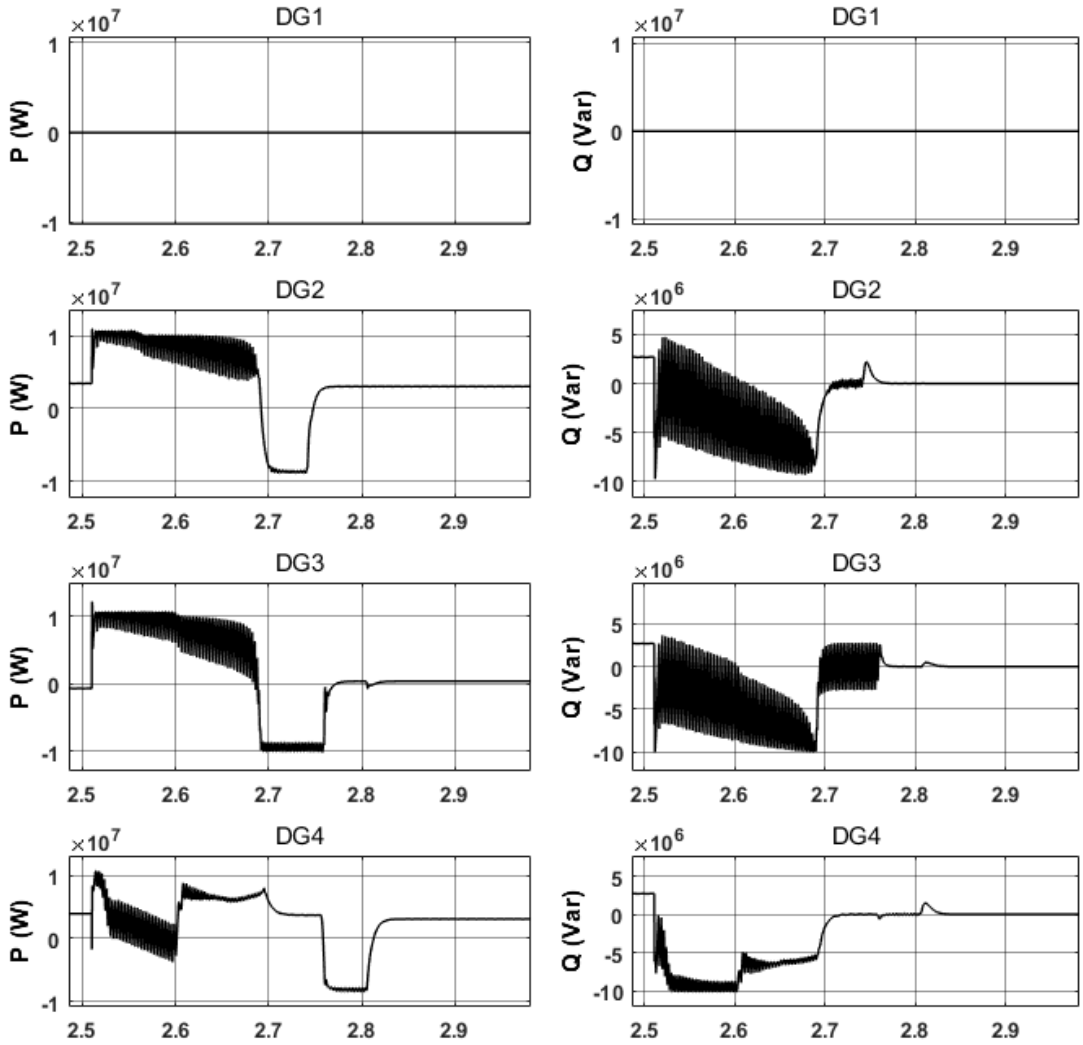

Figure 5.25 Power output of DGs during the time period of 2.5s-3s

d) PCC power deviation compensation on new system voltage and frequency

Figure 5.26 and *Figure 5.27* show the power flow on PCC bus and DG buses respectively. The compensation performance in this section is similar as it is in the time period of 0.5s-1.5s. The only difference is the power flow mismatch from the schedule is not completely eliminated. The

microgrid finally fed 1.9MW power into the main grid rather than the object 2.1MW.

The changes of system voltage and frequency lead to the change of the power consumed by the load and transmission lines with constant impedances. The precisely power exchange has to be assisted by the backup generator. DG1is shut down during this light load period. There is a start-up cost for back up DG, frequently start-up and shut down is not cost effective. Due to this over voltage situation is a short-term event in a practical distribution network, no further operations are needed to be applied to eliminate this power deviation.

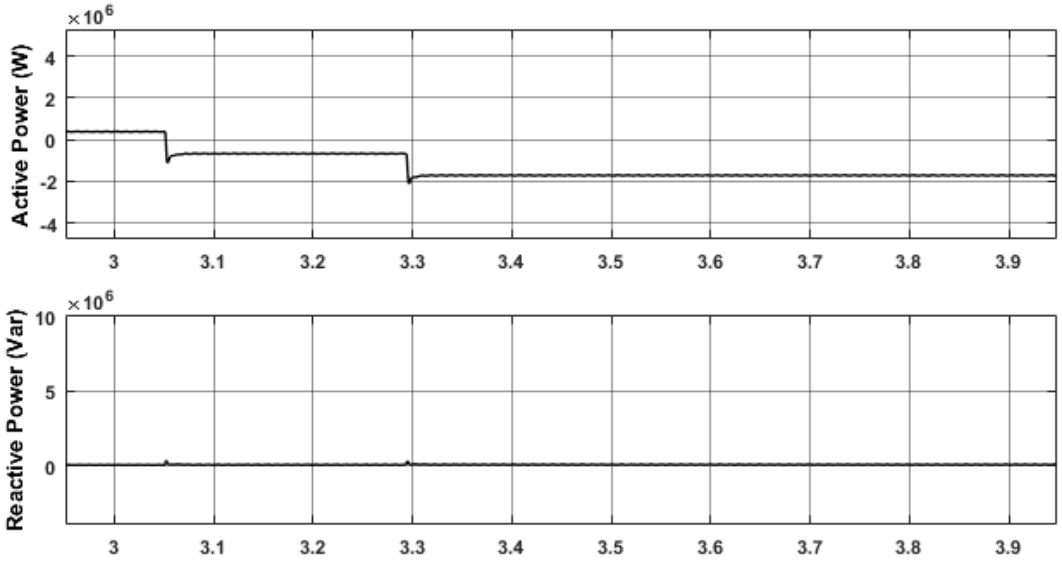

Figure 5.26 Power flow on PCC during the time period 3s-4s

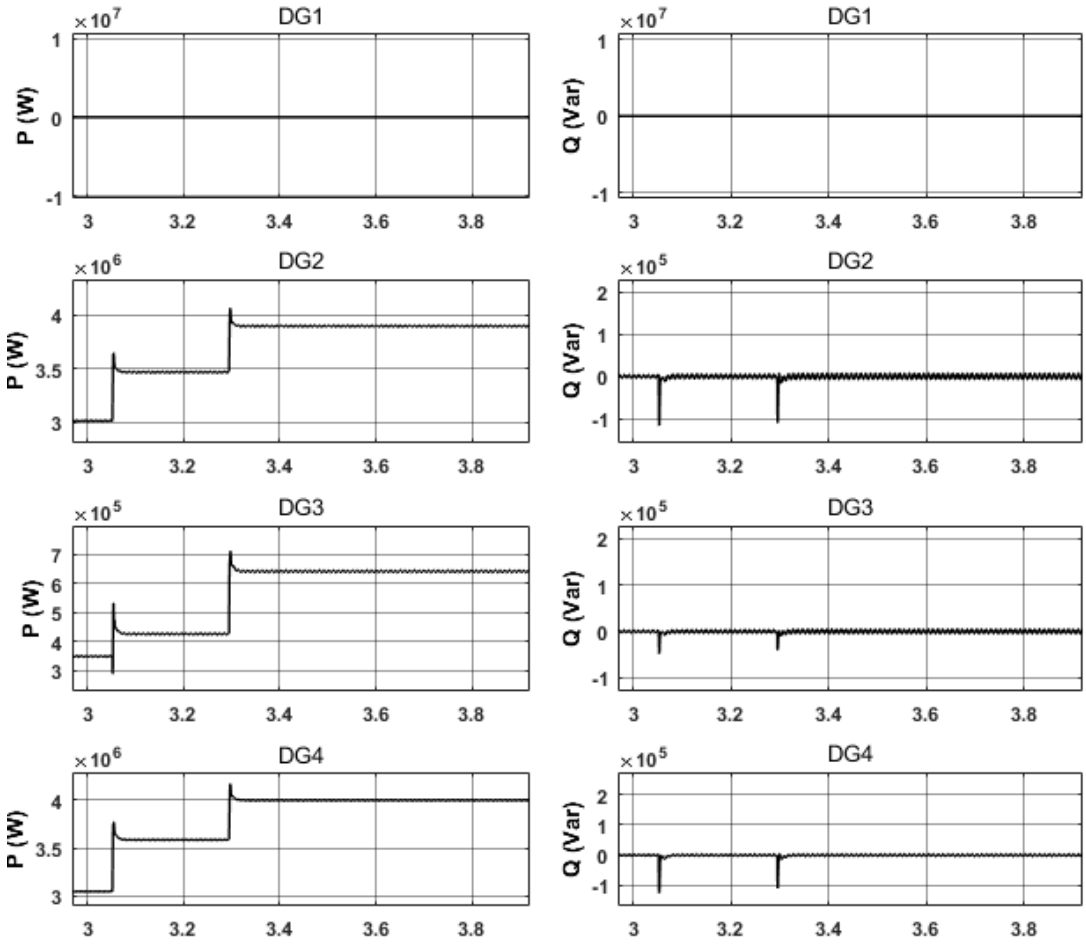

Figure 5.27 Power output of DGs during the time period of 3s-4s

5.5 Summary

In this chapter, an simulation microgrid model built in MATLAB/Simulink is used to evaluate the performance of the proposed hierarchical control method in chapter 4. With the proposed control theory, a grid connected medium voltage microgrid can perform as either controllable DG or load. A microgrid system operating schedule is generated from the statistical model proposed in previous chapters. The long-term stability of this microgrid is verified in the simulation results of 24-hours running without compensation. With the backup DG and controllable load commitment decision and initial references generated from control centre, this microgrid system performs well following the schedule.

The proposed local controller with P/V and Q/δ droop characteristics can achieve accurate power sharing of each DGs during normal conditions. It also can maintain the short-term system stability individual when the voltage and/or frequency variations happened on PCC bus. The deviations caused by these variations can be eliminated by updating local controller settings generated from the central controller. The compensation strategy which eliminates the deviations caused by non-linear components and inaccurate system parameters can be easily applied in this control system as well.

Chapter 6: High wind power penetrated medium voltage microgrid state transition and islanded operation with the proposed hierarchical control theory

6.1 Introduction

A hierarchical controlled microgrid simulation system has been built up and tested with grid connected mode in chapter 5. However, a microgrid system is often required to be capable for both connected and islanded modes. It can be either manually disconnected from the main grid or insulated from the main grid by protection devices when abnormal situations happened in upstream. When a microgrid switched from the connected mode to the islanded mode, the power balance has to be maintained without the support of the main grid. The control strategies designed for the grid-connected microgrid cannot directly applied in these situations. In this chapter, the specific control strategies are proposed and evaluated in two main sections: state transition and islanded microgrid. A critical load shedding or wind power curtailing time, which is depending on the initial energy storage devices charged status, backup DG capacity, wind generation power and the loads, is proposed in the section 6.2. A case study of 24-hours critical time probability distributions of 12 months based on the 20-bus simulation microgrid is presented.

In section 6.3, the challenges during both disconnecting and reconnecting periods are discussed. The previous steady state power balance within the microgrid network will be interrupted as there is no power exchange from the main grid when disconnection happened. The operating mode of backup DG has to be changed to feed the power-demand gap. The energy storage devices also have to be charged to consume the over generated

power or discharged to provide the over loaded power in a short term. For the system stability consideration, the further operations have to be executed within the critical time. The wind power embedded microgrid system proposed in this thesis is designed to be operated with the main grid. In that event, the islanded microgrid will be finally reconnected to the main grid. When a microgrid reconnecting procedure begins, there are often differentials of voltage magnitude, phase angle and frequency exist at the PCC. The procedures which minimize the system disturbance during reclosing period are introduced in this chapter as well. The control strategies for solving these issues are proposed and evaluated in the 20-bus simulation microgrid system.

Besides the very short time period during state transition, the microgrid system has to be operated in the islanded mode for a certain duration. In section 6.4, the control strategies for short-term islanded microgrid are studied and discussed. As there are backup DG and energy storage devices in the proposed microgrid system, the microgrid has the capability of picking up all the existed demands and maintaining the power balance in a short term. To maximize the duration capability, a DG power sharing rule is proposed. For economic consideration, the power output of backup generator should be as small as possible. An optimization procedure which is looking for the smallest backup generator's output is proposed. A case study based on the simulation microgrid system is presented and discussed. The chapter summary is given in the last section.

6.2 Critical time for load shedding and wind power curtailing

When a microgrid disconnected from the main grid, both system frequency and voltage magnitude will be determined by the DGs within the microgrid. It has to meet the potential situations of missing balanced power supply and demand. In the proposed microgrid system, each WECS is coupled with a FESS which can output high power in a short term. In case of that, the effect of wind turbine output variations can be neglected in the very short disconnecting duration. The power balance gap is supplied by the energy storage devices and backup generator.

6.2.1 The critical time definition

Because of the energy stored in the FESS is limited, there is a critical time during which load shedding, wind power curtailing and/or load increasing have to be applied to maintain the power balance. In this thesis, the critical time $t_{critical}$ is defined as the equation *(6.1)*.

$$t_{critical=}\begin{cases} \dfrac{\sum_{i=1}^{j}[c_{dischar}\cdot E_i\cdot C_i]}{P_{Load}-c_{ol}\cdot P_{backup}-\sum_{i=1}^{k}P_i} & P_{Load}>\sum_{i=1}^{k}P_i+c_{ol}\cdot P_{backup} \\ \infty & \sum_{i=1}^{k}P_i\le P_{Load}\le\sum_{i=1}^{k}P_i+c_{ol}\cdot P_{backup} \\ \dfrac{\sum_{i=1}^{j}[(1-E_i)\cdot C_i]}{c_{char}\cdot(\sum_{i=1}^{k}P_i-P_{Load})} & P_{Load}<\sum_{i=1}^{k}P_i \end{cases} \quad (6.1)$$

Where:

P_{Load} is the current total demand power in the microgrid (MW)

P_i is the current output power of the i_{th} wind power generator in the microgrid (MW)

P_{backup} is the installed capacity of the backup generator (WM)

c_{ol} is the overload capability of the backup generator (%)

C_i is the installed capacity of the i_{th} energy storage device (MWh)

E_i is the current energy stored percentage in the i_{th} energy storage device (%)

$c_{dischar}$ is the discharge efficiency of the energy storage device (%)

c_{char} is the charge efficiency of the energy storage device (%)

j is the total number of energy storage devices in the microgrid

k is the total number of wind power generators in the microgrid

$t_{critical}$ is the critical time of load shedding when $P_{Load} > \sum_{i=1}^{n} P_i$ or the wind power curtailing time when $P_{Load} < \sum_{i=1}^{n} P_i$ (hour)

Refer to this equation, when the load is larger than the total power can be provided by the WECSs and the backup generator, the energy storage devices will be discharged to feed the gap. The critical time is determined by the amount of energy stored in the energy storage devices and the differential between the power supply and demand. Alternatively, if the power from the WECS is more than the demand, the energy storage devices will be charged to absorb the over generated power. The critical time is determined by the amount of energy the energy storage devices can take in. Besides these two situations, when the power balance can be maintained by tuning the backup generator's output, the further operations are not required. The critical time is considered as infinite.

6.2.2 Case study: The critical time of the simulation microgrid

This case study is executed on the simulation microgrid model which is proposed in Chapter 5. This section is going to figure out what the operations needs to be done and how long the operations must be executed after the microgrid disconnect from the main grid.

The system parameters of the microgrid system are given in Table 6.1. There are three 4MW rated wind power generators in the microgrid, each of them is coupled with a 2.7MWh FESS. Both the charge efficiency c_{char} and discharge efficiency $c_{dischar}$ of the FESS are 90%. A 2MW diesel generator is installed as the backup generator. The overload capacity of the backup generator c_{ol} is 110%. The demand in the microgrid is consisted of 7*0.6MW industrial loads and 4*0.6MW residential loads. The instant wind power generators' output, energy stored in the energy storage devices and the demand are variable.

Table 6.1 System parameters in the simulation microgrid

P_{Load}	From 1.65 MW to 5MW variates
P_i	From 0MW to 3*4MW depending on the current wind speed
P_{backup}	2MW diesel generator
c_{ol}	110%
C_i	3*2.7MWh fly wheel energy storage devices
E_i	From 0%-100% depending on the current running status
$c_{dischar}$	90%
c_{char}	90%
j	3
k	3

The seasonal WECS power output and FESS energy stored status probability distributions of Wensum have been studied in chapter 4. The 24-hours demand distribution characteristics of the simulation microgrid is presented in chapter 5. To make this section clear, the Weibull distribution parameters for the 12-months wind speed of Wensum are given in *Figure 6.1*. The Weibull shape parameter k indicates the wind power strength, and the Weibull scale parameter c describes the fluctuation character of the wind speed. The daily demand curve is shown in *Figure 6.2*.

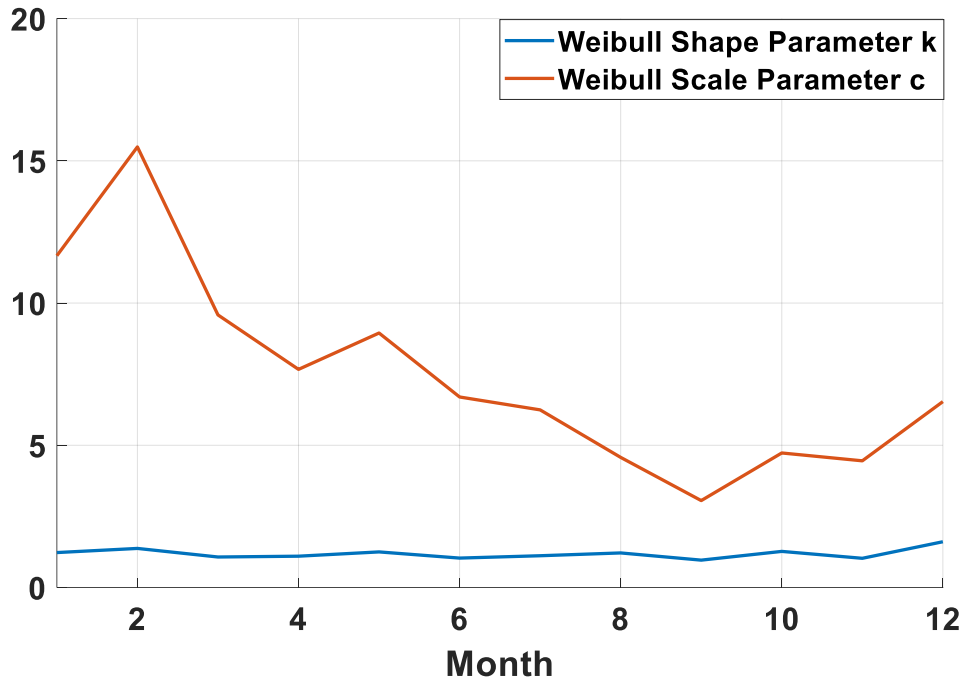

Figure 6.1 12-months Weibull Distribution parameters of wind speed

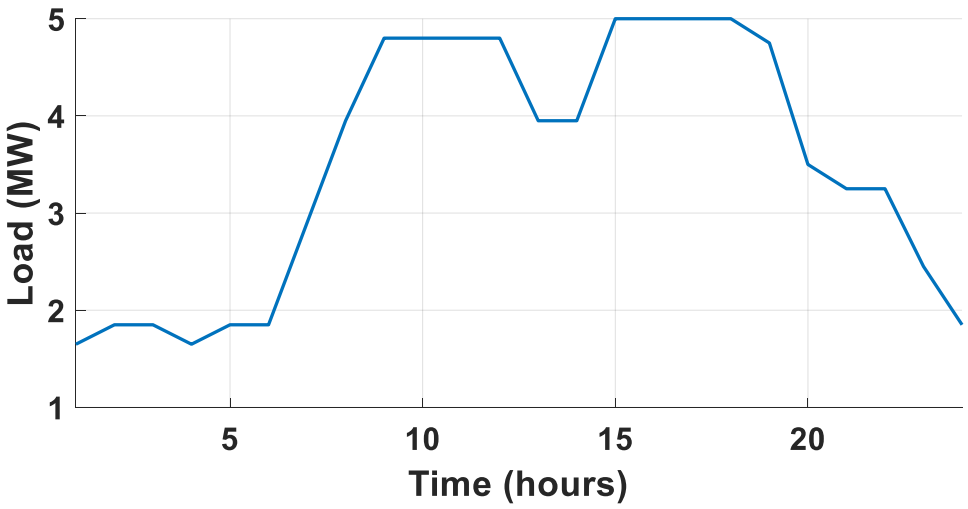

Figure 6.2 Daily load curve of the simulation microgrid

The critical time probably distribution characteristics can be derived based on the equation *(6.1)* by using Monte Carlo method. *Figure 6.3* and *Figure 6.4* show the 12-months daily critical operating time probability distribution characteristics which are derived by 100000 times repeated Monte Carlo simulations. In these two figures, the positive operating time means the FESSs are discharging to supply the power gap. Alternatively, the negative operating time means charging. In this case, when the critical operating time is over 1 hour, the microgrid is considered as an islanded microgrid rather than in the state transition period. In this situation, the load changing or wind power curtailing operations for disconnecting is not necessary.

Referring to the section 4.5.1.4 in Chapter 4, in August, September and October, the WECS/FESS combined system has the largest installed capacity requirements of FESS as the wind power is relatively weak in these three months. The value for these three months is chosen as the final installed capacity of FESS. In which case the other 9 months, the energy

storage devices have relatively larger reservation capability. This makes the probability of FESS charging and discharging in these 9 months distributed relatively average.

It can be observed from the figures that, the probability of the situations in which the load changing, or wind power abandoned have to be executed is relatively small. In most cases, the probability is less than 30% in the morning and midnight. During the daytime working hours, this probability is further reduced to less than 5%. To be noticed, in the further operation required situations, the negative critical time shares over 99.9% probability. It means in this simulation microgrid, only picking up controllable loads and wind power curtailing need to be considered during the disconnecting period.

As the wind power curtailing can be achieved by the local controller, the critical time requirement for the further action from up level controller can be relatively loose. In case of that, for the disconnecting operation, there is no requirement of additional fast communication channels in the proposed hierarchical control system. The FESS installed in the microgrid, which is designed to maintain the power output of the WECS and FESS combined energy source over half of average power generated by the standalone wind power generator, also has good capability for secure the critical loads during the transition period.

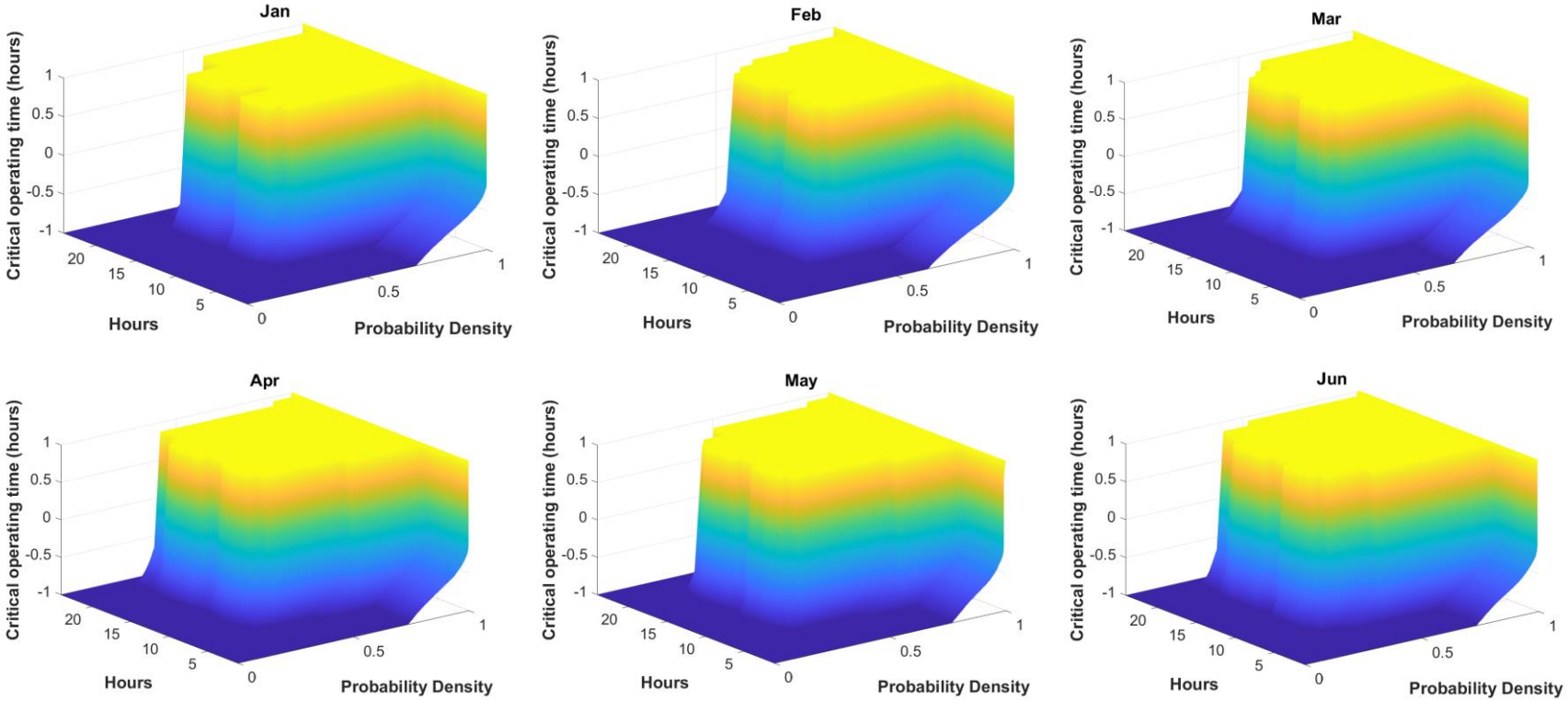

Figure 6.3 24-hours Critical operating time Probability distribution characteristics from January to Jun

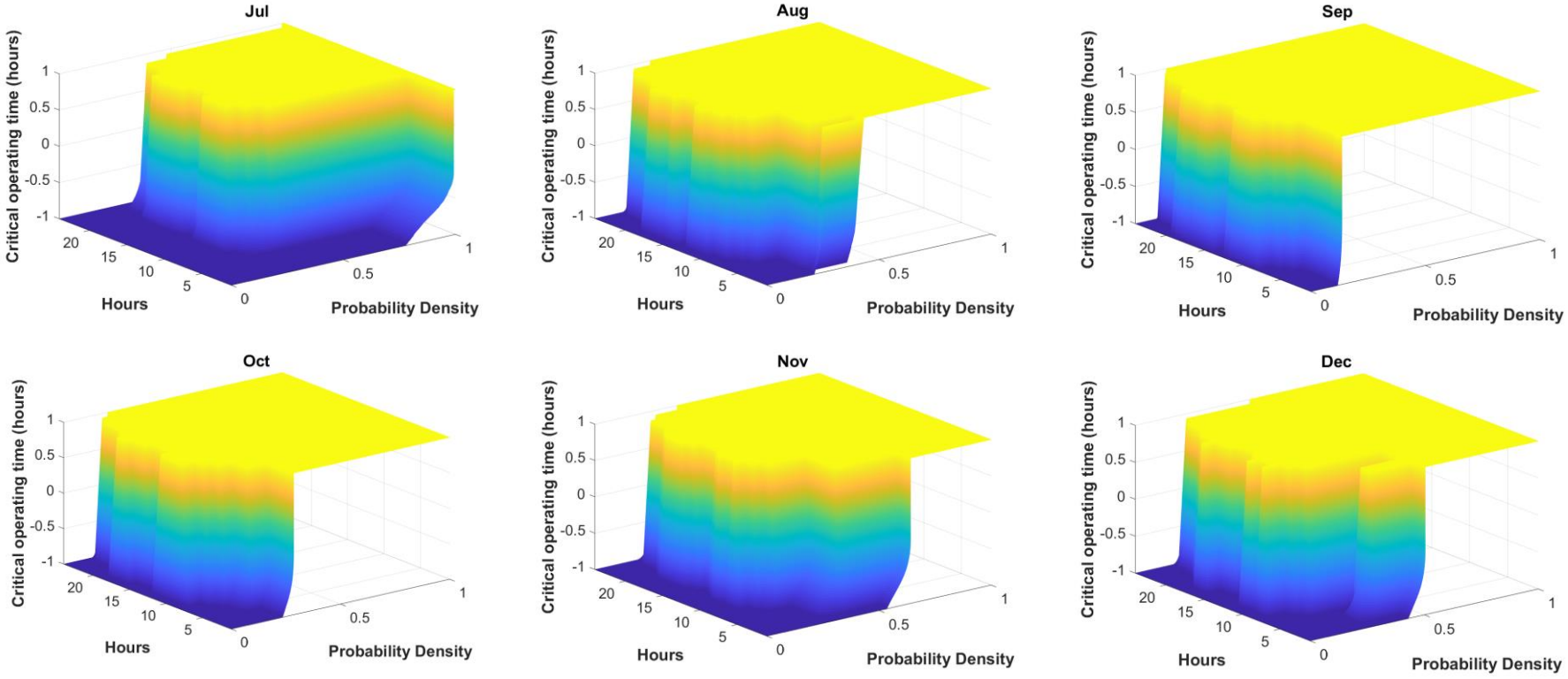

Figure 6.4 24-hours Critical operating time Probability distribution characteristics from July to December

6.3 Control strategies for microgrid state transition

6.3.1 Control strategies for the microgrid disconnection

A microgrid may disconnected from the main grid for different reasons. It could be accidently isolated by the protection devices when there are abnormal situations or faults happened in the main grid. If it is not a permanent fault, this microgrid will reconnect to the main grid in several seconds. The microgrid also can be manually disconnected for the purpose such as device maintenance and repairing. In this situation, a short-term islanded microgrid is formed.

In this section, the control procedure which is capable for different disconnecting situations is achieved by adding time delay to different strategies as *Figure 6.5* shows. After the islanding situation detected by the monitoring system, the backup generator has to be switch to constant voltage output mode as there has to be a reference bus in a power system. A delay time is added to determine which control strategy should be applied. If the time limit is not reached, the control strategy for the temporarily disconnection will be activated. This control strategy will be continuously working until the microgrid be reconnected to the main grid or the delay time is exceeded. Alternatively, if the islanded state lasts over the time limit, the control strategy will be switched to another one which is designed for short-term islanded microgrid. This short-term islanded microgrid control strategy will be discussed in the Section 6.4.

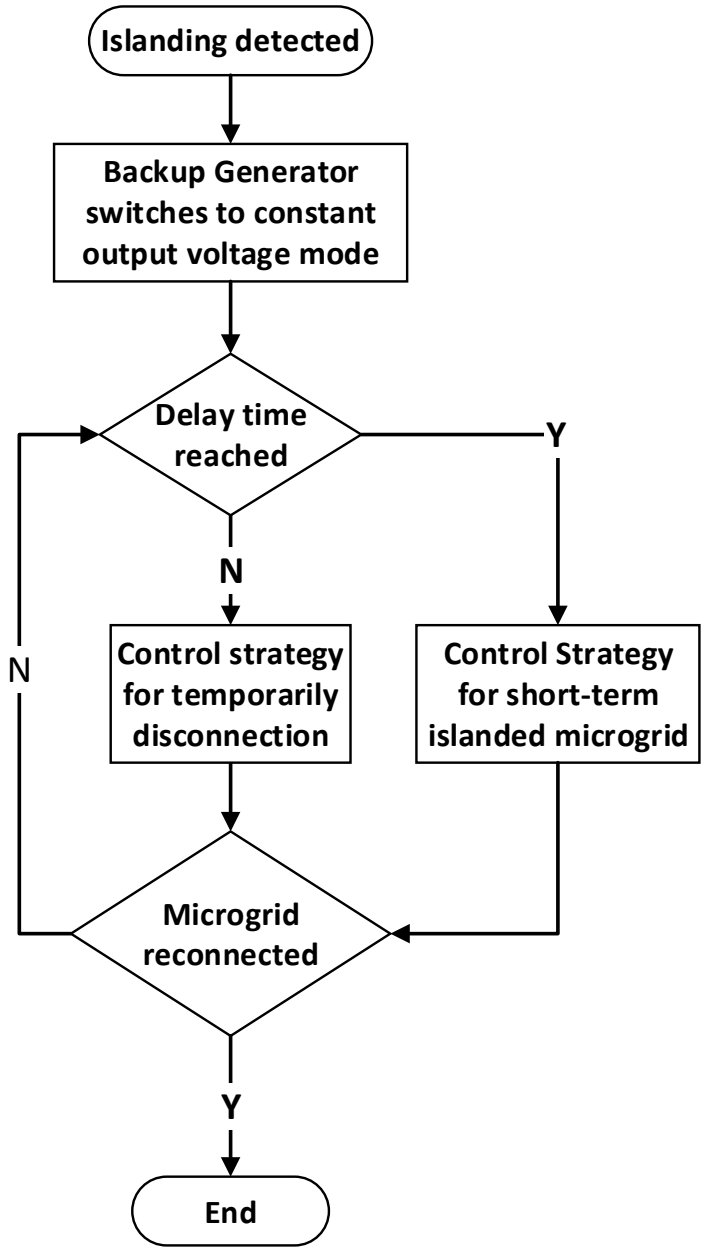

Figure 6.5 Control procedure for the microgrid disconnection

The control objective for temporarily disconnection contains two parts: maintaining the power balance within the microgrid and keeping the voltage magnitude and phase angle the same as before disconnecting. The power balance can be instantaneously maintained by the droop control-based level 1 controller. The voltage magnitude and phase angle control

are achieved by the deviation compensation procedure which is addressed in the upper level controller.

The overall control strategy for temporarily disconnection is proposed in *Figure 6.6*. This procedure is started with gathering the system information which includes the microgrid topology, demands, the capacity of generators. A case file which describes the system information is generated for power flow calculation. In this thesis, the description file is generated using the format of MATPOWER case file. A set of new references for level 1 controllers are generated by the MATPOWER optimal power flow function. The voltage at the microgrid side of PCC bus is compared to the previous value to determine whether the compensation procedure will be introduced in. If the differential is out of the allowance, the compensation procedure which is proposed in chapter 4 will be used to generate and add compensation parameters into the description file. The new references based on the latest case file are applied to the level 1 controllers. The loop of power flow regulation will be continuously executed until the voltage deviation at the PCC bus within the limitation.

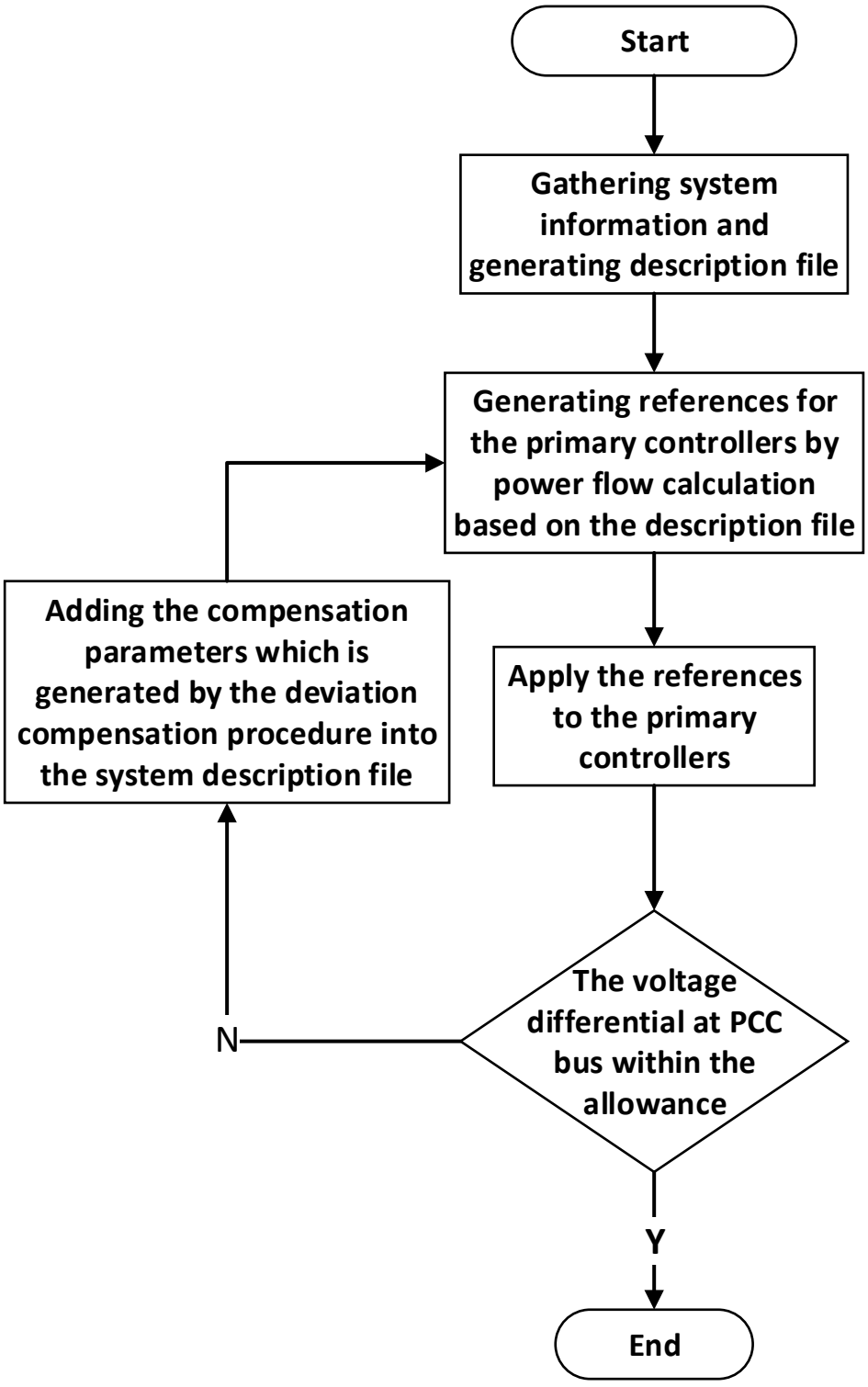

Figure 6.6 Control strategy for temporarily disconnection

6.3.2 Control strategies for the microgrid reconnection

The reconnecting operation is executed in mainly three kinds of situations: automatically reclosing, reclosing from an islanded state and black start. In this thesis, the microgrid is assumed continuously running, in case of that, the black start situation is not discussed. The automatically reclosing usually happened in several seconds to minutes after disconnecting operation. As the PCC bus voltage is regulated the same as before disconnecting by the control strategy for this short-term temporarily disconnection, additional operations before reclosing are not necessary.

After the microgrid operated in islanded mode for a certain time period, the voltage magnitude, phase angle and frequency may have shifted from the original values depending on the control strategies. To minimize the reclosing impact to the power quality, the voltage magnitude, phase angle and frequency at microgrid side of the PCC bus should be synchronized to the main grid side values before closing. The preclosing procedure is similar to the control strategy for the temporarily disconnection. The only difference is, the real time tracked main grid side values are used to evaluating the deviations instead of the before disconnecting parameters.

6.3.3 Simulation results and discussion

In this section, the experiment is divided into two scenarios. In the first scenario, the microgrid is operated with only the level 1 controller. The experiment here is simulating the communication loss of the control system to evaluate the robustness of the proposed control theory. In the second scenario, the proposed hierarchical control system is introduced in to evaluate the smooth transition function.

6.3.3.1 Scenario1: Microgrid state transition without higher level controller

a) Backgrounds of this experiment

In this scenario, the experiment is scheduled in three main time periods as Table 6.2 shows. The initial running status of the experiment system is picked from the operating schedule which is introduced in chapter 5. To evaluate the robust of the proposed control system, the data for 10 a.m. in July which has relatively heavy load and large power provided by the main grid before disconnection is applied in this section. There are 4.8MW loads in total. The power output of the 4 DGs and the main grid are 1.5MW, 0.6MW, 1.0MW, 0.6MW, 1.1MW respectively.

Table 6.2 Experiment events schedule

Time period	Events
0s-1s	Simulation initialization
1s-2s	Microgrid disconnected from the main grid, and the system is regulated by the level 1 controllers
2s-3s	Microgrid reconnected to the main grid, and the system is regulated by the level 1 controllers

b) Simulation results and discussion

The simulation results of power output of DGs, voltages of DG buses are recorded in *Figure 6.7*, *Figure 6.6.8* respectively. After the microgrid disconnected from the main grid at t=1s, each DGs is supposed to share the demand by their droop characteristics. It can be observed from *Figure 6.6.8*, the response time of these 4 DGs for the microgrid state transitions

are gradually increased. This is because the distance from the PCC bus to the DGs are different. In case of that, at the first 0.15 second, the backup generator DG1 which is close to the PCC bus, takes most of the demand originally supplied by the main grid. After the steady state reached, the entire microgrid voltage level decreased about 0.35 p.u.. Although it is acceptable for power grid, the disconnection effect on the voltage deviation do exist.

At t=2s, the microgrid is directly reconnected to the main grid without any synchronization operations. As all three DGs are operated under droop control mode, there is no reference for the phase angle regulation. The phase angle differential at two ends of PCC bus cannot be guaranteed in a certain area. Although the microgrid finally back to the steady state the same as the initial state, the voltage differentials cause large fluctuation during the reconnection period.

All in all, the microgrid system can survive, but the power quality cannot perfectly be guaranteed if only the control level 1 works properly.

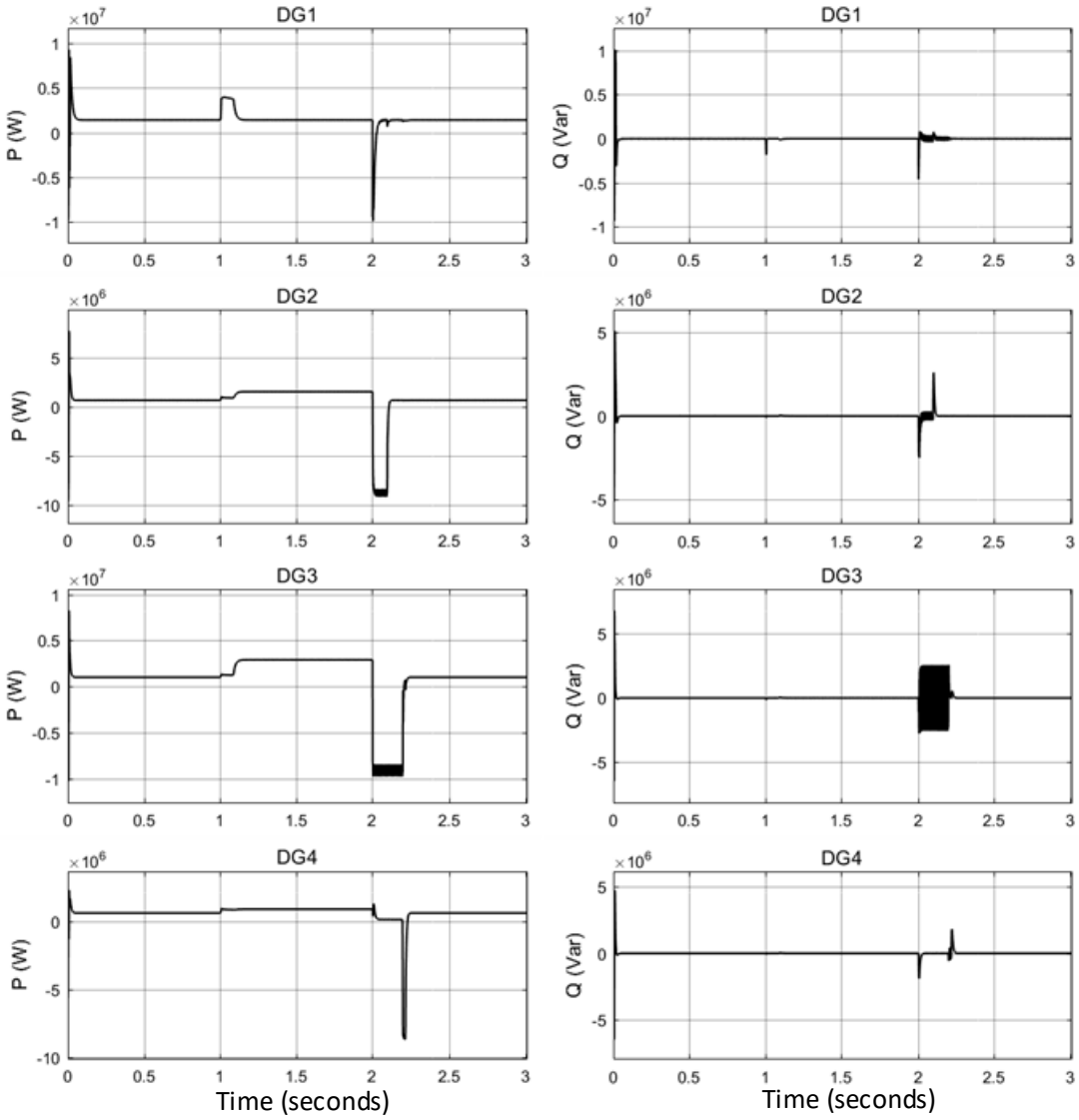

Figure 6.7 Power output of DGs

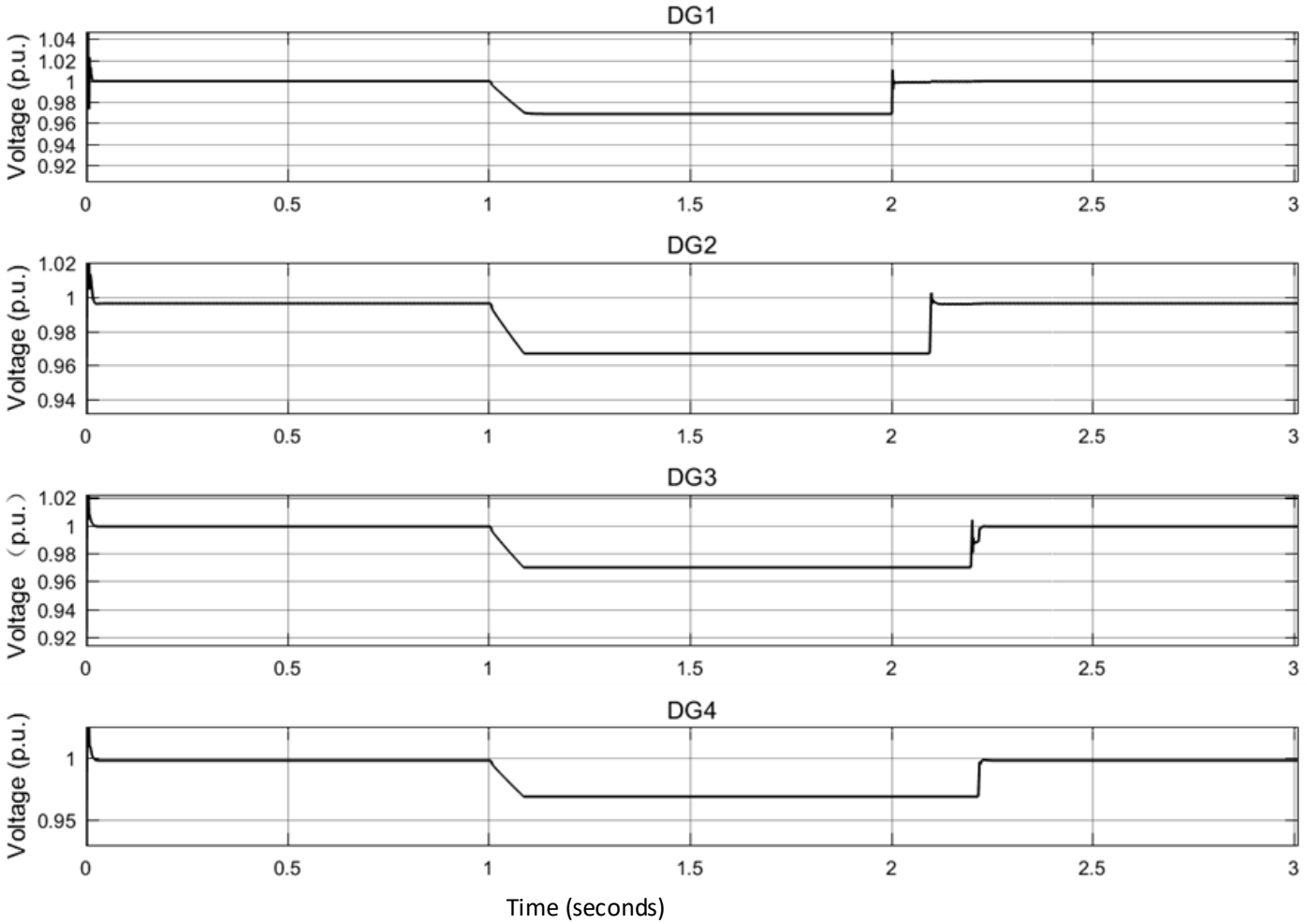

Figure 6.6.8 Voltage on DG buses

6.3.3.2 Scenario 2: Microgrid state transition with the hierarchical control system

a) Backgrounds of this experiment

In this scenario, the experiment is scheduled in 4 time periods as shown in Table 6.3. The initial status is the same as it is in scenario 1. In contrast to the last scenario, the higher-level controllers are involved in and improve the system performances.

Table 6.3 Experiment events schedule

Time period	Events
0s-1s	Simulation initialization
1s-1.5s	DG1 operating mode switched when Microgrid disconnection
1.5s-2s	Higher level controller involved, and new references applied
2s-2.5s	reconnection

b) Simulation results

The simulation results of power output of DGs and voltages of DG buses on each DG bus are recorded in *Figure 6.9* and *Figure 6.10* respectively. The backup generator DG1 switched to constant voltage output mode after the microgrid disconnection happened. As it is located close to the PCC bus, the bus voltage on the PCC bus is supported by DG1 and changed little after the microgrid disconnected. This makes the disconnection effects are isolated to the other DGs. In which case, the output voltage and power of DG2-4 are almost the same as before disconnecting. However, DG1 has to pick up the demand supplied by the main grid before. At t=1.5s,

this situation is dealt with by applying new references from the higher-level controllers to the level 1 controllers. The output voltage of DG2-4 are slightly increased, and they share more demand after this operation executed.

The microgrid is reconnected to the main grid at t=2s, the only thing affected is the power output of DG1. This is because it is operated in constant voltage output mode, the power output cannot automatically self-adjust. In contrast to scenario 1, the fluctuations on both of the active power and reactive power during transition periods are significantly reduced. The system voltage deviation is maintained in a very little area.

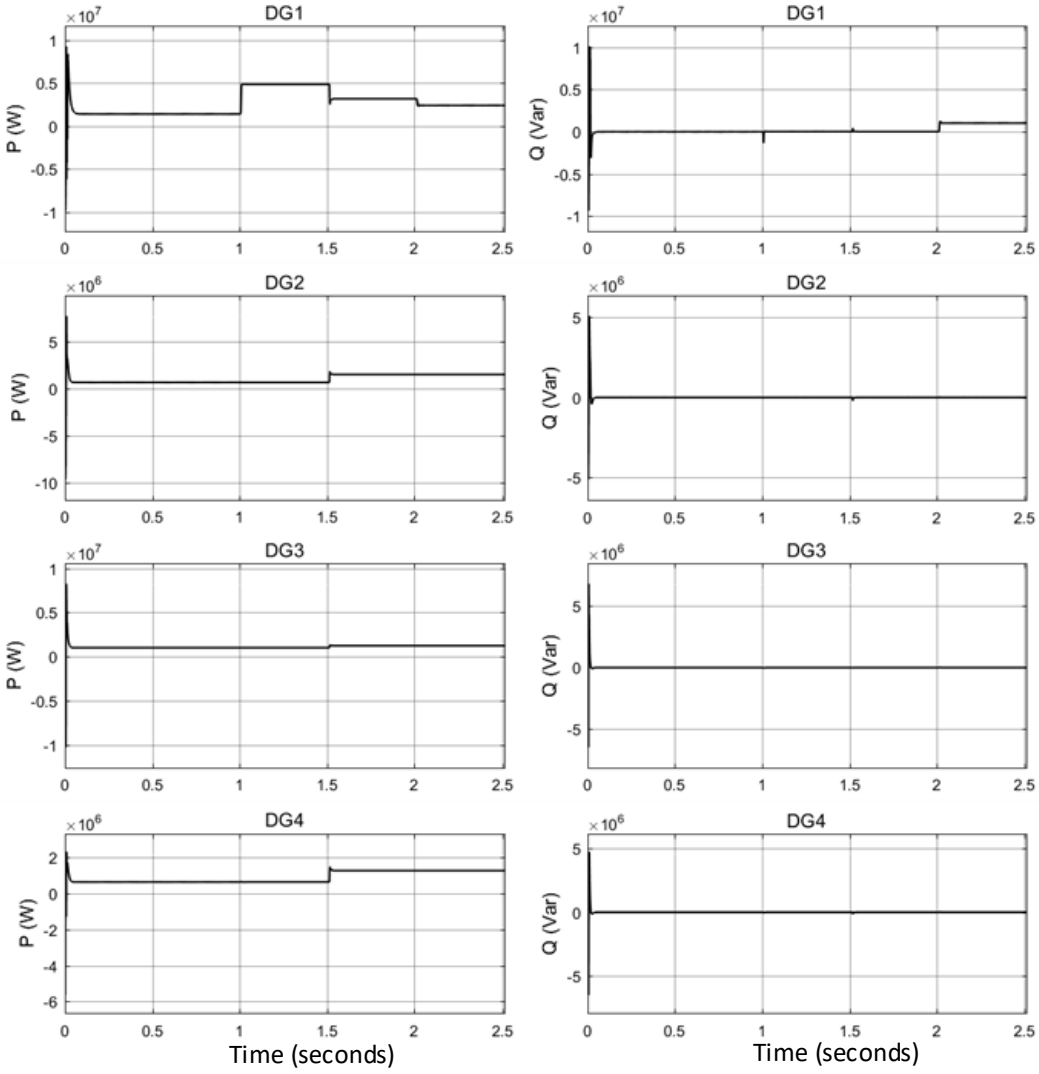

Figure 6.9 Power output of DGs

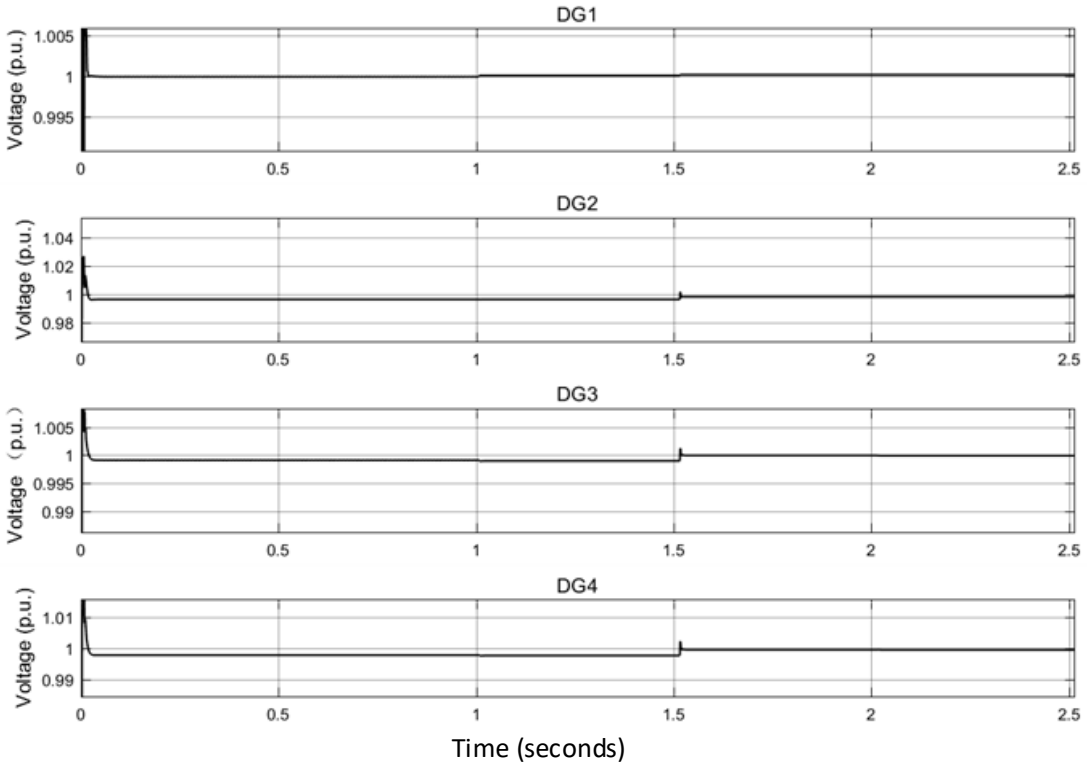

Figure 6.10 Voltage on DG buses

6.4 Control strategies for short-term islanded microgrid

For the highly randomly output characteristic of wind power generator, the wind power embedded microgrid which is operated in long-term islanded mode has to install a huge amount of energy storage devices or controllable loads to maintain the power balance. The large investment cost makes this type of microgrid not feasible. In case of that, in this chapter, only short-term islanded microgrid is discussed.

6.4.1 Power sharing among DGs

As discussed in section 6.2, with the proposed WECS/FESS combined DG, there is no overload risk in the short-term islanded situation. In which case, the control strategy for the short-term islanded microgrid is about power

sharing among DGs. In the proposed microgrid system, each DG is consisted of a wind power generator and a flywheel energy storage device. To maximize the duration of the system power balance in the short-term islanded period, besides the wind power generator output, the power sharing ratio of each DG is also related to the energy stored in the storage devices. The output of each DG is regulated following the equation *(6.2)*.

$$P_i = \frac{C_i + t \cdot P_{wi}}{\sum_{i=1}^{n}(C_i + t \cdot P_{wi})} \cdot (P_L - P_{BG}) \quad (6.2)$$

Where:

P_i is the output power of the i_{th} DG (MW)

P_{wi} is the output power of the i_{th} wind power generator part in the DG (MW)

C_i is the energy stored in the energy storage device which is coupled with the i_{th} wind power generator (MWh)

P_L is the total loads (MW)

P_{BG} is the output power of backup generator (MW)

t is a time constant (hour)

n is the total number of the energy resources

6.4.2 The backup generator's output optimization

As the load is consisted of controllable load and inelastic load, P_L can variate to a certain level if needed. The output power of backup generator P_{BG} is also flexible. For economic considerations, the output power of

backup generator P_{BG} should be as small as possible when the power balance is maintained. The optimized P_{BG} has to be satisfied the constraints as *(6.3)* presents. The constraints have two rules: the backup generator has to be running within its capable operating range, and the energy stored in the storage devices can support the request power output in the certain time period.

$$\text{constraints}\begin{cases} P_{BGmin} \le P_{BG} \le P_{BGmax} \\ C_i - t \cdot (P_i - P_{wi}) > 0 \end{cases} \tag{6.3}$$

The procedure which used to find the minimum P_{BG} is given in *Figure 6.11*. This procedure is achieved by a step increase in the value of P_{BG} from P_{BGmin} until the first one which meets the constraints.

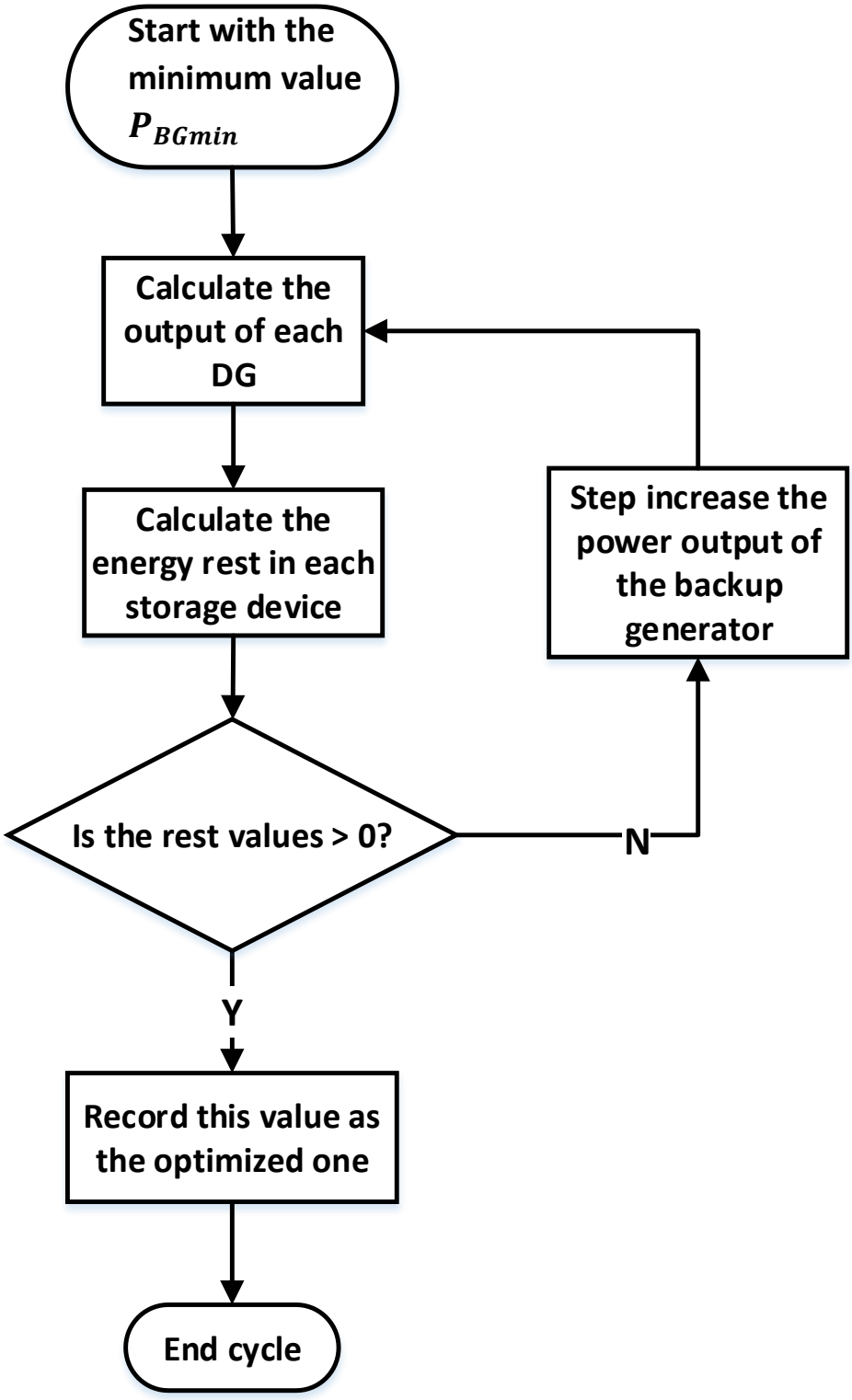

Figure 6.11 Procedure for finding the minimum backup generator's output

6.4.3 Case: The backup DG's output in the simulation short-term islanded microgrid

In the simulation microgrid, the wind speed is assumed to change every 15 minutes, in which case, the time constant *t* in the equation *(6.2)* is chosen to be 0.25 hours. As the generating cost of diesel generator is much higher than wind generators, it always be preferred to generate minimum power. In this case study, how much power need to be generated by backup DG to maintain the maximum reliability is discussed.

It can be observed from the *Figure 6.12* and *Figure 6.13*, that for each hour in different months, there are only several times the backup DG cannot operated with 0.8MW output, which is the minimum operating mode of this diesel generator, during the 100000 times Monte Carlo simulation. This backup generators minimum output power requirement in 12 months has the similar trends of the critical time probability distribution which is discussed in the case study of section 6.2. It means more energy storage device installed capacity can reduce the operating cost. However, for this particular system, even in August, the probability of output power over 0.8MW is around 10 times over 100000 times simulation, which is much less than 0.1%.

In which case, the output of the backup DG can always set to the minimum value which is 0.8MW in the simulation microgrid to reduce the response time. The FESS installed capacity which is designed for the purpose of reducing the WECS power output variation is capable for the short-term islanding situation.

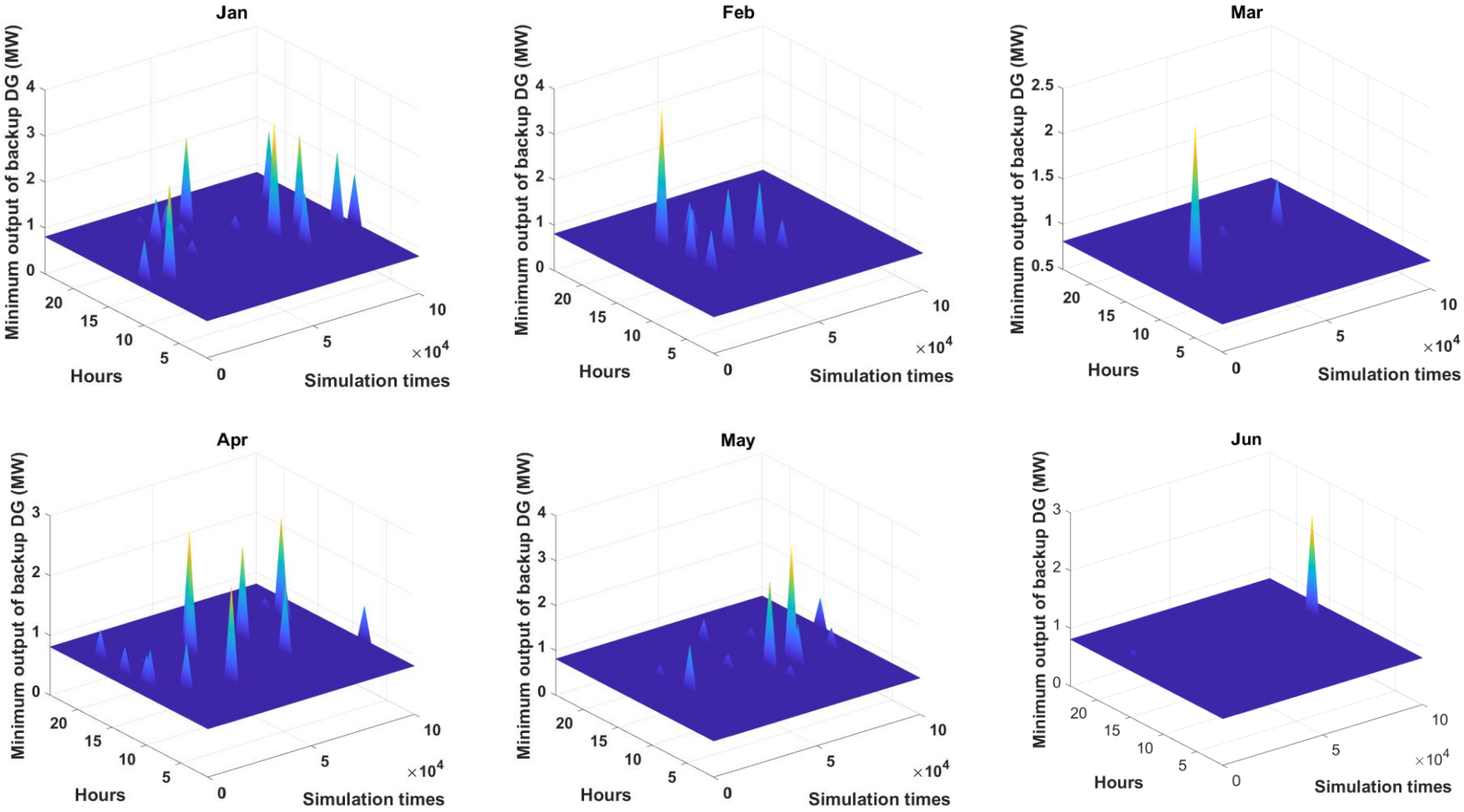

Figure 6.12 The optimized backup DG's output power from January to June

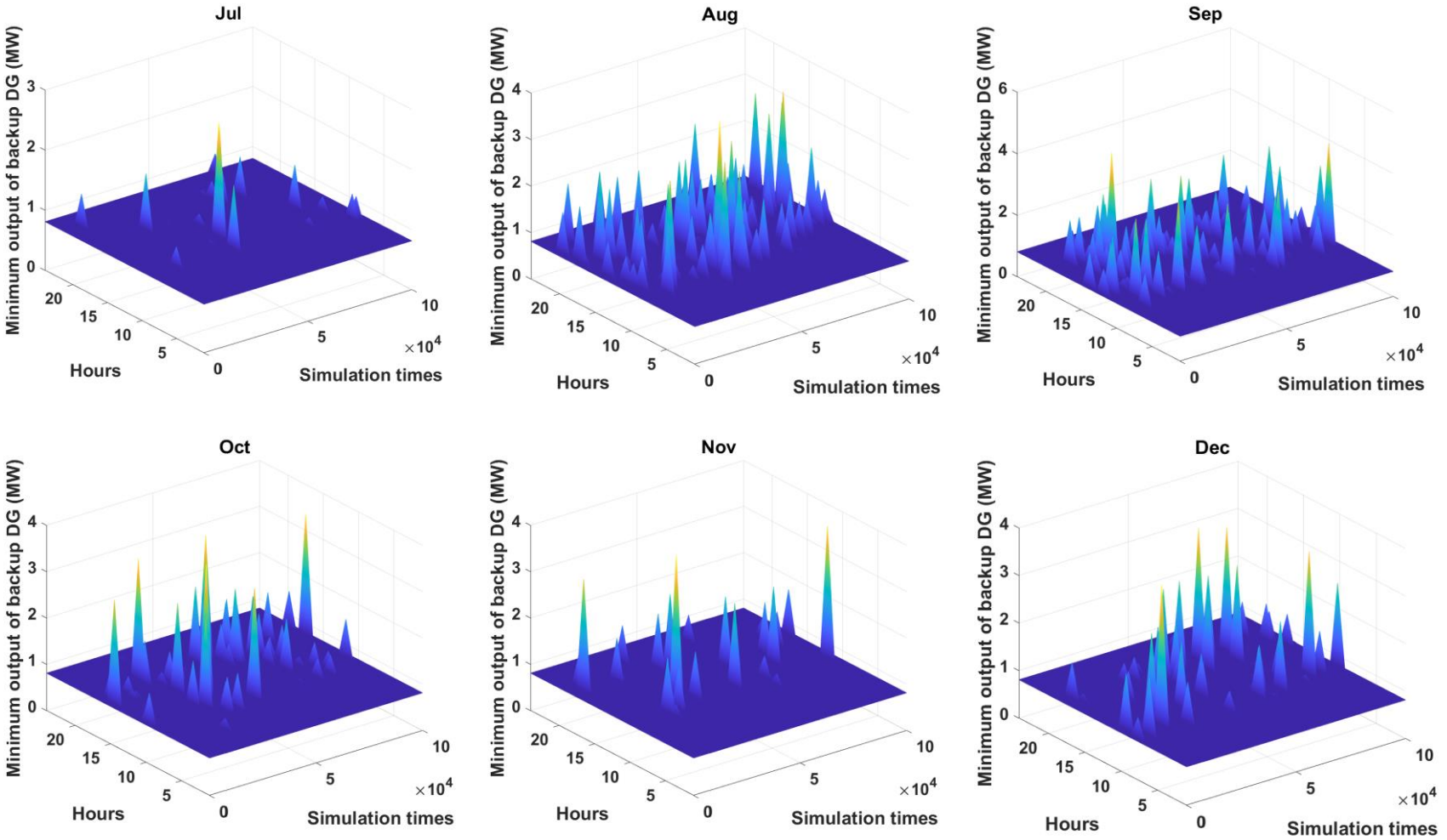

Figure 6.13 Optimized backup DG's output from July to December

6.5 Summary

In this Chapter, the control strategies for smooth transition and short-term islanded operation are proposed. For the proposed wind power embedded microgrid, the existing components which are designed for the grid-tied operations also can be applied in the short-term islanding situation and achieve smooth transition function. The smooth transition function is achieved by the combination of PCC voltage deviation compensation and switching the operating mode of backup DG to constant voltage output mode. With the proposed hierarchical control strategies, there is no load shedding operation required for disconnected period. Besides, with the proposed load sharing method, for the first 15 minutes of islanded situation, the backup generator can operate in minimum mode even for the heavy load periods.

Chapter 7: Conclusions

7.1 Conclusions and Contributions

The proposed hierarchical control system enables to make a wind power generation embedded microgrid to be effectively operated, and minimize the power quality and safety issues caused by the features of wind power generator. In which case, it provides a feasible solution for improving wind power penetration. To achieve this object, the works have been done and the achievements in this thesis are concluded as follows.

7.1.1 Development of the wind power generator's output model

For the purpose of evaluating the wind generator embedded microgrid system performance, the wind power output statistical model which is based on the artificial wind speed and aerodynamic characteristic of wind turbine generator is investigated in this thesis. The wind speed characteristic is described by the Weibull Distribution. The shape and scale parameters of Weibull Distribution are derived from the historical data by the moment method.

There are three factors which are used to derive the wind power generator's output model: wind speed, aerodynamic of wind turbine and the generator efficiency. The wind speed data used for evaluation experiment is generated by repeating Monte Carlo simulation. The aerodynamic performance of the wind turbine is determined by the factors of wind power velocity, air density, the area swept by rotor blades and the power conversion efficiency of rotor blades. In this thesis, these factors are obtained from the commercial generator's instructions. The generator's power conversion efficiency is determined by the generator

type. The DFIG and PMSG wind generator model are the two most commonly used commercial models currently. According to the comparisons in Chapter 2, the DFIG model is the PMSG model is chosen as the simulation wind generator model in this thesis as it has better performances during weak wind power durations.

A case study, which used the historical wind speed data from Wensum weather station and the PMSG type wind turbine model Vestas V150-4.2MW^{TM}IEC III B, demonstrated the feasibility of this artificial model. This statistical model has the advantages of easy to obtain, good probability distribution characteristic which is close to the observed data characteristic. The power output distribution characteristics are sensitive to the features of wind speed data, it is sufficient for describing or evaluating a system in different seasons and/or different areas.

7.1.2 Development of the wind power integrated microgrid with the hierarchical control system

In this research, the three-levels hierarchical control method is proposed to achieve the promising microgrid functions. This proposed control system can adapt to various situations such as frequency and voltage variations on PCC without relying on the communication channels. The advanced functions such as economic running, deviation elimination are achieved in real-time by using low bandwidth communication channels. Besides, the system regulations are operated in non-real-time domain.

A 4-bus LV microgrid model built in MATLAB/Simulink is used to preliminary test the proposed control system. The further simulation scenarios are taken in the CERTS 20-bus microgrid model. The proposed hierarchical control method is easy to apply and robust with the simple

decentralized control level 1 structure. It is also good at system parameters regulation and function flexible with the assistant of the higher-level control systems. This proposed control system also can be extended to any inverter-based energy source with randomly power output. The key findings and contributions are concluded as follows:

- **Decentralized control level 1**

In contrast to the conventional control methods which normally consider the voltage magnitude and frequency at the PCC as a constant, the proposed control level 1 is designed to provide the instantaneous functions of voltage stability provision, frequency stability preserving, plug and play capability of DERs and circulating current avoidance among DERs during voltage and frequency variations. With the simulation results the 4-bus microgrid system, the advantages of the proposed level 1 control theory are proved.

In this research, the DGs in microgrid is connected to the grid through inverter interfaces. The generator unit is operated as a current controlled voltage source and be regulated by the combination of an inner current control loop and an outer voltage control loop. It has the advantage of limit the abnormal current.

The decentralized features which is not rely on the communication channels are achieved by the adjustable load sharing method. Its dynamic response can be adjusted without affecting the droop characteristics. In contrast to conventional P/f and Q/V droop characteristics, the modified P/V and Q/δ droop characteristics are proposed as the transmission lines in microgrid has relatively large R/X ratios.

The frequency signal tracked by PLL in conventional droop methods is replaced by the VPLL which directly generate the phase angle signal with constant frequency. The VPLLs in different generator units are synchronized by GPS signal. Be compared with the conventional control theories which use the frequency as the global reference, the proposed system is more stable as there always no frequency differences among DGs.

- **Centralized control level 2**

The control level 2 cooperates with the control level 1 to obtain the advantages of both droop control techniques (non-communication required and certain level of autonomy) and the active load sharing methods (voltage and frequency regulation). There are two main control objectives of the control level 2 in the proposed hierarchical control method: initial steady state values generation and deviations compensation.

The initial steady state settings are generated by the power flow calculation function of the MATPOWER tools box in MATLAB. As a single microgrid system is relatively simple, the initial settings can be obtained in tens of milliseconds.

The control level 2 gives compensation of the voltage and/or frequency deviation caused by control level 1 by modifying the settings of level 1 controllers through low bandwidth communication channels. The deviations compensation is achieved by recalculating power flows after adding correction parameters which is generated from the comparisons of observed values and the initial calculated results. The simulation results

show that the lack accuracy regulation problem caused by the droop controllers can be eliminated in several seconds.

Besides the features of both the fast-dynamic response capability and accurate power flow regulation, the limitation of load variation capability of the standalone level 1 controller is extended after the level 2 controller introduced.

- **Centralized control level 3**

The control level 3 which can take place in several minutes to hours. There are two groups of functions are proposed in this control level: non-real-time and real-time operating functions.

A WECS/FESS combined system which improves the system performances is proposed. The features of high-power density and low-energy density make the FESS has the capability of providing large power output in short terms. Besides, this combined system is economical because of the good durability of FESS. The supplementary optimization function for the combined system is addressed in the level 3 controller as a non-real-time function. The generator power output variance is reduced to 1/3 of the original WECS after optimized.

The real time optimization functions which utilized in this level, such as economic operating and smooth state transition, are achieved by sending compensation requests to the level 2 controller. The simulation result of reclosing procedure in chapter 4 demonstrates the good cooperation among the control systems in these different three levels.

7.1.3 Wind power embedded microgrid operated by the proposed hierarchical control method

In chapter 5 and chapter 6, the further experiments and demonstrations are executed in an 11kV CERTS 20-bus simulation microgrid model built in MATLAB/Simulink. This main components in the microgrid contains: 2.6MW load (0.8MW is controllable), a 2MW diesel generator which used as the backup generator and three 4MW wind power generator which are coupled with FESSs. Assisted with the hierarchical control system, this experiment model can be operated in grid connected mode, islanded mode and achieved smooth transition.

Under grid connected mode, the microgrid system can be operated as a controllable unit which is connected to the main grid through PCC. The behaviour of this microgrid is operated follow the schedule generated by level 3 controller. The experiment results prove that the power exchange between the hierarchical controlled microgrid and the main grid can be kept constant in certain time periods with high reliability. This makes the impacts caused by the intermittent and variating features of wind power be minimized. In case of that, the wind power penetrated level in a power system can be increased without causing problems by introducing this microgrid system.

The simulation microgrid is designed for increasing wind power penetration level which means it is usually operated in the grid connected mode. Furthermore, the simulation results show its capabilities for state transition and short-term islanded mode with the proposed control strategies. The control strategies for fast reclosing, reconnecting from islanded and the load sharing during short-term islanded scenarios were

proposed. The simulation results demonstrated these control strategies can improve the microgrid system robustness and achieve the promised smooth transition function.

7.2 Future work

There are some potential areas for the future research:

- Harmonics distortion emulation

  In a microgrid system, there are large amount of power electronic devices in a relatively small power system. The harmonic distortion hazard has to be considered. There are mainly three potential ways that can minimize the harmonics: installing more filters, using Proportional-Resonant controllers which has the anti-harmonic capability instead of PI controller, and using advanced converter techniques. In this thesis, two-level converter and LC filter are implemented in the inverter interfaced DG model. The AC side voltage converted by this two-level converter has the shortcoming on the waveform quality. Besides, this PWM driven converter has to be operated in high frequency switching mode which can cause relatively large power losses. In contrast to the conventional two-level and three-level converter, the Modular Multi-Level Converter (MMC) which is already used in the HVDC industry has significant advantages on the quality of waveform and switching frequency [137, 138]. When there are certain number of the submodules, the output voltage waveform is very close to the sine wave. In which case, the filter part is not necessary.

- State-of-the-art communication protocols

  The communication system between different control levels in this research is achieved by using TCP/IP communication protocol through a data base in a local area network. There are some particular communication protocols which have the potentials of consuming less system resources and/or reducing the communication delay. For instance, the IEC 61850 protocol, which is a standard for the design of electrical substation automation [139]. There are two types of message structure of this protocol, Generic Object Oriented Substation Events (GOOSE) and Generic Substation State Events (GSSE). By using GOOSE message, a data set contains any format of data is transmitted within 4 milliseconds. In contrast to GOOSE message, GSSE format is simpler, only a status list which is consisted of a string of bits is used and exchanged among devices. In that case, GSSE message could be handled faster than GOOSE message in certain devices. As their different features, which type of message should be implemented depends on the circumstances. For the practical situation it is necessary to establish the best communication protocols.

- Multi microgrids

  The WECSs are located in the same microgrid network in this thesis. There are situations that the WECSs could be operated in several microgrids. These microgrids could be operated together as a larger entity, as well as running as an individual microgrid. For instance, if the distributed energy resources cannot be contained in a single microgrid became of geographic or economic reasons, they could be operated in multi microgrids. These multi microgrids cooperation can

be regulated by the third level control system. In contrast to the previous situation, when there are abnormal situations happened inside a microgrid, to minimize the impact, it could be divided into several groups which contains power resources and loads. It forms another type of multi microgrids. As the network topology significantly changed, the settings of the level 1 controller have to be modified. How to deal with these situations could be investigated in the future researches.

- Market behaviour

  To maintain the power balance and scheduled power exchange at the PCC, there are controllable loads and backup generators in the microgrid. In this thesis, the demands are simply divided into two groups: inelastic loads and controllable loads. In a competitive electricity market, only part of the demands is fully inelastic or fully controllable, the electricity price and demands usually have an inverse relationship. More detailed and accurate demand side model need to be investigated to evaluate market behaviour of a microgrid. Besides, there are some situations that the microgrid cannot meet the demands, there have to be a priority list of loads and a compensation agreement in the event of a blackout. The research is the market behaviour and would need to be considered for future work.

References

1. ; Available from: https://www2.gov.scot/renewableenergy.
2. C. Luo, H. G. Far, H. Banakar, P. Keung, and B. Ooi, *Estimation of Wind Penetration as Limited by Frequency Deviation.* IEEE Transactions on Energy Conversion, 2007. **22**(3): p. 783-791.
3. Paul Gardner Frans Van Hulle. *PART 2: GRID INTEGRATION*. Available from: https://www.wind-energy-the-facts.org/wind-energy-penetration-and-integration.html [Accessed: 01/10/2018].
4. T. h. m. El-Fouly, H. H. Zeineldin, E. f. El-Saadany, and M. M. A. Salama, *Impact of wind generation control strategies, penetration level and installation location on electricity market prices.* IET Renewable Power Generation, 2008. **2**(3): p. 162-169.
5. D. Yang, J. Kim, Y. C. Kang, E. Muljadi, N. Zhang, J. Hong, S. Song, and T. Zheng, *Temporary Frequency Support of a DFIG for High Wind Power Penetration.* IEEE Transactions on Power Systems, 2018. **33**(3): p. 3428-3437.
6. Y. Wang, G. Delille, H. Bayem, X. Guillaud, and B. Francois, *High Wind Power Penetration in Isolated Power Systems—Assessment of Wind Inertial and Primary Frequency Responses.* IEEE Transactions on Power Systems, 2013. **28**(3): p. 2412-2420.
7. N. Nguyen and J. Mitra, *Reliability of Power System with High Wind Penetration Under Frequency Stability Constraint.* IEEE Transactions on Power Systems, 2018. **33**(1): p. 985-994.
8. D. Gautam, V. Vittal, and T. Harbour, *Impact of Increased Penetration of DFIG-Based Wind Turbine Generators on Transient and Small Signal Stability of Power Systems.* IEEE Transactions on Power Systems, 2009. **24**(3): p. 1426-1434.
9. Y. Ding, C. Singh, L. Goel, J. Østergaard, and P. Wang, *Short-Term and Medium-Term Reliability Evaluation for Power Systems With High Penetration of Wind Power.* IEEE Transactions on Sustainable Energy, 2014. **5**(3): p. 896-906.
10. D. Westermann and A. John, *Demand Matching Wind Power Generation With Wide-Area Measurement and Demand-Side Management.* IEEE Transactions on Energy Conversion, 2007. **22**(1): p. 145-149.
11. A. Ahmadi-Khatir, A. J. Conejo, and R. Cherkaoui, *Multi-Area Unit Scheduling and Reserve Allocation Under Wind Power Uncertainty.* IEEE Transactions on Power Systems, 2014. **29**(4): p. 1701-1710.
12. F. Alismail, P. Xiong, and C. Singh, *Optimal Wind Farm Allocation in Multi-Area Power Systems Using Distributionally Robust Optimization Approach.* IEEE Transactions on Power Systems, 2018. **33**(1): p. 536-544.
13. Y. Liu, W. Du, L. Xiao, H. Wang, and J. Cao, *A Method for Sizing Energy Storage System to Increase Wind Penetration as Limited by Grid Frequency Deviations.* IEEE Transactions on Power Systems, 2016. **31**(1): p. 729-737.
14. X. Dui, G. Zhu, and L. Yao, *Two-Stage Optimization of Battery Energy Storage Capacity to Decrease Wind Power Curtailment in Grid-Connected Wind Farms.* IEEE Transactions on Power Systems, 2018. **33**(3): p. 3296-3305.
15. P. Wang, Z. Gao, and L. Bertling, *Operational Adequacy Studies of Power Systems With Wind Farms and Energy Storages.* IEEE Transactions on Power Systems, 2012. **27**(4): p. 2377-2384.
16. B. Cleary, A. Duffy, A. OConnor, M. Conlon, and V. Fthenakis, *Assessing the Economic Benefits of Compressed Air Energy Storage for Mitigating Wind Curtailment.* IEEE Transactions on Sustainable Energy, 2015. **6**(3): p. 1021-1028.

17. F. Díaz-González, F. D. Bianchi, A. Sumper, and O. Gomis-Bellmunt, *Control of a Flywheel Energy Storage System for Power Smoothing in Wind Power Plants.* IEEE Transactions on Energy Conversion, 2014. **29**(1): p. 204-214.
18. M. A. Hozouri, A. Abbaspour, M. Fotuhi-Firuzabad, and M. Moeini-Aghtaie, *On the Use of Pumped Storage for Wind Energy Maximization in Transmission-Constrained Power Systems.* IEEE Transactions on Power Systems, 2015. **30**(2): p. 1017-1025.
19. G. Cai and L. Kong, *Techno-economic analysis of wind curtailment/hydrogen production/fuel cell vehicle system with high wind penetration in China.* CSEE Journal of Power and Energy Systems, 2017. **3**(1): p. 44-52.
20. J. Merley, G. Lorenz, P. Mandatova, P. O. Granström, and F. Chapalain. *EU-wide network codes: Process, role of DSOs and possible impacts*. in *22nd International Conference and Exhibition on Electricity Distribution (CIRED 2013)*. 2013.
21. E. H. Allen, R. B. Stuart, and T. E. Wiedman, *No Light in August: Power System Restoration Following the 2003 North American Blackout.* IEEE Power and Energy Magazine, 2014. **12**(1): p. 24-33.
22. C. Sulzberger, *History - When the lights went out remembering 9 November 1965.* IEEE Power and Energy Magazine, 2006. **4**(5): p. 90-95.
23. Xinyao Li, *Thesis: Enhanced Control and Protection for Inverter Dominated Microgrids*, in *Department of Electronics and Electrical Engineering*. 2014, University of Strathclyde.
24. H. Kuang, S. Li, and Z. Wu. *Discussion on advantages and disadvantages of distributed generation connected to the grid*. in *2011 International Conference on Electrical and Control Engineering*. 2011.
25. B. Lasseter. *Microgrids [distributed power generation]*. in *2001 IEEE Power Engineering Society Winter Meeting. Conference Proceedings (Cat. No.01CH37194)*. 2001.
26. R. H. Lasseter. *MicroGrids*. in *2002 IEEE Power Engineering Society Winter Meeting. Conference Proceedings (Cat. No.02CH37309)*. 2002.
27. D. E. Olivares, A. Mehrizi-Sani, A. H. Etemadi, C. A. Cañizares, R. Iravani, M. Kazerani, A. H. Hajimiragha, O. Gomis-Bellmunt, M. Saeedifard, R. Palma-Behnke, G. A. Jiménez-Estévez, and N. D. Hatziargyriou, *Trends in Microgrid Control.* IEEE Transactions on Smart Grid, 2014. **5**(4): p. 1905-1919.
28. Dan T. Ton and Merrill A. Smith, *The U.S. Department of Energy's Microgrid Initiative.* The Electricity Journal, 2012. **25**(8): p. 84-94.
29. Grid Integration Group. *Examples Of Microgrids*. 2018; Available from: https://building-microgrid.lbl.gov/examples-microgrids [Accessed: 04/10/2018].
30. Adam Hirsch, Yael Parag, and Josep Guerrero, *Microgrids: A review of technologies, key drivers, and outstanding issues.* Renewable and Sustainable Energy Reviews, 2018. **90**: p. 402-411.
31. Navigant Research. *Microgrid Deployment Tracker 2Q18*. 2018; Available from: https://www.navigantresearch.com/reports/microgrid-deployment-tracker-2q18 [Accessed: 01/08/2018].
32. M. S. Mahmoud, S. Azher Hussain, and M. A. Abido, *Modeling and control of microgrid: An overview.* Journal of the Franklin Institute, 2014. **351**(5): p. 2822-2859.
33. *<Microgrid control and management of state transition period.pdf>.*
34. ; Available from: https://ec.europa.eu/commission/index_en [Accessed: 20/02/2019].
35. A. Elmitwally and M. Rashed, *Flexible Operation Strategy for an Isolated PV-Diesel Microgrid Without Energy Storage.* IEEE Transactions on Energy Conversion, 2011. **26**(1): p. 235-244.

36. S. Mishra, D. Ramasubramanian, and P. C. Sekhar, *A Seamless Control Methodology for a Grid Connected and Isolated PV-Diesel Microgrid.* IEEE Transactions on Power Systems, 2013. **28**(4): p. 4393-4404.
37. K. Yu, Q. Ai, S. Wang, J. Ni, and T. Lv, *Analysis and Optimization of Droop Controller for Microgrid System Based on Small-Signal Dynamic Model.* IEEE Transactions on Smart Grid, 2016. **7**(2): p. 695-705.
38. S. Parhizi, H. Lotfi, A. Khodaei, and S. Bahramirad, *State of the Art in Research on Microgrids: A Review.* IEEE Access, 2015. **3**: p. 890-925.
39. H. Vasconcelos, C. Moreira, A. Madureira, J. P. Lopes, and V. Miranda, *Advanced Control Solutions for Operating Isolated Power Systems: Examining the Portuguese islands.* IEEE Electrification Magazine, 2015. **3**(1): p. 25-35.
40. K. V. Vidyanandan and N. Senroy, *Frequency regulation in a wind-diesel powered microgrid using flywheels and fuel cells.* IET Generation, Transmission & Distribution, 2016. **10**(3): p. 780-788.
41. *IEEE Standard for the Testing of Microgrid Controllers.* IEEE Std 2030.8-2018, 2018: p. 1-42.
42. *IEEE Standard for the Specification of Microgrid Controllers.* IEEE Std 2030.7-2017, 2018: p. 1-43.
43. *IEEE Draft Recommended Practice for the Planning and Design of the Microgrid.* IEEE P2030.9/D9, December 2018, 2018: p. 1-42.
44. O. Cornea, G. Andreescu, N. Muntean, and D. Hulea, *Bidirectional Power Flow Control in a DC Microgrid Through a Switched-Capacitor Cell Hybrid DC–DC Converter.* IEEE Transactions on Industrial Electronics, 2017. **64**(4): p. 3012-3022.
45. M. Kwon and S. Choi, *Control Scheme for Autonomous and Smooth Mode Switching of Bidirectional DC–DC Converters in a DC Microgrid.* IEEE Transactions on Power Electronics, 2018. **33**(8): p. 7094-7104.
46. V. Nasirian, S. Moayedi, A. Davoudi, and F. L. Lewis, *Distributed Cooperative Control of DC Microgrids.* IEEE Transactions on Power Electronics, 2015. **30**(4): p. 2288-2303.
47. N. Pogaku, M. Prodanovic, and T. C. Green, *Modeling, Analysis and Testing of Autonomous Operation of an Inverter-Based Microgrid.* IEEE Transactions on Power Electronics, 2007. **22**(2): p. 613-625.
48. M. C. Chandorkar, D. M. Divan, and R. Adapa, *Control of parallel connected inverters in standalone AC supply systems.* IEEE Transactions on Industry Applications, 1993. **29**(1): p. 136-143.
49. J. A. P. Lopes, C. L. Moreira, and A. G. Madureira, *Defining control strategies for MicroGrids islanded operation.* IEEE Transactions on Power Systems, 2006. **21**(2): p. 916-924.
50. T. Kawabata and S. Higashino, *Parallel operation of voltage source inverters.* IEEE Transactions on Industry Applications, 1988. **24**(2): p. 281-287.
51. J. M. Guerrero, J. Matas, L. Garcia de Vicuna, M. Castilla, and J. Miret, *Decentralized Control for Parallel Operation of Distributed Generation Inverters Using Resistive Output Impedance.* IEEE Transactions on Industrial Electronics, 2007. **54**(2): p. 994-1004.
52. C. K. Sao and P. W. Lehn, *Autonomous load sharing of voltage source converters.* IEEE Transactions on Power Delivery, 2005. **20**(2): p. 1009-1016.
53. C. T. Lee, C. C. Chu, and P. T. Cheng, *A New Droop Control Method for the Autonomous Operation of Distributed Energy Resource Interface Converters.* IEEE Transactions on Power Electronics, 2013. **28**(4): p. 1980-1993.
54. W. Yao, M. Chen, J. Matas, J. M. Guerrero, and Z. M. Qian, *Design and Analysis of the Droop Control Method for Parallel Inverters Considering the Impact of the Complex*

Impedance on the Power Sharing. IEEE Transactions on Industrial Electronics, 2011. **58**(2): p. 576-588.
55. H. Mahmood, D. Michaelson, and J. Jiang, *Accurate Reactive Power Sharing in an Islanded Microgrid Using Adaptive Virtual Impedances.* IEEE Transactions on Power Electronics, 2015. **30**(3): p. 1605-1617.
56. Y. Li and Y. W. Li, *Power Management of Inverter Interfaced Autonomous Microgrid Based on Virtual Frequency-Voltage Frame.* IEEE Transactions on Smart Grid, 2011. **2**(1): p. 30-40.
57. T. Iwade, S. Komiyama, Y. Tanimura, M. Yamanaka, M. Sakane, and K. Hirachi. *A novel small-scale UPS using a parallel redundant operation system*. in *Telecommunications Energy Conference, 2003. INTELEC '03. The 25th International*. 2003.
58. H. M. Hsieh, T. F. Wu, Y. E. Wu, H. S. Nien, and Y. E. Wu. *A compensation strategy for parallel inverters to achieve precise weighting current distribution*. in *Fourtieth IAS Annual Meeting. Conference Record of the 2005 Industry Applications Conference, 2005.* 2005.
59. Tan Jingtao, Lin Hua, Zhang Jun, and Ying Jianping. *A novel load sharing control technique for paralleled inverters*. in *Power Electronics Specialist Conference, 2003. PESC '03. 2003 IEEE 34th Annual*. 2003.
60. T. Caldognetto and P. Tenti, *Microgrids Operation Based on Master/Slave Cooperative Control.* IEEE Journal of Emerging and Selected Topics in Power Electronics, 2014. **2**(4): p. 1081-1088.
61. Lee Woo-Cheol, Lee Taeck-Ki, Lee Sang-Hoon, Kim Kyung-Hwan, Hyun Dong-Seok, and Suh In-Young. *A master and slave control strategy for parallel operation of three-phase UPS systems with different ratings*. in *Applied Power Electronics Conference and Exposition, 2004. APEC '04. Nineteenth Annual IEEE*. 2004.
62. V. Verma and G. G. Talpur. *Decentralized Master-Slave operation of microgrid using current controlled distributed generation sources*. in *2012 IEEE International Conference on Power Electronics, Drives and Energy Systems (PEDES)*. 2012.
63. Wu Tsai-Fu, Chen Yu-Kai, and Huang Yong-Heh, *3C strategy for inverters in parallel operation achieving an equal current distribution.* IEEE Transactions on Industrial Electronics, 2000. **47**(2): p. 273-281.
64. M. Farhadi and O. Mohammed, *Energy Storage Technologies for High-Power Applications.* IEEE Transactions on Industry Applications, 2016. **52**(3): p. 1953-1961.
65. Bin Wu Venkata Yaramasu, *Model Predictive Control of Wind Energy Conversion Systems*. 2016, Wiley-IEEE Press.
66. M. Liserre, R. Cardenas, M. Molinas, and J. Rodriguez, *Overview of Multi-MW Wind Turbines and Wind Parks.* IEEE Transactions on Industrial Electronics, 2011. **58**(4): p. 1081-1095.
67. Samuela Bassi and Naomi Hicks. *Onshore wind energy: what are the pros and cons?* ; Available from: https://www.theguardian.com/environment/2012/sep/25/climate-change-windpower [Accessed: 10/07/2018].
68. *Global wind report: Annual market update*. 2016: Global Wind Energy Council (GWEC).
69. International Renewable Energy Agency (IRENA). *Renewable Energy Technologies: Cost Analysis Series*. Wind Power 2012; Available from: http://www.irena.org/publications/2012/Jun/Renewable-Energy-Cost-Analysis---Wind-Power [Accessed: 10/07/2018].
70. I. Erlich and U. Bachmann. *Grid code requirements concerning connection and operation of wind turbines in Germany*. in *IEEE Power Engineering Society General Meeting, 2005*. 2005.

71. Magdi Ragheb and Adam M. Ragheb, *Wind Turbines Theory - The Betz Equation and Optimal Rotor Tip Speed Ratio*, in *Fundamental and Advanced Topics in Wind Power*, R. Carriveau, Editor. 2011, InTech: Rijeka. p. Ch. 02.
72. *IEC 61400-1: Wind turbines - Part1: Design requirements*. 2005, International Electrotechnical Commission.
73. Javier González and Roberto Lacal Arantegui, *Technological evolution of onshore wind turbines—a market-based analysis*. 2016.
74. S. Alshibani, V. G. Agelidis, and R. Dutta, *Lifetime Cost Assessment of Permanent Magnet Synchronous Generators for MW Level Wind Turbines.* IEEE Transactions on Sustainable Energy, 2014. **5**(1): p. 10-17.
75. Xin Li, *Reduction of Wind Power Curtailment in Power System Operation*, in *Electronics and Electrical Engineering*. 2015, University of Strathclyde.
76. Jun Xia, *Future Power System Dynamic Frequency Response Under High Penetration Levels of Wind*, in *Electronics and Electrical Engineering*. 2015, Strathclyde.
77. Junji Tamura, *Calculation Method of Losses and Efficiency of Wind Generators*, in *Wind Energy Conversion Systems: Technology and Trends*, S. M. Muyeen, Editor. 2012, Springer London: London. p. 25-51.
78. S. H. Pishgar-Komleh, A. Keyhani, and P. Sefeedpari, *Wind speed and power density analysis based on Weibull and Rayleigh distributions (a case study: Firouzkooh county of Iran).* Renewable and Sustainable Energy Reviews, 2015. **42**: p. 313-322.
79. Y. A. kaplan, *Determination of the best Weibull methods for wind power assessment in the southern region of Turkey.* IET Renewable Power Generation, 2017. **11**(1): p. 175-182.
80. A. K. Azad, M. G. Rasul, M. M. Alam, S. M. Ameer Uddin, and Sukanta Kumar Mondal, *Analysis of Wind Energy Conversion System Using Weibull Distribution.* Procedia Engineering, 2014. **90**: p. 725-732.
81. Kasra Mohammadi and Ali Mostafaeipour, *Using different methods for comprehensive study of wind turbine utilization in Zarrineh, Iran.* Energy Conversion and Management, 2013. **65**: p. 463-470.
82. Siegfried Heier, *Grid Integration of Wind Energy Conversion Systems*. 2006: John Wiley & Sons.
83. Y. Zhao and C. Ding. *Wind Power Generator Output Model Based on the Statistical Wind Speed Distribution Derived From the Historical Data*. in *2018 2nd IEEE Conference on Energy Internet and Energy System Integration (EI2)*. 2018.
84. F. Nejabatkhah and Y. W. Li, *Overview of Power Management Strategies of Hybrid AC/DC Microgrid.* IEEE Transactions on Power Electronics, 2015. **30**(12): p. 7072-7089.
85. H. Lasseter Robert, A. Akhil Abbas, Marnay Chris, Stephens John, E. Dagle Jeffery, T. Guttromson Ross, A. Sakis Meliopoulous, J. Yinger Robert, and H. Eto Joseph, *Integration of Distributed Energy Resources: The CERTS MicroGrid Concept*. 2003, CERTS.
86. F. Katiraei, R. Iravani, N. Hatziargyriou, and A. Dimeas, *Microgrids management.* IEEE Power and Energy Magazine, 2008. **6**(3): p. 54-65.
87. A. G. Tsikalakis and N. D. Hatziargyriou, *Centralized Control for Optimizing Microgrids Operation.* IEEE Transactions on Energy Conversion, 2008. **23**(1): p. 241-248.
88. B. V. Solanki, K. Bhattacharya, and C. A. Cañizares, *A Sustainable Energy Management System for Isolated Microgrids.* IEEE Transactions on Sustainable Energy, 2017. **8**(4): p. 1507-1517.
89. N. D. Hatziargyriou, A. Dimeas, A. G. Tsikalakis, J. A. P. Lopes, G. Karniotakis, and J. Oyarzabal. *Management of microgrids in market environment*. in *2005 International Conference on Future Power Systems*. 2005.

90. A. Bidram and A. Davoudi, *Hierarchical Structure of Microgrids Control System.* IEEE Transactions on Smart Grid, 2012. **3**(4): p. 1963-1976.
91. Stephen Gillette. *Microturbine Technology Matures*. 2010; Available from: http://www.powermag.com/microturbine-technology-matures/ [Accessed: 20/09/2017].
92. Mohd Azrik Bin Roslan, *Thesis: Parallel Connected Inverter Operation in an Islanded Microgrid*, in *Department of Electronics and Electrical Engineering*. 2013, University of Strathclyde.
93. M. Hamzeh, H. Karimi, and H. Mokhtari, *A New Control Strategy for a Multi-Bus MV Microgrid Under Unbalanced Conditions.* IEEE Transactions on Power Systems, 2012. **27**(4): p. 2225-2232.
94. A. Ghazanfari, M. Hamzeh, H. Mokhtari, and H. Karimi, *Active Power Management of Multihybrid Fuel Cell/Supercapacitor Power Conversion System in a Medium Voltage Microgrid.* IEEE Transactions on Smart Grid, 2012. **3**(4): p. 1903-1910.
95. F. Kroupa Venceslav, *Phase-Locked Loops*, in *Frequency Stability:Introduction and Applications*. 2012, Wiley-IEEE Press. p. 328.
96. IEEE education society. *Pulse Width Modulated Inverter Model*. 1998; Available from: http://www.ewh.ieee.org/soc/es/Nov1998/08/PWMINV.HTM [Accessed: 10/07/2018].
97. A. M. Gole. *Sinusoidal Pulse width modulation*. 2000; Available from: http://encon.fke.utm.my/nikd/SEM4413/spwm.pdf [Accessed: 20/09/2017].
98. T. C. Green and M. Prodanović, *Control of inverter-based micro-grids.* Electric Power Systems Research, 2007. **77**(9): p. 1204-1213.
99. A. Morales, X. Robe, M. Sala, P. Prats, C. Aguerri, and E. Torres, *Advanced grid requirements for the integration of wind farms into the Spanish transmission system.* IET Renewable Power Generation, 2008. **2**(1): p. 47-59.
100. E. Fagan, S. Grimes, J. McArdle, P. Smith, and M. Stronge. *Grid code provisions for wind generators in Ireland*. in *IEEE Power Engineering Society General Meeting, 2005*. 2005.
101. S. Bernard, D. Beaulieu, and G. Trudel. *Hydro-Quebec grid code for wind farm interconnection*. in *IEEE Power Engineering Society General Meeting, 2005*. 2005.
102. R. M. Zavadil and J. C. Smith. *Status of wind-related US national and regional grid code activities*. in *IEEE Power Engineering Society General Meeting, 2005*. 2005.
103. National Grid. *THE GRID CODE*. 2017; Available from: http://www2.nationalgrid.com/uk/industry-information/electricity-codes/grid-code/the-grid-code/ [Accessed: 10/09/2017].
104. Hannele Holttinen, Peter Meibom, Antje Orths, Bernhard Lange, Mark O'Malley, John Olav Tande, Ana Estanqueiro, Emilio Gomez, Lennart Söder, Goran Strbac, J. Charles Smith, and Frans van Hulle, *Impacts of large amounts of wind power on design and operation of power systems, results of IEA collaboration.* Wind Energy, 2011. **14**(2): p. 179-192.
105. M. Tsili and S. Papathanassiou, *A review of grid code technical requirements for wind farms.* IET Renewable Power Generation, 2009. **3**(3): p. 308-332.
106. *IEEE Guide for Design, Operation, and Integration of Distributed Resource Island Systems with Electric Power Systems.* IEEE Std 1547.4-2011, 2011: p. 1-54.
107. DCode. 2017; Available from: http://www.dcode.org.uk/ [Accessed: 10/07/2018].
108. DCode. *The distribution code of licensed distribution nerwork operators of Great Britain*. 2017; Available from: http://www.dcode.org.uk/assets/uploads/DCode_v28_May_2017__020517_final.pdf [Accessed: 10/07/2018].

109. G. J. Kish and P. W. Lehn. *Microgrid design considerations for next generation grid codes*. in *2012 IEEE Power and Energy Society General Meeting*. 2012.
110. M. Amin and M. Molinas, *Small-Signal Stability Assessment of Power Electronics Based Power Systems: A Discussion of Impedance- and Eigenvalue-Based Methods.* IEEE Transactions on Industry Applications, 2017. **53**(5): p. 5014-5030.
111. E. A. A. Coelho, P. C. Cortizo, and P. F. D. Garcia, *Small-signal stability for parallel-connected inverters in stand-alone AC supply systems.* IEEE Transactions on Industry Applications, 2002. **38**(2): p. 533-542.
112. J. M. Guerrero, L. G. de Vicuna, J. Matas, M. Castilla, and J. Miret, *A wireless controller to enhance dynamic performance of parallel inverters in distributed generation systems.* IEEE Transactions on Power Electronics, 2004. **19**(5): p. 1205-1213.
113. GE Fanuc Intelligent Platforms Information Centers. *Switched Ethernet Latency Analysis*. 2009; Available from: https://www.edn.com/Pdf/ViewPdf?contentItemId=4135948 [Accessed: 10/07/2018].
114. Cheng Yeong Jia and E. K. K. Sng, *A novel communication strategy for decentralized control of paralleled multi-inverter systems.* IEEE Transactions on Power Electronics, 2006. **21**(1): p. 148-156.
115. M. S. Marhaba, S. Farhangi, H. Iman-Eini, and R. Iravani, *Reactive power sharing improvement of droop-controlled DFIG wind turbines in a microgrid.* IET Generation, Transmission & Distribution, 2018. **12**(4): p. 842-849.
116. Y. Sun, G. Shi, X. Li, W. Yuan, M. Su, H. Han, and X. Hou, *An f-P/Q Droop Control in Cascaded-Type Microgrid.* IEEE Transactions on Power Systems, 2018. **33**(1): p. 1136-1138.
117. B. M. Eid, N. A. Rahim, J. Selvaraj, and A. H. El Khateb, *Control Methods and Objectives for Electronically Coupled Distributed Energy Resources in Microgrids: A Review.* IEEE Systems Journal, 2016. **10**(2): p. 446-458.
118. R. Majumder, G. Ledwich, A. Ghosh, S. Chakrabarti, and F. Zare, *Droop Control of Converter-Interfaced Microsources in Rural Distributed Generation.* IEEE Transactions on Power Delivery, 2010. **25**(4): p. 2768-2778.
119. Inc. Cavium. *Introduction to Ethernet Latency - An Explanation of Latency and Latency Measurement*. 2017; Available from: https://www.cavium.com/Documents/TechnologyBriefs/Adapters/Tech_Brief_Introduction_to_Ethernet_Latency.pdf [Accessed: 10/07/2018].
120. Official U.S. government. *GPS Accuracy*. Available from: https://www.gps.gov/systems/gps/performance/accuracy/ [Accessed: 10/07/2018].
121. M. Edrah, K. L. Lo, and O. Anaya-Lara, *Reactive power control of DFIG wind turbines for power oscillation damping under a wide range of operating conditions.* IET Generation, Transmission & Distribution, 2016. **10**(15): p. 3777-3785.
122. Xu Lie and P. Cartwright, *Direct active and reactive power control of DFIG for wind energy generation.* IEEE Transactions on Energy Conversion, 2006. **21**(3): p. 750-758.
123. S. Sayeef, N. Mendis, K. Muttaqi, and S. Perera. *Enhanced reactive power support of a PMSG based wind turbine for a Remote Area Power system*. in *2010 20th Australasian Universities Power Engineering Conference*. 2010.
124. B. Stott, *Review of load-flow calculation methods.* Proceedings of the IEEE, 1974. **62**(7): p. 916-929.
125. Ray D. Zimmerman, Carlos E. Murillo-Sánchez, and others. *MTAPOWER - A MATLAB Power System Simulaiton Package*. Available from: http://www.pserc.cornell.edu/matpower/ [Accessed: 10/07/2018].

126. R. Engleitner, A. Nied, M. S. M. Cavalca, and J. P. da Costa, *Dynamic Analysis of Small Wind Turbines Frequency Support Capability in a Low-Power Wind-Diesel Microgrid.* IEEE Transactions on Industry Applications, 2018. **54**(1): p. 102-111.
127. S. Krishnamurthy, T. M. Jahns, and R. H. Lasseter. *The operation of diesel gensets in a CERTS microgrid*. in *2008 IEEE Power and Energy Society General Meeting - Conversion and Delivery of Electrical Energy in the 21st Century*. 2008.
128. S. F. Rafique and Z. Jianhua, *Energy management system, generation and demand predictors: a review.* IET Generation, Transmission & Distribution, 2018. **12**(3): p. 519-530.
129. L. Hernandez, C. Baladron, J. M. Aguiar, B. Carro, A. J. Sanchez-Esguevillas, J. Lloret, and J. Massana, *A Survey on Electric Power Demand Forecasting: Future Trends in Smart Grids, Microgrids and Smart Buildings.* IEEE Communications Surveys & Tutorials, 2014. **16**(3): p. 1460-1495.
130. Z. Chen, J. M. Guerrero, and F. Blaabjerg, *A Review of the State of the Art of Power Electronics for Wind Turbines.* IEEE Transactions on Power Electronics, 2009. **24**(8): p. 1859-1875.
131. G. Koutitas and L. Tassiulas, *Periodic Flexible Demand: Optimization and Phase Management in the Smart Grid.* IEEE Transactions on Smart Grid, 2013. **4**(3): p. 1305-1313.
132. *Diesel Generator Sets P2000 / P2250E*. Available from: https://www.fgwilson.com/en_GB/products/new/fg-wilson/diesel-generator-sets/large-range-730-kva/1000004947.html [Accessed: 10/07/2018].
133. *Average price of diesel fuel in the United Kingdom (UK) between January 2015 and December 2017 (in pence per liter)*. 2017; Available from: https://www.statista.com/statistics/299552/average-price-of-diesel-in-the-united-kingdom/ [Accessed: 10/07/2018].
134. Energy & Industrial Strategy Department for Business. *International industrial energy prices*. 2017; Available from: https://www.gov.uk/government/statistical-data-sets/international-industrial-energy-prices [Accessed: 10/07/2018].
135. U.A.Bakshi M.V.Bakshi, *Elements Of Power Systems*. First ed. 2008: Technical Publications Pune.
136. Nexans. *6-36kV Medium Voltage Underground Power Cables*. Available from: http://www.nexans.co.uk/UK/files/Underground%20Power%20Cables%20Catalogue%2003-2010.pdf [Accessed: 10/07/2018].
137. M. Amin, A. Rygg, and M. Molinas, *Self-Synchronization of Wind Farm in an MMC-Based HVDC System: A Stability Investigation.* IEEE Transactions on Energy Conversion, 2017. **32**(2): p. 458-470.
138. Z. Zhao, K. Li, Y. Jiang, S. Lu, and L. Yuan, *Overview on reliability of modular multilevel cascade converters.* Chinese Journal of Electrical Engineering, 2015. **1**(1): p. 37-49.
139. International Electrotechnica Commissionl. *IEC 61850: Power Utility Automation*. [Accessed: 10/07/2018].

Appendix

A. MATLAB codes for WECS electrical power output data generating

The MATLAB codes here is used for generating artificial wind power generator's output mentioned in chapter 2.

A.1 Overall wind power generator's output data

```
%% WECS electrical power output
%% v is the wind speed data
%% vr is the rated wind speed
%% vci is the cut in wind speed
%% vco is the cut out wind speed
%% Pr is the rated power of wind generator
function P=WECSout(v,vr,vci,vco,Pr)
    n=length(v);
    P=zeros(n,1);
    [a,b,c]=abcCal(vci,vr); % coefficient
    % generate electrical power output
    for i=1:1:n
        if v(i)<vci||v(i)>vco
            P(i)=0;
          elseif v(i)>=vci&&v(i)<vr
     P(i)=(Pr/(a*vr^2+b*vr+c)/vr^3)*(a*v(i)^5+b*v(i)^4+c*v(i)^
     3);% Pt=Pr/kr
        elseif v(i)>vr&&v(i)<vco
            P(i)=Pr;
        end
    end
end
```

A.2 Function of Weibull Distribution parameters generating

```
%% Weibull parameters for 100 meters height generating from
original observed ground wind speed data
function [k,c]=weibullPGen(windSpeed)
%% mean annual wind speed =mean(WSAnual)=1.9, 100 meters
annual ave wind speed is 7.05, this data should multiply a
ecoefficiency 3.71
windSpeed=windSpeed*3.71;
k=(0.9874/(std(windSpeed)/mean(windSpeed)))^1.0983;
c=mean(windSpeed)/(gamma(1+1/k));
end
```

A.3 Function of artificial wind speed generating

```
%% Artificial wind speed generating by Monte Carlo Simulation,
n is the repeating times
function v=windSpeedGen(k,c,n)
    v=zeros(n,1);
    for i=1:1:n
        M=rand(1);
        v(i)=c*(-log(M^(1/k)));
    end
end
```

A.3 Function of generator's parameters calculating

```
%% PMSG a b c parameters calculation based on cut in speed and
rated speed
function [a,b,c]=abcCal(vci,vr)
a=-0.14/(vr-vci)^2;
b=(0.31*vr-0.03*vci)/(vr-vci)^2;
c=(0.78*vr^2-1.87*vr*vci+0.95*vci^2)/(vr-vci)^2;
end
```

B. MATLAB codes for WECS/FESS combined system optimization

B.1 Overall setting points optimization

```
%% full optimization procedure
% initialize variant value
clear;
variant=0.5;

%% generate wind speed data
% weibull distribution parameters k c, repeat times of monte
carlo
% sumulation n
kAnnual=[1.2285;1.3741;1.0725;1.1010;1.2515;1.0334;1.1169;1.21
55;0.9622;1.2695;1.0267;1.6089];
cAnnual=[11.6642;15.4889;9.5832;7.6686;8.9463;6.6980;6.2448;4.
5742;3.0555;4.7300;4.4539;6.5354];
k=kAnnual(1);
c=cAnnual(1);
n=20000;% monte carlo repeat times
v=windSpeedGen(k,c,n);
%% generate WECS output data
% rated wind speed vr, cut in wind speed vi, cut out wind
speed vco, rated
% power capacity Pr
Pr=2;
vr=9.1;
vci=3;
vco=22.5;
P=WECSout(v,vr,vci,vco,Pr);
%%%%%%%%%%%%%%%%%%%initial
guesses%%%%%%%%%%%%%%%%%%%%%%%%%%%%%%%%%%%%%%%%%%%%
acc=20;% accuracy
P1=mean(P)/Pr/2;% P1=0.2;
Cmax=0.95;
Cinitial=Cmax;% initial energy stored in FESS
C1initial=P1*Pr*0.25/0.9/Cmax*2;
P2interval=[(P1+(0.5-P1)/acc):((0.5-P1)/acc):0.5];
for i=1:1:acc
    P2=P2interval(i);
    P3interval=[(P2+(0.8-P2)/acc):((0.8-P2)/acc):0.8];% P3
interval
    for j=1:1:acc
        P3=P3interval(j);
        C1interval=[(C1initial+((0.5-C1initial)/acc)):((0.5-
C1initial)/acc):0.5];
        for k=1:1:acc
            C1=C1interval(k);
```

```
            C2interval=[(C1+(1-C1)/acc):((1-C1)/acc):1];
            for h=1:1:acc
                C2=C2interval(h);
%%%%%%%%%%%%%%%%%%%%%%%%%%%%%%%%%%%%%%%%%%%%%%%%%%%%%%%%%%%%%%%%%%%%%%%%%%%%
%%%%%%%%%%%

[Pcomb,Cfess]=combOut(P,Pr,P1,P2,P3,Cinitial,C1,C2,Cmax);%
combined system output
                failurePer=sum(Pcomb<P1*Pr)/length(Pcomb);
                latestVariant=var(Pcomb);
                if failurePer<=0.01&&var(Pcomb)<variant
                %record opt values and break out
                    optP1=P1;
                    optP2=P2;
                    optP3=P3;
                    optC1=C1;
                    optC2=C2;
                    optvariant=latestVariant;
                    optfailurerate=failurePer;

[optPcomb,optCfess]=combOut(P,Pr,P1,P2,P3,Cinitial,C1,C2,Cmax)
;
                    optC=max(optCfess);
%                     break;
                end
            end
        end
    end
end
```

B.2 Function of generating WECS/FESS combined system output data

```
%% generate combined system output data and latest FESS stored
energy level
%% Original WECS output P MW, installed capacity of WECS Pr MW
%% initial guess of percentage setting points P1,P2,P3,C1,C2
%% initial guess of FESS installed capacity Cmax
%% Initial FESS energy stored Cinitial MJ(MVA)
%% assume the FESS has 90% efficiency of energy exchange
%% assume 15 min interval of wind speed variations

function
[Pcomb,Cfess]=combOut(P,Pr,P1,P2,P3,Cintial,C1,C2,Cmax)
    n=length(P);
    Pcomb=zeros(n,1);
    Cfess=zeros(n+1,1);
    Cfess(1)=Cintial; %initial energy stored in FESS
    %%%%%%%%%%%%%%%%%%%%%%%%%%%%%%%%%%%%%%%%%%%%%%%%%%%%%%%%%%%%
    % transfer percentage value to real value
    P1=P1*Pr;
```

```
    P2=P2*Pr;
    P3=P3*Pr;
    C1=C1*Cmax;
    C2=C2*Cmax;
    %%%%%%%%%%%%%%%%%%%%%%%%%%%%%%%%%%%%%%%%%%%%%%%%%%%%%%%%%%%%
    Cmin=P1*0.25*1.1; %minimum energy has to be stored in FESS
prevent stopping rotate
    for i=1:1:n
        %%%%%%%%%% combined output P1%%%%%%%%%%%%%%%%%%%%%%%%
        if P(i)<=P1&&Cfess(i)>Cmin&&Cfess(i)<=C2 %discharge
            Pcomb(i)=P1;
            Cfess(i+1)=Cfess(i)-(P1-P(i))*0.25*1.1;
        elseif P(i)>P1&&P(i)<=P3&&Cfess(i)<=Cmin %charge
            Pcomb(i)=P1;
            Cfess(i+1)=Cfess(i)+(P(i)-P1)*0.25*0.9;
        %%%%%%%%%% combined output P2%%%%%%%%%%%%%%%%%%%%%%%%
        elseif P(i)<=P1&&Cfess(i)>C2 %discharge
            Pcomb(i)=P2;
            Cfess(i+1)=Cfess(i)-(P2-P(i))*0.25*1.1;
        elseif
P(i)>P1&&P(i)<=P2&&Cfess(i)>C1&&Cfess(i)<=C2 %discharge
            Pcomb(i)=P2;
            Cfess(i+1)=Cfess(i)-(P2-P(i))*0.25*1.1;
        elseif
P(i)>P2&&P(i)<=P3&&Cfess(i)>Cmin&&Cfess(i)<=C1 %charge
            Pcomb(i)=P2;
            Cfess(i+1)=Cfess(i)+(P(i)-P2)*0.25*0.9;
        elseif P(i)>P3&&Cfess(i)<=C1 %charge
            Pcomb(i)=P2;
            Cfess(i+1)=Cfess(i)+(P(i)-P2)*0.25*0.9;
         %%%%%%%%%% combined output P3%%%%%%%%%%%%%%%%%%%%%%%%
        elseif P(i)>P1&&P(i)<=P3&&Cfess(i)>C2 %discharge
            Pcomb(i)=P3;
            Cfess(i+1)=Cfess(i)-(P3-P(i))*0.25*1.1;
        elseif P(i)>P3&&Cfess(i)>C2&&Cfess(i)<=Cmax %charge
            Pcomb(i)=P3;
            Cfess(i+1)=Cfess(i)+(P(i)-P3)*0.25*0.9;
        %%%%%%%%%%%%%%%standby%%%%%%%%%%%%%%%%%%%%%%%%%%%%%%%%
        else
            Pcomb(i)=P(i);
            Cfess(i+1)=Cfess(i);
        end
    end
end
```

C. DFIG and PMSG wind turbine model

C.1 DFIG model

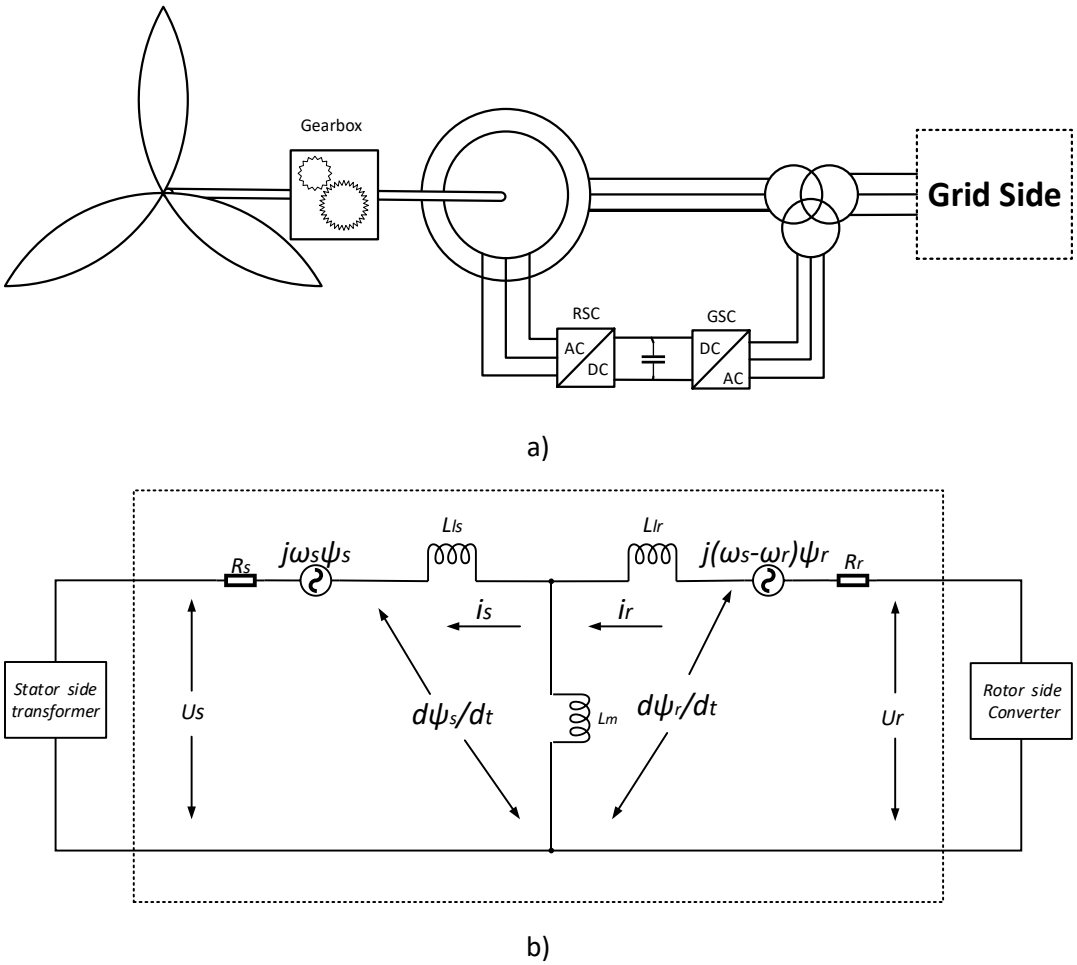

Figure 0.1 a) schematic diagram of DFIG and b) single phase equivalent circuit

Steady-state machine stator and rotor voltages is presented in equation (0.1) and (0.2) which derived by Kirchhoff's law from the single phase equivalent circuit in Figure 0.1.

$$u_s = R_s i_s + j\omega_s \psi_s + \frac{d\psi_s}{dt} \tag{0.1}$$

$$u_r = R_r i_r + j(\omega_s - \omega_r)\psi_r + \frac{d\psi_r}{dt} \tag{0.2}$$

Where:

u_s is the stator voltage (V)

u_r is the rotor voltage (V)

R_s is the stator resistance (Ω)

R_r is the rotor resistance (Ω)

i_s is the stator current (A)

i_r is the rotor current (A)

ψ_s is the stator flux (Wb)

ψ_r is the rotor flux (Wb)

ω_s is the synchronous speed (rad/s)

ω_r is the rotor speed (rad/s)

The **stator and rotor flux** are defined as:

$$\psi_s = (L_{ls} + L_m)i_s + L_m i_r \quad (0.3)$$

$$\psi_r = (L_{lr} + L_m)i_r + L_m i_s \quad (0.4)$$

Where:

L_{ls} is the stator leakage induction (H)

L_{lr} is the rotor leakage induction (H)

L_m is the mutual induction (H)

Generators can be analysed in two-axis theory either in αβ, xy or dq frames. To eliminate coupling issues and simplify the power system analysis, dq frame is preferred. In dq frame analysis, AC power system is transformed into a DC circuit. The axis rotating at synchronous speed is usually chosen as the reference axis for induction machine. In this thesis, q-axis is assumed to be 90° leading d-axis.

Equation (0.1) - (0.4) are rewritten as equation (0.5) - (0.12) by a dq transformation.

$$u_{ds} = R_s i_{ds} - \omega_s \psi_{qs} + \frac{d\psi_{ds}}{dt} \tag{0.5}$$

$$u_{qs} = R_s i_{qs} + \omega_s \psi_{ds} + \frac{d\psi_{qs}}{dt} \tag{0.6}$$

$$u_{dr} = R_r i_{dr} - (\omega_s - \omega_r)\psi_{qr} + \frac{d\psi_{dr}}{dt} \tag{0.7}$$

$$u_{qr} = R_s i_{dr} + (\omega_s - \omega_r)\psi_{dr} + \frac{d\psi_{qr}}{dt} \tag{0.8}$$

$$\psi_{ds} = (L_{ls} + L_m) i_{ds} + L_m i_{dr} \tag{0.9}$$

$$\psi_{qs} = (L_{ls} + L_m) i_{qs} + L_m i_{qr} \tag{0.10}$$

$$\psi_{dr} = (L_{ls} + L_m) i_{dr} + L_m i_{ds} \tag{0.11}$$

$$\psi_{qr} = (L_{ls} + L_m) i_{qr} + L_m i_{qs} \tag{0.12}$$

When a generator is running in steady state operation mode, the derivative terms in equation (0.5) and (0.6) become 0. The stator flux and rotor flux can be obtained in dq-axis frame as:

$$\psi_{ds} = \frac{u_{qs} - R_s i_{qs}}{\omega_s} \tag{0.13}$$

$$\psi_{qs} = -\frac{v_{ds} - R_s i_{ds}}{\omega_s} \tag{0.14}$$

The **electrical power** generated by the DFIG are

$$P_s = \frac{3}{2}\left(u_{ds} i_{ds} + u_{qs} i_{qs}\right) \tag{0.15}$$

$$Q_s = \frac{3}{2}\left(u_{qs} i_{ds} - u_{ds} i_{qs}\right) \tag{0.16}$$

$$P_r = \frac{3}{2}\left(u_{dr} i_{dr} + u_{qr} i_{qr}\right) \tag{0.17}$$

$$Q_r = \frac{3}{2}\left(u_{qr} i_{dr} - u_{dr} i_{qr}\right) \tag{0.18}$$

$$P_{DFIG} = P_s + P_r \tag{0.19}$$

$$Q_{DFIG} = Q_s + Q_r \tag{0.20}$$

The **electromagnetic torque** is defined as the real part of the product of flux vector and current vector in (0.21):

$$T_e = \frac{3}{2} P\left(\psi_{ds} i_{qs} - \psi_{qs} i_{ds}\right) \tag{0.21}$$

Here *P* is the DFIG pole pairs.

C.2 PMSG model

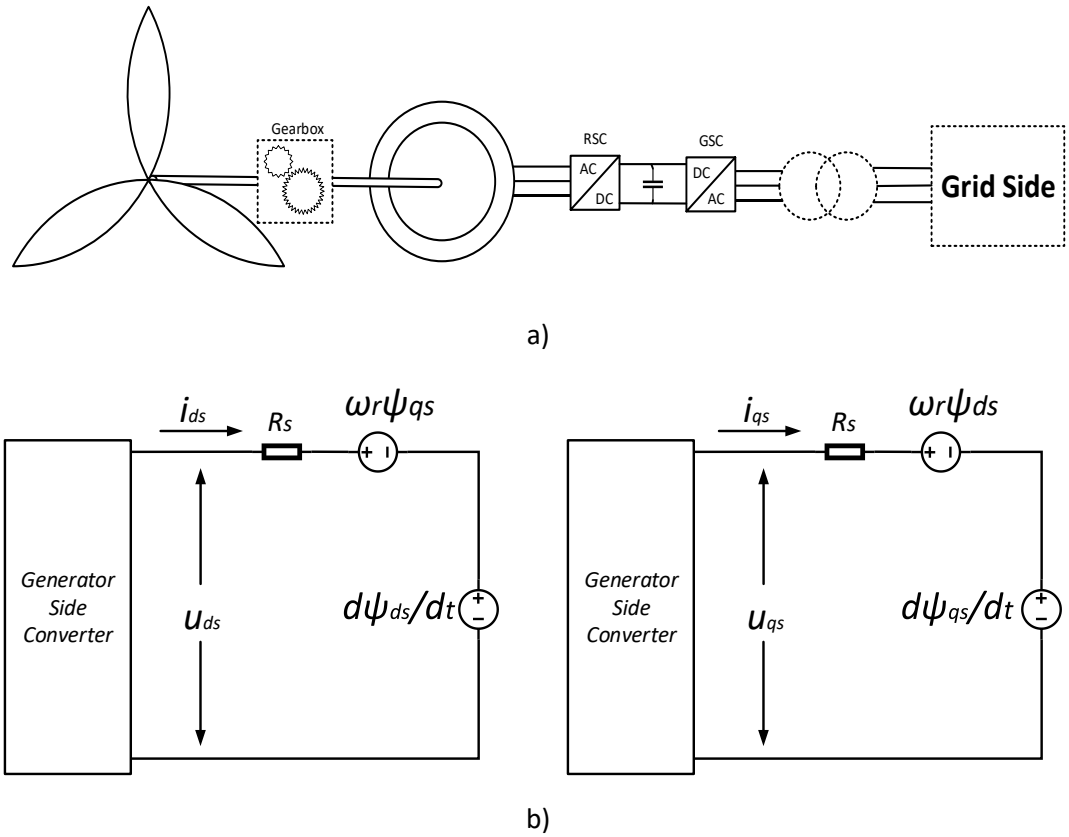

Figure 0.2 a) schematic diagram of PMSG and b) dq frame equivalent circuit

Similar to the section 2.3.2, the features of PMSG can be derived based on Figure 0.2 as follows:

Steady-state machine stator voltages

$$u_{ds} = R_s i_{ds} - \omega_r \psi_{qs} \quad (0.22)$$

$$u_{qs} = R_s i_{qs} + \omega_r \psi_{ds} \quad (0.23)$$

Stator flux linkages

$$\psi_{ds} = L_{ds} + \psi_r \quad (0.24)$$

$$\psi_{qs} = L_{qs} i_{qs} \quad (0.25)$$

Electrical power generated by PMSG

$$P_{PMSG} = P_s = \frac{3}{2}\left(u_{ds} i_{ds} + u_{qs} i_{qs}\right) \quad (0.26)$$

$$Q_{PMSG} = Q_s = \frac{3}{2}\left(u_{qs} i_{ds} - u_{ds} i_{qs}\right) \quad (0.27)$$

Electromagnetic torque

$$T_e = \frac{3}{2} P\left(\psi_{ds} i_{qs} - \psi_{qs} i_{ds}\right) \quad (0.28)$$